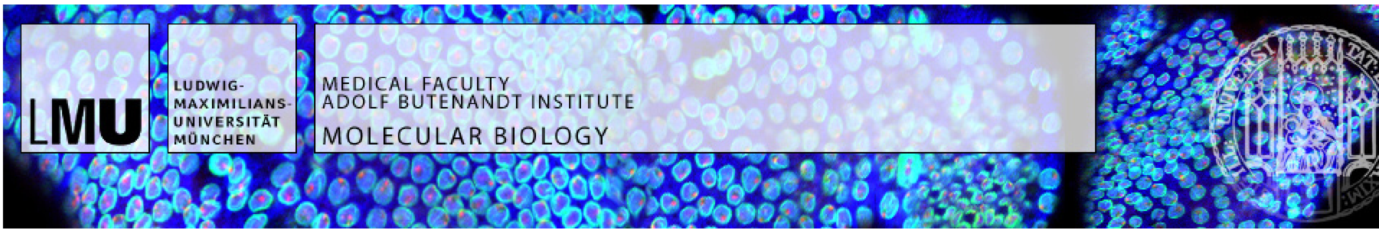
LMU
LUDWIG-
MAXIMILIANS-
UNIVERSITÄT
MÜNCHEN
MEDICAL FACULTY
ADOLF BUTENANDT INSTITUTE
MOLECULAR BIOLOGY

Dissertation zur Erlangung des Doktorgrades
der Naturwissenschaften an der Fakultät für Biologie
der Ludwig-Maximilians-Universität München

Physical and Functional Interaction between DOM-B and ACF1

The Interception of Two Distinct Nucleosome Remodeling Principles

Sandra Vengadasalam
München

Juni 2011

Ehrenwörtliche Versicherung

Ich versichere hiermit ehrenwörtlich, dass die vorgelegte Dissertation von mir selbständig und ohne unerlaubte Hilfe angefertigt wurde.

München, den ....

....
Sandra Vengadasalam

Eingereicht am 15. Juni 2011

Mündliche Prüfung am 1. August 2011

1. Gutachter: Professor Dr. Peter Becker

2. Gutachter: Professor Dr. Charles David

3. Gutachter: Professor Dr. Thomas Cremer

4. Gutachter: Professor Dr. Angelika Böttger

5. Gutachter: Professor Dr. Gerhard Wanner

6. Gutachter: Professor Dr. Kirsten Jung

ACKNOWLEDGEMENTS

First of all I would like to thank Dr. Anton Eberharter for offering me the research on this very exciting "Domino and ACDC" project. Thank you for your guidance, motivation and advice whenever needed and for letting me follow my own path. You strengthened my interest in science and taught me how to become an independent scientist.

I am especially grateful to Professor Dr. Peter Becker who gave me the opportunity to continue my work and always had time for me even in busy days. Thank you for carefully reading this manuscript, your valuable scientific input, useful criticism and all the fruitful discussions.

I also want to express my gratitude to Dr. Mariacristina Chioda not only for teaching me her technical expertise and never running out of ideas when the project was stuck, but also for her right words bringing back my enthusiasm for our fascinating research field. Thank you for picking me up in my green coat, sharing chocolate and your extraordinary friendship.

I also would like to thank Florian Dreisbach for his great work and help in the lab as well as in the flyroom.

I wish to acknowledge Dr. Natascha Kunert for scientific comments and discussions especially during the last months. In addition, I want to thank Professor Dr. Ralph Rupp for being a member of my thesis advisory committee and Dr. Sandra Hake for her time and helpful advice.

Heartfelt thanks go to all past and present members of the molecular biology department for creating a scientifically motivating environment and an enjoyable lab atmosphere. Unforgettable will be the "ABI-orchestra" and its members Dr. Verena Maier, Dr. Franziska Ertel, Florian Dreisbach, Dr. Sonja Wiedemann and Dr. Alexandra Lantermann. You made it fun to work here!

My special thanks go to Dr. Franziska Ertel, Dr. Annette Scharf, Dr. Verena Maier, Dr. Stephanie Socher and Cordula Marschal for being great friends.

I am also grateful to my parents, Siegrun and Sakthy Vengadasalam, for supporting me throughout my life and education and for their unwavering confidence in me.

Most of all I thank Dr. Felix Gußmann for always being there for me. I couldn't have wished for more.

CONTENTS

Summary..1

Zusammenfassung..3

1 **Introduction**..7

  1.1 Chromatin 8
    1.1.1 DNA Compaction Levels in Chromatin..8
    1.1.2 Chromatin Is a Highly Dynamic Structure..9
    1.1.3 Histone Variants..10

  1.2 ATP-Dependent Chromatin Remodeling..13
    1.2.1 Composition and Basic Domains of Different Chromatin Remodeling Families..........14
    1.2.2 Subfamilies of Chromatin Remodelers and Their Known Biological Function 15
      1.2.2.1 The SWI/SNF Family..16
      1.2.2.2 The CHD Family..17
      1.2.2.3 The ISWI Family..18
      1.2.2.4 The INO80 Family..19

  1.3 The Chromatin Remodeler Domino..21
    1.3.1 The Structure of Domino..21
    1.3.2 The Functions of Domino A and Domino B Are Just Beginning to Be Uncovered........21

  1.4 *Drosophila melanogaster* – a Model Organism to Study Chromatin Remodeling during Development..23
    1.4.1 The Life Cycle of *Drosophila Melanogaster*..24
    1.4.2 Embryogenesis..25
    1.4.3 Morphogenesis and Eye Development..27
    1.4.4 Oogenesis..31
    1.4.5 Stem Cell Maintenance during Oogenesis..33

  1.5 Objective..35

2 **Material and methods**..**37**

  2.1 Material Sources..38
    2.1.1 Laboratory Chemicals and Biochemicals..38
    2.1.2 Enzymes..39
    2.1.3 Antibodies..39
    2.1.4 Organisms..40
    2.1.5 Oliogonucleotides, Plasmids and Baculoviruses..40
    2.1.6 Other Materials..41
    2.1.7 Buffers and Solutions..41

2.2 Methods for Preparation and Analysis of DNA........44

2.2.1 General Methods for Working with DNA........44

2.2.1.1 Agarose Gel Electrophoresis........44

2.2.1.2 DNA Quantification........45

2.2.1.3 Transformation of Competent Bacteria........45

2.2.1.4 Plasmid Preparation........45

2.2.2 Cloning of *UAS*-Reporter Constructs........45

2.2.3 Site-Directed Mutagenesis........45

2.2.4 DNA Purification for P-Element-Mediated Germline Transformation via Microinjection of *Drosophila* Embryos........46

2.2.5 DNA Biotinylation........46

2.2.6 Chromatin Assembly on Immobilized DNA........46

2.3 Methods for Protein Purification and Analysis........47

2.3.1 Protein Quantification........47

2.3.2 SDS Polyacrylamide Gel Electrophoresis (SDS-PAGE)........47

2.3.3 Western Blotting........48

2.3.4 Bacterial Expression and Purification of GST- and FLAG-Tagged DOM-B Proteins.....48

2.3.4.1 Induction of Protein Expression........48

2.3.4.2 Preparation of Bacterial Cell Extract........49

2.3.4.3 Purification of GST-Tagged DOM-B Proteins from Bacterial Cell Extract........49

2.3.5 Expression and Purification of Recombinant Proteins in *Sf9* Cells........49

2.3.5.1 Cultivation of *Spodoptera Frugiperda* Cells........49

2.3.5.2 Infection of *Sf9* Cells with Baculoviruses........49

2.3.5.3 Preparation of *Sf9* Cell Extract........50

2.3.5.4 Purification of FLAG-Tagged DOM-B Proteins from *Sf9* Cell Extract........50

2.3.6 Purification of DOM-B from *Drosophila* Embryos........50

2.3.6.1 Harvesting of *Drosophila* Embryos........50

2.3.6.2 Large Scale Preparation of *Drosophila* Embryo Nuclear Extract (TRAX)........51

2.3.6.3 Purification of DOM-B Proteins from TRAX by Ion Exchange Chromatography........51

2.3.6.4 Superose 6 Gel Filtration Analysis of DOM-B, ACF1 and ISWI from TRAX......51

2.3.6.5 Small Scale Preparation of Nuclear Extract from *Drosophila* Embryos........52

2.4 ATPase assay........52

2.5 Generation of New Antibodies........53

2.6 General Methods for Working with *Drosophila*........53

2.6.1 Fly Maintenance........53

2.6.2 Microinjection of *Drosophila* Embryos for P-Element-Mediated Germline Transformation........53

2.6.3 Screening and Mapping Chromosomal Insertion Sites of Transgenes........54

2.6.4 Novel Established Transgenic Fly Lines........55

2.6.5 Fly Crosses........56

2.7 *In Vivo* Analysis of *Drosophila* Transgenic Fly Lines..........56
  2.7.1 Ectopic Expression of DOM-B in Adult Fly Ovaries..........56
    2.7.1.1 Preparation of Adult Fly Ovaries..........56
    2.7.1.2 Ovary Extract Preparation and Quantitative Western Blotting..........57
    2.7.1.3 Immunofluorescence Staining and Analysis of Fly Ovaries..........57
  2.7.2 Ectopic Expression of DOM-B in Larval Imaginal Discs and Salivary Glands..........58
    2.7.2.1 Preparation of Imaginal Discs and Salivary Glands..........58
    2.7.2.2 Immunofluorescence Analysis of Imaginal Discs and Salivary Glands..........58
    2.7.2.3 BrdU Labeling of Imaginal Eye-Antenna Discs..........59

3 Results..........**61**

In Vitro Analysis of Domino B

3.1 Distinct DOM-B Complexes Exist in *Drosophila* Embryos..........62
  3.1.1 DOM-B Expression Is Developmentally Regulated in *Drosophila*..........62
  3.1.2 DOM-B Is Part of a High Molecular Weight Complex in *Drosophila* Embryos..........63
  3.1.3 DOM-B, ACF1 and ISWI Cofractionate in *Drosophila* Embryos after Several Distinct Ion Exchange Chromatography Columns..........63

3.2 Recombinant DOM-B Proteins Can Be Expressed in *E.coli* and *Sf9* Cells..........66
  3.2.1 Expression and Purification of Recombinant DOM-B Proteins and Derivatives in Bacteria..........67
  3.2.2 Purification of Recombinant DOM-B Proteins and Derivatives in *Sf9* Cells..........69

3.3 The ATPase Domain of DOM-B Is Required for Direct Binding to ACF1..........70

3.4 The ATPase Activity of DOM-B Is Inhibited by Its C-terminus..........72

In Vivo Analysis of Domino B

3.5 DOM-B Expression and Distribution on Chromatin of Salivary Glands Is Similar to ACF1..........75
  3.5.1 Characterization of a New α-H2AV-Specific Antibody..........76
  3.5.2 Characterization of New Specific α-DOM-B Monoclonal Rat Antibodies..........77
  3.5.3 Characterization of a New Specific α-DOM-B Polyclonal Chicken Antibody..........79
  3.5.4 Ectopic Expression of ACF1 in Salivary Glands Upregulates DOM-B Signals..........80

3.6 Chromatin Formation in Salivary Glands Is Disturbed by Ectopic Expression of DOM-B..........81

3.7 DOM Depletion Disturbs Normal Development during Fly Morphogenesis..........83
  3.7.1 Knock-Down of DOM in Salivary Glands Causes Pupal Lethality..........83
  3.7.2 Depletion of DOM during Eye Development Impairs Eye and Antenna Morphology..........85
  3.7.3 Differentiation of Precursor Cells in Imaginal Eye-Antenna Discs Is Perturbed by DOM Depletion..........86

3.8 Ectopic Expression of DOM-B in Imaginal Eye-Antenna Discs Disturbs Eye Development....87
  3.8.1 Ectopic Expression of DOM-B in Imaginal Eye-Antenna Discs Caused Phenotypic Abnormalities in Adult Compound Eyes....87
  3.8.2 Ectopic Expression of DOM-B Disturbes Cell Differentiation in Larval Imaginal Eye-Antenna Discs....89
  3.8.3 Ectopic Expression of DOM-B Delays Cell Cycle Progression during S-Phase and Perturbs Apoptotic Events....90

3.9 Combined Ectopic Expression of DOM-B and ACF1 Leads to Major Defects and Lethality....92
  3.9.1 Ectopic Expression of DOM-B in Fly Eyes Leads to a Rough Eye Phenotype....92
  3.9.2 Coexpression of DOM-B and ACF1 Affects Cell Fate in Imaginal Eye-Antenna Discs....95

3.10 DOM-B and ACF1 Are Important during Oogenesis....97

3.11 Ectopic Coexpression of DOM-B and ACF1 Has a Dramatic Synergistic Effect on Fly Viability during Early *Drosophila* Development....101

4 Discussion....**103**

4.1 DOM-B Is a Subunit of the Putative Novel Chromatin Remodeling Complex ACDC....104

4.2 Developmental Expression of DOM-B in *Drosophila* Is Similar to ACF1....106

4.3 DOM-B Plays an Important Role during *Drosophila* Development Similar to ACF1....107
  4.3.1 DOM-B and ACF1 Influence the Stem Cell Maintenance in *Drosophila* Female Ovaries....107
  4.3.2 DOM-B Is Important for Chromatin Formation at Larval Stage....108
  4.3.3 DOM-B Is Essential for Cell Differentiation and Cell Cycle Progression....109

4.4 Synergistic Effects upon DOM-B and ACF1 Overexpression Are Restricted to Oogenesis and Early Embryogenesis....111

4.5 Outlook....114
  4.5.1 Future *in Vivo* and *in Vitro* Studies of DOM-B and ACDC....114
  4.5.2 The Connection between DOM-Containing Nucleosome Remodelers and ACF/CHRAC Might Be the Metabolism of H2AV....115

5 Abbreviations....**120**

6 Bibliography....**124**

7 List of Figures and Tables....**134**

8 Curriculum Vitae....**137**

SUMMARY

The life of multicellular organisms starts with the fertilization of a single egg cell. This cell develops into a mature organism through complex mechanisms such as cell proliferation, cell fate determination and cell differentiation as well as cell interactions and movement. These developmental processes depend on selective gene expression and hence on a dynamic nature of chromatin, which is regulated by epigenetic programs. One molecular mechanism to change gene expression is ATP-dependent chromatin remodeling, which can change the contact between histones and DNA, catalyze nucleosome repositioning or eviction and replace histones with their variants. A known chromatin remodeling factor that is involved in histone exchange is the highly conserved ATPase Domino A of the TIP60 complex. The isoform Domino B is so far less characterized. Previous studies found this enzyme involved in essential processes during development of flies and mammals, but the biological function and the molecular context of Domino B is poorly understood. During my PhD thesis, I have analyzed the expression pattern of Domino B, characterized some associated factors in a putative novel complex and explored its potential functions.

Domino belongs to the SWR1-type chromatin remodelers and contains the characteristic bipartite ATPase domain. By fractionation of *Drosophila* embryo nuclear extracts a so far unappreciated diversity of nucleosome remodeling complexes emerged. In distinct fractions, Domino B was associated with known TIP60 subunits and to our surprise, with ACF1 and ISWI. Both factors belong to the ACF/CHRAC complexes, which change the chromatin structure through nucleosome sliding. The physical interaction of Domino B, ACF1 and ISWI is specific to earliest stages of embryonic development in *Drosophila*, since all of them were predominantly detected in preblastodermal embryos and were absent in later stages. To analyze Domino B *in vitro* as well as *in vivo*, three different expression systems (in *E.coli*, *SF9* cells and *D. melanogaster*) were established. *In vitro*, recombinant ACF1 and ISWI bound directly to Domino B and its split ATPase domain was mapped as the binding region to ACF1. These findings indicate a novel putative remodeling complex consisting among others of Domino B, ACF1 and ISWI, which we referred to as ACDC (ACF-Domino containing) complex. The functional role of Domino B and ACDC were characterized in *in vivo* experiments studying loss- and gain-of-function phenotypes in *Drosophila*. Domino B is involved in cell fate determination, cell differentiation and cell cycle related processes in specific cell types. Remarkably, phenotypic abnormalities of Domino B correspond to them of ACF1 indicating their functional relationship *in vivo*. A coexpression of both factors during early developmental stages resulted in synergistic effects and synthetic lethality. A putative ATPase deficient form of Domino B (Domino B KR) could “rescue” observed synthetic lethal phenotypes of ACDC. Synthetic actions of Domino B and ACF1 are restricted to oogenesis and early embryogenesis in agreement with their association in ovaries and preblastodermal embryos.

In conclusion, the results of this work show that Domino B is involved in cell differentiation and cell cycle related processes in *Drosophila*. A novel physical and functional interaction between Domino B and ACF that was unappreciated so far was found in early embryogenesis. This reveals a novel type of complex combining two distinct remodeling mechanisms, nucleosome sliding and histone variant exchange.

ZUSAMMENFASSUNG

Das Leben vielzelliger Organismen beginnt mit der Befruchtung einer Eizelle. Diese Zelle entwickelt sich im Zuge komplexer Mechanismen wie Zellproliferation, Zelldifferenzierung und der Bestimmung des Zellschicksals so wie Zellinteraktion und Zellbewegung zu einem ausgereiften Organismus. Diese Entwicklungsprozesse sind von einer gezielten Genexpression und damit von einer flexiblen Chromatinstruktur, welche durch verschiedene epigenetische Programme reguliert wird, abhängig. Einer dieser molekularen Mechanismen zur Beeinflussung der Genexpression ist ATP-abhängiges „chromatin remodeling“, welches die DNA-Histon-Kontakte verändert und dadurch Nukleosomen verschieben, ausbauen oder durch den Austausch kanonischer Histone mit ihren Varianten umformen kann. Ein bekannter „chromatin remodeling“ Faktor, welcher am Histonaustausch beteiligt ist, ist die hoch konservierte ATPase Domino A des TIP60 Komplexes. Seine zweite Isoform Domino B wurde bis jetzt nur wenig beschrieben und wird gerade erst näher erforscht. Frühere Studien belegen, dass dieses Enzym an essentiellen Prozessen während der Entwicklung von Fliegen und Säugetieren beteiligt ist. Die biologische Funktion und die genaue Funktionsweise von Domino B sind jedoch weitgehend unbekannt. Während meiner Dissertation habe ich das Expressionsmuster von Domino B analysiert, einige seiner Partner innerhalb eines eventuell neuartigen Komplexes beschrieben und seine potentielle Funktion untersucht.

Domino gehört zu der Familie der SWR1 „chromatin remodeler“ und zeichnet sich durch die charakteristische zweigeteilte ATPase Domäne aus. Nach der Fraktionierung von *Drosophila* Kernextrakten zeigte sich eine bisher unbeachtete Vielfältigkeit nukleosomaler „remodeling Komplexe“. In bestimmten Fraktionen assoziierte Domino B mit bekannten Untereinheiten des TIP60 Komplexes und überraschenderweise mit ACF1 und ISWI. Diese beiden Faktoren gehören zu den ACF/CHRAC Faktoren, welche Chromatin durch das Verschieben von Nukleosomen verändern können. Die physische Interaktion von Domino B, ACF1 und ISWI ist für die sehr frühe Embryonalentwicklung in *Drosophila* spezifisch, da alle drei Faktoren überwiegend in preblastodermalen Embryos nachgewiesen wurden und ihre Proteine im Verlauf der weiteren Entwicklung abnahmen. Um Domino B *in vitro* sowie *in vivo* erforschen zu können, wurden drei verschiedene Expressionssysteme (in *E.coli*, *SF9* Zellen und *D. melanogaster*) etabliert. *In vitro* interagierten rekombiniertes ACF1 und ISWI direkt mit Domino B, dessen geteilte ATPase Domäne als Binderegion zu ACF1 identifiziert werden konnte. Diese Daten weisen auf einen möglicherweise neuartigen „remodeling“ Komplex hin, der sich unter anderem aus Domino B, ACF1 und ISWI zusammensetzt und den wir als ACDC (ACF-Domino containing) Komplex bezeichnen. Die funktionelle Bedeutung von Domino B und des ACDC Komplexes wurde in *in vivo* Experimenten durch die Analyse von phänotypischen Veränderungen nach einer gezielten Terminierung oder Überexpression (loss- and gain-of-function) von Domino B erforscht. Domino B ist an der Bestimmung des Zellschicksals sowie an der Zelldifferenzierung und an Zellzyklus gekoppelte Prozesse in bestimmten Zelltypen beteiligt. Bemerkenswerterweise ähneln sich hierbei die Phänotypen von Domino B und ACF1, was auf ihre funktionelle Beziehung auch *in vivo* deutet. Eine Koexpression beider Faktoren während frühen Entwicklungsphasen führte zu synergistischen Effekten bis hin zur synthetischen Letalität. Eine möglicherweise ATPase defekte Form von Domino B (Domino B KR) konnte letale Phänotypen von ACDC aufheben. Die synergistische Wirkung von Domino B und ACF1 ist gemäß ihrer Assoziation in Ovarien und preblastodermalen Embryos beschränkt auf die Oogenese und frühe Embryogenese.

Zusammengenommen zeigen diese Ergebnisse, dass Domino B an der Zelldifferenzierung und an

Prozessen während des Zellzyklus in *Drosophila* beteiligt ist. Eine bisher völlig unbeachtete und neuartige physische und funktionelle Interaktion zwischen Domino B und ACF besteht während der frühen Embryogenese und möglicherweise während der Oogenese. Diese deutet auf eine ganz neue Art von Komplex hin, welcher zwei individuelle Mechanismen, Verschiebung von Nukleosomen und Austausch von Histonvarianten, kombiniert.

1 INTRODUCTION

1.1 Chromatin

1.1.1 DNA Compaction Levels in Chromatin

DNA is the prime macromolecule that stores genetic information of all known living organisms, with the exception of some viruses (Avery et al., 1944). Each human cell contains approximately 2 meters of DNA, which is packed into a microscopic space of the eukaryotic nucleus with about 10 µm in diameter. How can that 2 m long fiber be squeezed into a small nucleus? This challenge to compact DNA is accomplished by specialized proteins that bind to and fold the DNA into chromatin – the complex that combines DNA and proteins. These DNA binding proteins are termed histones and act as spools around which DNA winds (Figure 1.1). Histones are a family of small, positively charged proteins that interact with DNA very tightly due to the negatively charged phosphodiester backbone of the DNA double helix (Van Holde, 1988).

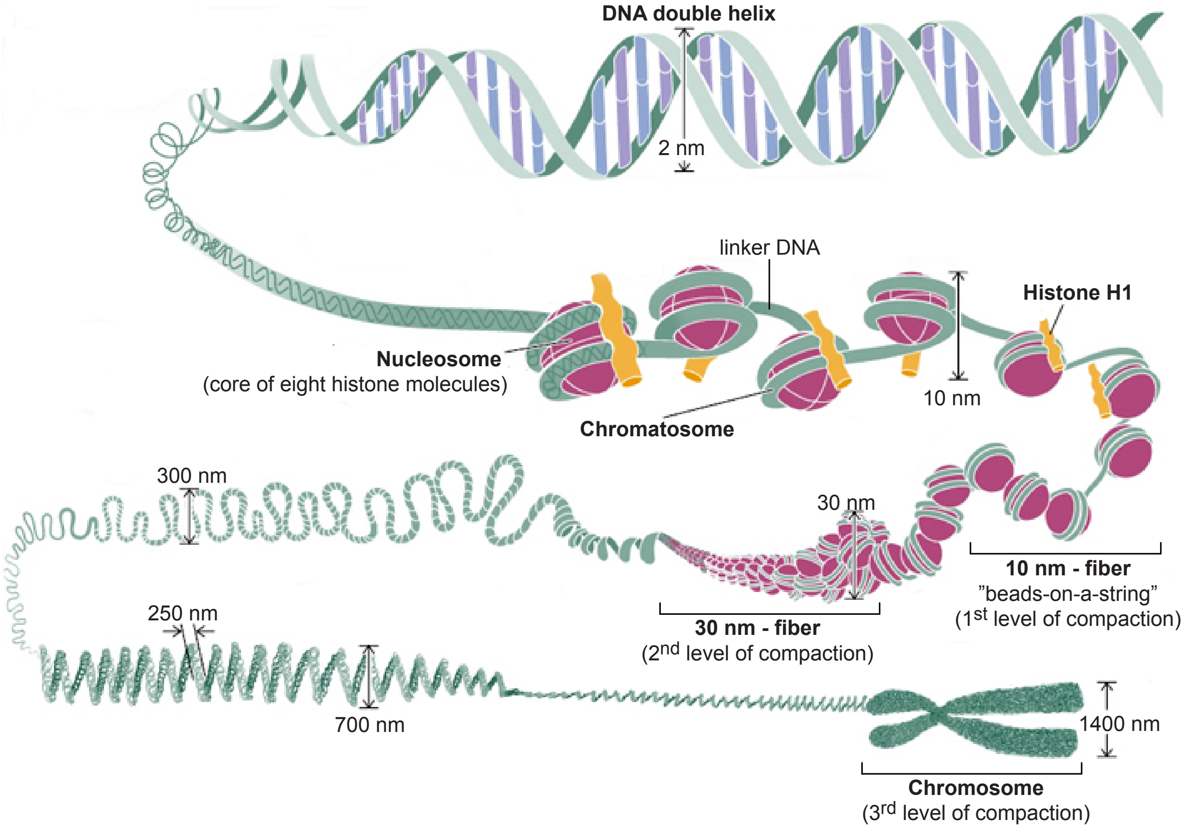
DNA double helix
2 nm
linker DNA
Histone H1
Nucleosome
(core of eight histone molecules)
10 nm
Chromatosome
300 nm
30 nm
10 nm - fiber
"beads-on-a-string"
(1st level of compaction)
250 nm
30 nm - fiber
(2nd level of compaction)
700 nm
1400 nm
Chromosome
(3rd level of compaction)

Figure 1.1: The major structures in DNA compaction
Schematic overview of the highly complex chromatin structure depicting major levels of its compaction (modified from Annunziato, 2008).

The basic unit of chromatin is the nucleosome, which contains 147 bp of DNA wrapped around a histone octamer in 1.67 left-handed superhelical turns (Van Holde, 1988; Luger et al., 1997; Wolffe, 1998). The histone octamer is formed by two of each of the core histone proteins H2A, H2B, H3 and H4 (Thomas and Kornberg, 1975). Nucleosomes are bound by a fifth histone, the linker histone H1, which wraps another 20 bp of DNA around the octamer resulting in two full turns (Wolffe, 1998). In chromatin, nucleosomes are connected by 10 to 80 bp of DNA, which usually is referred to as linker

DNA. A nucleosome with a short stretch of linker DNA bound by H1 is called chromatosome (Brown et al., 2006; Sheng et al., 2006). These chromatosomes form the fundamental repeating entity of chromatin and build a long chain, which gives the appearance of a string of beads called 10 nm fibre (Olins and Olins, 1974; van Holde, 1988). The 10 nm fiber represents the first level of DNA compaction and folds into the second level - the 30 nm fiber, which generates a series of coils and loops that provide successively higher levels of organization. The compaction beyond the 30 nm fiber is so far not well understood. Folding at the tertiary level probably involves additional non-histone nucleosomal binding proteins to finally build the mitotic chromosome with a fiber diameter of 1.4 µm (Tremethick 2007; Woodcock and Gosh, 2010).

Thus, chromatin can be folded into a small volume through a series of higher order structures to chromosomes in nuclei of many higher eucaryotic cells. In general, two types of chromatin exist: highly condensed, transcriptionally silent chromatin known as heterochromatin and more accessible chromatin termed as euchromatin. Euchromatin defines most of interphase chromosomes and probably corresponds to looped domains of 30 nm fibers. It comprises the most active portion of the genome within the cell nucleus. Heterochromatin, in contrast, includes additional proteins and probably represents more compact levels of organization. Heterochromatin that is always silenced is termed as "constitutive heterochromatin" and mainly comprises repetitive genetic elements, such as telomeres and centromeres. "Facultative heterochromatin" is only silenced under specific developmental or environmental signaling cues like in the inactive X chromosome in female mammals and can lose its condensed structure to become transcriptionally active (Oberdoerffer and Sinclair, 2007).

1.1.2 Chromatin Is a Highly Dynamic Structure

For many years biologists thought that chromatin is an inflexible and highly compact structure. Once the nucleosome is formed in a particular position on DNA, it remained fixed in place because of the tight association between the core histones and DNA. Despite of the strong DNA-histone interface and the high degree of DNA compaction into chromatin, its structure must be highly dynamic to allow the DNA to become easily accessible to canonical processes in the cell such as DNA replication, cell cycle progression, coordinated gene expression or DNA repair and recombination events. All these essential processes depend on a dynamic alteration of nucleosome formation. For reversibly changing

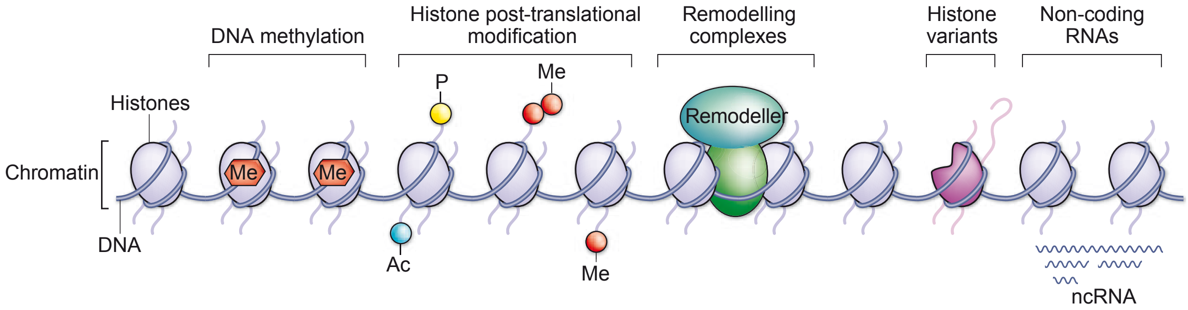

Figure 1.2: Epigenetic mechanisms involved in chromatin modifications
Chromatin is a highly dynamic structure and can be altered by five known mechanisms: DNA methylation, histone modification, chromatin remodeling, insertion of histone variants, and the effects of non-coding RNAs (ncRNAs). Ac, acetyl; Me, methyl; P, phosphate (adapted from Dulac, 2010).

local chromatin structure and altering DNA compaction, several epigenetic mechanisms have evolved: DNA methylation, posttranslational modifications of histones, effects of non-coding RNAs, insertion of histone variants and ATP-driven chromatin remodeling (Figure 1.2). Epigenetic alterations of chromatin are heritable changes in genome function that occur without modifications of the DNA sequence (Probst et al., 2009). Interestingly, the chromatin structure encodes the epigenetic information that governs the expression of the underlying genes (Korber and Becker, 2010). Korber and colleagues speculate that chromatin remodelers for example, may add structural information and confer epigenetic stability to chromatin on several levels. Since this work investigates in an ATP-dependent chromatin remodeler that might be involved in histone exchange, these two principles will be described below in details.

1.1.3 Histone Variants

As described above, the chromatin structure can be modulated by the incorporation of variant histone subspecies, which have evolved particular characteristics that impact on the transcriptional capacity of the nucleosomal regions they inhabit. Histone variants can be enriched in specialized domains of chromatin and differ in their individual amino-acid sequence relative to the major canonical histone (Figure 1.3). The four canonical histones H2A, H2B, H3 and H4 constitute the major part of histone proteins within an organism and are encoded by multiple genes. These genes are found clustered in repeat arrays with a highly conserved sequence similarity and lack introns (March-Diaz and Reyes, 2009; Talbert and Henikoff, 2010). The expression of canonical histones is tightly regulated during cell cycle and strictly coupled to DNA replication, since their genes are expressed mostly during S-phase (Sarma and Reinberg, 2005; March-Diaz and Reyes, 2009). In contrast to the canonical histones, histone variants are often encoded by a single gene that contains introns and which is constitutively expressed throughout the cell cycle. As a consequence, histone variants can be incorporated into nucleosomes during the entire cell cycle (Sarma and Reinberg, 2005). They often work in concert with other remodeling strategies like variant-specific post-translational histone modifications (PTMs) - an enzymatic modification of N-terminal histone tails to ensure the proper functioning of these domains (Fuks, 2005). For example, N-terminal histone tails are subject to several types of covalent modifications, including acetylation, methylation and ubiquitination of lysine residues, methylation of arginine residues or phosphorylation of serine and threonine residues (Figures 1.2 and 1.3) (Bönisch et al., 2008). Histones are known as the slowest evolving proteins and the specializations of their variants have developed to perform additional tasks during their long evolutionary history. Some histone variants are found in nearly all eukaryotes, reflecting conserved common functions in eukaryotic cells, whereas lineage-specific variants are specialized for the unique biology of their host organisms (Talbert and Henikoff, 2010; Wiedemann et al., 2010).

During the last several years, extensive experimental evidence suggests that the functions of canonical histones are primarily in genome packaging and gene regulation, whereas non-canonical variants play an important role in divers processes such as DNA repair, meiotic recombination, transcription initiation and termination or sex chromosome condensation (Talbert and Henikoff, 2010). This functional diversity of histone variants reflects also their differences from canonical histones. The incorporation of histone variants at certain loci or certain regions of the genome leads to structural alterations in the core octamers, which subsequently confers specific functional features to chromatin and alters the nucleosome dynamics (Bernstein and Hake, 2006; March-Diaz and Reyes, 2009; Talbert and Henikoff, 2010). At present, numerous histone variants from the H2A and H3 families and to a lesser extent, the H2B and H4 histone families, have been identified (Figure 1.3). Each histone or histone variant possess the common structure of a histone fold domain (HFD), which consists of three α-helices separated by two loops (van Attikum and Gasser, 2005; Talbert and Henikoff, 2010). The HFDs fold together in antiparallel pairs and build the histone dimers of H3-H4 and H2A-H2B. From this dimeric structure of HFDs, tetramers, hexamers and octamers can be assembled in a stepwise manner (Sarma and Reinberg, 2005; Talbert and Henikoff, 2010).

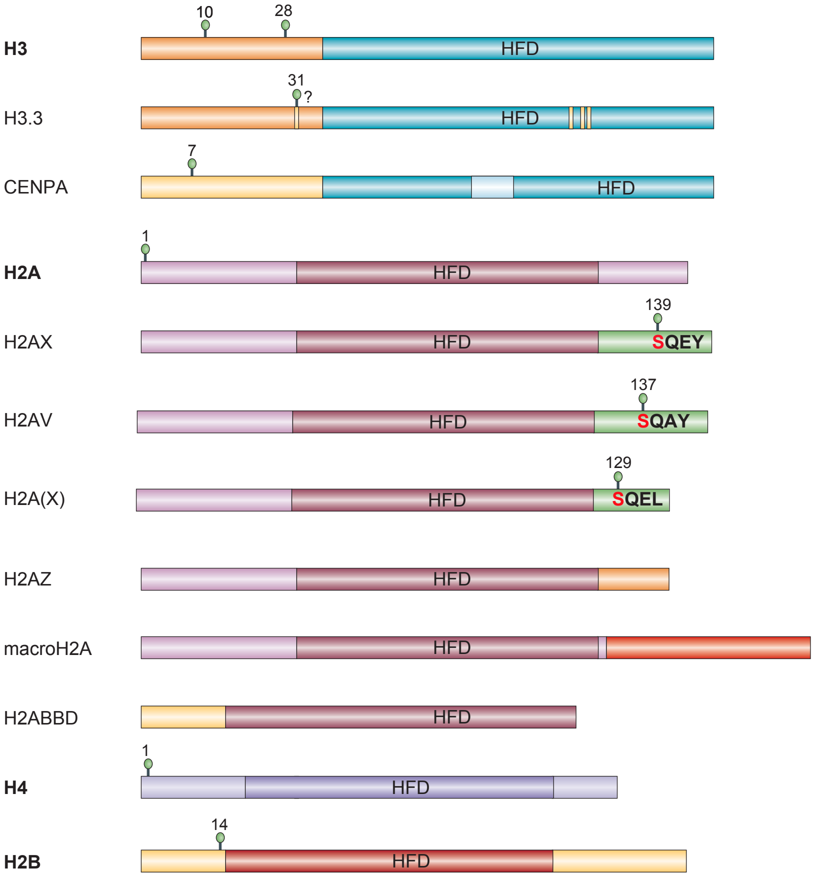

Figure 1.3: Canonical core histones and their major variants
Schematic overview of the four canonical core histones H2A, H2B, H3, H4 and their major variants possessing a histone-fold domain (HFD). Histone variants differ significantly in their primary amino-acid sequence from their canonical paralogues. The most variable core histone is H2A. C-terminal residues of the human H2AX and the fly H2AV are almost identical to those of yeast histone H2A(X) and contain the conserved SQ-motif of which the serine residue is phosphorylated (green circles) in response to DNA damage and DBS repair (adapted from Sarma and Reinberg, 2005).

Among all these histone proteins and their variants, subspecies of the H2A family are more specified in the following, since this study focus on a chromatin remodeler that might be involved in exchange of the histone variant H2AV. The H2A family possesses the most diverse and largest number of variants, including the well characterized H2AZ, H2AX and H2AV, as well as the less described variants macroH2A and H2ABBD. Although all H2A proteins retain a high degree of sequence similarity at the HFD region, they differ significantly throughout their amino-acid sequences, and are much more divergent from their canonical form than other variants (Figure 1.3). MacroH2As are highly conserved H2As that are characterized by an extended C-terminal macro domain (> 200 residues). This histone variant is enriched on the X chromosome of female mammals and is supposed to be involved in

X chromosome inactivation and transcriptional silencing (Sarma and Reinberg, 2005; Talbert and Henikoff, 2010). The smallest of the H2A variants is the mammal-specific H2A Barr body-deficient (H2ABBD) variant, which contains a short C-terminus with a truncation of the HFD region and a distinct N-terminus lacking all of the conserved modification sites that are present in H2A. H2ABBD is found to be associated with active chromatin and might be involved in the formation of accessible chromatin, but no specific function has yet been identified for this interesting variant (Sarma and Reinberg, 2005; Talbert and Henikoff, 2010).

The H2AZ variant has been identified in a wide variety of species, including *Saccharomyces cerevisiae* (H2AZ, also called Htz1), *Drosophila melanogaster* (H2AV) and human (H2AZ) (Figure 1.4). Phylogenetic analysis indicates that H2AZ diverged from the major H2A early in eukaryotic evolution and developed specialized conserved functions, which are distinct from that of the canonical H2A (Figure 1.4.A). Indeed, the H2AZ variant differs from the major H2A at many positions throughout the primary sequence. Only 60% of the amino-acid sequence of the H2AZ variant is identical to the canonical H2A within the same organism, while H2AZ-like variants from different organisms are more homologous across the species and show a high sequence similarity of about 90% to each other (Jin et al., 2005; March-Diaz and Reyes, 2009; Morrison and Shen, 2009). To date, diverse and apparently contradictory roles are known for H2AZ such as gene activation and silencing, nucleosome turnover, DNA repair, heterochromatin and chromatin fiber formation as well as embryonic stem cell differentiation. These conflicting associations of H2AZ with active and silenced chromatin might be partially explained by the variant-specific PTMS like phosphorylation, acetylation and monoubiquitylation that affect most H2A variants (Talbert and Henikoff, 2010).

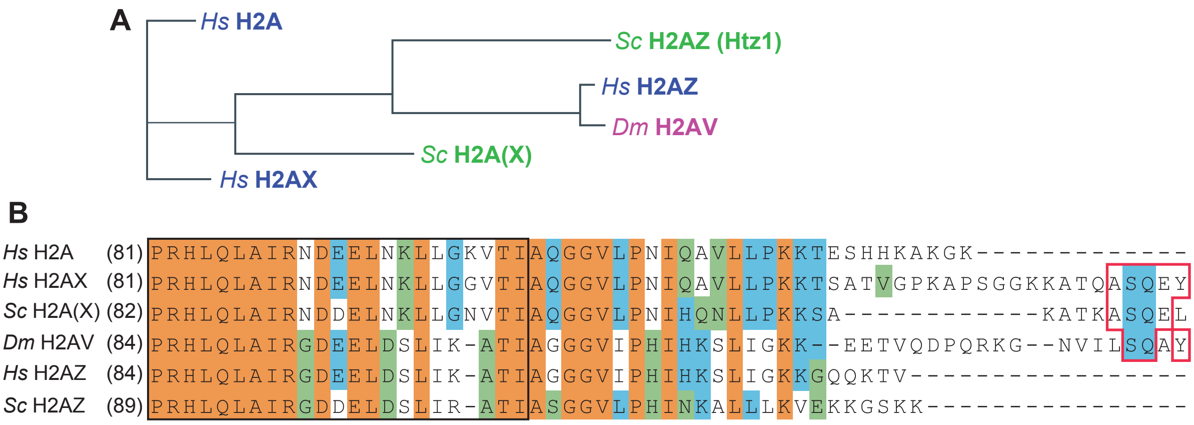
A
Hs H2A
Sc H2AZ (Htz1)
Hs H2AZ
Dm H2AV
Sc H2A(X)
Hs H2AX
B
Hs H2A (81) PRHLQLAIRNDEELNKLLGKVTIAQGGVLPNIQAVLLPKKTESHHKAKGK-------------
Hs H2AX (81) PRHLQLAIRNDEELNKLLGGVTIAQGGVLPNIQAVLLPKKTSATVGPKAPSGGKKATQASQEY
Sc H2A(X) (82) PRHLQLAIRNDDELNKLLGNVTIAQGGVLPNIHQNLLPKKSA------------KATKASQEL
Dm H2AV (84) PRHLQLAIRGDEELDSLIK-ATIAGGGVIPHIHKSLIGKK--EETVQDPQRKG--NVILSQAY
Hs H2AZ (84) PRHLQLAIRGDEELDSLIK-ATIAGGGVIPHIHKSLIGKKGQQKTV-----------------
Sc H2AZ (89) PRHLQLAIRGDDELDSLIR-ATIASGGVLPHINKALLLKVEKKGSKK----------------

Figure 1.4: Major histone variants of the H2A family in different species
(A) Phylogeny of histone H2A variants in *Homo sapiens* (*Hs*, blue), *Saccharomyces cerevisiae* (*Sc*, green) and *Drosophila melanogaster* (*Dm*, purple). **(B)** Amino-acid (aa) sequence alignment (in one letter code) of H2A and H2A variants in different species. Sequence similarity is encoded by background color: identical aa = orange, conserved aa = blue, similar aa = green and unique aa are not shaded. aa in the core histone domains are boxed with a black line and the SQ motif at their C-termini is highlighted in red. The numbers in parentheses indicate the position of aa in the sequence (adapted from Morrison and Shen, 2009).

Compared to H2AZ-like variants, H2AX-like histone variants show a highly conserved sequence similarity in their HFD region with the canonical human H2A and contain a conserved SQ motif (Figures 1.3 and 1.4.B). H2AX is the main form of H2A in *Saccharomyces cerevisiae* and is often contradictory termed as H2A(X), H2A or H2a1 in yeast (van Attikum and Gasser, 2005; Bernstein and Hake, 2006;

Morrison and Shen, 2009). In *Drosophila*, only H2AV is known as variant of the H2A family, which is a chimeric molecule consisting of the H2AZ globular domain and coupled to the C-terminal H2AX tail including the SQ motif (Figures 1.3 and 1.4) (Sarma and Reinberg, 2005; Morrison and Shen, 2009). H2AV of *Drosophila* is an example of a convergent acquisition of the SQ motif and suggests multiple origins of canonical H2A from an ancestral H2AX (Talbert and Henikoff, 2010). H2AV is localized to the centromeric heterochromatin of chromosomes and is required for euchromatic silencing and heterochromatin formation (Swaminathan et al., 2005).

The serine residue of the SQ motif in all H2AX-like histone variants becomes rapidly phosphorylated in response to DNA damage (S129 in yeast H2A(X), S139 in human H2AX and S137 in fly H2AV) (Figures 1.3 and 1.4.B). The resulting phosphorylated forms ɣ-H2AX or ɣ-H2AV, are involved in the recruitment of DNA repair proteins or histone modifying enzymes and promote chromatin remodeling (Sarma and Reinberg, 2005; Bao and Shen, 2007a; Hargreaves and Crabtree, 2011). Especially the latter is described in yeast and also in *Drosophila*. It has been shown that the large chromatin remodeling complex TIP60 of flies catalyzes the exchange of ɣ-H2AV and replaces it with the unmodified H2AV variant in an ATP-dependent manner (*see* Chapter 1.2) (Kusch et al., 2004).

The catalytic subunit of TIP60 is the ATPase Domino - the chromatin remodeler of this study and an ortholog of the yeast SWR1 protein (*see* next chapter). The SWR1 complex in yeast is a member of the ATP-dependent INO80 family of chromatin-remodeling factors. SWR1 exchanges the conventional histone H2A (as the H2A-H2B dimer) with its variant H2AZ (as the H2AZ-H2B dimer) in nucleosome arrays of *Saccharomyces cerevisiae*, which prevents the spreading of heterochromatin regions into regions of euchromatin (Mizuguchi et al., 2004; van Attikum and Gasser, 2005; Hargreaves and Crabtree, 2011). Also in humans, the SRCAP complex appears to be structurally related to the SWR1 and the TIP60 complexes. Recently, SRCAP has been shown to be involved in the incorporation of the H2AZ variant into nucleosomes (Wong et al., 2007).

Taken together, the diverse functions of histone variants and their specific PTMs are just beginning to be uncovered. Especially studies of the molecular machines that catalyze the specific deposition, exchange or replacement of histones and variants provide new insights into gene regulation and expression throughout the cell cycle and during development. The chromatin remodeler Domino is part of this study and involved in histone exchange. The discovery of such chromatin remodeling machines will give us a fuller appreciation of how chromatin dynamics is linked with developmental processes and cell differentiation. A brief overview of ATP-dependent chromatin remodeling factors and their mechanisms is therefore given in the next chapter.

1.2 ATP-Dependent Chromatin Remodeling

Chromatin remodeling is the enzyme-assisted change of the local chromatin state to enable dynamic access to DNA for divers DNA-binding proteins (DBPs). Remodeling enzymes use the energy of ATP hydrolysis to reversibly disrupt the tight ionic association of DNA with histones or histone variants, which in turn may lead to nucleosome repositioning or ejection, localized unwrapping or histone exchange with certain variants including entire dimer eviction (Figure 1.5). Despite the high dynamics of

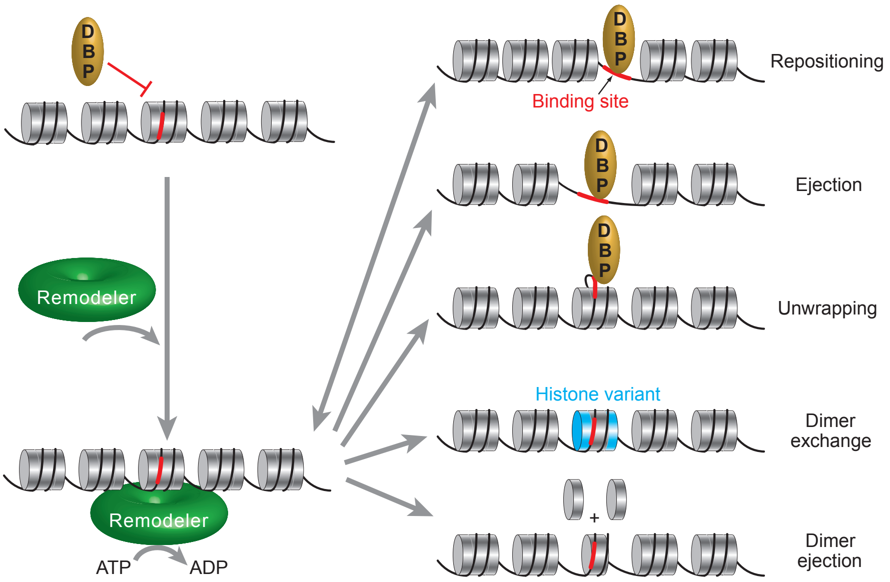

Figure 1.5: Mechanisms of ATP-driven chromatin remodeling
Chromatin remodelers (green) can bind to DNA of nucleosomal arrays and use the energy of ATP-hydrolysis to provide a regulated DNA accessibility to DNA-binding proteins (DBPs) through different strategies: Repositioning of nucleosomes, in which a binding site (red) for DBPs, initially occluded by the histone core, becomes accessible; nucleosomal eviction (ejection); localized unwrapping. They also can eject or exchange histone dimers and replace them with histone variants (blue) (adapted from Clapier and Cairns, 2009).

chromatin achieved by remodelers, nucleosome remodeling is also fundamentally involved in the assembly of stable chromatin structures. They can establish transcriptional active as well as repressive chromatin states (Becker und Hörz, 2002; Korber and Becker, 2010).

1.2.1 Composition and Basic Domains of Different Chromatin Remodeling Families

To date, 24 subfamilies of chromatin remodeling enzymes are known, which are defined by similarity in sequence and domain organization (Flaus et al., 2006). Four of these subfamilies are mainly studied during the past decade: SWI/SNF, ISWI, CHD and INO80 (Bao and Shen, 2011; Kasten et al., 2011; Sims and Wade, 2011; Yadon and Tsukiyama, 2011). All of them contain a similar ATPase subunit of the SWI/SNF type that is defined by a bipartite ATPase domain (Figure 1.6). The linker region between the two parts is distinctively short in remodelers of the SWI/SNF, ISWI, and CHD families, whereas remodelers of the INO80 family contain a three times longer insertion.

Each class is further characterized by a unique domain composition flanking the ATPase region: a Bromodomain and a HSA domain in the SWI/SNF family, a SANT – SLIDE module in the ISWI family, tandem chromodomains in the CHD family, and a HSA domain in the INO80 family (Eberharter and Becker, 2004; Mohrmann and Verrijzer, 2005; Clapier and Cairns, 2009; Hargreaves and Crabtree, 2011). All modifying enzymes share basic properties like direct binding to DNA sequence and to histone octamers or variants and the ability to recognize covalent histone modifications. Furthermore, they contain domains for interaction with associated factors (Clapier and Cairns 2009). Together,

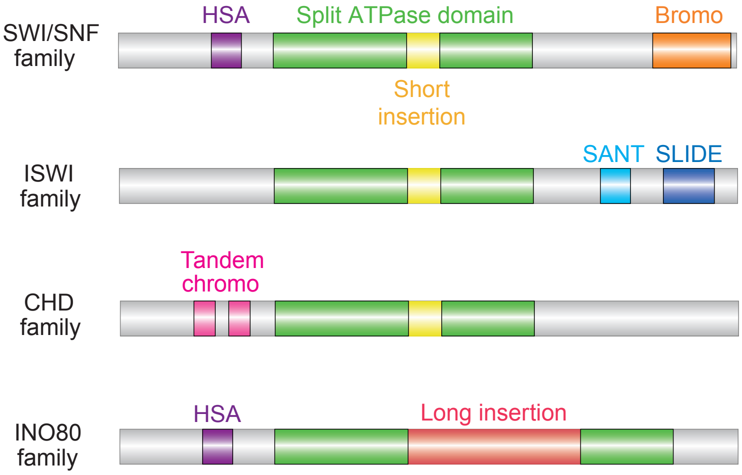

Figure 1.6: Families of ATP-dependent chromatin remodelers and their basic domains
All remodeler families contain an ATPase subunit (green) of the SWI2/SNF2 family that is split in two parts. The short insertion (yellow) between the ATPase domains distinguishes remodelers of the SWI/SNF, ISWI, and CHD families from remodelers of the INO80 family comprising a long insertion (red). Each family is further characterized by individual domains (adapted from Clapier and Cairns, 2009).

these shared properties allow chromatin flexibility and dynamics in order to quickly adapt to regulatory needs. The wide variety of regulatory tasks such as efficient transcriptional regulation, DNA replication and DNA-damage repair, require multiple remodelers with distinct targeting and specialized functions. In the cell, ATP-dependent remodelers work in concert with other factors, most notably histone chaperones and histone modifying enzymes, which are part of larger, multisubunit protein complexes. Simple remodeling machines can comprise just two subunits, complicated remodeling contain more than 15 subunits (Clapier and Cairns, 2009)

1.2.2 Subfamilies of Chromatin Remodelers and Their Known Biological Function

The four subfamilies of chromatin remodelers are classified by their central ATPase subunit that was first identified. They comprise highly conserved key domains from yeast to humans (Table 1.1), which reflects their importance for chromatin regulation and essential mechanisms revolving around DNA metabolism (Eberharter and Becker, 2004; Bao and Shen, 2007; Hargreaves and Crabtree, 2011). An impaired regulation of these processes has been linked to transcriptional deregulation and cancer development. Malfunctions in remodeling factors often lead to severe consequences in developmental or cell growth defects (Wang et al., 2007; Chioda et al., 2010; Keenen et al., 2010; Hargreaves and Crabtree, 2011).

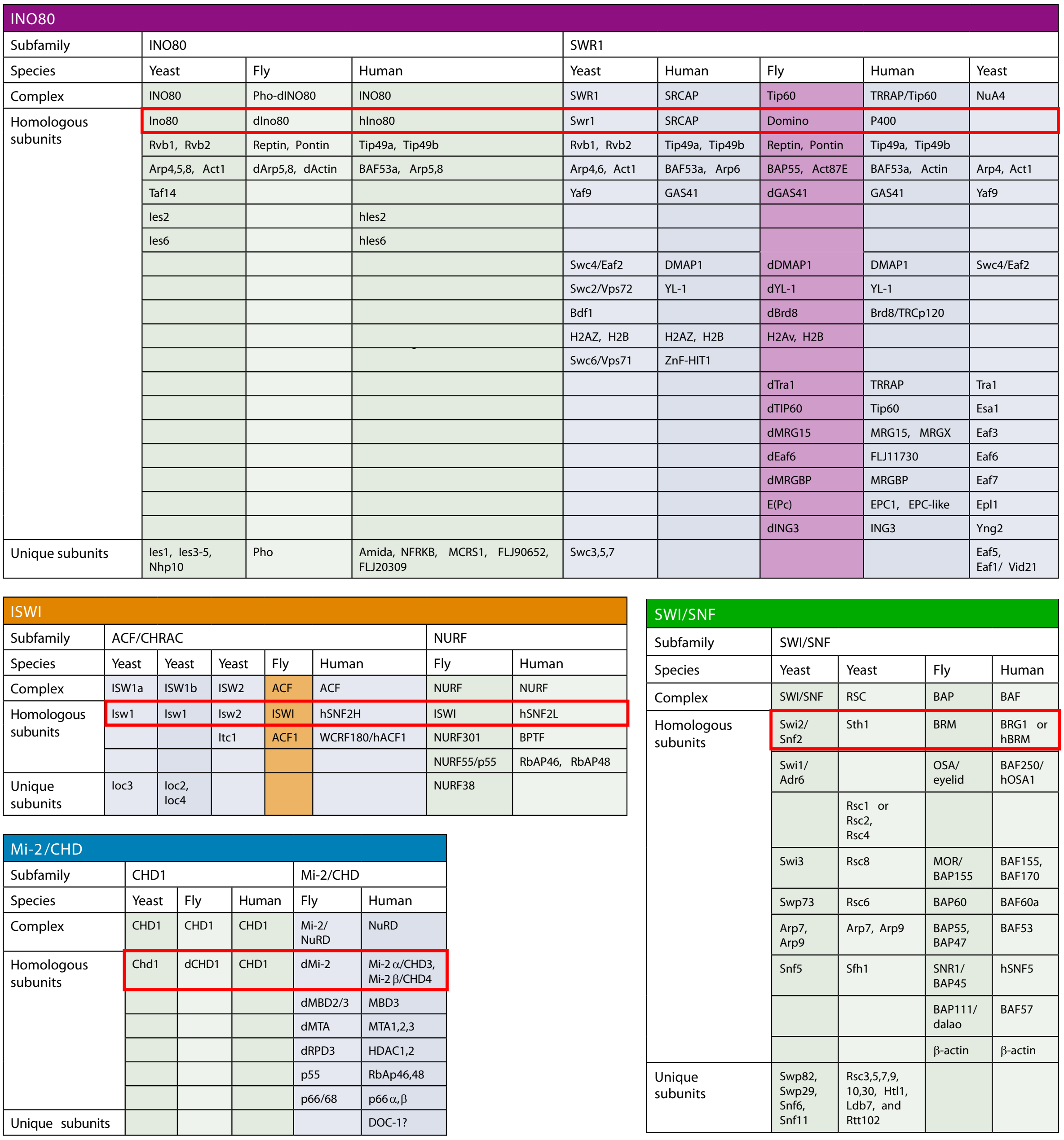

INO80								
Subfamily	INO80			SWR1				
Species	Yeast	Fly	Human	Yeast	Human	Fly	Human	Yeast
Complex	INO80	Pho-dINO80	INO80	SWR1	SRCAP	Tip60	TRRAP/Tip60	NuA4
Homologous subunits	Ino80	dIno80	hIno80	Swr1	SRCAP	Domino	P400	
	Rvb1, Rvb2	Reptin, Pontin	Tip49a, Tip49b	Rvb1, Rvb2	Tip49a, Tip49b	Reptin, Pontin	Tip49a, Tip49b	
	Arp4,5,8, Act1	dArp5,8, dActin	BAF53a, Arp5,8	Arp4,6, Act1	BAF53a, Arp6	BAP55, Act87E	BAF53a, Actin	Arp4, Act1
	Taf14			Yaf9	GAS41	dGAS41	GAS41	Yaf9
	Ies2		hIes2					
	Ies6		hIes6					
				Swc4/Eaf2	DMAP1	dDMAP1	DMAP1	Swc4/Eaf2
				Swc2/Vps72	YL-1	dYL-1	YL-1	
				Bdf1		dBrd8	Brd8/TRCp120	
				H2AZ, H2B	H2AZ, H2B	H2Av, H2B		
				Swc6/Vps71	ZnF-HIT1			
						dTra1	TRRAP	Tra1
						dTIP60	Tip60	Esa1
						dMRG15	MRG15, MRGX	Eaf3
						dEaf6	FLJ11730	Eaf6
						dMRGBP	MRGBP	Eaf7
						E(Pc)	EPC1, EPC-like	Epl1
						dING3	ING3	Yng2
Unique subunits	Ies1, Ies3-5, Nhp10	Pho	Amida, NFRKB, MCRS1, FLJ90652, FLJ20309	Swc3,5,7				Eaf5, Eaf1/ Vid21

ISWI							
Subfamily	ACF/CHRAC					NURF	
Species	Yeast	Yeast	Yeast	Fly	Human	Fly	Human
Complex	ISW1a	ISW1b	ISW2	ACF	ACF	NURF	NURF
Homologous subunits	Isw1	Isw1	Isw2	ISWI	hSNF2H	ISWI	hSNF2L
			Itc1	ACF1	WCRF180/hACF1	NURF301	BPTF
						NURF55/p55	RbAP46, RbAP48
Unique subunits	Ioc3	Ioc2, Ioc4				NURF38	

Mi-2/CHD					
Subfamily	CHD1			Mi-2/CHD	
Species	Yeast	Fly	Human	Fly	Human
Complex	CHD1	CHD1	CHD1	Mi-2/ NuRD	NuRD
Homologous subunits	Chd1	dCHD1	CHD1	dMi-2	Mi-2 α/CHD3, Mi-2 β/CHD4
				dMBD2/3	MBD3
				dMTA	MTA1,2,3
				dRPD3	HDAC1,2
				p55	RbAp46,48
				p66/68	p66 α,β
Unique subunits					DOC-1?

SWI/SNF				
Subfamily	SWI/SNF			
Species	Yeast	Yeast	Fly	Human
Complex	SWI/SNF	RSC	BAP	BAF
Homologous subunits	Swi2/ Snf2	Sth1	BRM	BRG1 or hBRM
	Swi1/ Adr6		OSA/ eyelid	BAF250/ hOSA1
		Rsc1 or Rsc2, Rsc4		
	Swi3	Rsc8	MOR/ BAP155	BAF155, BAF170
	Swp73	Rsc6	BAP60	BAF60a
	Arp7, Arp9	Arp7, Arp9	BAP55, BAP47	BAF53
	Snf5	Sfh1	SNR1/ BAP45	hSNF5
			BAP111/ dalao	BAF57
			β-actin	β-actin
Unique subunits	Swp82, Swp29, Snf6, Snf11	Rsc3,5,7,9, 10,30, Htl1, Ldb7, and Rtt102		

Table 1.1: Subfamilies of main chromatin remodeling complexes and their orthologous subunits
The four chromatin remodeling subfamilies comprise multisubunit complexes, which are evolutionary highly conserved. They are classified according to their ATPase subunits. Red frames mark the core ATPase of each complex. Two important complexes for this study, TIP60 and ACF, are highlighted in purple and orange, respectively (adapted from Bao and Shen, 2007).

1.2.2.1 The SWI/SNF Family

The individual subunits of yeast SWI/SNF were originally identified through screens for mutants that were unable to grow on sucrose because of defective transcription of one gene (sucrose non-fermenting or SNF) and for mutants with faulty mating-type switching (SWI) because of defective transcriptional activation (Peterson and Herskowitz,1992). The screening identified about 11 subunits of the SWI/SNF complex including its ATPase SWI2 or SNF2. This catalytic ATPase comprises an

HSA, a post-HSA, and a C-terminal bromodomain - the distinguishing feature, since this domain is absent in ISWI, CHD/MI-2 and INO80 type ATPases. The bromodomain is involved in recognizing specific acetylated lysines in histone tails and may serve as a protein–protein interaction module (Mohrmann and Verrijzer, 2005; Kasten et al., 2011). It is important to mention that homologous remodeling complexes often share many subunits. For example, in *Drosophila* the homolog of the ATPase SWI2/SNF2 is BRM. BRM resides in two closely related complexes – the BAP complex, which is related to human BAF and yeast SWI/SNF complex and the PBAP complex (not shown) homolog to the yeast RSC complex (Mohrmann and Verrijzer, 2005; Moshkin et al., 2007).

This family has many activities, and it repositions and ejects nucleosomes at many loci for diverse processes like activation but also repression of certain genes as demostrated by studies on SWI/SNF and RSC (Gangaraju and Bartholomew 2007; Clapier and Cairns 2009). Several subunits of this complex either possess intrinsic tumor-suppressor activity or are required for the activity of other tumor-suppressor genes. A homozygous inactivation of *snf5* is embryonic lethal in mice or results in extremely rapid and fully penetrant cancer development. In human, SNF5 is specifically inactivated in malignant rhabdoid tumours, a highly aggressive cancer of early childhood (Roberts and Orkin, 2004).

1.2.2.2 The CHD Family

Remodeling complexes of the CHD subfamily are also involved in the suppression of cellular invasive behavior in multiple cancers. LSD1, for example, a subunit of the most prominent member NuRD, targets the metastasis programs in human breast cancer and inhibits the invasion of cancer cells and cancer metastatic potential (Wang et al., 2009). NURD contains the ATPase Mi-2 and associates with MBD3 and the histone deacetylases HDAC1 and HDAC2. This might target CHD complexes to methylated DNA and couple ATP-dependent remodeling to histone deacetylation, resulting in regulated gene silencing (Clapier and Cairns 2009; Wang et al., 2009).

Originally, CHD was purified from *Xenopus laevis* and subsequently found in yeast and fly. Characteristic features include two tandem chromodomains N-terminal to the ATPase domain (Sims and Wade, 2011). In *Drosophila*, the CHD1 chromatin remodeling factor is required for the deposition of histone variant H3.3 into the male pronucleus during embryogenesis and is important for proper wing development and fertility (Konev et al., 2007; McDaniel et al., 2008). *In vitro* it was demonstrated that CHD1 assembles nucleosome arrays together with the chaperone NAP-1 (Lusser et al., 2005). Lusser and colleges further suggest a role for CHD1 in the assembly of active chromatin and a function of ACF, a remodeling complex of the ISWI subfamily, in the assembly of repressive chromatin state. This reflects the concept of the apparent antagonism between remodelers that organize chromatin and those that disorganize/eject nucleosomes to set up a dynamic flux of assembly and disassembly.

However, certain remodeler families can not only be related to assembly or organization and other families to disorganization and ejection of nucleosomes (Lorch et al., 2006; Clapier and Cairns 2009; Lorch et al., 2010). It is well studied that chromatin remodeling factors within the same class can have opposite effects on transcription even though they share common subunits as known from ISWI-containing complexes.

1.2.2.3 The ISWI Family

Originally, ACF, NURF and CHRAC (Figure 1.7, Table 1.1) were identified in *Drosophila* by fractionation of embryonic extracts (Tsukiyama and Wu, 1995; Ito et al., 1997; Varga-Weisz et al., 1997). All three complexes share the catalytic subunit ISWI, which is evolutionary highly conserved and the homologue to human SNF2h (Yadon and Tsukiyama, 2011). ISWI-type remodelers are characterized by their C-terminal SANT domain adjacent to a SLIDE domain, which together form a nucleosome recognition module (*see* Figure 1.6) (Grüne et al., 2003; Eberharter et al., 2004). The SANT domain binds unmodified histone tails, while the SLIDE domain binds nucleosomal DNA (Yadon and Tsukiyama, 2011). They increase the chromatin dynamics by altering the histone-DNA contacts in an ATP-dependent manner in order to modulate the access of transcription factors, to incorporate core and linker histones into chromatin and to slide nucleosomes on DNA (Längst and Becker, 2001; Corona and Tamkun, 2004; Varga-Weisz, 2010). One remarkable feature of ISWI remodelers is the conversion of an irregular succession of nucleosomes into an array with regular spacing (Becker, 2002; Becker and Hörz, 2002; Varga-Weisz, 2010). For example, the chromatin remodeling complexes ACF and CHRAC optimize chromatin spacing predominantly through nucleosome sliding on DNA to promote heterochromatin assembly and repression of transcription as shown in *Drosophila* (Fyodorov et al., 2004).

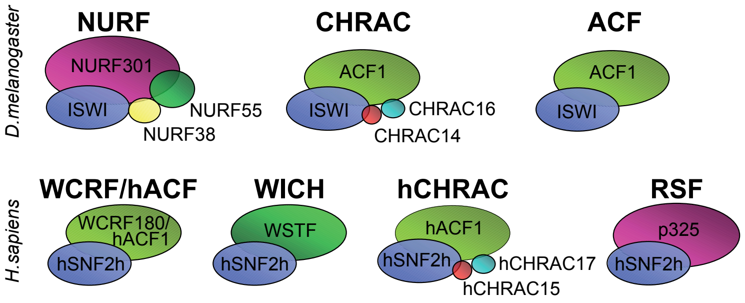

Figure 1.7: Chromatin remodeling complexes of the ISWI family and their homologous subunits
Composition of the *D.melanogaster* NURF, CHRAC and ACF complexes and the human WCRF/hACF, WICH, CHRAC and RSF complexes. Conserved subunits are color coded (*see* also Table 1.1). The catalytic subunit (blue) of all complexes is the ATPase ISWI – the counterpart of human SNF2h. In flies and humans, the remodeling machines CHRAC and ACF share the essential subunit ACF1 (green) that is similar to WSTF in the human WICH complex (adapted from Corona and Tamkun, 2004).

Also *in vitro* ACF promotes the assembly of regular arrays of nucleosomes or chromatosomes and catalyze the movement of nucleosomes and chromatosomes in arrays (Eberharter et al., 2004; Lusser et al., 2005; Maier et al., 2008). In contrast, NURF is able to disrupt regular nucleosomal arrays and has been implicated in transcriptional activation, showing that the diversity can be imparted by subunits and the outcome of the nucleosome mobilization can be different (Längst and Becker, 2004; Fyodorov et al., 2004; Chioda and Becker 2010). ACF and CHRAC differ also from NURF by their large subunit ACF1, which is known to play an essential role during early development of *Drosophila*. A recent study showed that the expression of ACF1 is under developmental control and strongly diminished during *Drosophila* embryonic development (Chioda et al., 2010). Chioda and colleagues detected high levels of ACF1 predominately in undifferentiated cells, including the germ cell precursors and larval neuroblasts (Chioda et al., 2010). They propose that ACF1-containing factors are involved in the initial establishment of diversified chromatin structures, such as heterochromatin, since misexpression of ACF1 compromised fly viability and survivors displayed defects in chromatin assembly and chromatin-mediated gene repression at all developmental stages. Furthermore, by altering the levels of ACF1 in a developmental and tissue-specific manner, they observed global and variegated deviations from normal chromatin organization with pleiotropic defects and perturbed nuclear programs. ISWI or ACF1-containing complexes were also subsequently found in other organisms, including yeast and humans. Another complex of this family is WICH, which consists of two subunits: WSTF, which is related in its subdomain architecture to ACF1 and ISWI as motor protein (Bochar et al., 2000; Guschin et al., 2000; Eberharter et al., 2001). It was shown that WSTF contains a novel tyrosine kinase that phosphorylates Tyr 142 of the histone variant H2AX during DNA damage response in mammalian cells (Xiao et al., 2009). Also the human RSF complex, which also exists in flies, is known to interact with histone variants. A recent study demonstrated that the subunit of the RSF complex Rsf-1, the counterpart of human p325, interacts with histone H2AV (human H2AX) and the H2AV-exchanging machinery TIP60 complex in *Drosophila* (Hanai et al., 2008). Since TIP60 belongs to the INO80 family of chromatin remodelers (*see* next Chapter), an interaction between different chromatin remodelers of different families combining two remodeling principles is conceivable. Hanai and colleagues proposed that the RSF complex plays a role in silent chromatin formation by promoting histone H2AV replacement (Hanai et al., 2008).

1.2.2.4 The INO80 Family

Histone variant replacement or exchange, was originally only observed with yeast SWR1 complexes of the INO80 family (Kobor et al., 2004; Morillo-Huesca et al., 2010). It was shown that SWR1 efficiently replaces the canonical histone H2A with histone H2AZ in an ATP-dependent manner in *S.cerevisiae* (Mizuguchi et al., 2004; Wu et al., 2005). Moreover, INO80 type complexes contribute to a wide variety of chromatin-dependent nuclear transactions, including transcription, DNA repair and DNA replication (Conaway and Conaway, 2008; Bao and Shen, 2011). The INO80 ATPase is a member of the SWI/SNF family but is characterized by a large insertion between the split ATPase domains. INO80 complexes are conserved from yeast to man and share a set of core subunits, which include the INO80 ATPase, two AAA+ ATPases (ATPases associated with variety of cellular activities) referred to as Rvb1 and Rvb2, actin and three actin-related proteins Arp4, Arp5 and Arp8 (Figure 1.8) (Bakshi et al., 2004; van Attikum and Gasser, 2005; Clapier and Cairns, 2009). Many INO80 type complexes are complicated remodeling machines as they often contain more than 10 subunits (Bao and Shen, 2007; Clapier and Cairns, 2009; Bao and Shen, 2011; Hargreaves and Crabtree, 2011). Recent findings have revealed that fly and human INO80 complexes have evolved from the yeast INO80 complex. Although they share a common core of conserved subunits, the complexes have diverged substantially during evolution and have acquired new subunits with apparently species-specific functions (Conaway and Conaway, 2008).

This transition from yeast to vertebrate chromatin-remodeling complexes involved the expansion of several genes encoding the subunits of remodeling complexes and the use of a combinatorial diversity, as proposed for the large TIP60 or the human SCRAP remodeling complex. TIP60 and SCRAP are examples, which have lost, gained and shuffled subunits during evolution from yeast to vertebrates. In particular, TIP60, which exists in man and flies, and the human SCRAP complex are putative hybrids of at least two and possibly all three *S. cerevisiae* complexes INO80, SWR1 and NuA4, since all of them share many subunits (van Attikum and Gasser, 2005; Auger et al., 2008). Accordingly, remodelers of higher organisms like humans and flies (SCRAP and TIP60 with p400/Domino) may be composite HAT remodeler complexes, whereas yeast separate these activities, since the yeast NuA4 complex lacks a remodeler ATPase (Clapier and Cairns, 2009).

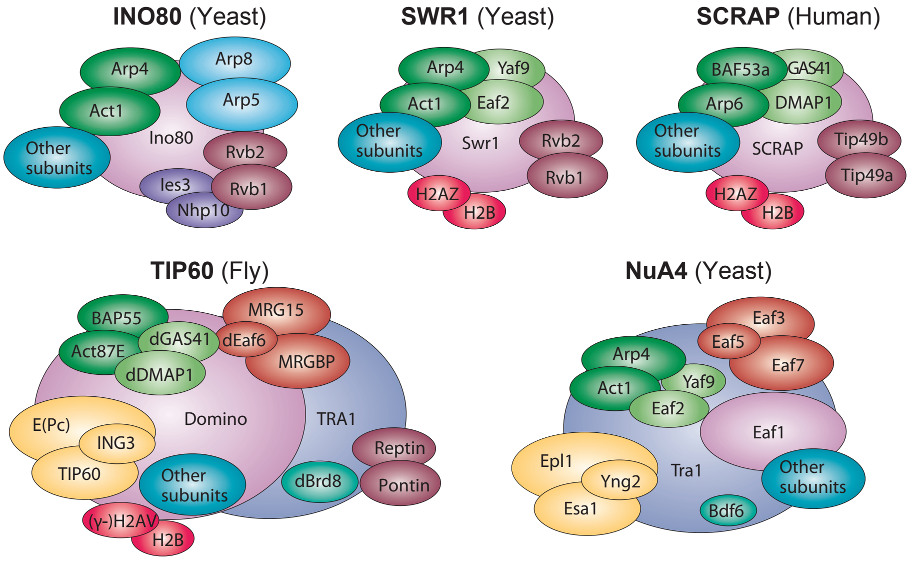
INO80 (Yeast)
Arp4
Arp8
Act1
Arp5
Ino80
Other subunits
Rvb2
Ies3
Rvb1
Nhp10
SWR1 (Yeast)
Arp4
Yaf9
Act1
Eaf2
Other subunits
Swr1
Rvb2
Rvb1
H2AZ
H2B
SCRAP (Human)
BAF53a
GAS41
Arp6
DMAP1
Other subunits
SCRAP
Tip49b
Tip49a
H2AZ
H2B
TIP60 (Fly)
BAP55
MRG15
dGAS41
dEaf6
Act87E
MRGBP
dDMAP1
E(Pc)
Domino
TRA1
ING3
Reptin
TIP60
Other subunits
dBrd8
Pontin
(γ-)H2AV
H2B
NuA4 (Yeast)
Eaf3
Eaf5
Arp4
Eaf7
Yaf9
Act1
Eaf2
Eaf1
Epl1
Yng2
Tra1
Other subunits
Esa1
Bdf6

Figure 1.8: Major chromatin remodeling complexes of the INO80 family and their homologous subunits
Composition of the *S.cerevisiae* SWR1, INO80, NuA4 complexes, the human SCRAP and the *D. melanogaster* TIP60 complex. Conserved subunits are color coded (*see* also Table 1.1). The catalytic subunit (purple) of all complexes, except NuA4, is related to the SWI2/SNF2 type ATPase but contains a large insertion between the split ATPase domains. The catalytic subunit of NuA4 is the histone acetyltransferase Esa1, which has its counterpart in TIP60 of the TIP60 complex. The NuA4 subunit Eaf1 has homology with the SWR1 and Domino/p400 ATPase subunits. Because the yeast NuA4, SWR1 and INO80 complexes share many subunits with TIP60 and SCRAP complexes of flies and humans, it is proposed that TIP60 and SCRAP are hybrids of at least two and possibly all three *S. cerevisiae* complexes (adapted from van Attikum and Gasser, 2005).

The large TIP60 complex exists in a stable nuclear multiprotein complex of approximately 18 subunits. However, depending on the cellular process in which TIP60 participates, it can also form distinct transient complexes with appropriate binding partners (Sapountzi et al., 2006). In humans, the TIP60 complex performs most transcriptional and DNA damage-related functions. The acetyltransferase TIP60 of the TIP60 complex has divergent functions and plays a role in many processes such as cellular signaling, DNA damage repair, cell cycle and checkpoint control or apoptosis (Sapountzi et al., 2006). Another essential component of the human TIP60 complex is the subunit p400/Domino, an ATPase that has chromatin remodeling and histone exchange activity (Ikura et al., 2000; Sapountzi et al., 2006). In flies, the homologue catalytic subunit of the human p400/Domino protein is termed Domino, which is the homologous subunit to the yeast SWR1 and the human SCRAP.

In summary, many of the INO80 remodeling complexes are involved in histone replacement and exchange (*see* also Chapter 1.1.3). Surprisingly, even though the TIP60 complex and its emergence is well characterized in human and flies, little is known about its motor protein Domino except for its exchange function as TIP60 subunit. Therefore, one aspect of this study was the analysis of the ATP-dependent chromatin remodeling enzyme Domino with focus on the isoform Domino B, since distinct biological functions and putative interaction partners of Domino remain to be elucidated. More details about Domino will be given in the following chapter.

1.3 The Chromatin Remodeler Domino

1.3.1 The Structure of Domino

The *domino* gene was isolated in a screen for mutations that cause hematopoietic disorders in *Drosophila melanogaster* (Braun et al., 1997). Braun and colleagues used a screen of *P-lacZ* enhancer trap lines to identify fly lines with transgene expression in larval hemocytes at the end of the 3rd instar larval stage. One mutation with a very striking lymph gland phenotype that results in mutant larvae with two black dots, they named Domino (Braun et al., 1997). *domino* generates two forms of transcripts by alternative splicing: *domino A* is encoded by 14 exons and *domino B* by 11 exons (Ruhf et al., 2001). The splicing products encode two isoforms of the Domino (DOM) protein - Domino A (DOM-A) composed of 3202 amino acids (aa) and Domino B (DOM-B) of 2498 aa. Both proteins share a common N-terminal region and are distinguishable by their divergent C-termini (Figure 1.9). The N-terminal common region contains a Proline (P) -rich (9%) domain and an acidic domain (42% Glutamic acid (E) and Aspartic acid (D)) with several putative PEST sequences. Both isoforms are characterized by a 500 aa ATPase domain, which is separated by a long insertion of 451 aa (Ruhf et al., 2001). There is no significant similarity to known proteins except the SWR1 class ATPase subunit (Ruhf et al., 2001; Mizuguchi et al., 2004; Ueda et al., 2007).

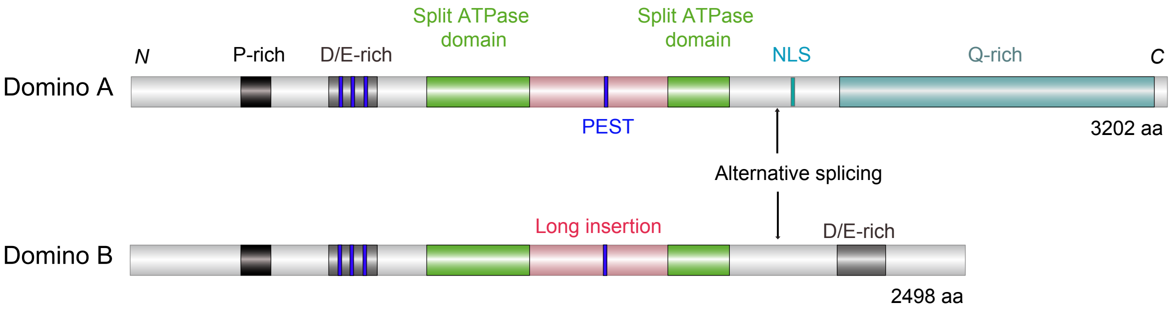

Figure 1.9: The two isoforms of Domino and their domains
The schematic overview depicts the two isoforms of Domino: Domino A (DOM-A, 3202 aa) and Domino B (DOM-B, 2498 aa). The common N-terminal region contains a P-rich domain, an acidic region (D/E-rich) and the bipartite ATPase domain. In the divergent C-terminal regions, only DOM-A bears a nuclear localization signal (NLS) and a large domain with poly-Q repeats, whereas DOM-B exhibits an additional acidic region. Blue stripes show the localization of PEST sequences (adapted from Ruhf et al., 2001).

The C-terminal divergent part of DOM-A bears a bipartite nuclear localization signal and a long domain with numerous poly - Glutamine (Q) repeats. The C-terminal domain of DOM-B, however, contains an additional acidic domain (43% Glutamic acid and Aspartic acid) (Ruhf et al., 2001).

1.3.2 The Functions of Domino A and Domino B Are Just Beginning to Be Uncovered

In comparison to the human and fly ACF/CHRAC or the yeast SWR1/INO80 remodeling complexes, which were analyzed over the last couple of years, functions and characteristics of DOM proteins are just beginning to be uncovered. Also differences between DOM-A and DOM-B await further specification. Initially, mutations of *domino* have been found to cause hematopoietic disorders in *Drosophila* *melanogaster* (Braun et al., 1997). Not only in flies, also in mice the homolog p400/mDomino plays a critical role in embryonic hematopoiesis by regulating the expression of essential genes (Ueda et al., 2007). A recent study showed that a knock-out of p400/mDomino in mice resulted in an acute loss of hematopoietic progenitor cells (Fujii et al., 2010). Fujii and colleagues monitored by p400/mDomino deletion a drastic reduction of nucleated cells in the bone marrow, including committed myeloid and erythroid cells as well as stem cells. Moreover, they exhibited in the cell-cycle progression of mouse embryonic fibroblasts a pleiotropic cell cycle defect between S and G2/M phases, and a strong growth of cells in concert with polyploid and multinucleated cells (Fujii et al., 2010). These results indicate that in mice mDomino plays not only a key role in embryonic hematopoiesis, it is also involved in cellular proliferation and in cell-cycle progression. Ruhf and colleagues studied *domino* by imprecise P-element excision and analysis of resulting loss-of-function alleles. They monitored phenotypes that are typical for proliferation gene mutations indicating that DOM is necessary for cell viability and proliferation, as well as for the oogenesis in flies (Ruhf et al., 2001). The necessity of DOM proteins for fly viability, proper development, and hematopoiesis was monitored by the latest study, where deletions of *Drosophila* ELP3 - a subunit of the fly Elongator complex containing a histone acetyltransferase domain - resulted in a functional overlap of ELP3 with DOM and a compelling similarity in overall effects on gene expression (Walker et al., 2011). Walker and colleagues speculate that similar phenotypes of DOM and ELP3 deletions, such as delayed growth, poor disc formation, pupal lethality and melanotic nodule formation, arise from coordinate regulation of similar sets of target genes and imply functional collaboration between DOM-mediated chromatin remodeling (Walker et al., 2011). All analyses indicate that DOM is involved in several essential processes at certain developmental stages of *Drosophila*.

The expression of DOM proteins during *Drosophila* development was first determined by Ruhf and colleagues (Ruhf et al., 2001). They could localize by immunofluorescence staining with α-DOM-A and α-DOM-B antisera both proteins in embryos; DOM-B is expressed ubiquitously in all nuclei of early embryos, while DOM-A is not expressed until embryonic stage 10, which suggests a specialized function of DOM-B during early *Drosophila* development. At larval stages, DOM-B was enriched in brain cells, in all cells of the imaginal discs, in lymph glands and in salivary glands, whereas the expression of DOM-A was found to be restricted to some brain regions and to the photoreceptor precursor cells posterior to the morphogenetic furrow in the imaginal eye disc (*see* Chapter 1.4). In adult flies, only DOM-B was found strongly expressed in follicle cells, nurse cells and the oocyte of the female ovary. In contrast, DOM-A protein was not monitored in the ovary even though the transcript was there (Ruhf et al., 2001). The fact that especially DOM-B is expressed in all embryonic nuclei, in most nuclei of larval tissues during morphogenesis and in stem cells of adult ovaries supports the notion that DOM-B is a factor that fulfils essential functions during oogenesis and early development. A recent study confirmed the presence of DOM-B in adult ovaries and detected DOM-B protein with higher amounts in germ stem cells (GSCs) and in somatic stem cells (SSC) than in other cells of the germarium by immunofluorescence analysis of ovaries (*see* Chapter 1.4.4) (Xi and Xie, 2005). Xi and colleagues linked the function of DOM-B to somatic stem cell (SSC) self-renewal, while ISWI is important for the GSCs maintenance (Xi and Xie, 2005).

However, functional mechanisms for DOM-B are not well understood and remain to be elucidated. DOM-B was found on a large number of euchromatic sites on polytene chromosomes of larval salivary glands (Ruhf et al., 2001). The functional overlap and the remarkable similarity between Elp3 and DOM indicates a further contribution of DOM to transcriptional regulation, as Elp3 is known to associate with active genes and participates in RNA polymerase II transcript elongation (Walker et al., 2011). Hitherto, the notion that DOM-B participates in chromatin remodeling is based on several studies and Domino`s similarity to known SWI2/SNF2 proteins for which interactions with chromatin and remodeling have been biochemical established (Ruhf et al., 2001). Initially, DOM proteins could be purified and isolated by Ruhf and colleagues from nuclei extracts of 0-12 h AED embryos. The native molecular weight (MW) of DOM-A and DOM-B was examined using gel filtration chromatography. Both proteins appeared as more than 2 MDa, which led to the hypothesis that both proteins are incorporated into large complexes (Ruhf et al., 2001). Indeed, the isoform DOM-A was found as a part of the large TIP60 complex in *Drosophila* S2 cells (*see* Table 1.1 and Figure 1.8) (Kusch et al.; 2004). Kusch and colleagues showed that the histone acetyltransferase dTIP60 of the TIP60 complex acetylates nucleosomal phosphorylated H2AV, which is subsequently exchanged by the ATPase subunit DOM-A with the unmodified H2AV variant (Kusch et al.; 2004). Another recent study identified the human Domino/p400 ATPase as a novel DNA damage response protein in mammalian cells, which may regulate together with the TIP60 acetyltransferase apoptotic responses to DNA damage (Xu et al., 2010). Xu and colleagues demonstrated that both, hDomino/p400 and hTIP60, promote chromatin ubiquitination at sites of DNA damage and mediate the alteration of nucleosome and chromatin structures during DSB repair (Xu et al., 2010).

So far, mechanisms and functions of DOM were predominately studied *in vitro* using *Drosophila* embryonic or mammalian cells that do not recapitulate the three-dimensional complexity of chromatin structure *in vivo*, such as its organization into heterochromatin and euchromatin or its dynamics. It is clear that further *in vitro* assays as well as *in vivo* analyses are needed to tease apart biological functions of DOM. Therefore, DOM was studied *in vitro* as well as *in vivo* using *Drosophila melanogaster* as a model organism. For a better understanding the development of *Drosophila* with respect to the used organs and tissues are described in the following chapter.

1.4 *Drosophila melanogaster* – a Model Organism to Study Chromatin Remodeling during Development

The fruit fly *Drosophila melanogaster* has a pre-eminent place in biological research, particularly in genetics and developmental biology, as it is most widely used and genetically best-known of all eukaryotic organisms. The developmental processes in flies provide a unique opportunity to study common regulatory principles and essential functions of genes and proteins. The key molecular pathways required for the development of a complex animal, such as patterning of the primary body axes, organogenesis or control of cell proliferation and differentiation processes have been highly conserved since the evolutionary divergence of flies and humans (Reiter et al., 2001). Therefore, studies in *Drosophila* provide deeper insights into these key mechanisms in other eukaryotes, including humans. Over the last years, *Drosophila* is being used as a genetic model for several human diseases and developmental defects, including the neurodegenerative disorders Parkinson’s or Alzheimer’s disease, and to study mechanisms underlying cell proliferation and death to achieve normal tissue size, as well as oncogenesis and tumor formation (Potter et al., 2000; Reiter et al., 2001; Vidal and Cagan, 2006). As described above, perturbed cell growth or cancer development are often caused by malfunctions in remodeling factors (Chapter 1.2.2). When these pathways are disrupted in either flies or mammals, similar defects are often observed. Recently, chromatin-remodeling enzymes appeared to have instructive and programmatic roles during development (Ho and Crabtree, 2010), which also will be delineated in the following chapters. Furthermore, the different developmental stages of *Drosophila* provide an ideal system to analyze chromatin-related processes in a tissue- and developmental-specific manner, as each developmental stage offers its own experimental system with diverse techniques and approaches. In the next sections the main developmental stages of *Drosophila* used during this study will be introduced.

1.4.1 The Life Cycle of *Drosophila Melanogaster*

Drosophila melanogaster belongs to ectothermic animals whose developmental period varies with temperature. Under ideal conditions at 25°C, the development time (egg to adult) of wildtype flies is about 9 days (Figure 1.10).

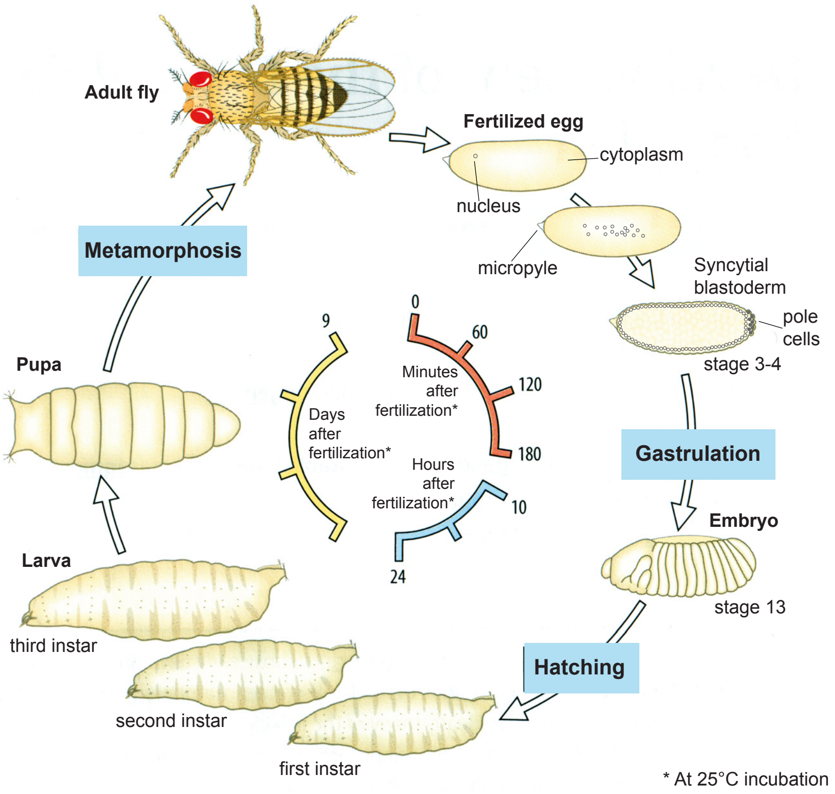
Adult fly
Fertilized egg
cytoplasm
nucleus
micropyle
Syncytial blastoderm
pole cells
stage 3-4
Gastrulation
Embryo
stage 13
Hatching
first instar
second instar
third instar
Larva
Pupa
Metamorphosis
0
60
120
180
Minutes after fertilization*
10
24
Hours after fertilization*
9
Days after fertilization*

* At 25°C incubation

Figure 1.10: The life cycle of *Drosophila melanogaster*
The major stages of the *Drosophila* life cycle are depicted: embryonic phases, three larval periods (termed instars), a pupal stage and finally adulthood. At 25°C, the development time (egg to adult) of wild type flies takes approximately 9 days after hatching (adapted from Wolpert et al., 2007).

The shortest development time, 7 days, is achieved at 28°C while the required time span increases with lower temperatures (e.g. at 18°C it takes 19 days) (Sullivan et al., 2000). After fertilization, female flies lay embryos that undergo cleavage and gastrulation and hatch after 24 h (at 25°C) as feeding larvae. During this stage, the larva grows for about 4 days and goes through two molts (2nd and 3rd instar), at about 24 h and 48 h after hatching. Then, the larva encapsulates in the puparium for four days during which metamorphosis occurs.

1.4.2 Embryogenesis

Embryogenesis in *Drosophila* has been extensively studied. A network of genes governs the early development of the fruit fly embryo and is one of the best understood gene networks to date. Furthermore, embryos can be easily collected in large quantities, which make them ideal for biological research.

Female virgins become receptive to courting males at about 8–12 hours after emergence and can lay up to 100 eggs per day. Already during the egg formation (oogenesis) in the ovaries of female flies (*see* Chapter 1.4.4), the building-blocks of the anterior-posterior (A/P) and the dorsal-ventral (D/V) axis patterning are laid out before the egg is fertilized and deposited. This polarization is due to differentially localized mRNA molecules, encoded by the 50 so called "maternal effect genes", as they are synthesized and expressed by the mother fly and not by the embryo (Johnston and Nüsslein-Vollhardt, 1992; Lasko, 2011). Upon fertilization, these genes encode proteins that get translated to establish concentration gradients that span the egg. For example, important genes responsible for this maternal contribution are *bicoid* and *hunchback*, which are required for the formation of the head and the thorax, or *nanos* and *caudal,* which are essential in the formation of more posterior abdominal segments. "Maternal gene" products provide positional information, which activates the zygotic gene expression required for the determination of cell fate in an embryo. In contrast to "maternal genes", "zygotic genes" are expressed in the nuclei of the embryo itself (Johnston and Nüsslein-Vollhardt, 1992; Janody et al., 2000; Lasko, 2011). Also maternal chromatin remodeling proteins like BAP of the SWI/SNF family are required for the early stages of specifying segmental identity in *Drosophila*. It was shown that a depletion of the subunit BRM or other components of the BAP complex from the zygote leads to multiple defects in organ and gamete formation and to embryonic lethality at late stages of development (Brown et al., 2007; Ho and Crabtree, 2010)

The anterior end of an egg is marked by the "micropyle" in the external coat, through which the sperm can enter (Figure 1.10). After the fusion of sperm and egg nuclei, the zygote nucleus undergoes 13 rapid mitotic divisions without cell division, until approximately 6000 nuclei accumulate in the unseparated cytoplasm creating a multinucleate syncytium (Foe and Alberts, 1983; Frescas et al., 2006). This makes early embryos of *Drosophila* so special, as the cleavage occurs in a syncytium, where even large molecules such as proteins can diffuse between nuclei during the first 3 h of embryogenesis. During cleavage, the chromatin in nuclei of embryos is largely decondensed and in a highly plastic state. There, the transition of chromatin into somatic and germline chromatin occurs (Rudolph et al., 2007). This involves a step-wise implementation of chromatin structures from a hyperdynamic to a fully structured state through epigenetic mechanisms like histone modifications or chromatin remodeling (Meshorer and Misteli, 2006; Rudolph et al., 2007; Chioda et al., 2010). Thus, *Drosophila* early embryos have become valuable systems for the detailed study of translational control, cell intercalation mechanisms, protein expression patterns and chromatin structure.

By the end of the 8th division (approximately 2 h after fertilization) most nuclei migrate to the periphery to form a monolayer - the syncytial blastoderm (Figure 1.10 and 1.11). At the apical pole of early blastoderm nuclei heterochromatin becomes visible (Rudolph et al., 2007). Preblastoderm embryos are known to contain high amounts of nucleosome remodeling factors, especially those of the ISWI type like CHRAC or ACF (Varga-Weisz et al., 1997; Ito et al., 1999; Corona and Tamkun, 2004; Chioda et al., 2010). Chromatin remodelers and associated factors play global roles in chromatin assembly and nucleosome dynamics as shown for the remodeling subunit ACF1. The expression of ACF1 is strongly diminished during embryonic development and persists at high levels only in undifferentiated cells (Chioda et al., 2010). Chioda and colleagues showed that ACF1 is involved in the initial establishment of diversified chromatin structures, such as heterochromatin. Unbalancing the expression of ACF1 perturbs chromatin organization, which results in faulty proliferation and differentiation decisions (Chioda et al., 2010). During the formation of the syncytial blastoderm also the A/P and D/V axes become fully established by the “maternal effect genes” and future segmented regions are already determined (Figure 1.11).

Figure 1.11: The three major stages during *Drosophila* embryogenesis
Schematic side view drawings of *Drosophila* embryos. At 2 h AED the syncytial blastoderm is established in an embryo. A fate map depicts future segmented regions (color coded according to the predicted structures in adult flies). Between 5-8 h the embryo is at the “extended germ band stage” involving the gastrulation, where segmentation already starts. After 10 h the germ-band contracts and the segmentation divides the embryo into 14 parasegments, which are clearly defined (adapted from Alberts et al., 2002).

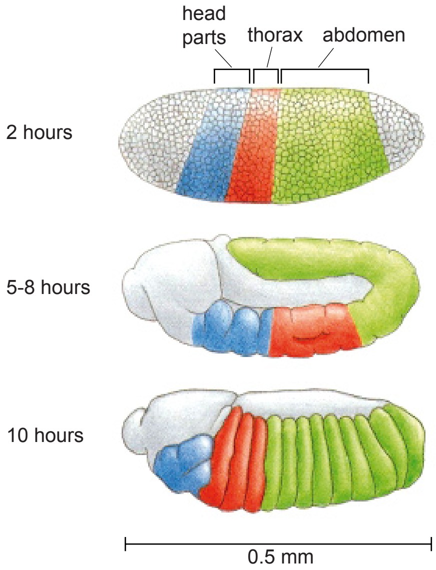

A few nuclei do not transform into blastodermal cells and move towards the posterior end of the embryo after the 10th division. They develop into the “pole cells”, which are the germ-line precursors that will give rise to eggs or sperm during further development (*see* Chapter 1.4.4) (Foe and Alberts, 1983; Johnston and Nüsslein-Vollhardt, 1992). Early embryos that are not older than stage 2 are used for P-element-mediated germline transformation to generate transgenic fly lines. At this stage, a transgene can be integrated into the genome of embryonic pole cells (*see* Chapter 2.6.2).

Finally, after the 13th division, cell membranes invaginate at the periphery to enclose each nucleus. Thereby, the “syncytial blastoderm” converts into a “cellular blastoderm” with individual somatic cells (approximately 3 h after fertilization) (Foe and Alberts, 1983). Before this cellularization is fully completed, gastrulation starts with the ventral invagination of the prospective mesoderm forming a furrow. Gastrulation starts about 3 h after fertilization and segregates the presumptive mesoderm, endoderm, and ectoderm (Foe and Alberts, 1983; Johnston and Nüsslein-Vollhardt, 1992). The furrow becomes a ventral tube within the embryo and forms a layer of mesodermal tissue beneath the ventral ectoderm. At the same time, the prospective endoderm invaginates as two pockets at the anterior and posterior ends of the ventral furrow. Along with the endoderm the pole cells are internalized. Between 5-8 h, the embryo is at the “extended germ band stage” (Figure 1.11): Ectodermal cells on the surface and the mesoderm undergo convergence and extension to form the germ band. This band extends posteriorly and wraps around the dorsal surface of the embryo (Johnston and Nüsslein-Vollhardt, 1992; Keller, 2006). Recent studies have shown that the *Drosophila* germ-band extension depends on cell shape change in addition to cell intercalation in the embryonic tissues. While cell intercalation requires A/P patterning, cell shape change is under the control of D/V patterning and a passive response to mechanical forces caused by the invaginating mesoderm (Butler et al., 2009). The establishment of polarized cell intercalation and cell shape changes during germ-band elongation depends on zygotic factors such as the pair-rule gene *even-skipped* or gap genes like *krüppel* and *knirps* along the A/P or *twist* and *snail* defining the mesoderm along the D/V axis (Johnston and Nüsslein-Vollhardt, 1992; Butler et al., 2009).

At the time of the germ band extension the body segments begin to appear and demarcate the parasegments, which become clearly defined after 10 h. During segmentation, the germ-band retracts and 14 parasegments are formed out of register: 3 for the mouthparts of the head (blue), 3 for the thoracic region (red) and 8 for the abdomen (green) (Figure 1.11). Later on, the parasegments give rise to the segments of the larva and the adult fly (Martinez-Arias and Lawrence, 1985). The segmentation of *Drosophila* embryos depends on the establishment of complex spatiotemporal gene expression patterns, like the so called "segmentation gene network". This network consists of maternal and zygotic factors such as "pair-rule genes" (e.g. *fushi tarazu, even-skipped*) or "segmentation genes" (e.g. *engrailed, hedgehog*) that act in a hierarchical fashion to generate increasingly refined and complex expression patterns along the A/P axis in the blastoderm embryo (Martinez-Arias and Lawrence, 1985; Johnston and Nüsslein-Vollhardt, 1992; Schroeder et al., 2004). Also other key morphogenetic processes occur at this stage, like organogenesis and the segregation of imaginal discs precursors. Finally, the embryo hatches from the surrounding cuticle of the egg shell to become a 1st instar larvae.

1.4.3 Morphogenesis and Eye Development

After the embryonic phase, the *Drosophila* larva grows for about 4 days (at 25°C) while molting twice into 2nd and 3rd instar. During this time, they feed on the microorganisms that decompose the fruit, as well as on the sugar of the fruit itself or the food within the culture bottle. The anterior region of the head is marked by a specialized structure called acron, while the posterior end is marked by a structure termed telson. Between head and telson, 12 segments (thoracic and abdominal) divide the cuticle, which were set aside as 14 parasegments during the segmentation of the embryo. The 14 parasegments have been converted into 12 larval segments, which are separated by bristles and denticles on the cuticle. A characteristic structure protruding outwards of the anterior segment is referred to as spiracles, which starts to develop after the first molt and allows to discern 1st instar larvae from older larvae. 3rd instar larvae are also called "wandering larvae" as they leave the food and usually crawl up to a side of the culture bottle to encapsulate in the puparium and to undergo metamorphosis. This behavior makes wandering larvae so useful for biological research, as they can be easily collected at the same developmental stage.

Drosophila larvae harbor small sheets of prospective epidermal cells derived from the cellular blastoderm that grow throughout the entire larval life and form sacs of single epithelia. These pouches contain usually a cluster of 23 to 40 undifferentiated cells, set aside during embryonic development. These structures are called imaginal discs and give rise to adult organs during morphogenesis. Different imaginal discs have their particular size and shape and are named after the corresponding external appendages they form: six leg, two wing, two haltere, two eye and antenna discs, the genitalia discs, a pair of salivary glands and other adult head structures can be distinguished (Figure 1.12). Already during larval stages imaginal discs undergo complex events in terms of cell signalling and gene function, such as patterning and differentiation, before they go through a complete metamorphosis at the pupal stage in which nearly all larval structures desintegrate and are replaced by the structures of the adult fly (Morata, 2001; Atkins and Mardon, 2009). During the last 20 years, researchers have

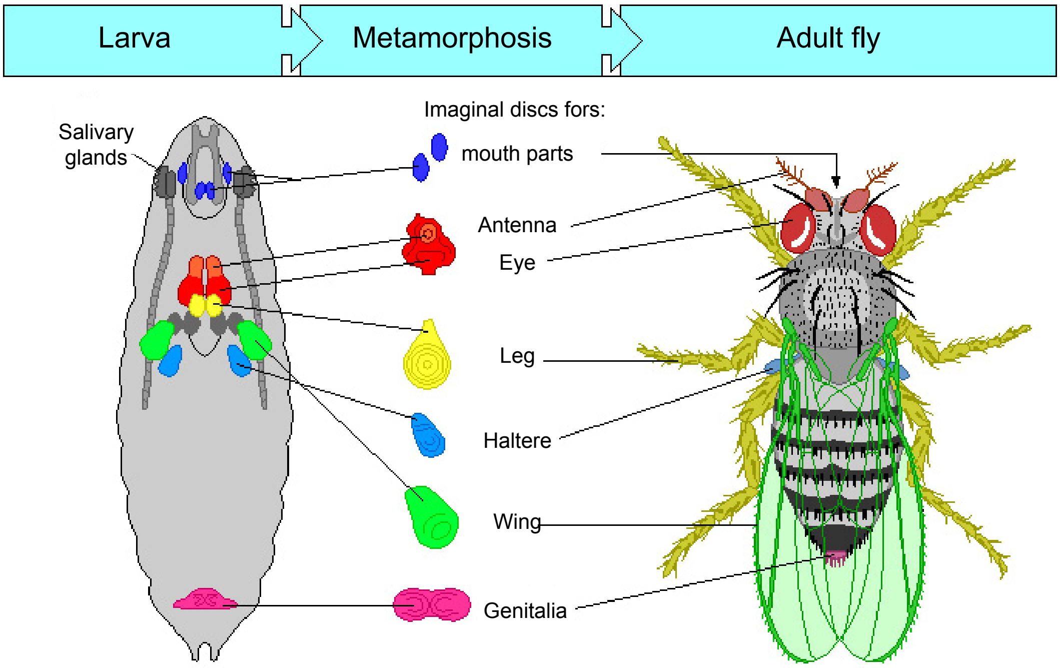

Figure 1.12: Imaginal discs in the *Drosophila* larva and corresponding structures in an adult fly
Single epithelial sheets are termed imaginal discs and develop into a variety of adult structures during metamorphosis. A schematic 3rd instar larvae shows the position of all imaginal discs (color coded according to the organs that they will develop into). The schematic body of a *Drosophila* depicts the adult structures (adapted from Wolpert et al., 2007).

applied molecular and genetic techniques to elucidate how processes and mechanisms work together for proper tissue development. These include the hormonal control mechanisms of disc development, as well as the molecular genetics of cell proliferation and differentiation or cell fate determination and cell cycle control. One of the best-understood examples of how such cellular and molecular interactions generate a proper adult organ is the development of the compound *Drosophila* eye. The imaginal disc of the compound eye is subdivided into two major morphogenetic fields. The anterior lobe of the epithelium - the antennal disc - gives rise to the antenna, while the posterior pouch - the eye disc - gives rise to the eye. The eye field includes separate primordia for eye, cuticle, and ocelli, whereas the antennal field includes an antenna and a cuticle primordium (Figure 1.13). Each field also gives rise to substantial portions of the head cuticle (Kenyon et al., 2003). The identities of the eye and the antenna are not determined until mid or late 2nd larval instar with the restricted expression of genes such as *eyeless*, *twin of eyeless*, *eyes absent*, *sine oculis* and *Dachshund*. These master control genes are first coexpressed in cells of the eye field and interact with each other through direct transcriptional regulation and/or the formation of biochemical complexes. They do not function as a linear biochemical or enzymatic pathway but rather exist in a regulatory network that is referred to as the retinal determination gene network (RDGN) (Kumar, 2001; Kenyon et al., 2003; Duong et al., 2008). Signals like RDGN, *hedgehog*, *decapentaplegic*, the epidermal growth factor (EGF) and Notch govern the initiation of a progressive wave - the morphogenetic furrow (MF) - which sweeps across the eye disc from posterior to anterior over a period of about two days. Cells anterior to the MF are undifferentiated and proliferate asynchronously. The furrow itself is the physical consequence of constriction of apical actin cytoskeletal rings, and is coincident with a band of cell cycle arrest at the G1 stage (Figure 1.14). After the arrest of proliferation within the MF, cells undergo a synchronous

S-phase just posterior to the MF followed by the G2-phase. The ommatidial preclusters lose this synchrony around the time that they begin mitosis. (Figure 1.14.B) (Hsiung and Moses, 2002; Leong et al., 2009; Roignant and Treisman, 2009; Popov et al., 2010). As the MF passes through a region of cells, those cell clusters begin to differentiate in a specific order and are regularly spaced in a hexagonal array. With a rate of two hours per row of ommatidial clusters, the MF moves forward and transforms the unpatterned and undifferentiated field of cells into eight photoreceptor neurons (R1-R8), in response to a wave of signals that trigger the development of ommatidia to become ultimately the photoreceptors of the adult eye.

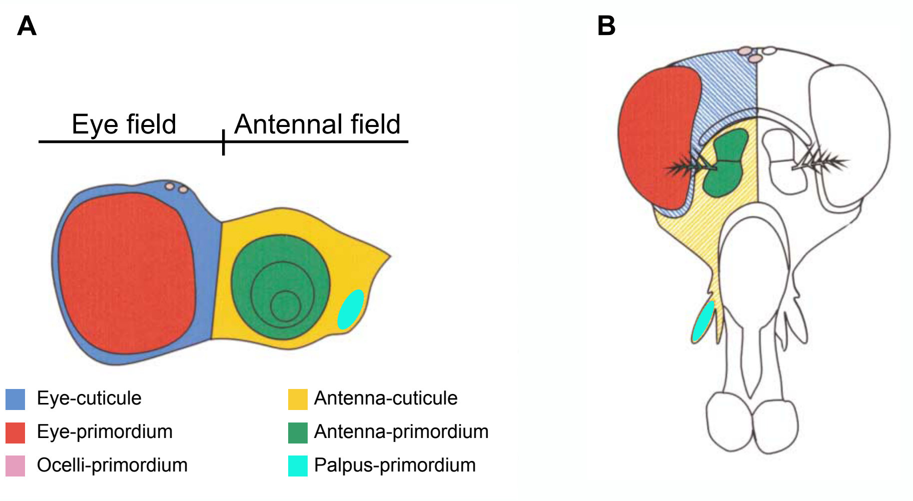

Figure 1.13: Schematic fate map of the eye-antenna disc and the corresponding structures
(A) Schematic fate map of the eye-antenna imaginal disc, which is established during the 1st - and 2nd instar of the *Drosophila* larva. The disc epithelium is shaped as a flattened sack and gives rise to the adult compound eye and the antenna as well as to some of the head cuticle (color coded according to the structures that they will develop into). **(B)** The schematic adult fly head depicts the corresponding structures (adapted from Kenyon et al., 2003).

The first cell to differentiate is the central (R8) photoreceptor, which coordinates the incorporation of all other photoreceptors (Frankfort and Mardon, 2002; Hsiung and Moses, 2002). Regular spacing of the ommatidia is achieved by lateral inhibition of the R8 photoreceptors that are characterized by *atonal* gene expression. *Atonal* is initially expressed in a broad stripe just anterior to the MF. After the precursors pass the MF, *atonal* expression is gradually refined to single R8 cells within the ommatidial preclusters in a process requiring lateral inhibition mediated by the Notch receptor (Roignant and Treisman, 2009). Each R8 cell initiates a cascade of signals that recruits cells anterior to and posterior to R8 to become the R2 and R5 photoreceptors, which are functionally equivalent. Subsequently, signals from these cells induce four more adjacent cells on either side of them to become the R3 and R4 photoreceptors, which are slightly different types of photoreceptor cells, followed by the differentiation of R1 and R6 photoreceptors. The R2/R5, R3/R4 and R1/R6 photoreceptors are sequentially recruited in a pair-wise fashion and are arranged in a semi-circle with R8 in the center. Finally, the R7 photoreceptor appears and completes the circle (Frankfort and Mardon, 2002).

After recruitment of the R7 photoreceptor, the multicellular ommatidial precursors rotate 90° within the matrix of their undifferentiated, stationary neighbors, the “interommatidial cells” in the disc epithelium (Figure 1.14.A). This ommatidial rotation depends on mechanisms that change cell adhesion and polarize the adult *Drosophila* eye across its D/V midline - the “equator” (*see* Figure 1.15) (Fetting et al., 2009). The other cells around the ommatidial clusters become the lens producing cone cells and finally the surrounding ring of accessory cells. At the adult stage, the compound

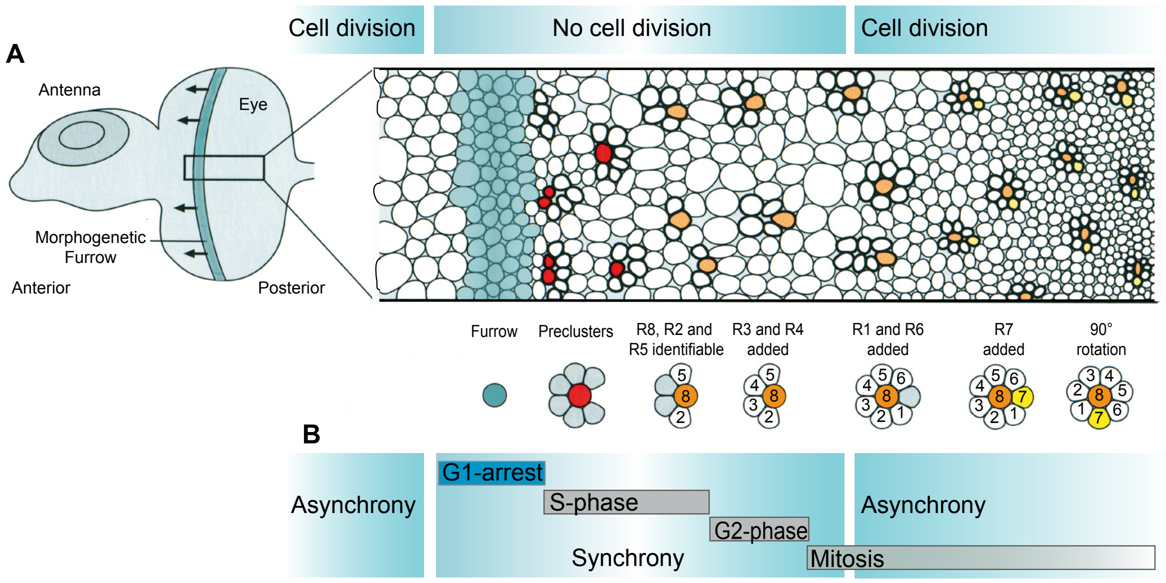
Cell division
No cell division
Cell division
A
Antenna
Eye
Morphogenetic Furrow
Anterior
Posterior
Furrow
Preclusters
R8, R2 and R5 identifiable
R3 and R4 added
R1 and R6 added
R7 added
90° rotation
B
Asynchrony
G1-arrest
S-phase
G2-phase
Synchrony
Mitosis
Asynchrony

Figure 1.14: Differentiation of photoreceptors in the *Drosophila* eye imaginal disc
(A) Section of a mature left eye disc. The morphogenetic furrow (MF) sweeps across the disc from posterior (right) to anterior (left). Behind the MF, the photoreceptor cells differentiate in a defined sequence (adapted from Wolpert et al., 2007). **(B)** Cell cycles of developing photoreceptor cell clusters depicted in (A). As cells enter the MF, they are arrested at the G1-stage and get synchronized. Subsequently cells undergo a synchronous S-phase followed by the G2-phase. Ommatidial preclusters lose this synchrony around the time that they begin mitosis (adapted from Held, 2005).

eye presents a regular hexagonal array of approximately 750 identical facets or ommatidia. An adult ommatidium is a precise 19-cell assembly of 8 photoreceptors and 11 accessory cells. Six of eight photoreceptor neurons (Figure 1.15, R1 - R6) lie in a ring and form the core of the ommatidium. Each of them project the light-gathering organelles termed as rhabdomeres (Rh, grey) into the central lumen carrying the photosensitive opsin. Six rhabdomeres (Rh1 - Rh6)

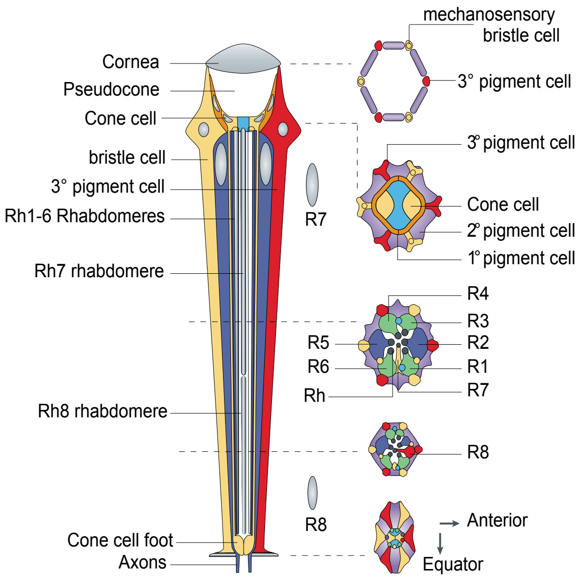
mechanosensory bristle cell
Cornea
Pseudocone
Cone cell
bristle cell
3° pigment cell
Rh1-6 Rhabdomeres
Rh7 rhabdomere
Rh8 rhabdomere
Cone cell foot
Axons
R7
R8
3° pigment cell
3° pigment cell
Cone cell
2° pigment cell
1° pigment cell
R4
R3
R2
R1
R7
R5
R6
Rh
R8
Anterior
Equator

Figure 1.15: Cells in one ommatidium of an adult compound eye in *Drosophila*
In the adult retina each ommatidium is made of 19 cells, shown in a longitudinal section to the left and five cross-sections to the right at the indicated levels. Eight photoreceptors neurons (R1–R8) build the core of the ommatidium and project the rhabdomeres (Rh, dark grey) — light-gathering organelles — into the central lumen. Above this lumen four cone cells secrete the overlying pseudocone and lens material. Pigment cells (1°, 2° and 3° type) and mechanosensory bristle cells surround the photoreceptors. Axons project basally (adapted from Kumar, 2001).

contain a blue-sensitive opsin and form a characteristic trapezoid. In the center of the apical retina, a smaller rhabdomere bearing ultraviolet-sensitive opsin is associated with the distal R7 photoreceptor cell. Below the Rh7 rhabdomere, the R8 photoreceptor neuron appears as inner central cell and contains the Rh8 rhabdomere, which is blue and green-sensitive (Kumar, 2001; Hsiung and Moses 2002).

Above the photoreceptors, a quartet of four cone cells secretes the dioptic elements of the ommatidium: the overlying pseudocone and the chitinous extracellular corneal lens, surrounded by a set of pigment cells. Two primary pigment cells are mirror-image twins and encircle the cone cells to secrete the lens material like the cone cells. The secondary pigment cells lie between two ommatidia, and the tertiaries are shared among three ommatidia at a vertex. The small mechanosensory bristles of the eye are products of the bristle cells surrounding the ommatidium. Eye bristles are developmentally distinct from ommatidia and project their sensory axons into the brain (Kumar, 2001; Hsiung and Moses 2002).

1.4.4 Oogenesis

The development of a multicellular organism from a single egg cell requires essential processes like intercellular signaling pathways regulating proliferation and differentiation of many cell types as well as the organization of these cells into a complex pattern. The *Drosophila* ovary provides an excellent system for studying such factors. In *Drosophila*, oogenesis occurs within the female ovary that is composed of 16–20 independent strings of egg chambers called ovarioles. Each ovariole contains a series of developing egg chambers harboring 15 sister nurse cells and one oocyte, which always takes the most posterior position (Figure 1.16). The egg chambers are surrounded by a somatic follicular epithelium and are connected by stalks, which are formed by specialized anterior polar follicle cells. The egg chambers develop over 7 days through 14 morphologically distinct stages to give rise to a mature egg (Becalska and Gavis, 2009; Roth and Lynch, 2009; Hartman et al., 2010). Throughout

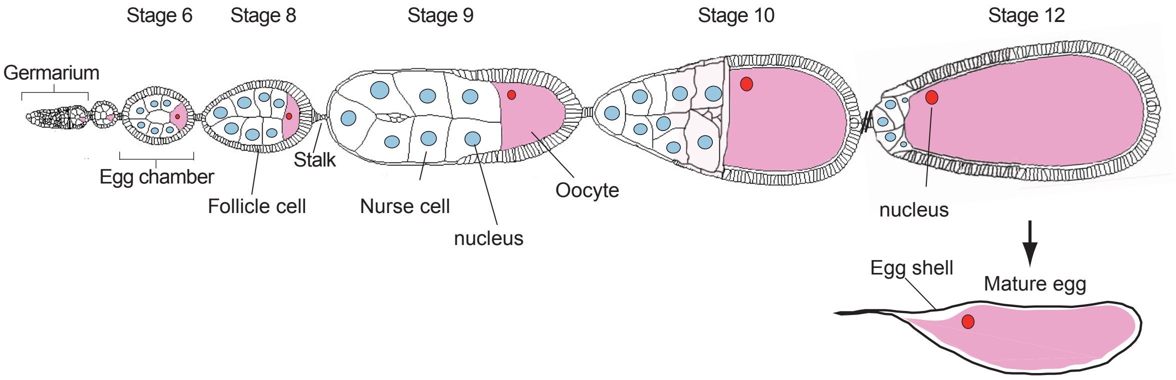

Figure 1.16: The *Drosophila* ovariole
Schematic drawing of an ovariole with the germarium at the anterior tip and egg chambers of increasing age. Each egg chamber is composed of one oocyte (nucleus in red) and 15 sister nurse cells (nuclei in blue). The egg chambers are surrounded by a monolayer of somatic follicle cells and connected by stalks. They undergo 14 morphologically distinct stages within 7 days to give rise to mature eggs. Eggs are produced from a germarium, which contains germline stem cells and somatic stem cells. Bottom: Mature egg (adapted from Becalska and Gavis, 2009; Wolpert et al., 2007).

oogenesis, the nurse cells produce large quantities of proteins and maternal RNAs that are delivered to the developing oocyte via cytoplasmatic bridges and microtubules. This supply of maternal factors by the nurse cells is essential for the development of the egg and the future embryo. As described above, maternal gene products set the basic framework like A/P and the D/V axis before the egg is fertilized and deposited (Chapter 1.4.2). The *Drosophila* remodeling complex CHD1 appeared to have an important role during gametogenesis, oogenesis and as a maternal product. Flies depend on the presence of functional CHD1, as a knock-down of CHD1 in male and female flies resulted in sterility of both sexes (Ho and Crabtree, 2010). At the end of stage 10, when the nurse cell cluster and the oocyte are similar in volume, the nurse cells extrude their maternal effect gene products such as *bicoid*, *nanos*, *gurken* or *oskar* into the oocyte through the microtubule cytoskeleton (Becalska and Gavis, 2009). Becalska and Gavis visualized the streaming of the oocyte cytoplasm (Figure 1.16, purple) mixing with the incoming nurse cell cytoplasm during stage 10 of oogenesis.

At the late phase of this stage, apoptotic pathways are initiated to subsequently eliminate the nurse cells from the egg chamber. The chromosomes of the polyploid nurse cells undergo DNA fragmentation at stage 12, followed by the completion of cytoplasm transfer from the nurse cells to the oocyte. During stage 13, nurse cells contain highly fragmented DNA and disappear from the egg chamber concomitantly with the formation of apoptotic vesicles (Foley and Cooley, 1998). Finally, the follicle cells enclose the egg chamber and secrete the vitelline membrane as well as the egg shell to protect the maturing egg (Figure 1.16, bottom).

Ovarian follicle formation requires a high level of coordination between the developmental programs of germline stem cells (GSCs), somatic stem cells (SSCs) and somatic cells. These three different cells types are located at the anterior tip of the ovariole in the germarium (Figure 1.17). In

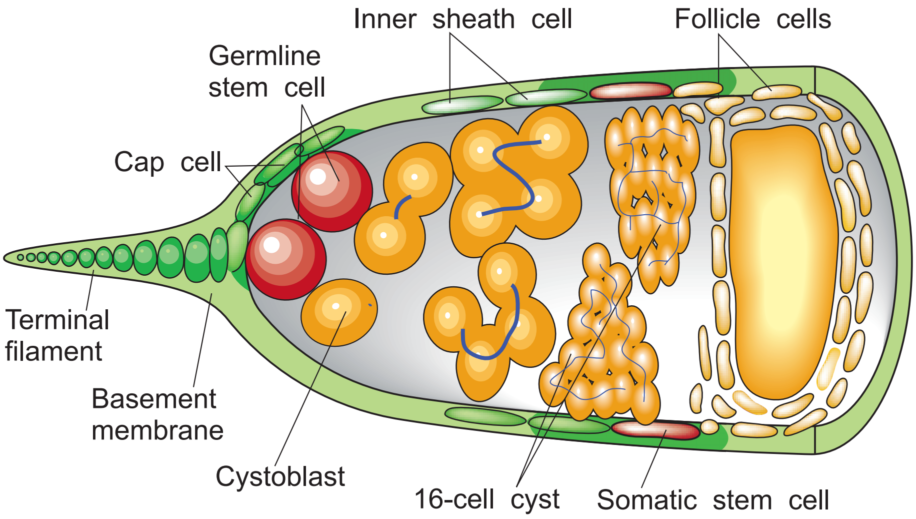

Figure 1.17: The *Drosophila* germarium
Schematic drawing of a germarium (sagittal section). 2-3 germ stem cells (GSCs) are located adjacent to the terminal filament and cap cells making up the germ cell niche (green). GSCs divide to produce another GSC and a cystoblast, which subsequently divides synchronously four times to produce a cyst of 16 cystocytes that are connected by fusomes (blue). The resulting structure is also called 16-cell cyst. The somatic stem cells (SSCs), located in their own niche (green), give rise to the follicle cells, which encapsulate each budding egg chamber harbouring the the 16-cell cyst (adapted from Spradling et al., 2001).

Drosophila, 2-3 GSCs are maintained throughout the entire lifetime of the adult female. GSCs are in close contact with quiescent somatic cells - the terminal filament and cap cells that make up the germ cell niche reside next to a basement membrane (Spradling et al., 2001; Niki et al., 2006). They divide asymmetrically and produce one daughter stem cell that retains its attachment to the cap cell and another daughter cell, called the cystoblast (Figure 1.17 and 1.18). The cystoblast (CB) leaves the niche and begins a series of differentiation steps while moving away from the anterior tip. The CB undergoes four rounds of synchronous cell division and yields to a cyst of 16 cystocytes, which are interconnected by actin-rich cytoplasmic bridges referred to as ring canals. One cell of the 16-cell cyst differentiates in the oocyte and enters meiosis, while the remainders become the polyploid nurse cells (Spradling et al., 2001; Niki et al., 2006; Roth and Lynch, 2009). The ring canals link all the cystocytes together and comprise cytoskeletal proteins, the fusomes. Later on, the fusomes are replaced by a polarized microtubule network. The mature germline cyst travels posteriorly through the germarium while contacting inner sheath cells until the cyst encounters a small population of 2-3 SSCs. The SSCs produce somatic follicle cells that centripetally encapsulating each germline cyst individually. The follicle cells differentiate into 3 cell types: the follicular cells that form the monolayered epithelium around each egg chamber, the polar cells that are pairs of cells that mark the anterior and posterior end of the egg chamber, and the interfollicular stalk cells that connect the mature egg chambers (Spradling et al., 2001; Roth and Lynch, 2009; Hartman et al., 2010). When follicle cells surround the cyst, the cyst flattens to become one cell thick disc spanning the whole width of the germarium.

1.4.5 Stem Cell Maintenance during Oogenesis

During the past several years, a remarkable progress in the understanding of stem cell formation and its underlying molecular mechanisms occurred. Especially studies of stem cells in *Drosophila* ovaries yielded exciting insights into signaling pathways and factors that regulate the stem cell maintenance and differentiation processes. Although cell signaling and stem cell formation are under intense investigation, little is known about how these events are regulated and maintained during oogenesis.

A stem cell is “the mother of all cells”: embryonic stem cells give rise to numerous differentiated cell types and are characterized by their ability to self-renew as well as by their extensive proliferative potential. They are involved in the generation and maintenance of tissues and organs. Stem cells depend on signals from cells within their microenvironment - the so called “stem cell niche” - as well as developmental specific factors (Spradling et al., 2001; Lin, 2002). Spradling and colleagues speculate that stem cells in a niche might contact the basement membrane asymmetrically and orientate their division plane to ensure that only one daughter cell inherits adhesive contacts with the basement membrane (Figure 1.18) (Spradling et al., 2001). They hypothesized that the stem cell niche is formed with respect to the extracellular matrices (ECMs) that locally modulate the concentration of adhesive and signaling molecules. The daughter cell adjacent to the stem cell niche is held in the niche, where it will be maintained as a GSC, whereas the other daughter cell starts to differentiate and becomes a CB, while moving away from the GSC (Spradling et al., 2001). Thus, a stem cell niche creates an inductive microenvironment that maintains the stem cell fate and prevents the differentiation of GSCs. A known key niche signal that promotes proliferation and self-renewal of the GSCs is the bone morphogenetic protein ligand decapentaplegic, whereas *hedgehog* is required for maintenance and cell division of the SCCs (Niki et al., 2006; Ables and Drummond-Barbosa, 2010). The regulation of

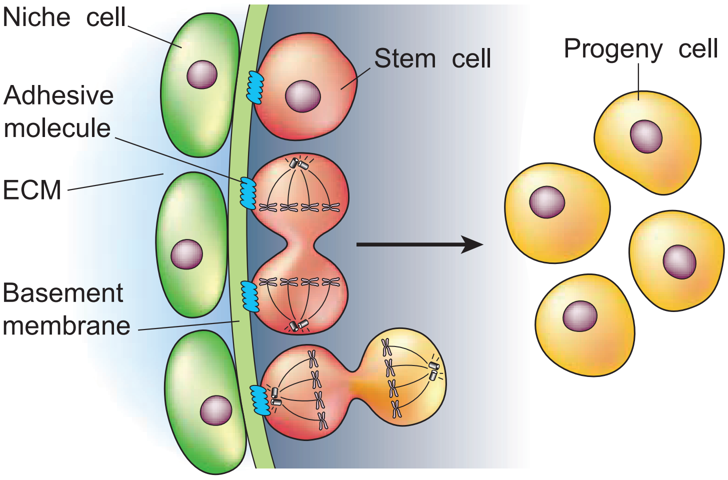

Figure 1.18: Proposed model of a stem cell niche
Adhesive molecules connect germ stem cells (GSCs, red) with the basement membrane in the specialized niche, where the self-renewing ability of GSCs is controlled by tissue specific transcriptional regulators and signals. These signals are predominantly expressed by the niche cells (green) to block the differentiation of GSCs and regulate their division. After the stem cell divides, one daughter cell retains its connections to the niche, while the other (yellow) differentiates. The cell fate determination depends besides other signals on epigenetic regulation of gene expression by chromatin remodeling factors. The extracellular matrix (ECM) can locally modulate the concentration of adhesive and signaling molecules (adapted from Spradling et al., 2001).

stem cells depends not only on tissue-specific transcriptional regulators but also on changes in chromatin organization. The chromatin structure imposes an additional level of regulation to keep the balance between stem cell self-renewal and cell differentiation. While the self-renewing ability of a stem cell is controlled by its specialized niche, the cell fate determination depends on epigenetic regulation of gene expression by chromatin remodeling factors (Xi and Xie, 2005). Xi and colleagues showed that the chromatin remodeling factors ISWI and DOM control GSCs and SSCs self-renewal in the *Drosophila* ovary (Xi and Xie, 2005). Chromatin remodeling factors can also cooperate with niche signals to coordinately regulate a common set of target genes to prevent premature stem cell differentiation. For example, the nucleosome-remodeling complex NURF ensures GSCs maintenance by positively regulating the known JAK-STAT signaling cascade to prevent differentiation within adjacent stem cells in *Drosophila* testis (Cherry and Matunis, 2010).

1.5 Objective

Since 1997, when *domino* was discovered within a screen for mutations that cause hematopoietic disorders in *Drosophila melanogaster* (Braun et al., 1997), Domino is noted as a potential candidate to remodel chromatin during development. It is surprising, that hitherto only a few studies analyzed some aspects of this apparently versatile and highly conserved chromatin remodeler, while other homologues such as yeast SWR1 or human SCRAP complexes are well explored during the last 20 years. To date, Domino`s mechanisms and its biological function during development regardless of fly, mouse or humans, are just beginning to be uncovered. Further investigations of Domino will make important contributions to the fascinating field of epigenetic regulation through chromatin remodeling also in the context of stem cell maintenance.

This thesis work focuses on the Domino B isoform. To explore the role of this essential protein during developmental processes such as differentiation, cell cycle progression or stem cell formation, *Drosophila melanogaster* was used as a model organism. Furthermore, to tease apart the biological functions and mechanisms, Domino B was also analyzed *in vitro.* This thesis aimed to characterize Domino B in terms of (A) a putative novel chromatin remodeling complex, (B) the expression and distribution during *Drosophila* development and (C) its biological function.

2 MATERIALS AND METHODS

2.1 Material Sources

2.1.1 Laboratory Chemicals and Biochemicals

Acrylamide (Rotiphorese Gel® 30)	Roth, Karlsruhe
Agar-Agar	Probio, Eggenstein
Agarose (ME, LE *GP* and low melting)	Biozym, Hessisch Oldendorf
Ampicillin	Roth, Karlruhe
Aprotinin	Sigma, Taufkirchen
ATP	Sigma, Taufkirchen
[γ-32P]- ATP	Perkin Elmer, Massachusetts
Bacto Agar	BD, France
Brewer´s yeast	Leiber, Bramsche
BSA (Bovine serum albumin), 98% pure	Sigma, Taufkirchen
BSA, purified	NEB, Frankfurt/Main
β-Mercaptoethanol Sigma,	Taufkirchen
Chloramphenicol	Roth, Karlsruhe
Coomassie G250	Serva, Heidelberg
Corn meal	Bäko, Nürnberg
dNTP-Mix	NEB, Frankfurt/Main
dNTP-Set	Roche, Mannheim
DTT	Roth, Karlsruhe
EDTA	Sigma, Taufkirchen
EGTA	Sigma, Taufkirchen
Ethidium bromide	Sigma, Taufkirchen
Fetal bovine serum	Sigma, Taufkirchen
HEPES	Roth, Karlsruhe
Kanamycin	Sigma, Taufkirchen
IPTG	Roth, Karlsruhe
Leupeptin	Sigma, Taufkirchen
Nipagin	Sigma, Taufkirchen
Normal goat serum	Dianova, Hamburg
NP40 (Igepal CA-630)	Sigma, Taufkirchen
Orange G	Sigma, Taufkirchen
Paraformaldehyde	Sigma, Taufkirchen
Pepstatin	Sigma, Taufkrichen
Phenol	Roth, Karlsruhe
PMSF (Phenylmethanesulfonyl fluoride)	Sigma, Taufkirchen
Raisins	Ökoring, Mammendorf
Semolina	Tengelmann KG, Germany
SDS (Sodium dodecyl sulfate)	Serva, Heidelberg
Sf-900II medium (GibCo)	Invitrogen, Karlsruhe
Sugar beet molasses	Ökoring, Mammendorf
Temed (N,N,N',N'-Tetramethylethylenediamine)	Roth, Karlsruhe
TO-PRO3 (Molecular Probes)	Invitrogen, Karlsruhe
Tris	Invitrogen, Karlsruhe
Triton X-100	Sigma, Taufkirchen
Tween 20	Sigma, Taufkirchen
Vectashield mounting medium	Vector Labs, U.K.
Yeast extract	Difco, Detroit

All other chemicals were purchased in analytical grade from Merck, Darmstadt.

2.1.2 Enzymes

DNA Polymerase I, Large (Klenow) Fragment	NEB, Frankfurt/Main
Micrococcal nuclease (MNase)	Sigma, Taufkirchen
Proteinase K	Roche, Mannheim
Restriction endonucleases	NEB, Frankfurt/Main
Taq DNA Polymerase	NEB, Frankfurt/Main

2.1.3 Antibodies

Primary antibodies

chicken α-DOM-B (polycl. Ch35)	Eurogentec, Netherlands
chicken α-DOM-B (polycl. Ch36)	Eurogentec, Netherlands
chicken α-DOM-B (polycl. Ch37)	Eurogentec, Netherlands
chicken α-DOM-B (polycl. Ch38)	Eurogentec, Netherlands
rat α-DOM-B (monocl. 2G5)	E. Kremmer, Munich, Germany
rat α-DOM-B (monocl. 2F4)	E. Kremmer, Munich, Germany
rat α-DOM-B (monocl. 3H1)	E. Kremmer, Munich, Germany
rat α-DOM-B (monocl. 8B8)	E. Kremmer, Munich, Germany
rat α-ACF1 (monocl. 8E3)	E. Kremmer, Munich, Germany
rabbit α-ISWI	JW. Tamkun,Florida, USA
rabbit α-H2A	Eurogentec, Netherlands
rabbit α-H2AV	Eurogentec, Netherlands
rabbit α-ɣ-H2AV	Rockland, Pennsylvania, USA
mouse α-HP1	S. Elgin, St. Louis, USA
rabbit α-Caspase	Cell Signalling, USA
mouse α-ELAV	Hybridoma bank, Iowa, USA
mouse α-DAC	Hybridoma bank, Iowa, USA
mouse α-FLAG	Sigma, Taufkirchen
mouse α-GFP	Molecular Probes, Karlsruhe
guinea pig α-PW35	C. Regnard, Munich, Germany
mouse α -BrdU (clone IU-4)	Accurate Chemicals, USA
mouse α-LAMIN	SantaCruz, USA
rabbit α-MRG 15	JL. Workman, Kansas city, USA
rabbit α-TIP60	JL. Workman, Kansas city, USA
rabbit α-GAS41	JL. Workman, Kansas city, USA
rabbit α-ING3	JL. Workman, Kansas city, USA
rabbit α-TRA1	JL. Workman, Kansas city, USA
rabbit α-INO80	JL. Müller, Heidelberg
rabbit α-Pontin	AJ. Saurin, Marseille, France
rabbit α-Reptin	AJ. Saurin, Marseille, France

Secondary antibodies

rabbit α-chicken HRP-conjugated	Promega, Mannheim
goat α-mouse HRP-conjugated	Promega, Mannheim
goat α-rabbit HRP-conjugated	Promega, Mannheim
goat α-rat HRP-conjugated	Promega, Mannheim
goat α-chicken Alexa 488-conjugated	Invitrogen, Karlsruhe
goat α-guinea pig Alexa 488-conjugated	Invitrogen, Karlsruhe
donkey α-mouse Alexa 488-conjugated	Invitrogen, Karlsruhe
donkey α-rabbit Alexa 488-conjugated	Invitrogen, Karlsruhe
donkey α-chicken Rhodamine Red X -conjugated	Dianova, Hamburg
donkey α-mouse Rhodamine Red X-conjugated	Dianova, Hamburg
goat α-rabbit Rhodamine Red X-conjugated	Dianova, Hamburg
donkey α-rat Rhodamine Red X-conjugated	Dianova, Hamburg

2.1.4 Organisms

E. coli TOP10	Invitrogen, Karlsruhe
E.coli BL21-CodonPlus	Stratagene, USA
E.coli DH10Bac	Invitrogen, Karlsruhe
Sf9 cells (*Spodoptera frugiperda*)	Novagen, USA

All *Drosophila* flies used for this study are listed and described in chapter 2.6.

2.1.5 Oligonucleotides, Plasmids and Baculoviruses

Primers
All primers were ordered from Biomers, Ulm

DOM-B WT fw	5’-GTCGACGGTACCATGAATGAAGGTAATTCAG-3’
DOM-B WT rv	5’-TGCGGCCGCTCACTTGTCGTCGTCGTCCTTGTAGTCCCTGGCTG TTCCGCT-3’
DOM-B K945R fw	5’-GAGATGGGTCTGGGCCGAACCATCCAGACCATTG-3’
DOM-B K945R rv	5’-CAATGGTCTGGATGGTTCGGCCCAGACCCATCTC-3’
DOM-B Δ1fw	5’-GTCGACGGTACCATGAATGAAGGTAATTCAG-3’
DOM-B Δ1rv	5’-TGCGGCCGCTCACTTGTCGTCGTCGTCCTTGTAGTCGAAGGGCACAGGAGTA A-3’
DOM-B Δ2 fw	5’-GTCGACGGTACCATGGTTACTCCTGTGCCCTTCC-3’
DOM-B Δ2 rv	5’-TGCGGCCGCTCACTTGTCGTCGTCGTCCTTGTAGTCTGAATTCGTCGCCGGTGTGAG-3’
DOM-B Δ3 fw	5’-GTCGACGGTACCATGAATGAAGGTAATTCAG-3’
DOM-B Δ3 rv	5’-TGCGGCCGCTCACTTGTCGTCGTCGTCCTTGTAGTCTGAATTCGTCGCCGGTGTGAG-3’
DOM-B Δ4 fw	5’-GTCGACGGTACCATGAATGAAGGTAATTCAG -3’
DOM-B Δ4 rv	5’-TGCGGCCGCTCACTTGTCGTCGTCGTCCTTGTAGTCAGTTTCTTCCACAAAGCGCAT-3’
DOM-B Δ5 fw	5’-CGACGAATTCAATGGCAGCAG-3’
DOM-B Δ5 rv	5’-TGCGGCCGCTCACTTGTCGTCGTCGTCCTTGTAGTCAGTTTCTTCCACAAAGCGCAT-3’
DOM-B Δ6 fw	5’-GTCGACGGTACCATGGTTACTCCTGTGCCCTTCC-3’
DOM-B Δ6 rv	5’-TGCGGCCGCTCACTTGTCGTCGTCGTCCTTGTAGTCAGTTTCTTCCACAAAGCGCAT-3’
DOM-B Δ7 fw	5’-GTCGACGGTACCATGCGCTTTGTGGAAGAAACT-3’
DOM-B Δ7 rv	5’-TGCGGCCGCTCACTTGTCGTCGTCGTCCTTGTAGTCCCTGGCTGTTCCGCT-3’

Plasmids

pBluescript KS	Stratagene, Netherlands
pFastBacHTc1-Vektor	Invitrogen, Karlsruhe
pCR-3.5-XL-TOPO	Invitrogen, Karlsruhe
pGEX	GE Healthcare, Munich
pUASp	Rorth, 1998

Baculoviruses raised in this study

DOM-B WT-FLAG
DOM-B KR-FLAG
DOM-B Δ1-FLAG
DOM-B Δ2-FLAG
DOM-B Δ3-FLAG
DOM-B Δ4-FLAG
DOM-B Δ6-FLAG
DOM-B Δ7-FLAG

Other baculoviruses kindly provided

ACF	JT. Kadonaga, San Diego, USA
ACF1-FLAG	JT. Kadonaga, San Diego, USA
ISWI	JT. Kadonaga, San Diego, USA
FLAG-ISWI	Adolf-Butenandt-Institute, Munich, Germany

2.1.6 Other Materials

1 kb DNA marker	NEB, Frankfurt/Main
100 bp DNA marker	NEB, Frankfurt/Main
Anti-FLAG M2 agarose	Sigma, Taufkirchen
DE81 anion exchanger chromatography paper	Whatman, Rothenburg
Dynabeads M280-Straptavidin	Invitrogen Dynal AS, Norway
EGGstract IgY purification system	Promega, Mannheim
ECL detection system	GE Healthcare, Munich
Gel Extraction Kit	QIAGEN, Hilden
Glutathion-Sepharose beads 4B	GE Healthcare, Munich
Immobilon-P PVDF membrane	Millipore, Massachusetts, USA
Kilobasebinder	Invitrogen Dynal AS, Norway
Miracloth (Calbiochem)	Merck, Darmstadt
Mono Q HR 5/5	GE Healthcare, Munich
Mutagenesis Kit	Invitrogen, Karlsruhe
peqGOLD Protein Marker	Peqlab, Erlangen
Plasmid Maxi Kit	QIAGEN, Hilden
Plasmid Mini Kit	QIAGEN, Hilden
Quick spin colums Sepahdex G 50	Roche, Mannheim
Q-Sepharose	GE Healthcare, Munich
Rotilabo syringe filters	Roth, Karlsruhe
Siliconised reaction tubes, 1.5 ml	Biozym, Hessisch Oldendorf,
SpectraPor dialysis membrane	Roth, Karlsruhe
SP-Sepharose column (5 ml)	GE Healthcare, Munich
Superose 6 HR 10/30	GE Healthcare, Munich
Super RX Fuji medical X-ray film	Fuji, Düsseldorf
TLC plates	Merck, Darmstadt
Wizard SV Gel and PCR clean up system	Promega, Mannheim

2.1.7 Buffers and Solutions

Agar plates for collecting *Drosophila* embryos	1.8%	Bacto-agar
	2%	Sucrose
	0.1%	Acetic acid

ATPase buffer	20 m	HEPES-KOH pH 7.6
	50 mM	KCl
	2.5 mM	$MgCl_2$
	0.02% v/v	NP40
	10% v/v	Glycerol
	1 mM	DTT
	proteinase inhibitors (just before use)	
Coomassie destaining solution	10% v/v	Acetic acid
Coomassie staining solution 1	0% v/v	Acetic acid
	0.25% w/v	Coomassie Brilliant Blue R-250
Chromatin assembly buffer1 (CAB1)	50 mM	HEPES-KOH pH 7.5
	1 mM	EDTA
Chromatin assembly buffer 2 (CAB2)	10 mM	Tris-HCl pH 7.4
	1 mM	EDTA pH 8.0
	5 mM	DTT
	0.5 mM	PMSF
Chromatin assembly buffer 3 (CAB3)	10 mM	Tris-HCl pH 7.4
	1 mM	EDTA pH 8.0
	5 mM	DTT
	200 µg/ml	BSA
	20 % v/v	Glycerol
	0.1% v/v	NP40
	0.5 mM	PMSF
DNA loading dye (6x)	30% v/v	Glycerol
	0.25% w/v	Bromophenol blue or orange G
Embryo wash buffer (EW)	120 mM	NaCl
	0.05% v/v	Triton X-100
Embryo buffer 1 (EB1)	15 mM	HEPES-KOH pH 7.6
	10 mM	KCl
	2 mM	$MgCl_2$
	0.5 mM	EGTA
	0.1 mM	EDTA pH 8.0
	350 mM	Sucrose
	1 mM	DTT (just before use)
	1 mM	NaMBS
	proteinase inhibitors (just before use)	
Embryo buffer 2 (EB2)	15 mM	HEPES-KOH pH 7.6
	110 mM	KCl
	2 mM	$MgCl_2$
	0.1 mM	EDTA pH 8.0
	1 mM	DTT (just before use)
	1 mM	NaMBS
	proteinase inhibitors (just before use)	

Embryo buffer 2 (EB3)	25 mM	HEPES-KOH pH 7.6
	100 mM	KCl
	2 mM	$MgCl_2$
	0.1 mM	EDTA pH 8.0
	1 mM	DTT (just before use)
	20% v/v	Glycerol
	1 mM	NaMBS
	proteinase inhibitors (just before use)	
Fly food	13.3% w/v	Brewer`s yeast
	26% w/v	Semolina
	13.3% w/v	Corn meal
	50% v/v	Sugar beet molasses
	9.5% w/v	Agar-agar
	40% w/v	Raisins
	1.6% v/v	Propionic acid
	24% v/v	Nipagin
Fixation buffer	50% v/v	Methanol
	10% v/v	Acetic acid
GST elution buffer	20 mM	HEPES-KOH pH 7.6
	100 mM	NaCl
	0.5 mM	EDTA
	1.5 mM	$MgCl_2$
	10%	Glycerol
	33mM	Glutathion-Tris-HCl pH 9.5
	proteinase inhibitors (just before use)	
HEMG 0/50/200/500/1000	20 mM	HEPES-KOH pH 7.6
	0/50/200/500/1000 mM	KCl
	0.5 mM	EDTA
	1.5 mM	$MgCl_2$
	10%	Glycerol
	0.05%	NP40
	proteinase inhibitors (just before use)	
Laemmli buffer (5x)	250 mM	Tris-HCl pH 6.8
	10% w/v	SDS
	50% v/v	Glycerol
	0.1% w/v	Bromophenol blue
	10%	β-mercaptoethanol
LB-agar plates	LB-medium	
	1.5% w/v	Bacto-agar
LB-medium	1.0% w/v	Tryptone
	0.5% w/v	Yeast extract
	1.0% w/v	NaCl
MNase buffer	10mM	HEPES-KOH pH 7.6
	10mM	KCl
	1.5 mM	$MgCl_2$
	34 mM	Sucrose
	10%	Glycerol
	1 mM	$CaCl_2$

MNase mix	5 mM	$CaCl_2$
	2.5 U	MNase
	in HEMG200	
Nuclei buffer (NB)	15 mM	Tris-Cl pH 7.4
	60 mM	KCl
	15 mM	NaCl
	5 mM	$MgCl_2$
	0.1 mM	EGTA pH 8.0
	proteinase inhibitors (just before use)	
Phosphate-buffered saline (PBS)	1.54 M	NaCl
	15 mM	KH_2PO_4
	27 mM	$Na_2HPO_4*12H_2O$
PBS-T	PBS	containing 0.1% Tween 20
PBS-1%T	PBS	containing 1% Tween 20
Sucrose buffer	15 mM	HEPES-KOH pH 7.6
	10 mM	KCl
	5 mM	MgCl2
	0.05 mM	EDTA
	0.25 mM	EGTA
	30 mM	Sucrose
	1 mM	DTT (just before use)
	proteinase inhibitors (just before use)	
TAE	40 mM	Tris-acetate
	1 mM	EDTA pH 8.0
Transfer buffer	48 mM	Tris base
	39 mM	Glycine
	20% v/v	Methanol

Proteinase inhibitors included 0.2 mM PMSF, 1 mg/l Aprotinin, 1 mg/l Leupeptin and 0.7 mg/l Pepstatin.

2.2 Methods for Preparation and Analysis of DNA

2.2.1 General Methods for Working with DNA

2.2.1.1 Agarose Gel Electrophoresis

Agarose gel electrophoresis was performed to analyze the quality, size and amount of linear DNA fragments (Sambrook and Russell, 2001). According to the size of DNA fragments, agarose solutions ranging from 0.7 to 2% w/v were dissolved in 1 × TAE by boiling. Gels contained a final concentration of 0.5 µg/ml ethidium bromide. Samples were prepared by adding 1/6 v/v of 6 × DNA loading dye. A DNA ladder was used as a size standard. Electrophoresis was performed in 1 × TAE by applying 10 V/cm gel length. After separation, DNA was examined on UV light (254-366 nm) in a gel documentation system (Peqlab, Erlangen).

2.2.1.2 DNA Quantification

The DNA concentration was determined by measuring the optical density (OD) at a wavelength of 260 nm with a NanoDrop® (Peqlab, Erlangen). One OD unit at 260 nm (OD260) corresponds to a concentration of 50 µg DNA/ml. The purity of the DNA can be judged by the ratio OD260/OD280. Pure DNA preparations should have a ratio between 1.8 and 2.0.

2.2.1.3 Transformation of Competent Bacteria

50 µl of chemically competent *E. coli* were thawed on ice and incubated with an appropriate amount of plasmid DNA for 30 min on ice. The cell suspension was heat-shocked for 45 sec at 42°C and immediately chilled on ice for 3 min. 200 µl LB were added and cells incubated at 37°C for 30 min. Transformed bacteria were plated on agar plates containing appropriate antibiotics. Plates were incubated overnight at 37°C.

2.2.1.4 Plasmid Preparation

Plasmids were prepared using the QIAGEN Plasmid Mini and Maxi kits (QIAGEN, Hilden) following the manufacturer's instructions.

2.2.2 Cloning of *UAS*-Reporter Constructs

The cDNA of full length DOM-B WT was kindly provided by Dr. Marie-Laure Ruhf (Friedrich Miescher Institute, Basel, Switzerland). All *Drosophila* DOM-B constructs and truncated versions (DOM-B WT/ KR – FLAG and DOM-B Δ1-7 - FLAG) were amplified by PCR from a cDNA clone containing the FLAG epitope sequence, generated by Dr. Mariacristina Chioda (Adolf-Butenandt-Institute, Munich, Germany). All DOM-B *UAS*-Reporter Constructs were verified by sequencing before further cloning. PCR products were gel-purified and cloned in a pCR3.5-XL TOPO vector (Invitrogen, Karlruhe) using *Sal I* / *Not I* restriction sites. All different DOM-B inserts were mobilised with *Sal I* and *Not I* and subcloned into pGEX vector (GE Healthcare, Munich) for bacterial expression in *E.coli* cells and in pFastBac1 vector (Invitrogen, Karlsruhe). The various fragments of Domino sub-cloned into pFastBac1 were used to generate recombinant viral particles using the Bac-to-Bac system (Invitrogen, Karlsruhe). DOM-B WT-FLAG and DOM-B KR-FLAG sequences were mobilised from pCR3.5-XL TOPO vector using *Kpn I* and *Not I* restriction sites and subcloned into pUASp vector (Rorth, 1998). After sequencing, transgenic fly lines were generated by injecting embryos of *y[1]w[1118]* with the appropriate column-purified plasmid DNA and P-element-mediated germline transformation (*see* 2.6.2). All primer pairs are listed in chapter 2.1.5.

2.2.3 Site-Directed Mutagenesis

The DOM-B KR mutant was previously generated by Dr. Angelika Loiberstetter (Adolf-Butenandt-Institute, Munich, Germany). The amplified DNA sequence of DOM-B WT was point mutated by site-directed mutagenesis (Mutagenesis Kit, Invitrogen, Karlsruhe) following the manufacturer's instructions and verified by sequencing. The primers used for site-directed mutagenesis are listed above (Chapter 2.1.5).

2.2.4 DNA Purification for P-Element-Mediated Germline Transformation via Microinjection of *Drosophila* Embryos

30 µg of pUAS-DOM-B WT-FLAG and pUAS-DOM-B KR-FLAG plasmid DNA were purified using the Wizard SV Gel and PCR clean up kit following according to the manufacturer's instructions (Promega, Mannheim). After purification, DNA concentration was quantified with a NanoDrop® (Peqlab, Erlangen). 9 µg of the appropriate plasmid DNA, 3 µg Δ 2.3 transposase encoding helper plasmid (Heike Mitlöhner, Adolf Butenandt Institute, Munich, Germany), 1.5 µl 10 × injectionbuffer (50 mM KCl, 1 mM Na_3PO_4) and food color (Schwartau, Bad Schwartau) diluted 1:10 were mixed in a total volume of 20 µl and stored at -20°C.

2.2.5 DNA Biotinylation

500 µg pBluescript KS (+) vector (Stratagene, Netherlands) was double digested o/n at 37°C with a mix of 10 µl *Cla I* and 10 µl *EcoR I* in a total volume of 1000 µl containing 10 µl BSA (10 µg/µl), 100 µl 10 x NEB buffer 4 and x µl ddH_20. This sample was spitted into 500 µl aliquots. Within the first four hours of restriction digestion tubes were vortexed every 60 min. 2 µl of digestion mix before incubation, after 1 h of incubation and after the entire incubation period were analyzed by agarose gel electrophoresis. The digested DNA was precipitated by adding 50 µl of sodium acetate pH 5.2 (3 M) and 550 µl cold isopropanol. Samples were mixed and incubated on ice for 1 h. DNA was pelleted by centrifugation (30 min, 13000 rpm, 4°C). Pellets were washed with 70% ethanol and re-centrifuged (5 min, 13000 rpm, RT). DNA pellets were dried and redissolved in 125 µl ddH_2O per aliquot. To biotinylate the DNA on the *Eco R I* restriction site, 3 mM dUTP biotinylated, 3 mM dATP biotinylated and 10 U Klenow was added in a final volume of 300 µl per aliqout. Samples were incubated for 2 h at 37°C. Afterwards, Klenow enzyme was heat inactivated for 20 min at 70°C and chilled for 10 min at RT. Biotinylated DNA was purified from unincorporated nucleotides using three subsequent sepharose G50 columns (Quick spin colums Sephadex G 50, Roche, Mannheim). Columns were centrifuged (1 min, 1000 rpm, 4°C) to remove the G50 storage buffer from the matrix. 100 µl of the biotinylated DNA was applied to each column and centrifuged for 2 min at 1000 rpm at 4°C. The flow-through was collected and the DNA concentration determined with a NanoDrop®.

2.2.6 Chromatin Assembly on Immobilized DNA

To bind biotinylated DNA to paramagnetic Streptavidin coated beads (Dynabeads M280) 4 µg of DNA (pBS KS +) were immobilized to 80 µl packed Dynabeads. DNA was mixed with 10 µl kilobase binder (Dynal) and x µl ddH_20 in a total volume of 20 µl. The optimal amount of Dynabeads was determined by titration. Samples were incubated for 2 h at RT on a metal free rotating wheel and washed once with 1 ml ddH_20. The supernatant was discarded and the beads stored in 300 µl ddH_20. To assemble chromatin on immobilized DNA, 50 µl of packed Dynabeads containing 4 µg biotinylated DNA (pBS KS +) was mixed with 8 µl chromatin assembly buffer 1 (CAB 1) and 8 µl NaCl (5 M) for a final concentration of 2 M NaCl. Recombinant histone octamers containing either the canonical H2A or the histone variant H2AV of a concentration of 8 µg (2 µg/µl) were added using tips preblocked with 20 mg/ml BSA to the assembly extract in a total reaction volume of 20 µl. The assembly extract was immediately incubated at 37°C while gently shaking (600 rpm) for 15 min. Chromatin arrays were reconstituted by a step wise reduction the salt concentration (2 M) to 0.1 M NaCl with adding chromatin assembly buffer 2 (CAB 2). The whole assembly was conducted as follow:

Sample volume	[NaCl]	Volume of buffer to add	Incubation
20 µl in IB	2 M	0 µl CAB 1	15 min, 37°C
33.3 µl	1.2 M	13.3 µl CAB 2	15 min, 30°C
50 µl	0.8 M	16.67 µl CAB 2	15 min, 30°C
66.67 µl	0.6 M	16.67 µl CAB 2	15 min, 30°C
100 µl	0.4 M	33.33 µl CAB 2	15 min, 30°C
200 µl	0.2 M	100 µl CAB 2	15 min, 30°C
400 µl	0.1 M	200 µl CAB 3	15 min, 30°C

Table 2.1: Chromatin assembly by gradually reducing the salt concentration

Finally, CAB 3 was added to reduce the salt concentration to final 0.1 M NaCl. The assembly was verified by micrococcal nuclease digestion. Assembled nucleosomal arrays were stored at 4°C in siliconized 1.5 ml tubes. All further handling of chromatin was performed in siliconized tubes using preblocked tips. Chromatin salt assembly was also performed with 4 µg DNA (pBS KS +) not bound to beads using identical conditions.

2.3 Methods for Protein Purification and Analysis

2.3.1 Protein Quantification

Protein concentrations were estimated in comparison to a protein standard (purified BSA) on an SDS polyacrylamide gel stained with Coomassie blue.

2.3.2 SDS Polyacrylamide Gel Electrophoresis (SDS-PAGE)

Denaturing SDS polyacrylamide gels were used to separate protein mixtures according to their molecular weight. SDS-PAGE - consisting of a 6 to 15% separation gel and a 5% stacking gel - was conducted as described in Novex Mini Cell chambers (Invitrogen, Karlsruhe) (Sambrook and Russell, 2001). Protein samples were mixed with Laemmli buffer and denatured for 10 min at 96°C before gel application. Size markers were used to determine the molecular weight of separated protein bands. After separation, the gel was further processed either by Coomassie staining or Western blotting. For Coomassie blue staining proteins were fixed by shaking the gel for 30 min in fixation buffer. Subsequently, the gel was incubated for 0.5 - 1 h in Coomassie blue staining solution and destained in Coomassie destaining solution until the appropriate level of coloration was achieved. The gel was dried for 2 h at 80°C on a 3 MM Whatmann paper.

2.3.3 Western Blotting

Proteins separated by SDS-PAGE were transferred from a polyacrylamide gel to a methanol-activated Immobilon-PVDF membrane using a Mini Trans-Blot cell wet chambers (Biorad, Munich). Western blotting was carried out as described previously (Sambrook and Russell, 2001) with following modifications: Protein transfer was conducted at 4°C for 12 h at 40 V, the membrane was rinsed in methanol and air dried at RT. After transfer, the gel was Coomassie blue stained to determine the blotting efficiency. For protein detection, the membrane was activated by soaking it in methanol again, washed twice for 5 min in 1 x PBS-T and blocked with 5% (w/v) milk in 1 x PBS-T for 1 h at RT on a shaker. Subsequently, the membrane was incubated with the primary antibody dissolved in blocking buffer overnight at 4°C and washed 4 times for 10 min at RT with 1 x PBS-T.

Primary antibody	Dilution (WB)	Primary antibody	Dilution (WB)
chicken α-DOM-B 35	1:500	rabbit α-H2A	1:500
chicken α-DOM-B 36	1:500	mouse α-FLAG	1:5000
chicken α-DOM-B 37	1:500	mouse α-GFP	1:5000
chicken α-DOM-B 38	1:500	rabbit α-MRG15	1:3000
rat α-DOM-B 2G5	1:2	rabbit α-TIP60	1:3000
rat α-DOM-B 2F4	1:2	rabbit α-GAS41	1:3000
rat α-DOM-B 3H1	1:2	rabbit α-ING3	1:3000
rat α-DOM-B 8B8	1:2	rabbit α-TRA1	1:1500
rat α-ACF1 8E3	1:50	rabbit α-INO80	1:1000
rabbit α-ISWI	1:5000	rabbit α-Pontin	1:500
rabbit α-H2AV	1:400	rabbit α-Reptin	1:500

Table 2.2: Primary antibodies and their dilution used in this study for Western blot analyses

HRP (horse radish peroxidase) conjugated secondary antibodies were incubated in blocking buffer or 1 x PBS-T for one hour at RT. Afterwards, the membrane was washed 5 times with 1 x PBS-T. All secondary antibodies (see 2.1.3) were diluted 1:10000. Proteins were detected by chemoluminescence using the GE Healthcare ECL detection system according to the manufacturer's instructions (GE Healthcare, Munich). Signals were exposed between 1 and 60 min to x-ray films (medical X-ray Super RX, Fuji, USA) and developed in a developing machine (AGFA curix 60, Mortsel, Belgium).

2.3.4 Bacterial Expression and Purification of GST- and FLAG-Tagged DOM-B Proteins

2.3.4.1 Induction of Protein Expression

For a purification of DOM-B proteins via the glutathione sepharose (GST) and/or FLAG-tag, pGEX-GST-DOM-B WT-FLAG plasmid, pGEX-GST-DOM-B KR-FLAG plasmid and all truncated versions of pGEX-GST-DOM-BΔ1-7-FLAG vectors were transformed into chemically competent BL21

Codon Plus *E. coli.* The cells were plated on agar plates containing 30 µg/µl kanamycine and 25 µg/µl chloramphenicol. A single colony was picked and inoculated o/n at 37°C in 10 ml LB (+ 30 µg/µl kanamycine, + 25 µg/µl chloramphenicol). This preculture was added to 200 ml LB (+ 30 µg/µl kanamycine, + 25 µg/µl chloramphenicol). Bacterial culture was grown at 37°C until the cells reached a density of OD_{600} = 0.45. Expression of DOM-B plasmids was induced for 3 h at 37°C by adding IPTG to a final concentration of 0.5 mM.

2.3.4.2 Preparation of Bacterial Cell Extract

Three hours after IPTG induction, bacterial cells were split in 50 ml aliquots and pelleted by centrifugation (20 min, 4000 rpm, 4°C, Eppendorf 5180R). Each pellet was resuspended in 5 ml cold 1 × PBS-T with freshly added protein inhibitors, transferred in a new 15 ml tube and frozen in liquid nitrogen. Pellets were stored at -80°C until preparation of cell extracts. Bacterial cell pellets were rapidly thawed and sonified in an ice water bath with a Digital Sonifier 250D (1 min, 40% amplitude, pulse 15 sec on / 30 sec off, Branson, Danbury, USA). All steps were performed on ice or at 4°C in presence of proteinase inhibitors. Cell debris and insoluble proteins were removed by centrifugation (30 min, 13000 rpm, 4°C, Eppendorf 5180R). The supernatant containing the soluble protein fraction was directly used for further protein purification.

2.3.4.3 Purification of GST-Tagged DOM-B Proteins from Bacterial Cell Extract

To purify the recombinant protein via the GST-tag, the supernatant – containing soluble proteins - was incubated with equilibrated Glutathion-Sepharose beads (GE Healthcare, Munich) for 2 h at 4°C on a rotating wheel. The GST-beads, corresponding to an amount of 150 µl per 500 ml culture, were equilibrated 3 times in 1.5 ml PBS-1%T. After binding to beads, the unbound fraction and the bound proteins were separated by centrifugation (5 min, 1000 rpm, 4°C). The supernatant was frozen in liquid nitrogen and stored at -80°C as a control. Beads were washed 3 times with 5 ml PBS-T for 10 min on a rotating wheel and subsequently transferred into a siliconized 1.5 ml tube. GST-beads were washed two times more in HEMG500 and two times in HEMG200 for each 5 min rotating. For an optimal elution of proteins from the Glutathion-Sepharose, beads were incubated for 2 h 1:1 with GST-elution buffer. The eluted proteins were separated from the Glutathion-Sepharose by centrifugation (2 min, 2000 rpm, 4°C) and rapidly frozen in liquid nitrogen for subsequent long-time storage at -80°C.

2.3.5 Expression and Purification of Recombinant Proteins in *Sf9* Cells

2.3.5.1 Cultivation of *Spodoptera Frugiperda* Cells

All solutions were warmed to RT before use. *Spodoptera frugiperda (Sf9)* cells were cultured in Sf-900 II medium (Gibco, Invitrogen, Karlsruhe) supplemented with 9 mg/ml gentamycine and 9% (v/v) fetal bovine serum. To determine the cell number, *Sf9* cells were counted in a hemacytometer and cultured in a density of 0.5 x 10^6 and 2.0 x 10^6 cells/ml. *Sf9* cells were grown in 1 l-spinner flasks in 100 - 300 ml medium at 27°C and were not cultured longer than 3 month.

2.3.5.2 Infection of *Sf9* Cells with Baculoviruses

Wildtype and mutated DOM-B, as well as truncated DOM-B proteins with a C-terminal FLAG-tag were expressed in *Sf9* cells using the baculovirus system. All recombinant baculoviruses were generated within this study using pFastBac1 vectors (*see* 2.1.5) and the Bac-to-Bac expression system (Invitrogen, Karlsruhe). Amplification and maintenance of viruses was performed according to the manufacture's instructions (Invitrogen, Karlsruhe). For an infection, 15 cm round Petri dishes were prepared with 1.2 x 10^7 *Sf9* cells per dish covered by 5 ml of Sf-900II medium (Gibco, Invitrogen, Karlsruhe), complemented with 9% (v/v) fetal bovine serum and gently rocked for 1 h at RT followed by addition of 20 ml fresh medium. Cells were infected with a discrete amount of each baculovirus, which was previously determined in advance by virus titration and in test expression studies. In addition, cells were also infected with viruses carrying constructs of FLAG-ISWI and ACF1-FLAG or coinfected with untagged ACF1 and ISWI to produce recombinant DOM-B complexes or ACF. Protein expression was allowed for 48 h - 72 h at 27°C.

2.3.5.3 Preparation of *Sf9* Cell Extract

After incubation with baculoviruses, *Sf9* cells were harvested using a cell scratcher and washed once by removing the medium and replacing it with 5 ml of cold PBS. Cells were pelleted by centrifugation (10 min, 900 rpm in a Heraeus Megafuge 2.0) and resuspended in 800 µl HEMG500 per dish. The cell suspension was frozen in liquid nitrogen and stored at -80°C until preparation of cell extracts.

2.3.5.4 Purification of FLAG-Tagged DOM-B Proteins from *Sf9* Cell Extract

To purify the recombinant proteins, frozen cells were rapidly thawed at 37°C, immediately sonicated in an ice water bath (10 sec, 50% amplitude, Digital Sonifier 250D, Branson, Danbury, USA) and centrifuged (30 min, 13000 rpm, at 4°C, Eppendorf 5180R) to clear the whole cell extract from cell debris. The supernatant was transferred into a fresh siliconized tube. From now on, all steps were performed on ice or at 4°C in the presence of proteinase inhibitors. Anti-FLAG M2 agarose beads were equilibrated 3 × in 1.5 ml HEMG500 and added to the supernatant. The amount of added beads corresponds to 10 µl per Petri dish. Binding of the tagged proteins to the FLAG beads was allowed for 3 h on a rotating wheel at 4°C. After this incubation, the tubes were centrifuged (2 min, 13000 rpm, at 4°C, Eppendorf 5180R) and the supernatant, containing the unbound fraction, was removed or frozen in liquid nitrogen and stored at -80°C. Beads were washed 5 × with 1.5 ml HEMG500 for 10 min and 2 × with HEMG200 for 10 min on a rotating wheel. Proteins were eluted for 2 h in an appropriate volume (ca. 25 µl/plate) of HEMG200 containing 0.5 mg/ml FLAG-peptide. The eluted proteins were separated from FLAG-beads by centrifugation, rapidly frozen in small aliquots (10 - 20 µl) in liquid nitrogen and finally stored at -80°C (modified after Eberharter et al., 2004a).

2.3.6 Purification of DOM-B from *Drosophila* Embryos

2.3.6.1 Harvesting of *Drosophila* Embryos

Wildtype *Drosophila* embryos (either 0-90 min or o/n AED) were collected on apple juice-agar plates. For harvesting precisely staged embryos, *Drosophila* embryos were collected 3 h AED and aged outside of the fly culture cages at 25°C for additional 3 h, 6 h, 9 h, 12 h and 15 h, respectively. Four successive collections were rinsed with tap water into sieves and allowed to settle into EW on ice to arrest further development. After the pooled embryo collection had settled, cold EW was replaced by warm EW (at RT), adjusted to a volume of 200 ml. To dechorionate embryos, 60 ml of 13% hypochlorite were added and the embryos were stirred for 3 min on a magnetic stirrer. After dechorionation, embryos were poured into a steel sieve (mesh size 125 µm) and rinsed with running tap water for 5 min. To remove the chorions, 200 ml wash buffer was added and embryos were allowed to settle. The supernatant containing chorions and not dechorionated embryos was removed and discarded. The volume of the successfully dechorionated embryos was estimated. Embryos were directly used for large scale nuclear extract preparation (TRAX) or frozen in liquid nitrogen and stored at -80°C.

2.3.6.2 Large Scale Preparation of *Drosophila* Embryo Nuclear Extract (TRAX)

About 200 g dechorionated embryos were subsequently washed in cold 0.7% w/v NaCl and in embryo buffer 1 (EB1) for 15 min on ice. All successive steps were carried out at 4°C. The supernatant was removed, and the embryos were resuspended in 2 ml/g embryos of EB1. Embryo solution was poured into a homogenizer (Yamato, LH 21) and homogenized with a single pass at 1000 rpm. The homogenate was filtered through a single layer of miracloth and filled with EB1 to a final concentration of 5 ml/g embryo. Embryo nuclei were pelleted by centrifugation for 15 min at 8000 rpm in a Sorvall SS34 rotor. The supernatant was carefully decanted and remaining white lipids were removed from the tube wall. The pellet was resuspended in 1 ml/g embryos of EB2. The volume of the isolated nuclei was estimated and the nuclei suspension precipitated by adding 1/10 volume of 4 M $(NH_4)_2SO_4$ (at RT). The mixture was rotated on a wheel for 20 min followed by centrifugation (2 h, 35000 rpm, Ti-45, ultracentrifuge). The supernatant was collected with a pipette, avoiding the floating layer of lipids and the pellet and precipitated again. For each ml of supernatant, 0.3 g finely grounded powder of $(NH_4)_2SO_4$ was added stepwise under constant stirring. After centrifugation (20 min, 15000 rpm, 4°C, Sorvall SS34) the resulting pellet was resuspended in 0.2 ml/g of EB3 and dialysed against 2 l of this buffer for about 4 h. The nuclear extract was centrifuged once more (5 min, 9000 rpm, Sorvall SS34). The supernatant of this centrifugation step, that we refer to as *Drosophila* embryo nuclear extract (TRAX) was collected and frozen in liquid nitrogen (modified from Nightingale et al., 1998).

2.3.6.3 Purification of DOM-B Proteins from TRAX by Ion Exchange Chromatography

Chromatography procedures were carried out at 4°C; all solutions were filtered (0.22 µm pore size) and chilled to 4°C. *Drosophila* embryo nuclei extract (TRAX prepared from 200 g of 0-15 h embryos) was fractionated on a Q-Sepharose column equilibrated in HEMG100. The flow-through was subsequently fractionated on a SP-Sepharose column equilibrated in HEMG100. The 0.5 M KCl eluate of the SP-Sepharose column was dialysed against an excess of HEMG100 and processed on a Mono Q HR 5/5 column washed with HEMG100. Bound material was eluted with a linear gradient from HEMG100 to HEMG1000 at a flow-rate of 0.5 ml/min in 0.5 ml fractions. Peak fractions were pooled, concentrated in Microsep 10K Omega centrifugal devices and applied to a Superose 6 HR 10/30 size exclusion column processed in HEMG250. Alternatively, the 0.5 M KCl eluate of the Q-Sepharose column was dialysed against an excess of HEMG100 and loaded directly onto a Mono Q HR 5/5 column. The column was washed with HEMG100 and proteins were eluted with a gradient from HEMG 100 to HEMG1000 at a flow-rate of 0.5 ml/min. 0.5 ml fractions were pooled, concentrated in Microsep 10K Omega centrifugal devices and also applied to a Superose 6 HR 10/30 size exclusion column in HEMG250 with a flow-rate of 0.2 ml/min. Collected fractions were frozen in liquid nitrogen and stored at -80°C. Fractions were analyzed by SDS-PAGE and determined by Western blotting (modified from Eberharter et al., 2001).

2.3.6.4 Superose 6 Gel Filtration Analysis of DOM-B, ACF1 and ISWI from TRAX

DOM-B, ACF1 and ISWI were analyzed by gel filtration using a Superose 6 HR 10/30 size exclusion column. Purified nuclear extract prepared from 0-2 h AED embryos and 0-16 h AED embryos were loaded onto the Superose 6 HR 10/30 column equilibrated in HEMG250. 0.5 ml fractions were collected at a flow-rate of 0.2 ml/min. Samples were subjected by SDS-PAGE and analyzed by subsequent Western blotting.

2.3.6.5 Small Scale Preparation of Nuclear Extract from *Drosophila* Embryos

Small scale preparation of nuclear extract was used to isolate and analyze nuclear proteins from transgenic fly lines. For that, 3-10 d old flies hatched from 6-8 bottles (10 cm height, 5 cm diameter) were pooled in cylindrical embryo collection cages (10 cm height and 9 cm diameter). Fly cages were covered on one side by a fine metal mesh to maintain the fly culture under a constant air circulation and on the other side by agar plates (9 cm diameter) with a fresh streak of yeast paste. Flies were kept at 25°C. Embryos layed on plates were rinsed into a small sieve (mesh size 125 μm) with PBS. After washing with 3 ml NB / 0.3 M sucrose the volume of settled embryos was estimated. From now on, all solutions were prechilled at 4°C and procedures were carried out on ice. The embryos were homogenized in 3 volumes of NB / 0.3 M sucrose without prior dechorionation in a 1.5 ml reaction tube with a pestle fitting these tubes (micro pistill, Kontes, New Jersey). Larger volumes of embryos were homogenized in a 5 ml glass homogenizer (B. Braun, Melsungen). 100 μl of the homogenate were loaded onto prepared Miracloth mesh clipped by the lid of the 1.5 ml reaction tubes. These reaction tubes were prepared as follows: The inner part of the lid of the tube was cut out and 400 μl of NB / 1.7 M sucrose were added and overlaid by 400 μl of NB / 0.8 M sucrose. A small piece of Miracloth was pinned in between the tube and the lid to cover the opening. By spinning these tubes for 5 sec, the extract was filtered through the mesh. This step was repeated four times to load a total volume of 400 μl of homogenate per tube. After centrifugation (10 min, 13000 rpm, 4°C) in a table-top centrifuge, the nuclei formed a white pellet. Lipids, cell debris, and cytosol were retained at different solution interfaces. Nuclei were taken out of the tube with a pipette tip penetrating the sucrose layers and pooled in a fresh tube containing 500 μl NB / 0.3 M sucrose. The nuclear extracts were washed and pelleted once more by centrifugation (5 min, 5000 rpm) and the supernatant was removed. For SDS-PAGE and/or Westernblot analysis one volume of 1 x Laemmli buffer was added, nuclei were solubilised and denatured at 96°C for 8 min (Quivy and Becker, 1997).

2.4 ATPase assay

To measure the ATPase activity of chromatin remodeling enzymes, approximately 10 pmol of the appropriate remodeler were mixed with 150 ng chromatinized DNA or 1 μg of recombinant histone octamers using tips preblocked with 20 mg/ml BSA (98% PURE). Recombinant histones H2A and H2AV were kindly provided by Dr. Verena Maier (Adolf- Butenandt-Institute, Munich, Germany). Histones were purified as described (Huynh et al., 2005). 10 μl ATPase buffer with × μl ddH_2O were added to a total volume of 29 μl. The ATPase assay was started by adding 1 μl of 0.3 mM unlabelled ATP spiked 1:200 with γ-^{32}P-ATP (5.55 GBq/ml, 150 mCi/mol) in 3 mM $MnCl_2$ and inbubated at 26°C for 1 h. After the incubation, 1 μl of the reaction was spotted onto a TLC plate (polyethyleneimine cellulose on polyester; Merck) (10 cm x 20 cm). The plate was dried for 5 min at RT and the edge near the samples was placed about 0.7 cm into a solution of 0.5 M LiCl and 1 M formic acid avoiding direct touch of sample-spots with liquid. The buffer was allowed to migrate upwards until it reached the top of the plate. Plates were dried for 5 min at 68°C and exposed to a phosphoimager screen for 20 min. The radioactive signals corresponding to hydrolyzed phosphate and non-hydrolyzed ATP were quantified by a Phosphoimager. The two species could be distinguished by their different mobility, which is higher for the phosphate. The percentage of hydrolysed ATP was calculated by using AIDA Image Analyzer software (modified after Eberharter et al., 2001).

2.5 Generation of New Antibodies

To generate polyclonal DOM-B antibodies, GST-DOM Δ3-FLAG and GST-DOM Δ7-FLAG proteins, respectively, were expressed in *E.coli* and purified on Glutathion-Sepharose beads. 130 µl of each elution were mixed with 25 µl loading dye (6×) and denatured at 96°C for 10 min. 155 µl of samples were loaded on a preparative 6% SDS-PAGE. After electrophoresis and Coomassie blue staining, gel slices were sent to a company (Eurogentec, Netherlands) to generate new DOM-B antibodies. For each construct, two hens were immunized. The egg-yolks, which were delivered by the company, were purified with a purification kit (EGGstract IgY purification kit, Promega, Mannheim) according to the manufacture's instruction. The polyclonal antibodies Ch35 and Ch36, specific for DOM-B, and Ch37 and Ch38, specific for DOM-A and B, were tested in Western blot and immunofluorescence analysis.

The monoclonal rat antibody 8B8 specific for DOM-B was raised against the peptide-sequence KKAPRTESTPKC (C was used for KLH coupling of peptide) at the C-terminus of DOM-B. The monoclonal rat antibodies 3H1, 2F4 and 2G5 specific for DOM-B were raised against the recombinant DOM Δ7-FLAG expressed and purified from *Sf9* cells. These antibodies (8B8, 3H1, 2F4 and 2G5) were generated in collaboration with Dr. Elisabeth Kremmer (Helmholz Zentrum, Munich, Germany) and tested in Western blot as well as in immunofluorescence experiments.

Another polyclonal rabbit antibody used in this study is specific for the histone variant H2AV, designed by Dr. Anton Eberharter (Adolf-Butenandt-Institute, Munich, Germany) and generated by Eurogentec (Netherlands). This H2AV-antibody was raised against the peptide-sequence QDPQRKGNVILC (C was used for KLH coupling of peptide) at the C-terminus of H2AV and tested in Western blot and in immunofluorescence experiments.

2.6 General Methods for Working with *Drosophila*

2.6.1 Fly Maintenance

Flies were maintained at 18°C in incubators (Percival, Plant Climatics, Wertingen) and flipped every 3-4 weeks in small vials (Buddeberg, Mannheim) or larger bottles (Greiner Bio-one, Frickenhausen). Vials and bottles were freshly filled with fly food and covered by rubber foam-stoppers (Klühspies, Retzstadt). Wildtype *Drosophila melanogaster* were grown and maintained in a separate humid room at 25°C.

2.6.2 Microinjection of *Drosophila* Embryos for P-Element-Mediated Germline Transformation

For P-element-mediated germline transformation, the fly strain *y[1]w[1118]* (*yw*)- homozygous for the mutant *white*$^-$ gene (http://flybase.bio.indiana.edu) - was used as a "host" strain. These flies have white eyes. *White*$^+$ served as a marker for a successful transformation. Transformants were detected by their coloured eyes as 3-10 d old *yw* flies hatched from 6-8 bottles (10 cm height, 5 cm diameter) were pooled in cylindrical embryo collection cages (10 cm height and 9 cm) with fresh agar plates. Embryos not older than stage 2 were collected every 30 min with a wet brush and transferred onto an 18 x 18 mm coverslip previously immobilized with a drop of water on a microscope slide. The edge of the coverslip was in parallel to the edge of the slide. 98-120 embryos were lined up vertically and in 3 mm distance to the left edge of the coverslip. The embryos were orientated with the posterior pole pointing to the left edge by using a fine brush within maximum 15 min. Lined embryos were covered with a drop of halocarbon oil (ATofina Voltalef 10S, Lehmann & Voss & Co.) to get transparent after 2-4 min incubation. The slide was moved under a phase contrast microscope (ICS Standard25, Zeiss) and the tip of a prepared needle was brought as close as possible to the first embryo. The quality of needles for microinjection of *Drosophila* embryos were critical for high through-put and prepared as follows: A borosilicate capillary with omega dot fiber 1.0 mm OD (Kwik-Fil, USA) was fixed in a horizontal needle puller (Sutter brand series). Suitable capillaries were pooled (heat: 850, pull: 45, vel: 34, time: 39) and loaded with DNA. The needle was fixed in a needle holder and connected to an air-pressure injecting device (Narishige IM-300 Microinjector). The needle tip was opened by breaking the tip carefully at the edge of a slide. Best results were obtained with a leaky needle continuously dropping a small amount of DNA. Further adjustments were made by either changing the injection time (10 - 40 ms) or by the pressure apply of the air-pressure injecting device. The slide on the microscope stage was moved with a micromanipulator until the first embryo to be injected was positioned to the left of the vision-field. The tip of the needle was brought into the focal plane of the embryo. All further movements were done only with the micromanipulator of the microscope while the needle was fixed to the holder. The first embryo was gently impaled onto the needle tip. Subsequently the embryo was injected with the red stained DNA droplet diffusing into the embryo body near the pole cells. After injection, the needle was moved out of the embryo in a quick but gentle motion, before poking the next embryo. Embryos were injected between 10 and maximum 15 min after line-up. Embryos older than stage 2 were recognized under the microscope by their darker appearance. These embryos were destroyed. Most of the oil on the coverslip was removed by gravity flow. Afterwards, the coverslip was transferred into a small food vial, placing the edge with the embryos against the food. Embryos were kept at 18˚C until adults hatched. For each construct about 300-800 embryos were microinjected with a success rate of 10-20% hatching tansformants.

2.6.3 Screening and Mapping Chromosomal Insertion Sites of Transgenes

To obtain transformants, adult flies (P0) from microinjected embryos were collected and separated according to their sex. All integrated P-elements of this P0-generation are still restricted to the germ cells (10-20%). To screen for inserted P-element transgenes, adult flies were back-crossed to *yw* flies, homozygous for the mutant *white*$^-$ gene. Each male was crossed to 3-4 virgin *yw* females and each female to 2 *yw* males. Crosses were performed in separate vials named with a letter (A-Z) at 25°C until offspring (F1) hatched. The adult offspring (F1) generation was screened for transformants using *white*$^+$ as a marker. Transformants were identified by their colored eyes and named with a number (1-100). To determine on which *Drosophila* chromosome the P-element was integrated, the F1 generation was mapped by crossing them to several *balancer* lines. P-elements integrated on the first chromosome were verified with *Y mof'/FM; p[81]-2/+* line (Matthias Prestel, Adolf-Butenandt-Institute, Munich, Germany); transgenes on the second chromosome with *yw; bcg/cyo* (http://flybase.bio.indiana.edu) and transgenes integrated on the third chromosome with *TM3/TM6* (http://flybase.

bio.indiana.edu) flies. Heterozygote flies were finally crossed to siblings to obtain homozygous stocks. Transgenic fly lines, which could not kept homozygous were maintained as heterozygotes with an appropriate *balancer* strain. All fly crosses were maintained at 25°C in humid chambers (RU/Med, Rubarth Apparate GmbH, Laatzen).

2.6.4 Novel Established Transgenic Fly Lines

All transgenic fly lines for DOM-B WT-FLAG and DOM-B KR-FLAG generated by P-element-mediated germline transformation are listed below (Table 2.3).

pUAS-DOM-B WT - FLAG	
Genotype	**Integration**
*yw; DOM-B WT -**A1**/ TM3*	
*yw; DOM-B WT -**A2**/TM3*	
*yw; DOM-B WT -**A3**/ TM3/6*	
*yw; DOM-B WT -**A5**/TM3*	
*yw; DOM-B WT -**A7**/ cyo*	
*yw; DOM-B WT -**A8**/ TM6*	
*yw; DOM-B WT -**A9**/cyo*	
*yw; DOM-B WT -**A11***	on III. Chr.
*yw; DOM-B WT -**B1**/ TM6*	
*yw; DOM-B WT -**B2**/ TM3/6*	
*yw; DOM-B WT -**B4***	on II. Chr.
*yw; DOM-B WT -**B5**/ TM3*	
*yw; DOM-B WT -**B6**/ cyo*	
*yw; DOM-B WT -**C1***	on III. Chr.
*yw; DOM-B WT -**C2**/ TM3/6*	
*yw; DOM-B WT -**C3**/ TM6*	
*yw; DOM-B WT -**C4**/ TM3*	
*yw; DOM-B WT -**C6**/ TM3/6*	
*yw; DOM-B WT -**C7**/TM6*	
*yw; DOM-B WT -**C8**/ TM3*	
*yw; DOM-B WT -**C9**/ TM6*	
*yw; DOM-B WT -**C10**/TM6*	
*yw; DOM-B WT -**C11**/ TM6*	
*yw; DOM-B WT -**C15**/ TM6*	
*yw; DOM-B WT -**C16**/ TM3/6*	
*yw; DOM-B WT -**C17**/ TM6*	
*yw; DOM-B WT -**C18**/ TM3*	
*yw; DOM-B WT -**C19**/ TM3*	
*yw; DOM-B WT -**C20**/ TM*	
*yw, DOM-B WT –**S1***	on I. Chr.

pUAS-DOM-B KR – FLAG	
Genotype	**Integration**
*yw, DOM-B KR -**A1***	on I. Chr.
*yw, DOM-B KR -**A2***	on I. Chr.
*yw; DOM-B KR -**B1**/bcg*	
*yw; DOM-B KR -**B2**/ cyo*	
*yw; DOM-B KR -**B3**/ cyo*	
*yw, DOM-B KR -**B5***	on I. Chr.
*yw; DOM-B KR -**B6***	on III. Chr.
*yw; DOM-B KR -**C1**/ cyo*	
*yw; DOM-B KR -**C2**/ cyo*	
*yw; DOM-B KR -**C3**/ cyo*	
*yw; DOM-B KR -**C4**/ cyo*	
*yw; DOM-B KR -**C5**/ cyo*	
*yw; DOM-B KR -**C6***	on II. Chr.
*yw; DOM-B KR -**C7***	on II. Chr.
*yw; DOM-B KR -**C8**/ cyo*	
*yw; DOM-B KR -**C9**/ cyo*	
*yw; DOM-B KR -**D1**/ bcg*	
*yw; DOM-B KR -**E1**/ TM3*	
*yw; DOM-B KR -**G1**/ TM3*	
*yw; DOM-B KR -**G2**/ TM3*	
*yw; DOM-B KR -**G3**/ bcg*	
*yw; DOM-B KR -**G4***	on III. Chr.
*yw; DOM-B KR -**G6**/ TM3*	
*yw; DOM-B KR -**G7***	on III. Chr.
*yw; DOM-B KR -**G8**/ TM6*	
*yw; DOM-B KR -**G10***	on III. Chr.
*yw, DOM-B KR -**G11***	on I. Chr.
*yw, DOM-B KR -**G12***	on I. Chr.
*yw, DOM-B KR -**H1***	on I. Chr.
*yw; DOM-B KR -**H2**/ cyo*	
*yw; DOM-B KR -**H4***	on III. Chr.
*yw; DOM-B KR -**H5***	on III. Chr.
*yw, DOM-B KR -**H6***	on I. Chr.
*yw; DOM-B KR -**H7**/ FM*	
*yw; DOM-B KR -**H8**/ cyo*	
*yw; DOM-B KR -**H9***	
*yw; DOM-B KR -**I1**/ TM3*	
*yw; DOM-B KR -**J1**/ cyo*	
*yw; DOM-B KR -**J2***	on II. Chr.
*yw; DOM-B KR -**K1**/ TM3*	
*yw, DOM-B KR -**L1***	on I. Chr.
*yw, DOM-B KR -**L2***	on I. Chr.
*yw; DOM-B KR -**L3**/ FM*	

Table 2.3: Novel established transgenic fly lines for *UAS-DOM-B WT-FLAG* and *UAS-DOM-B KR-FLAG*

A further transgenic fly line used in this study is *yw, ACF1-D2; +/+; +/+* kindly provided by Dr. Mariacristina Chioda (Chioda et al., 2010). To study RNA interference (RNAi)-mediated targeted depletion, transgenic flies carrying inverted repeats (IR) of *domino* (VDRC stock nr 7787), *acf1* (VDRC stock nr 33447) or *h2av* (VDRC stock nr 12768) under the control of an UAS (upstream activating) sequence were obtained from the Vienna *Drosophila* RNAi Centre (VDRC, Vienna, Austria). These flies are referred to as *UAS-IR* fly lines.

2.6.5 Fly Crosses

For *in vivo* analyses of DOM-B WT-FLAG or DOM-B KR-FLAG, homozygous transgenic fly lines bearing the transgene on different chromosomes were chosen (*see* Table 2.3). Most studies for DOM-B WT were performed with *yw; DOM-B WT-B4-FLAG*; +/+ or *yw; +/+; DOM-B WT-A11-FLAG* and for DOM-B KR with *yw, DOM-B KR-H6-FLAG; +/+; +/+*, *yw; DOM-B KR-J2-FLAG, +/+* or *yw; +/+; DOM-B KR-G10-FLAG*. Ectopic expression or targeted depletion was induced with the well established *UAS-GAL4* system. This strategy made use of various *GAL4* “driver” lines, which direct the ectopic expression or depletion of certain proteins in a developmental and tissue-specific manner. For ectopic expression or depletion in salivary glands homozygous *UAS-DOM-B WT/KR-FLAG* fly lines or *UAS-IR* strains were crossed to *yw; [w+, GAL4*^{2314}*]* (*sgs3-GAL4*) at 28°C (Isogai et al., 2007). To induce expression or depletion in eye discs, *UAS*-fly lines were crossed to an eye-specific GAL4 driver line homozygote with the following genotype [*yw; eye-GAL4, GFP*] (*eye-GAL4*) on the third chromosome (Schmitt et al., 2005). For expression or depletion behind the morphogenetic furrow the fly line [*w[*]; P(w[+mC]=GAL4-ninaE.GMR)12*] (*glass-GAL4*) (Bloomington nr 1104) on the second chromosome was obtained from the Bloomington *Drosophila* stock center (BDSC, Indiana, USA). These crosses were maintained at 25°C, avoiding phenotypic abnormalities in offspring of control crosses. To drive the expression of DOM-B in female ovaries, homozygous *UAS*-fly lines were crossed to germline specific transgenic flies (*vasa-GAL4*) homozygote on the third chromosome, kindly provided by Sandy Mietzsch (Martin-Luther-University Halle-Wittenberg, Germany). Virgin female progeny of this cross was crossed for 3-6 days again to *UAS-vasa* males to induce DOM-B WT or KR expression in their ovaries carried out at 28°C. As control, a fly line carrying the *UAS-LacZ-mini white* construct, which can express the *β-galactosidase* (*lacZ*) gene in response to *GAL4* induction (Zink and Paro, 1995) was crossed to the same *GAL4-driver* lines.

2.7 *In Vivo* Analysis of *Drosophila* Transgenic Fly Lines

2.7.1 Ectopic Expression of DOM-B in Adult Fly Ovaries

2.7.1.1 Preparation of Adult Fly Ovaries

3-6 d old F1 female flies (*see* above 2.6.5) were anaesthetized using a stream of carbon dioxide. Flies were submerged into 1 × PBS in a glass jar with a pair of tweezers and grabbed at the lower thorax. The lower abdomen was tugged gently and a pair of ovaries was dissected. Ovaries were cleaned from other organs and transferred into a new glass jar filled with 1 × PBS while dissecting next flies.

For Western blot detection, 5-8 ovaries were transferred with a glass pipette in a 1.5 ml tube and PBS was removed. The ovaries were immediately frozen in liquid nitrogen until preparation of Western blot detection. For immunofluorescence staining, 5-8 ovaries were opened on one side with forceps to separate the ovariols, transferred with a glass pipette in a 1.5 ml tube and stored on ice until fixation.

2.7.1.2 Ovary Extract Preparation and Quantitative Western Blotting

Frozen ovaries were grained while still frozen and immediately dissolved in Laemmli buffer (preheated at 98°C). Samples were denatured for 10 min at 98°C and loaded on a 6% or 15% SDS-PAGE gel. Gels were transferred on Immobilon P membrane (Millipore, Massachusetts) and processed for immunodetection as described in the following.

2.7.1.3 Immunofluorescence Staining and Analysis of Fly Ovaries

All steps for staining *Drosophila* ovaries were performed at RT. Opened ovaries were fixed in 500 µl 3.7% para-formaldehyde (PFA) in 1 × PBS without detergent by rocking gently for 20 min.

Primary antibody	Dilution (IF)	Secondary antibody	Dilution (IF)
chicken α-DOM-B Ch35	1:250	α-chicken Alexa 488	1:300
rat α-DOM-B 2G5	1:2	α-rat Rhod. Red-X	1:250
rat α-ACF1 8E3	1:2	α-rat Rhod. Red-X	1:250
rabbit α-ISWI	1:100	α-rat Rhod. Red-X	1:250
rabbit α-H2AV	1:200	α-rabbit Alexa 488	1:300
rabbit α-ɣ-H2AV	1:100	α-rabbit Alexa 488	1:300

Table 2.4: Dilutions of primary antibodies and their appropriate secondary antibodies
Antibodies were used in immunofluorescence (IF) analyses of ovaries. Further details about the antibodies are listed above (Chapter 2.1.3).

To remove the PFA, discs were shortly rinsed and twice washed in 1 × PBS with 0.1% Triton (1 ml) for 20 min on a rotating wheel. The tissues were then extracted in 1 × PBS with 1% Triton (1 ml) for 90 min and afterwards blocked in 600 µl blocking buffer (1 × PBS, 0.1% Triton, 5% NGS) for 1 h on a rotating wheel. The blocking solution was carefully removed and two primary antibodies (*see* Table 2.4), diluted in 200 µl blocking buffer, were added and incubated o/n on a rotating wheel. Ovaries were washed 3 × for 15 min in 1 ml 1 × PBS-0.1% Triton. Appropriate secondary antibodies conjugated with Alexa 488 (Invitrogen, Karlsuhe) or Rhodamin Red-X (Dianova, Hamburg) were diluted in 250 µl blocking buffer and added to the samples for 2 h while rotating.Afterwards, the tissues were washed 3 × in 1 ml 1 × PBS-0.1% Triton for 10 min and DNA was stained with 500 µl of 1 µM TO-PRO3 (Molecular Probes, Invitrogen, Karlsruhe) in PBS for 10 min. DNA counterstaining was removed by washing the tissues twice with 1 ml 1 × PBS-0.1% Triton for 5 min. Ovaries were then rinsed with 1 × PBS without detergent and after removing PBS, incubated in Vectashield mounting medium (Vector Labs, U.K.) o/n at 4°C. Subsequently, tissues were transferred on slides (Roth, Karlsruhe) and mounted by separating the ovariols under a binocular microscope (Stemi 2000, Carl Zeiss, Jena). Images were acquired with a Zeiss LSM 510 META confocal microscope (Carl Zeiss, Jena) equipped with an Ar- and two He- ion lasers and imaged processed with Zeiss LSM 510 META Software.

2.7.2 Ectopic Expression of DOM-B in Larval Imaginal Discs and Salivary Glands

2.7.2.1 Preparation of Imaginal Discs and Salivary Glands

Wandering third instar larvae were dissected in 1 × PBS in a glass jar under a binocular microscope at RT. They were cut into two pieces and the anterior mouthpart was invaginated with forceps until the imaginal discs and a pair of salivary glands came outside. The inner part - now outside - was removed from larval fat body and gut. Imaginal discs and glands still attached to the cuticle were transferred with a glass pipette in a 1.5 ml reaction tube.

2.7.2.2 Immunofluorescence Analysis of Imaginal Discs and Salivary Glands

All steps for staining imaginal discs and salivary glands were performed at RT. Discs and glands, still attached to the larval cuticle, were fixed in 500 µl 3.7% PFA in 1 × PBS without detergent for 20 min. To remove the PFA, cuticles were rinsed and 3 times washed in 1 ml 1 × PBS with 0.3% Triton for 10 min on a rotating wheel. The tissues were blocked in 600 µl blocking buffer (1 × PBS, 0.1% Triton, 5% NGS) for 1 h on a rotating wheel. The blocking solution was carefully removed and two primary antibodies diluted in 200 µl blocking buffer were added and incubated o/n on a rotating wheel (*see* Table 2.5). The imaginal discs and salivary glands were washed 4 × for 15 min in 1 ml 1 × PBS-0.3% Triton. Appropriate secondary antibodies conjugated with Alexa 488 (Invitrogen, Karlsruhe) or Rhodamin Red-X (Dianova, Hamburg) were diluted in 250 µl blocking buffer and added to the samples. After 1 h incubation on a rotating wheel, tissues were washed 4 × in 1 ml 1 × PBS-0.3% Triton for 15 min and rinsed once in 1 ml 1 × PBS-0.1% Tween 20 for 5 min.

Primary antibody	Dilution (IF)	Secondary antibody	Dilution (IF)
chicken α-DOM-B 35	1:200	α-chicken Alexa 488	1:300
rat α-DOM-B 2G5	1:2	α-rat Rhod. Red-X	1:250
rat α-ACF1 8E3	1:2	α-rat Rhod. Red-X	1:250
rabbit α-ISWI	1:100	α-rabbit Rhod. Red-X	1:250
rabbit α-H2AV	1:200	α-rabbit Alexa 488	1:300
rabbit α-Caspase	1:100	α-rabbit Alexa 488	1:300
mouse α-HP1	1:100	α-mouse Rhod. Red-X	1:250
mouse α-Elav	1:100	α-mouse Alexa 488	1:300
mouse α-DAC	1:100	α-mouse Alexa 488	1:300
mouse α-Lamin	1:20	α-mouse Alexa 488	1:300
guinea pig α-PW35	1:500	α-guinea pig Alexa 488	1:400

Table 2.5: Dilutions of primary antibodies and their appropriate secondary antibodies
Antibodies were used in immunofluorescence (IF) analyses of larval imaginal discs and salivary glands. Further details about the antibodies are listed above (Chapter 2.1.3).

DNA counterstaining was performed with 500 µl of 1 µM TO-PRO3 in PBS for 10 min and removed by washing the tissues 2 × with 1 ml 1 × PBS-0.1% Tween 20 for 5 min. PBS-Tween was replaced by 200 µl 1×PBS without detergent. 4-6 cuticles per sample were transferred onto one slide. Under a binocular microscope imaginal eye discs or salivary glands were separated from the cuticle and mounted with Vectashield mounting medium (Vector Labs). Images were acquired with a Zeiss LSM 510 META confocal microscope equipped with an Ar- and two He- ion lasers and imaged processed with Zeiss LSM 510 META Software (Chioda et al, 2010).

2.7.2.3 BrdU Labeling of Imaginal Eye-Antenna Discs

Imaginal discs were dissected in PBS from wandering third instar larvae as described above. Cuticles with imaginal discs were incubated in PBS, containing 150 µg/ml 5'-Bromo-2-deoxyuridine (BrdU, Sigma, Taufkirchen) for 10 and 30 min. After BrdU incorporation the tissues were fixed in 5% PFA in PBS for 30 min at RT. To denature the DNA, discs were incubated in freshly prepared 3 M HCl for 30 min. Afterwards, the samples were neutralized by rinsing 3 × in PBS-0.3% Triton for 10 min. Blocking was performed for 1 h at RT in PBS with 0.1% Triton and 5% NGS on a rotating wheel. Blocking solution was carefully removed, replaced by primary antibodies diluted in 200 µl blocking buffer and samples were incubated o/n at 4°C. BrdU was detected with a mouse monoclonal α-BrdU antibody (clone IU-4, Accurate Chemicals, USA) diluted 1:100. Imaginal discs were then washed and incubated with appropriate secondary antibodies and a donkey α-mouse IgG conjugated with Alexa 488 (Invitrogen, Karlsruhe, 1:300) as described above (2.7.2.2). Imaginal eye-antenna discs were mounted with Vectashield mounting medium (Vector Labs, U.K.) and analyzed with a Zeiss LSM 510 META confocal microscope (Chioda et al. 2010).

3 RESULTS

IN VITRO ANALYSIS OF DOMINO B

3.1 Distinct DOM-B Complexes Exist in *Drosophila* Embryos

3.1.1 DOM-B Expression Is Developmentally Regulated in *Drosophila*

To date, the existence and composition of DOM-B containing multisubunit protein complexes remains to be elucidated. One approach was to analyze the developmental expression profile of DOM-B and to identify novel interaction partners thereof. Since the expression pattern of DOM-B during *Drosophila* embryogenesis had so far not been characterized, staged embryos (0-3 h, 3-6 h, 6-9 h, 9-12 h and 12-15 h AED) were collected to prepare nuclear protein extracts. These extracts were analyzed by SDS-PAGE and Western blotting using the polyclonal antibody Ch35 against DOM-B. (All DOM antibodies used in this study were tested in Western blot analysis (*see* Chapter 3.2) and characterized in immunofluorescence experiments explained in Chapter 3.7. DOM-B expression was found to be developmentally regulated (Figure 3.1). DOM-B specific signals were detected in protein extracts of early embryos (0-3 h AED, lane 1), which undergo the first nuclear divisions until the cellular blastoderm forms (*see* Chapter 1.4.2). During the subsequent gastrulation and germ-band extension of embryos between 3-9 h AED no significant DOM-B signal was observed (lanes 2 and 3); whereas between 9-15 h AED, when the segmentation starts to divide the embryo into 14 parasegments, a DOM-B signal was detected again (lanes 4 and 5).

Figure 3.1: DOM-B expression is developmentally regulated in *Drosophila* embryos
Small scale preparation of nuclear protein extracts from indicated developmental stages (0-3 h, 3-6 h, 6-9 h, 9-12 h, 12-15 h AED) were analyzed by SDS-PAGE and Western blotting. Equal volumes of nuclear extracts were tested for the presence of proteins indicated on the right. The size of marker proteins is shown left in kDa.

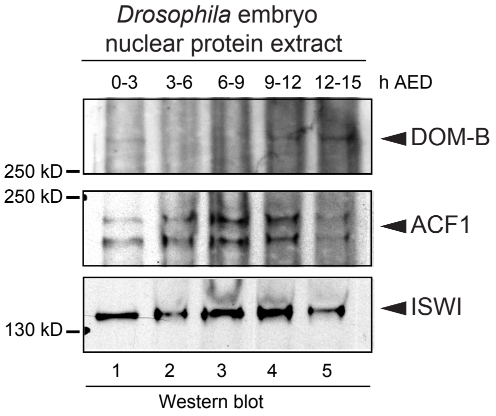

In addition, protein extracts were analyzed for the presence of other chromatin remodeling factors during embryonic development. For example, the chromatin remodeling factor ACF, consisting of ACF1 and the ATPase subunit ISWI, is known to be expressed in *Drosophila* embryos. In previous studies both proteins were found in protein extracts of 0-12 h AED and to a lesser extend in 12-15 h AED old *Drosophila* embryos (Elfring et al., 1994; Ito et al., 1999). According to these findings, nuclear protein extracts of indicated developmental stages were tested for the presence of ACF1 and ISWI proteins by Western blot analysis. ISWI signals were detected in all nuclear extracts, while ACF1 signals peaked between 6-12 h AED (Figure 3.1, lanes 3 and 4), which is in agreement with earlier findings (Elfring et al., 1994; Ito et al., 1999) .

The developmentally regulated expression of DOM-B during embryogenesis led to further analysis of its expression pattern also in context with other proteins like ACF1 and ISWI.

3.1.2 DOM-B Is Part of a High Molecular Weight Complex in *Drosophila* Embryos

Since the expression of DOM-B was different in early and late embryos, nuclear protein extracts from 0-2 h versus 0-16 h AED embryos were size-fractionated in 0.5 ml fractions by FPLC using a Superose 6 column in collaboration with Dr. Anton Eberharter (Adolf-Butenandt-Institute, Munich, Germany) (Figure 3.2). In preblastodermal embryos (0-2 h AED) DOM-B eluted in a single peak (fraction 14) corresponding to a molecular weight (MW) of approximately 2 MDa. ACF1 and ISWI signals were detected in fractions 14 and 18 - 26 and peaked in fractions 22–24 corresponding to a MW of 670 kDa (Figure 3.2.A). In 0-16 h AED embryos ACF1 cofractionated with ISWI in fractions 22-26 (Figure 3.2.B) corresponding to a MW of 670 kDa of the ACF complex in agreement with prior studies (Ito et al., 1999). Major differences between DOM-B and ACF in 0-16 h versus 0-2 h AED embryos were observed in fractions corresponding to a MW of 2 MDa: DOM-B was still detectable in fraction 14, while ACF1 was only observed in corresponding fractions from 0-2 h AED embryos (fraction 22-26).

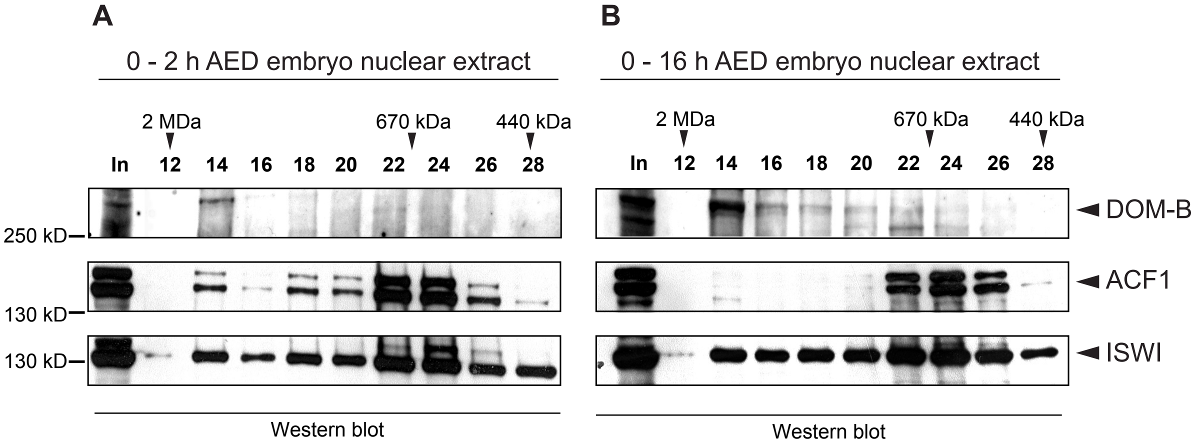
A
0 - 2 h AED embryo nuclear extract
2 MDa
670 kDa
440 kDa
In 12 14 16 18 20 22 24 26 28
250 kD
130 kD
130 kD
Western blot
B
0 - 16 h AED embryo nuclear extract
2 MDa
670 kDa
440 kDa
In 12 14 16 18 20 22 24 26 28
◄ DOM-B
◄ ACF1
◄ ISWI
Western blot

Figure 3.2: DOM-B, ACF1 and ISWI cofractionate in nuclear protein extracts of early embryos
Nuclear protein extracts were prepared from 0–2 h AED **(A)** and 0–16 h AED **(B)** old embryos, and size-fractionated by FPLC using a Superose 6 column. 0.5 ml fractions were analyzed by SDS-PAGE and Western blotting. Equal amounts of fractions were tested for the proteins indicated on the right. The size of marker proteins is shown left and above, IN indicates input protein (500µl).

Decreasing amounts of DOM-B were monitored in fractions 14 to 20, while the intensity of ISWI signals remained constant. The selective cofractionation of DOM-B and ACF1 in preblastodermal embryos (0-2 h AED) suggests that more than one ACF1-containing chromatin remodeling complex exists in early embryos. Whether these proteins indeed form a complex was the approach of the following investigations.

3.1.3 DOM-B, ACF1 and ISWI Cofractionate in *Drosophila* Embryos after Several Distinct Ion Exchange Chromatography Columns

In order to test whether DOM-B associates with ACF1 and ISWI in a large multisubunit protein complex, nuclear extracts from *Drosophila* embryos (0-12 h AED) were extensively fractionated in collaboration with Dr. Anton Eberharter (Adolf-Butenandt-Institute, Munich, Germany). DOM-B was monitored in collaboration with Florian Dreisbach (Adolf-Butenandt-Institute, Munich, Germany) using Western blot analysis. The purification scheme is shown in Figure 3.3.A. Crude nuclear protein extracts were

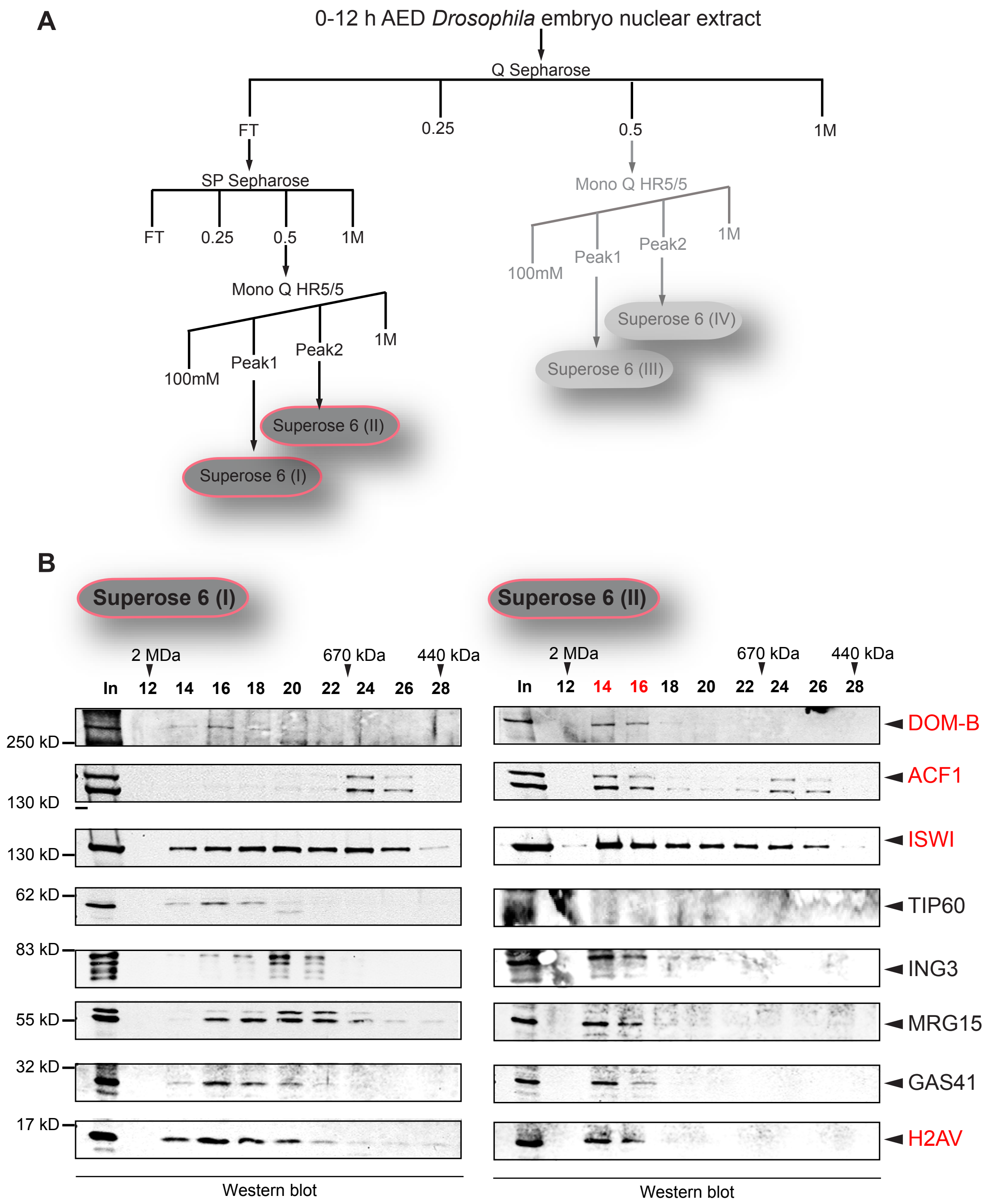
A
0-12 h AED Drosophila embryo nuclear extract
Q Sepharose
FT
0.25
0.5
1M
SP Sepharose
FT
0.25
0.5
1M
Mono Q HR5/5
100mM
Peak1
Peak2
1M
Superose 6 (II)
Superose 6 (I)
Mono Q HR5/5
100mM
Peak1
Peak2
1M
Superose 6 (IV)
Superose 6 (III)
B
Superose 6 (I)
Superose 6 (II)
2 MDa
670 kDa
440 kDa
In 12 14 16 18 20 22 24 26 28
250 kD
130 kD
130 kD
62 kD
83 kD
55 kD
32 kD
17 kD
DOM-B
ACF1
ISWI
TIP60
ING3
MRG15
GAS41
H2AV
Western blot
Western blot

Figure 3.3: DOM-B is part of a high molecular weight complex in *Drosophila* Embryos
(A) Fractionation scheme of nuclear protein extracts by ion exchange and size-exclusion chromatography. **(B)** Nuclear extracts were prepared from 0–12 h AED old embryos and size-fractionated as shown in (A). Superose 6 fractions were analyzed by SDS-PAGE and Western blotting. Equal volumes of selected fractions were tested for the presence of proteins indicated on the right. The size of marker proteins is shown left and above, IN indicates input protein (500 µl). DOM-B signals were detectable in fraction 16 of the first Mono Q peak (Superose 6 (I)) and in fractions 14-16 in the second peak (Superose 6 (II)).

loaded on a Q Sepharose FF (Fast Flow) column. The flow-through was purified using a SP Sepharose (for details *see* Chapter 2.3.6). The 0.5 M eluate of the SP Sepharose was further applied onto a Mono Q HR5/5 column. After elution with a 0.1 to 1 M salt gradient, two distinct peaks of DOM-B were detected and subsequently size-fractionated through a Superose 6 column. Fractions were analyzed by SDS-PAGE and Western blotting (Figure 3.3.B). Since DOM-A was found as a subunit of the

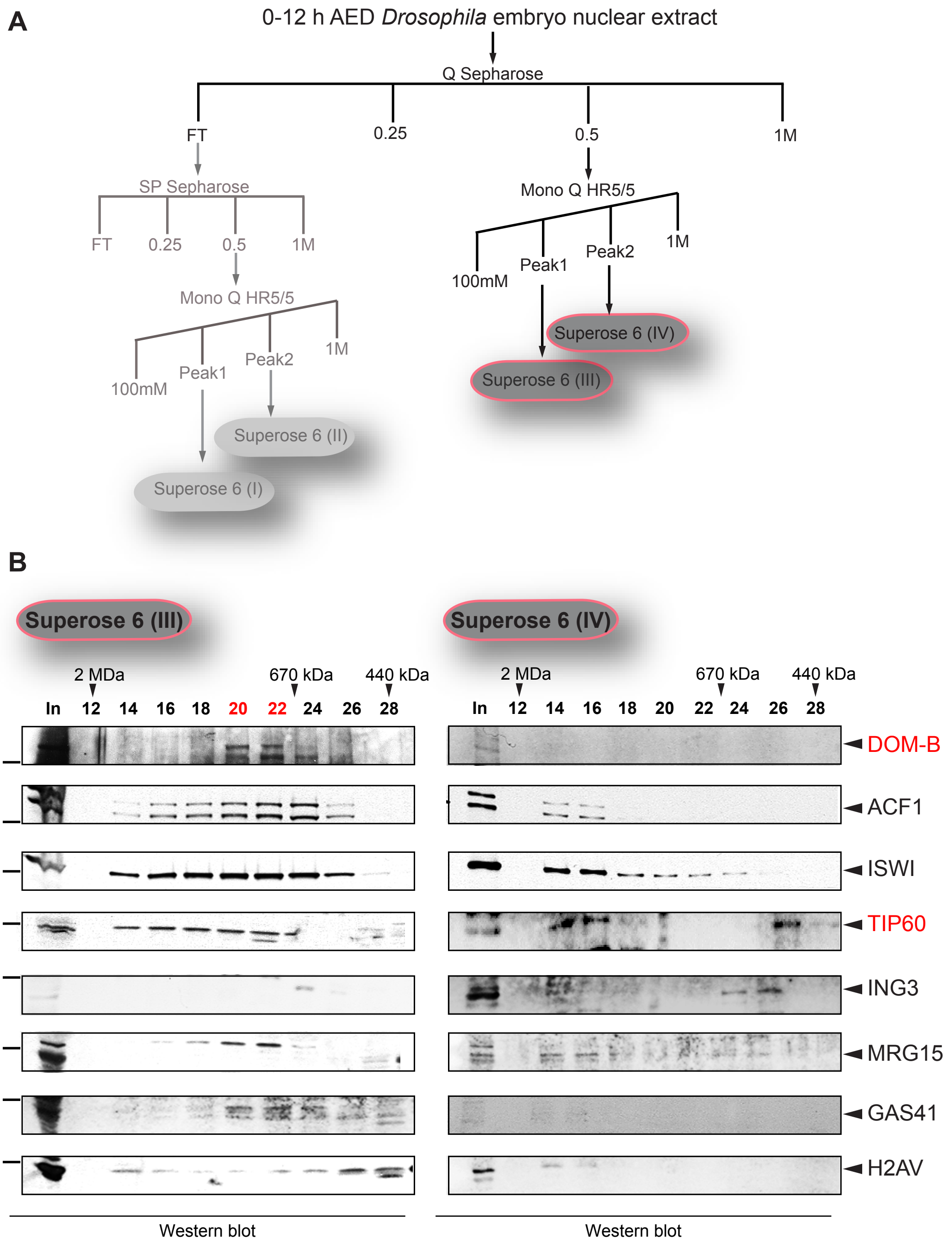

Figure 3.4: DOM-B is part of a high molecular weight complex in *Drosophila* Embryos
(A) Fractionation scheme of nuclear protein extracts by ion exchange and size-exclusion chromatography. **(B)** Nuclear extracts were prepared from 0–12 h AED old embryos and size-fractionated as shown in (A). Superose 6 fractions were analyzed by SDS-PAGE and Western blotting. Equal volumes of selected fractions were tested for the presence of proteins indicated on the right. The size of marker proteins is shown left and above, IN indicates input protein (500 µl). DOM-B signals were detectable in fraction 20-22 of the first Mono Q peak (Superose 6 (III)). No DOM-B signal is monitored in fractions eluted from the Superose 6 (IV).

large TIP60 complex in embryonic *Drosophila* S2 cells (Kusch et al.; 2004), fractions were analyzed for the presence of known subunits of this complex. DOM-B was identified in fraction 16 of the Superose 6 (I) column (Figure 3.3.B, left panel) together with five known subunits of the TIP60 complex: H2AV, GAS41, MRG15, ING3 and TIP60. This cofractionation suggests that DOM-B may reside in a similar TIP60 complex. In line with previous findings, DOM-B peak fractions of the Mono Q HR5/5 gradient were further analyzed with antibodies against ACF1 and ISWI. Only ISWI co-eluted with DOM-B in fraction 16, whereas ACF1 was detected in fractions 24-26. In striking contrast, ACF1 cofractionated with DOM-B in fractions 14 and 16 of the second DOM-B peak from the Mono Q HR5/5 separated with Superose 6 (II) column (Figure 3.3.B, right panel). Interestingly, in these fractions a clear TIP60 signal was not detectable. This might suggest that DOM-B could be part of an additional multisubunit protein complex lacking TIP60 in addition to being present in a free form. ISWI was found in all fractions, indicating that other ISWI-containing complexes are also present in these fractions. According to these findings, a putative DOM-B complex with a molecular weight of approximately 2 MDa appeared to be associated with ACF, ING3, MRG15, GAS41, H2AV and possibly with TIP60. Remarkably, this association resists four fractionation steps.

In addition, the 0.5 M eluate of the Q Sepharose column was loaded directly onto a Mono Q HR5/5 column. Also in this case, two distinct DOM-B peaks were monitored and further fractionated over Superose 6 columns. DOM-B peaked in the 1 MDa range in fractions 20-22. TIP60, ACF1, ISWI, MRG15, GAS41 and INO80 showed a broad distribution indicating complex heterogeneity. H2AV was present in fewer amounts; ING3 could not be detected (Figure 3.4.B, left panel). In contrast, DOM-B signals were not detected after Superose 6 size fractionation of the second gradient peak (Figure 3.4.B, right panel). These fractions contained also less ACF1 and ISWI, as well as small amounts of TIP60, MRG15, ING3 and INO80.

Taken together, these data reveal a hitherto unappreciated diversity of nucleosome remodeling complexes during embryogenesis. By fractionating embryo extracts different multisubunit protein complexes that associates with some components of known complexes, like TIP60 or ACF, appeared. Therefore we postulate the existence of a large complex containing at least DOM-B, ACF1 and ISWI.

3.2 Recombinant DOM-B Proteins Can Be Expressed in *E.coli* and *Sf9* Cells

In order to investigate a potential direct interaction between DOM-B and ACF, DOM-B proteins were expressed in *E.coli* and *Sf9* cells and purified. A series of DOM-B deletion mutants (DOM Δ1- Δ7) was generated to identify key domains involved in ATP-dependent chromatin remodeling. Besides the wildtype form of DOM-B (DOM-B WT), a DOM-B mutant (DOM-B KR) containing a point mutation in a conserved lysine residue (K945 → R) within the ATPase domain, was generated as a control for a more detailed enzymatic and functional evaluation. In context of the well-known ATPase ISWI, an analogous arginine substitution eliminated the ATPase and chromatin remodeling activities (Deuring et al., 2000). A schematic representation of all constructs investigated in this study is shown in Figure 3.5.A.

For bacterial expression, all DOM constructs were fused to N-terminal GST- and C-terminal FLAG-tags. In parallel, these DOM derivatives were expressed via a baculovirus expression system in *Sf9* cells and were purified via the C-terminal FLAG-tag. The expected molecular weight of DOM-B derivatives expressed in *E.coli* and in *Sf9* cells were calculated for a convenient identification on gels (Figure 3.5.B).

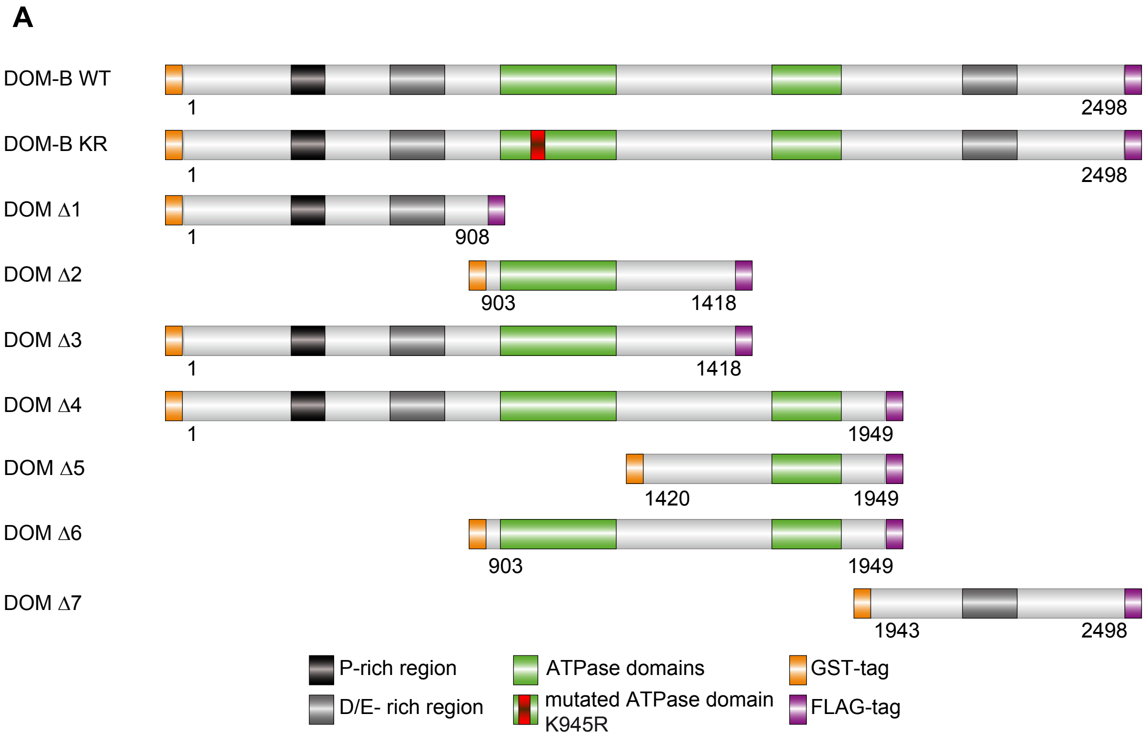
A
DOM-B WT
1
2498
DOM-B KR
1
2498
DOM Δ1
1
908
DOM Δ2
903
1418
DOM Δ3
1
1418
DOM Δ4
1
1949
DOM Δ5
1420
1949
DOM Δ6
903
1949
DOM Δ7
1943
2498
P-rich region
D/E- rich region
ATPase domains
mutated ATPase domain K945R
GST-tag
FLAG-tag

B

	DOM-B WT	DOM-B KR	DOM Δ1	DOM Δ2	DOM Δ3	DOM Δ4	DOM Δ5	DOM Δ6	DOM Δ7
E.coli (+GST/+FLAG)	304 kDa	304 kDa	129 kDa	86 kDa	185 kDa	-----	87 kDa	144 kDa	90 kDa
Sf9 (-GST/+FLAG)	275 kDa	275 kDa	100 kDa	57 kDa	156 kDa	214 kDa	-----	115 kDa	61 kDa

Figure 3.5: Overview of DOM-B derivatives investigated in this study
(A) Schematic representation of the domain architecture of DOM-B wildtype (DOM-B WT) protein and a series of recombinant proteins representing parts of DOM. Constructs of DOM-B were fused to a FLAG-tag (purple) at the C-terminus for expression in *Sf9* cells and to C-terminal FLAG- and N-terminal GST-tag (yellow) for bacterial expression. Green boxes represent the split ATPase domain; the pink stripe indicates the K945R mutation (DOM-B KR). **(B)** Approximate calculated molecular weight of recombinant DOM-B proteins and truncated versions generated in *E.coli* and *Sf9* cells.

3.2.1 Expression and Purification of Recombinant DOM-B Proteins and Derivatives in Bacteria

For further *in vitro* studies of DOM-B, it was necessary to produce sufficient amounts of recombinant proteins. First, various DOM-B fragments were expressed as C-terminal glutathione-S-transferase (GST) and N-terminal FLAG fusion proteins in *E.coli*. The derivatives were purified using glutathione sepharose resin. The eluted DOM fragments were then analyzed by SDS- PAGE and Coomassie blue staining (Figure 3.6.A/C). A bacterial expression of the full length DOM-B WT or KR protein was possible but not satisfactory. Purification via the glutathione sepharose resin did not remove non-specific bound bacterial proteins. In addition, a strong degradation of DOM products was observed even though working strictly on ice or at 4°C. Also a double purification using the GST-tag and the FLAG-tag did not yield intact DOM-B proteins (data not shown). The GST-DOM Δ4-FLAG (DOM Δ4)

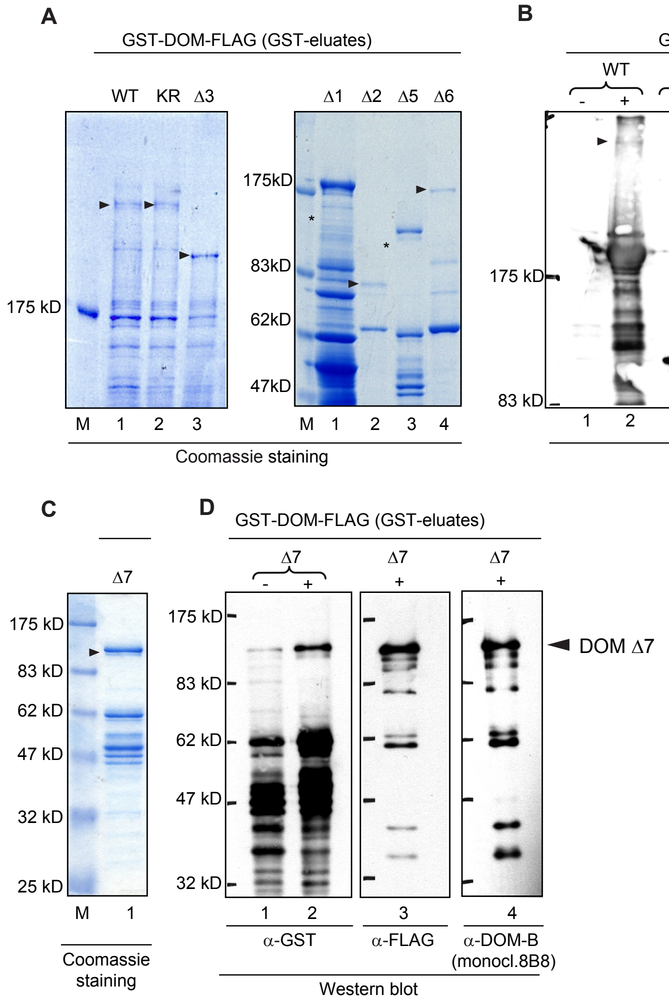
A
GST-DOM-FLAG (GST-eluates)
WT
KR
Δ3
Δ1
Δ2
Δ5
Δ6
175 kD
175kD
83kD
62kD
47kD
M 1 2 3
M 1 2 3 4
Coomassie staining
B
GST-DOM-FLAG (GST-eluates)
WT
Δ1
Δ2
Δ3
Δ5
Δ6
- + - + - + - + - + +
175 kD
83 kD
1 2 3 4 5 6 7 8 9 10 11
Western blot (α-FLAG)
C
Δ7
175 kD
83 kD
62 kD
47 kD
32 kD
25 kD
M 1
Coomassie staining
D
GST-DOM-FLAG (GST-eluates)
Δ7
Δ7
Δ7
- + + +
175 kD
83 kD
62 kD
47 kD
32 kD
DOM Δ7
1 2 3 4
α-GST
α-FLAG
α-DOM-B (monocl.8B8)
Western blot

Figure 3.6: DOM-B derivatives can be generated in *E.coli* and purified via GST-tag
(A) Different GST- and FLAG-tagged DOM-B derivatives as indicated at the top expressed in *E.coli*. Recombinant DOM-B proteins were purified via GST-tag. Eluted proteins were analyzed by SDS-PAGE and stained with Coomassie blue. The arrow marks DOM-B expression products with respect to their MW, the asterisk (*) indicates putative expression products of DOM-B. Lower bands are either degradation products of DOM-B or coeluted putative bacterial proteins. The size of marker proteins is shown left (M). **(B)** GST-eluates were verified by Western blotting with a specific antibody against the FLAG-tag (α-FLAG) before (-) and after (+) IPTG induction. **(C)** DOM Δ7 was purified and Coomassie blue stained as in (A). **(D)** The eluted protein DOM Δ7 was recognized by three different antibodies against the N-terminal GST-tag (lanes 1 and 2), the C-terminal FLAG-tag (lane 3) and by a monoclonal α-DOM-B (8B8) antibody (lane 4).

derivative could not be expressed at all. However, eluted DOM-B derivatives were identified by Western blot analysis using antibodies against the C-terminal FLAG-tag (Figure 3.6.B). Also in this case, degradation products were monitored with the FLAG antibody. The recombinant DOM Δ7 derivative was expressed to some degree and detected with three different specific antibodies against the N-terminal GST-tag (α-GST), the C-terminal FLAG-tag (α-FLAG) and by the monoclonal rat α-DOM-B 8B8 antibody (Figure 3.6.D). The latter antibody was specific for DOM-B was generated in collaboration with Dr. Elisabeth Kremmer (Helmholz Zentrum, Munich, Germany). Additional bands were detected in all lanes possibly belonging to degradation products of DOM-B. Considering the large MW of DOM derivatives, the low expression efficiency in *E.coli* is not surprising. Therefore, DOM-B fragments were generated and purified from insect cells using the baculovirus expression system.

3.2.2 Purification of Recombinant DOM-B Proteins and Derivatives in *Sf9* Cells

All DOM-B derivatives were generated in *Sf9* cells using the baculovirus expression system. Expressed proteins were purified from cell lysates by immuno affinity chromatography over an anti-FLAG resin and eluted by a competing FLAG peptide. FLAG elutions were analyzed by SDS-PAGE and Coomassie blue staining (Figure 3.7.A/C). For immunodetection of DOM-B in Western blots, the monoclonal rat antibody 2G5 and the polyclonal chicken antibody Ch35 were tested (for details *see* Chapter 2.5). (Both antibodies are further characterized in immunofluorescence experiments described in

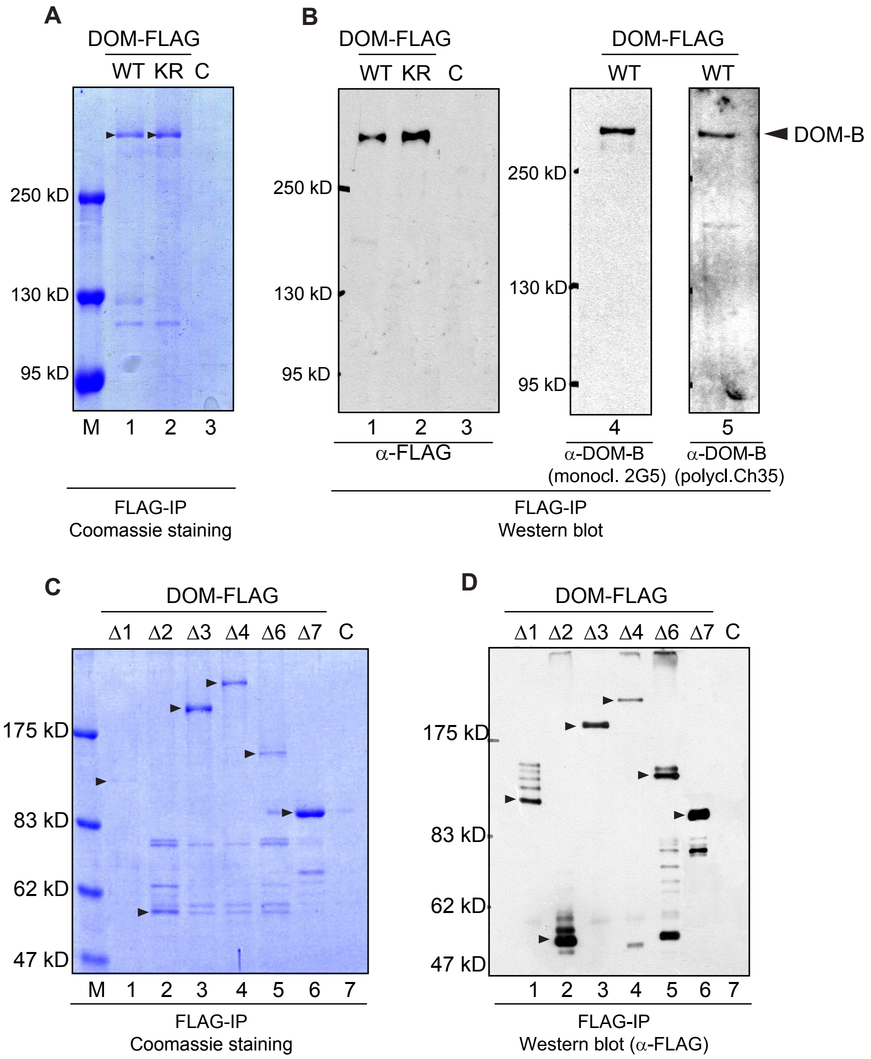
A
DOM-FLAG
WT KR C
250 kD
130 kD
95 kD
M 1 2 3
FLAG-IP
Coomassie staining
B
DOM-FLAG
WT KR C
250 kD
130 kD
95 kD
1 2 3
α-FLAG
DOM-FLAG
WT
WT
DOM-B
250 kD
130 kD
95 kD
4
α-DOM-B (monocl. 2G5)
5
α-DOM-B (polycl.Ch35)
FLAG-IP
Western blot
C
DOM-FLAG
Δ1 Δ2 Δ3 Δ4 Δ6 Δ7 C
175 kD
83 kD
62 kD
47 kD
M 1 2 3 4 5 6 7
FLAG-IP
Coomassie staining
D
DOM-FLAG
Δ1 Δ2 Δ3 Δ4 Δ6 Δ7 C
175 kD
83 kD
62 kD
47 kD
1 2 3 4 5 6 7
FLAG-IP
Western blot (α-FLAG)

Figure 3.7: DOM-B proteins can be expressed in *Sf9* cells and purified via FLAG-tag
Sf9 cells were infected with recombinant baculoviruses expressing various FLAG-tagged DOM-B derivatives as indicated at the top. Immuno affinity purification via FLAG-agarose of uninfected *Sf9* cells served as a control (C). The size of marker proteins is shown left (M). **(A)** Full length DOM-B WT-FLAG and KR proteins were affinity-purified via FLAG-tag. Eluted proteins were analyzed by SDS-PAGE and stained with Coomassie blue. **(B)** The eluted proteins were recognized by different antibodies against the C-terminal FLAG-tag (α-FLAG), the monoclonal rat α-DOM-B antibody 2G5 and the polyclonal chicken α-DOM-B antibody Ch35. **(C)** Truncated versions of DOM-B were purified and Coomassie blue stained as in (A). **(D)** Successful purifications of recombinant DOM-B proteins were verified by Western blotting with the α-FLAG antibody specific against the C-terminal FLAG-tag. Additional bands are proteolytic products of DOM-B proteins.

Chapter 3.5.) Both antibodies 2G5 and Ch35 recognized the full length DOM-B protein (Figure 3.7.B, lanes 4 and 5). This was verified by immunodetection with the α-FLAG antibody against the C terminal FLAG-tag of DOM-B (Figure 3.7.B, lanes 1 and 2). As a control, the cell lysate of uninfected *Sf9* cells - also processed via FLAG-agarose - was used. No signal was detected in all control (C) lanes, whereas all FLAG-tagged derivatives of DOM-B were detected by the α-FLAG antibody corresponding to their predicted molecular weight (in kDa) (Figure 3.7.D).

Compared to proteins generated in *E.coli*, sufficient amounts of protein for further studies and *in vitro* assays could be produced in *Sf9* cells. However, minor bands due to proteolytic degradation of DOM-B could not be avoided.

3.3 The ATPase Domain of DOM-B Is Required for Direct Binding to ACF1

Since DOM-B, ACF1 and ISWI may reside in a complex in *Drosophila* embryos, a reconstitution of a corresponding recombinant complex was attempted in *Sf9* cells to explore whether these proteins are able to directly interact *in vitro*. Therefore, DOM-B-FLAG derivatives were synthesized in *Sf9* cells as described previously. The different DOM-B complexes were generated by coexpression

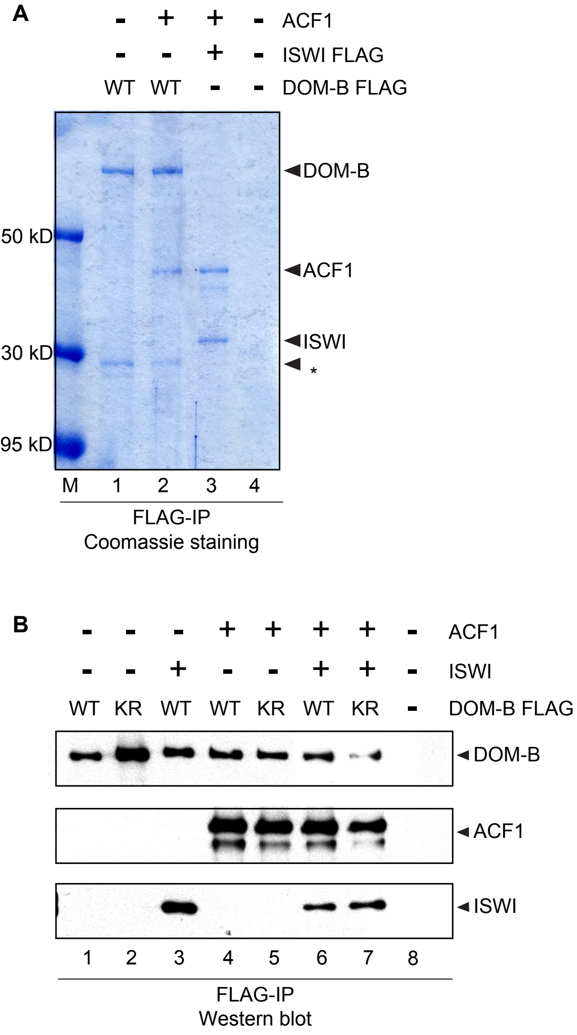

Figure 3.8: Recombinant DOM-B associates directly with ACF1 and ISWI *in vitro*
Sf9 cells were coinfected with recombinant baculoviruses expressing FLAG-tagged DOM-B derivatives and untagged ACF1 and ISWI as indicated at the top. Recombinant complexes or individual proteins were immuno affinity purified via FLAG-agarose and analyzed by SDS-PAGE. **(A)** Coexpression and coelution of FLAG-tagged DOM-B WT with untagged ACF1 (lane 2) was analyzed by Coomassie blue staining. Single expression of DOM-B WT-FLAG (lane 1) and reconstitution of the known recombinant ACF complex (lane 3) generated in *Sf9* cells served as controls. The asterisk (*) indicates a degradation product of DOM-B. α-FLAG immuno affinity purification of uninfected *Sf9* cells served as a control (lane 4). The size of marker proteins is shown left (M). **(B)** Recombinant proteins were analyzed by SDS-PAGE and Western blotting. FLAG-eluted proteins and associated partners were detected by different antibodies indicated on the right. α-FLAG immuno affinity purification of uninfected *Sf9* cells served as a control (lane 8) and immunodetection of the individual DOM-B WT and KR-FLAG proteins (lanes 1 and 2) served as further controls.

of FLAG-tagged DOM-B WT/KR with untagged ACF1 or ISWI. Recombinant complexes were purified from cell lysates by immuno affinity chromatography using α-FLAG resin and eluted with a competing FLAG peptide. Eluted material was separated by SDS-PAGE and analyzed by Western blotting. As a control α-FLAG immunopurified material of uninfected *Sf9* cell lysates was used to monitor all non-specific bound proteins. A successful coexpression and copurification via the FLAG-tag of DOM-B WT with untagged ACF1 could already be estimated by Coomassie blue staining (Figure 3.8.A). As a further control, the ACF complex was reconstituted in *Sf9* cells. Untagged ACF1 was purified with the FLAG-tagged ISWI, in agreement with previous studies (Eberharter et al. 2001).

To test and verify a direct interaction of DOM-B with ACF1 or ISWI, DOM-B-FLAG associated proteins were analyzed by immunodetection. Eluted material was probed with α-DOM-B WT/KR, α-ACF1 or α-ISWI specific antibodies (Figure 3.8.B). FLAG-tagged DOM-B WT was coimmunoprecipitated with untagged ACF1 (lane 4) and with untagged ISWI (lane 3), respectively. Copurification of all three proteins was also achieved after FLAG-elution of DOM-B WT-FLAG with untagged ACF1 and untagged ISWI (lane 6). This confirms that ACF1 and ISWI can directly interact with DOM-B and that these recombinant proteins can form a complex with DOM-B *in vitro*. Single expressions of DOM-B WT (lane 1) and KR (lane 2) served as controls. It was also tested whether the putative ATPase-deficient mutant DOM-B KR binds ACF1 and ISWI. Tagged DOM-B KR showed the same interactions as DOM-B WT (lanes 5 and 7), which suggests that the KR mutation region does not influence the binding of DOM-B to ACF1. Therefore, the region within DOM-B binding to ACF1 or ISWI was mapped more precisely. To delineate the ACF1 interacting domain of DOM-B a series of FLAG-tagged DOM-B derivatives were

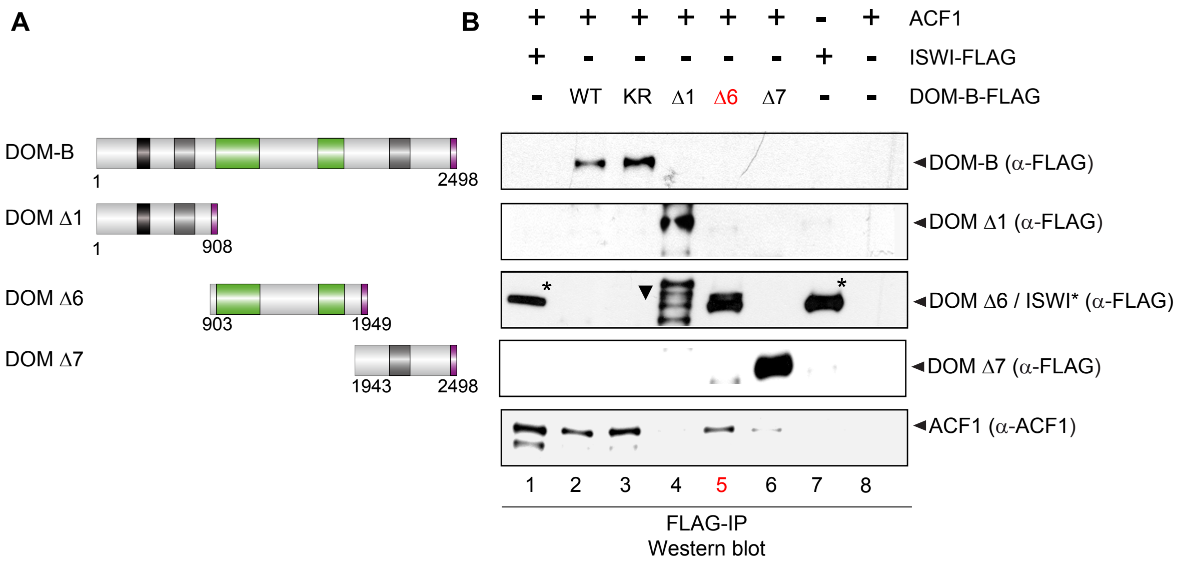

Figure 3.9: Mapping the ACF1 interacting domain of DOM-B
(A) Schematic representation of the domain architecture of recombinant DOM-B proteins used for the delineation of the ACF1 interacting domain. **(B)** *Sf9* cells were coinfected with recombinant baculoviruses expressing various FLAG-tagged DOM-B derivatives together with untagged ACF1 as indicated at the top. Recombinant protein complexes were immuno affinity purified via the FLAG-tag of DOM-B derivatives. Eluted proteins and associated partners were analyzed by SDS-PAGE and Western blotting and were identified by different antibodies indicated on the right. The size of marker proteins is shown left. The asterisks (*) indicate ISWI-proteins, the triangle (▼) indicates a degradation product of DOM-B Δ1. FLAG purification and Western blot analysis of DOM-B WT/KR-FLAG + untagged ACF1 (lanes 2 and 3), untagged ACF (lane 1), ISWI-FLAG (lane 7) and untagged ACF1 (lane 8) served as controls.

coexpressed with untagged ACF1 or untagged ISWI in *Sf9* cells using baculoviruses. Recombinant complexes were immuno affinity purified as above via the FLAG tag of DOM-B fragments and separated by SDS–PAGE. DOM derivatives, ACF1 and ISWI were identified by Western blotting using the appropriate antibodies (Figure 3.9). Deleting a rather long C-terminal region within the ATPase domain of DOM-B abolished the interaction with ACF1, as no ACF1 signal was detected in the FLAG elution of the N-terminal derivative DOM Δ1 (lane 4). A similar result was obtained with C-terminal DOM Δ7 fragment lacking the entire ATPase domain (lane 6). The interaction with ACF1 was only monitored with the derivate DOM Δ6 containing the entire center part, including the ATPase domain (lane 5). Therefore, the interacting region of DOM-B to ACF1 was mapped to the DOM-B split ATPase domain in these experiments.

3.4 The ATPase Activity of DOM-B Is Inhibited by Its C-terminus

As already mentioned, the bipartite SWR1 class ATPase domain relates DOM-B to the SWR1 and INO80 complexes of *S. cerevisiae* (Jin et al., 2005; Ueda et al., 2007). Recent studies demonstrated that the yeast SWR1 complex plays a role in histone variant exchange (Kobor et al., 2004; Morillo-Huesca et al., 2010). SWR1 in *S. cerevisae* can replace the canonical histone H2A with the histone variant H2AZ in an ATP-dependent manner (Mizuguchi et al., 2004; Wu et al., 2005). Furthermore, it has been demonstrated that the ATPase subunit of the TIP60 complex Domino/p400, catalyze the exchange of γ-H2AV (Kusch et al.; 2004). Since the *Drosophila* histone variant H2AV cofractionated with DOM-B in embryo nuclear extracts after successive ion exchange chromatographic steps (Figure 3.3), ATPase assays with reconstituted H2AV-containing histones in comparison to reconstituted canonical H2A-containing histones as substrates for chromatin remodeling enzymes were performed. Histones were incubated together with different chromatin remodeling enzymes and radioactively labeled γ^{32}P-ATP for 1 h at 26°C. As a control, FLAG- eluted material of uninfected *Sf9* cells was used instead of remodeling enzymes. ATPase activity was measured by visualizing the hydrolysis of γ^{32}P-ATP to γ^{32}P by thin layer chromatography (TLC) (Figure 3.10.A). The ATP hydrolysis was quantified with a Phospho Imager and the percentage of hydrolyzed ATP was calculated using the AIDA Image Analyzer software (Figure 3.10.B). Surprisingly, the full length DOM-B WT did not show any ATPase activity, similar to DOM-B KR, which was designed as the ATPase-deficient mutant. As expected, the C-terminal fragment DOM Δ7 lacking the entire ATPase subunit did not hydrolyze ATP. The enzyme activity was not stimulated by H2A or H2AV. In striking contrast, an ATP hydrolysis was only observed with DOM-B derivatives (DOM Δ3, Δ4 and Δ6) containing one or both domains of the split ATPase subunit but lacking the C-terminus. H2A or H2AV did not modulate the ATPase activity, which was also measurable in absence of histones. Highest ATPase activity independent of substrate was obtained with the DOM Δ4 derivate only missing the C-terminus, followed by DOM Δ6 comprising the ATPase domain. A decreased efficiency was observed for DOM Δ3 bearing only half part of the ATPase domain. Taken together, these results suggest that the C-terminus of DOM-B is involved in the regulation of the ATPase activity of this remodeler. The C-terminus distinguishes DOM-B from its isoform DOM-A, a further indication for distinct biological function of DOM-B. Conceivably, the C-terminal end of DOM-B may interact with the ATPase domain to influence the ATPase activity. However, this could not be clarified in this study. The ability of ACF1 to bind directly to the ATPase

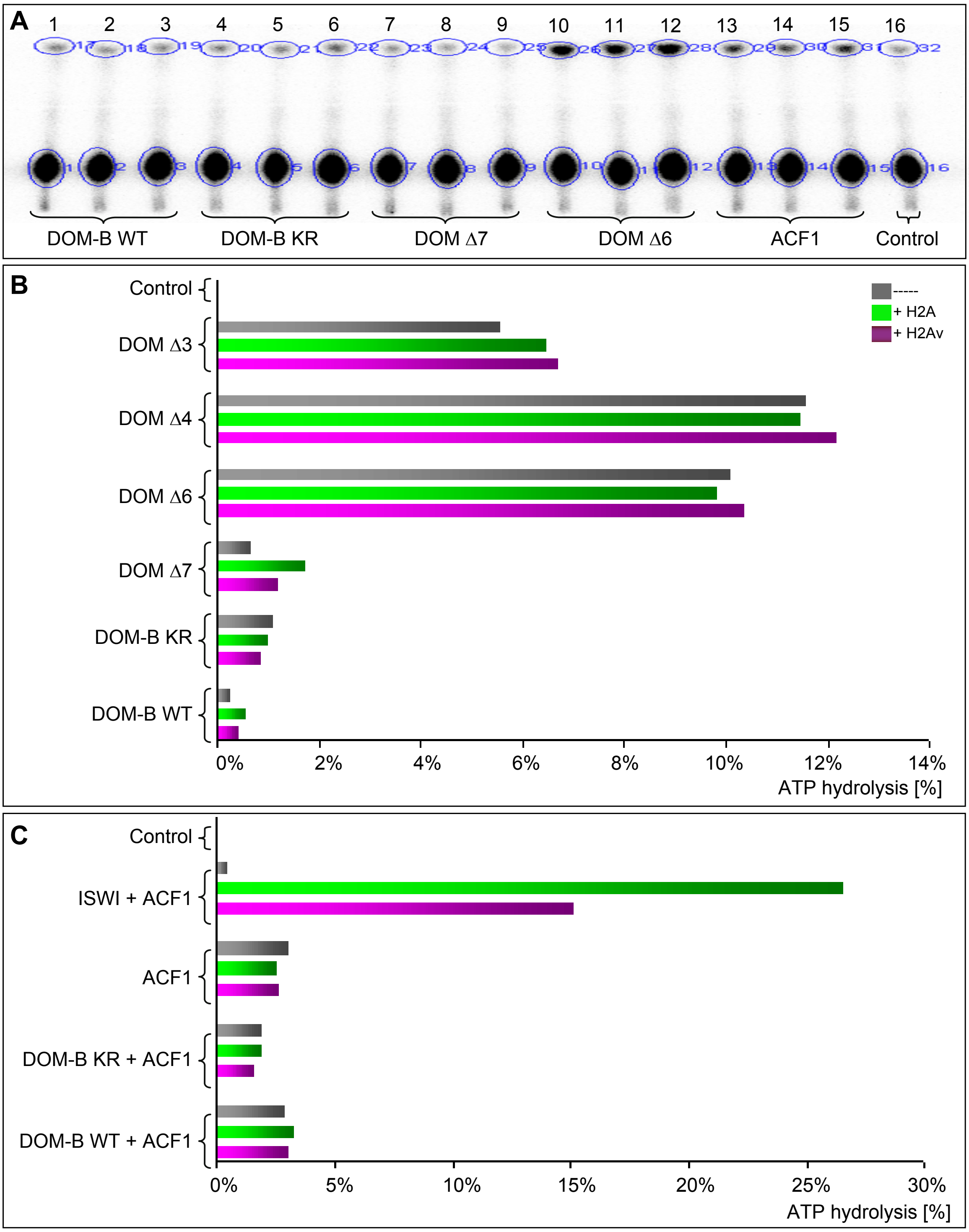

Figure 3.10: ATPase activities of DOM-B WT or KR, DOM-B derivatives and in combination with ACF1
ATPase assays with 1 µg of reconstituted histones (H2A or H2AV), 10 pmol of different chromatin remodeling enzymes and 1 µl of 0.3 mM unlabelled ATP spiked 1:200 with γ^{32}P-ATP (5.55 GBq/ml, 150 mCi/mol). After 1 h of incubation, reactions were stopped and spotted onto a TLC plate. ATP and hydrolyzed phosphate were separated by thin layer chromatography (TLC). The control was performed with FLAG-purified and eluted material of uninfected *Sf9* cells instead of remodeling enzymes. **(A)** Example of a TLC plate exposed to a Phospho Imager screen. Radioactive signals of ATP and hydrolyzed phosphate were quantified by a Phospho Imager. **(B)** The percentage of hydrolyzed ATP was calculated using AIDA Image Analyzer software. **(C)** ATPase assays were performed with equal amounts of DOM-B WT or KR mixed with ACF1. ATP hydrolysis was calculated as in (B).

domain of DOM-B (*see* Chapter 3.3) led to the question whether this interaction affects the ATPase activity of DOM-B. Therefore, ATPase assays were performed with equal amounts of DOM-B WT or KR mixed with ACF1 (Figure 3.10.C). None of the two samples – DOM-B WT + ACF1 or DOM-B KR + ACF1 showed ATPase activity.

As a positive control, ACF1 + ISWI (ACF) displayed approximately 25% of ATP-hydrolysis that was more stimulated in presence of H2A histones than of H2AV histones. ACF could not hydrolyze ATP in absence of histones. ACF1 alone served as a further negative control, since it does not hydrolyze ATP without ISWI.

Additionally, recombinant coexpressed and copurified DOM-B WT or KR with ACF1 in *Sf9* cells via FLAG-tag immuno affinity purification were used in ATPase assays. Also chromatin assembled H2A and H2AV-containing nucleosomes as substrates for the remodeling enzymes (data not shown) were tested in ATPase assays. In summary, ATPase assays were repeated 25 times in different combinations, various substrates and under different conditions. However, all results were similar to shown data.

In Vivo Analysis of Domino B

3.5 DOM-B Expression and Distribution on Chromatin of Salivary Glands Is Similar to ACF1

To gain further insight into the biological function of DOM-B during *Drosophila* development, it was essential to study the enzyme *in vivo*. For *in vivo* analysis, suitable novel antibodies were required, since available α-DOM-B antibodies specific in immunofluorescence experiments were only usable to a limited extend (Ruhf et al., 2001). Therefore, novel monoclonal rat and polyclonal chicken α-DOM-B antibodies were generated. Salivary glands of third instar larvae were chosen to verify the specificity of the novel α-DOM-B antibodies and to analyze the distribution of DOM-B on chromatin. Salivary glands of *Drosophila* are characterized by their large nuclei containing polytene chromosomes. The banding patterns of the polytene chromosomes are especially helpful in chromatin research, as they provide an excellent visualization of general interphase chromatin structure and allow the analysis of proteins binding to specific chromatin region. DOM-B is known to be expressed in nuclei of *Drosophila* larval tissues and had already been visualized on polytene chromosomes of salivary glands (Ruhf et al., 2001). Another known protein widely distributed on chromatin of *Drosophila* is the histone variant H2AV. H2AV is not only restricted to the centromeric heterochromatin of polytene chromosomes, but it is also localized in bands among the entire length of each chromosome arm (Leach et al., 2000; Swaminathan et al., 2005).

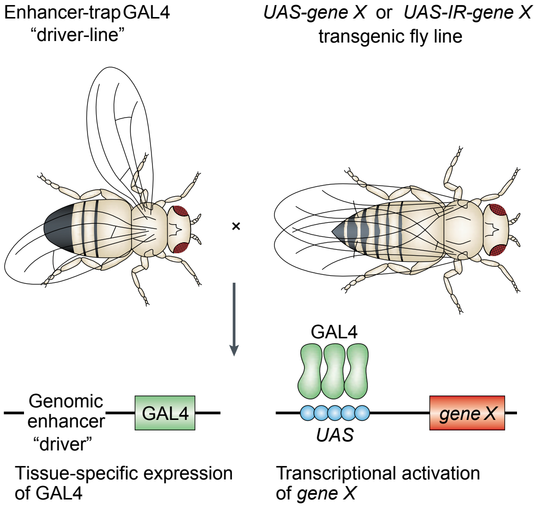
Enhancer-trap GAL4
"driver-line"
UAS-gene X or *UAS-IR-gene X*
transgenic fly line
×
GAL4
Genomic enhancer "driver"
GAL4
UAS
gene X
Tissue-specific expression of GAL4
Transcriptional activation of *gene X*

Figure 3.11: The *UAS-GAL4* system for targeted expression or deletion of proteins in *Drosophila*
Transgenic fly lines carry the gene of interest (*gene X*) next to the upstream activating sequence (*UAS*). To activate the *UAS-gene X* expression, transgenic flies are crossed to "driver fly lines" (Enhancer Trap GAL4 lines) expressing GAL4 under the control of genomic enhancers (*driver X-GAL4*). In progeny (F1) of this cross GAL4 binds specifically to *UAS* and activates the gene expression in a developmental- and tissue-specific manner. In absence of GAL4 the target gene is silent. This system was also used for RNAi-mediated depletion in *Drosophila*. Transgenic flies carrying inverted repeats (IR) of the gene of interest (*gene X*) under the control of the *UAS* (*UAS-IR-gene X*) are crossed to "driver fly lines". In offspring of this cross gene products are knocked-down in a developmental- and tissue-specific manner (adapted from Johnston, 2002).

This H2AV distribution on polytene chromosomes together with the fact that H2AV was cofractionated with DOM-B in nuclear extracts (*see* Chapter 3.1.3) renders this histone variant useful for costaining with DOM-B. The well-established *UAS-GAL4* system was used for *in vivo* analysis (Figure 3.11) (Brand and Perrimon, 1993). In this strategy homozygous transgenic fly lines bearing the transgene (*gene X*) next to the upstream activating sequence (*UAS*) are crossed to enhancer trap GAL4 lines also called "driver lines". These driver lines express GAL4 under the control of genomic enhancers ("drivers"), which are available in a variety of developmental and tissue-specific patterns (Brand and Perrimon, 1993; Johnston, 2002). For example, ectopic expression in salivary glands was induced by the *salivary glands 3-GAL4* driver line (*sgs-GAL4*) that is active at the mid-third instar transition in larval glands (Cherbas et al., 2003).The expression of the *UAS-gene X* is activated by the binding of GAL4 specifically to the *UAS* in the offspring (F1) of this cross. The genotype of this F1-generation is: *driver X-GAL4-UAS-gene X*, which is referred to as *driver X:gene X* (Figure 3.11). A fly line carrying the *UAS-LacZ-mini white* construct, which can express the *β-galactosidase* (*lacZ*) gene in response to GAL4 induction, served as a control. In absence of GAL4 the target gene should be silent.

3.5.1 Characterization of a New α-H2AV-Specific Antibody

The histone variant H2AV in *Drosophila* is localized throughout the euchromatic arms and prominently enriched on the heterochromatic chromocenter of polytene chromosomes (Leach et al. 2000; Swaminathan et al., 2005). It was used as an indicator of proper nuclear organization and chromatin formation. The new H2AV antibody, designed by Dr. Anton Eberharter (Adolf-Butenandt-Institute, Munich, Germany), was raised against a peptide sequence in the C-terminus of H2AV and tested in Western blot experiments (*see* Chapter 3.1.3). To explore its suitability for immunofluorescence experiments, it was tested on whole-mount salivary glands of a control fly line (Figure 3.12). For that

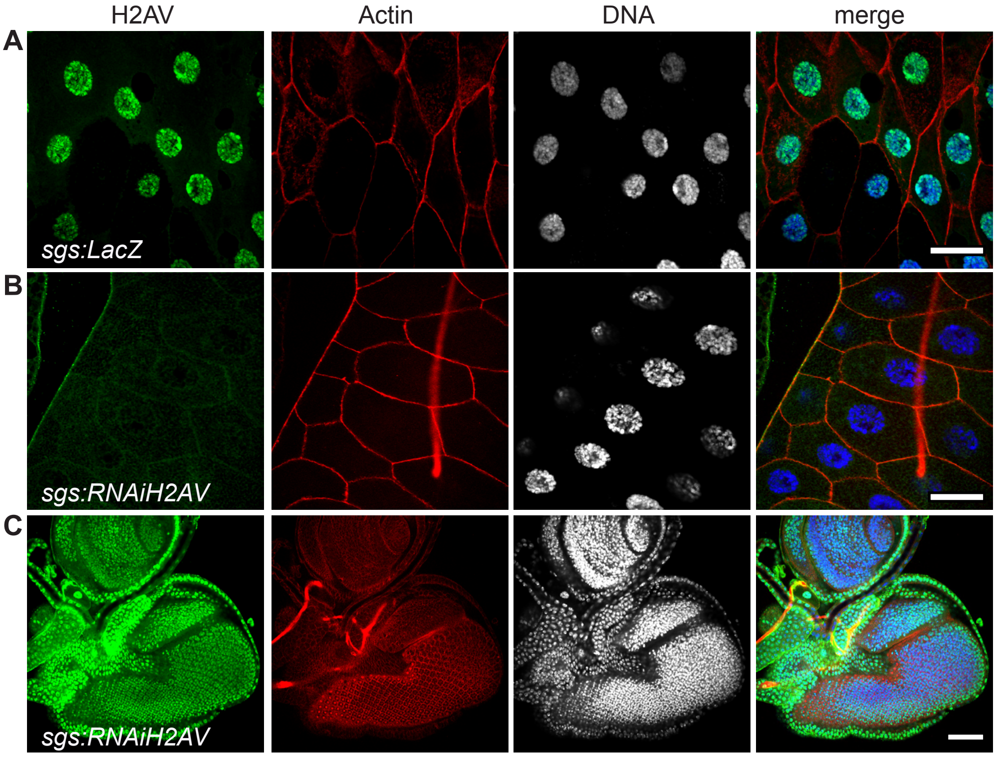

Figure 3.12: Establishment of a new α-H2AV antibody on larval tissues
(A) Immunofluorescence staining of whole-mount salivary glands of *sgs:LacZ* larvae expressing *UAS-β-galactosidase* as a control. A significant H2AV signal (green) could be detected. Actin staining by phalloidin (red) served as an internal reference for the quality of the staining procedure. DNA was stained by TO-PRO3 (white, blue in merge). **(B)** No H2AV signal was detectable upon H2AV depletion in salivary glands (*sgs:RNAiH2AV*). **(C)** As a control for the tissue-specificity of the *sgs3-GAL4* driver, staining of the eye-antenna disc of *sgs:RNAiH2AV* larvae was performed as in (A). Upon knock-down of H2AV in glands, a significant H2AV signal (green) was detected in all nuclei of the eye disc. Scale bars represent 50 µm.

purpose, homozygous *UAS-β-galactosidase* (*lacZ*) females were crossed to *sgs-GAL4* males. In polytene chromosomes of offspring (F1) larvae with the genotype *sgs-GAL4-UAS-lacZ* (*sgs:lacZ*) a clear banding pattern of H2AV signals could be detected along the entire chromosome arms (Figure 3.12.A). The observed H2AV signal distributions were similar to staining patterns of glands dissected from wildtype flies (data not shown) and are in line with previous studies of H2AV (Leach et al., 2000; Swaminathan et al., 2005). No H2AV signals were detected after the depletion of H2AV (*sgs: RNAiH2AV*), which verified the specificity of the novel α-H2AV antibody (Figure 3.12.B). To this end, transgenic females carrying inverted repeats (IR) of the *h2av* gene under the control of a GAL4-induced *UAS* sequence were crossed to *sgs-GAL4* males. As a reference for the staining procedure, glands were costained with phalloidin that marks actin filaments. No differences in phalloidin staining were monitored comparing the H2AV knock-down line (*sgs:RNAiH2AV*) with the control strain (*sgs: LacZ*).

In parallel, the H2AV antibody was tested on other tissues like imaginal eye-antenna discs dissected from the same larvae in which H2AV had been specifically depleted in salivary glands. Although the diploid nuclei of these tissues are very small, H2AV could be detected (Figure 3.12.C). This also demonstrated the specificity of the *sgs3-GAL4* driver, since a targeted depletion of H2AV was exclusively monitored in salivary glands and not in imaginal discs of these larvae.

3.5.2 Characterization of New Specific α-DOM-B Monoclonal Rat Antibodies

Since we were not satisfied with the performance of available antibodies against DOM-B in immunofluorescence experiments, we raised novel monoclonal rat antibodies directed against a peptide in the C-terminal end specific for the DOM-B isoform and against the recombinant derivative DOM Δ7 (*see* Chapter 3.1). In collaboration with Dr. Elisabeth Kremmer (Helmholz Zentrum, Munich, Germany), we obtained four monoclonal rat antibodies specific for DOM-B (8B8, 3H1, 2F4 and 2G5, as described in Chapter 2.5). These monoclonal rat antibodies were tested in Western blot experiments (Chapter 3.2), where DOM-B proteins were clearly detected with the antibodies 8B8 and 2G5 (Figures 3.6 and 3.7), as well as with 3H1 and 2F4 (data not shown). All four monoclonal rat antibodies were tested in immunofluorescence staining of whole mount salivary glands, in which only the antibody 2G5 recognized DOM-B on nuclei (Figure 3.13). Salivary glands of larvae expressing β-galactosidase as a control (*sgs*:*LacZ*) contained low levels of DOM-B (Figure 3.13.A/B). This is in line with previous studies, where DOM-B was found in nuclei of salivary glands and all imaginal discs of *Drosophila* larvae (Ruhf et al., 2001).

To further verify the specificity of this antibody and to increase the signal intensity on chromosomes, FLAG-tagged DOM-B WT and DOM-B KR were ectopically expressed in salivary glands. To this end, various independent transgenic fly lines for *UAS-DOM-B WT* and *UAS-DOM-B KR* were established by P-element-mediated germline transformation (Chapter 2.6), which allowed the expression of DOM-B WT or KR in a developmental and tissue-specific manner. Ectopic expression of DOM-B WT or KR in salivary glands using the *sgs-GAL4* driver increased the immunofluorescence signal of DOM-B detected with the α-DOM B 2G5 antibody (Figure 3.13.A; *sgs:DOM-B WT; sgs:DOM-B KR*). In addition, the specificity of this antibody was confirmed with a targeted depletion of DOM in salivary glands. For that purpose, both DOM isoforms that originate from alternative splicing were depleted by RNAi-mediated knock-down. Indeed, DOM lacking salivary glands displayed no DOM-B signal on their nuclei (*sgs:RNAiDOM*). In comparison to the control, variable intensities of H2AV signals were detected in salivary glands expressing DOM-B WT/KR (Figure 3.13.A). Additionally, a strong background staining of H2AV was observed upon DOM depletion (Figure 3.13.A). This variability may originate from defects of chromatin structure and will be further elucidated in Chapter 3.6. Therefore,

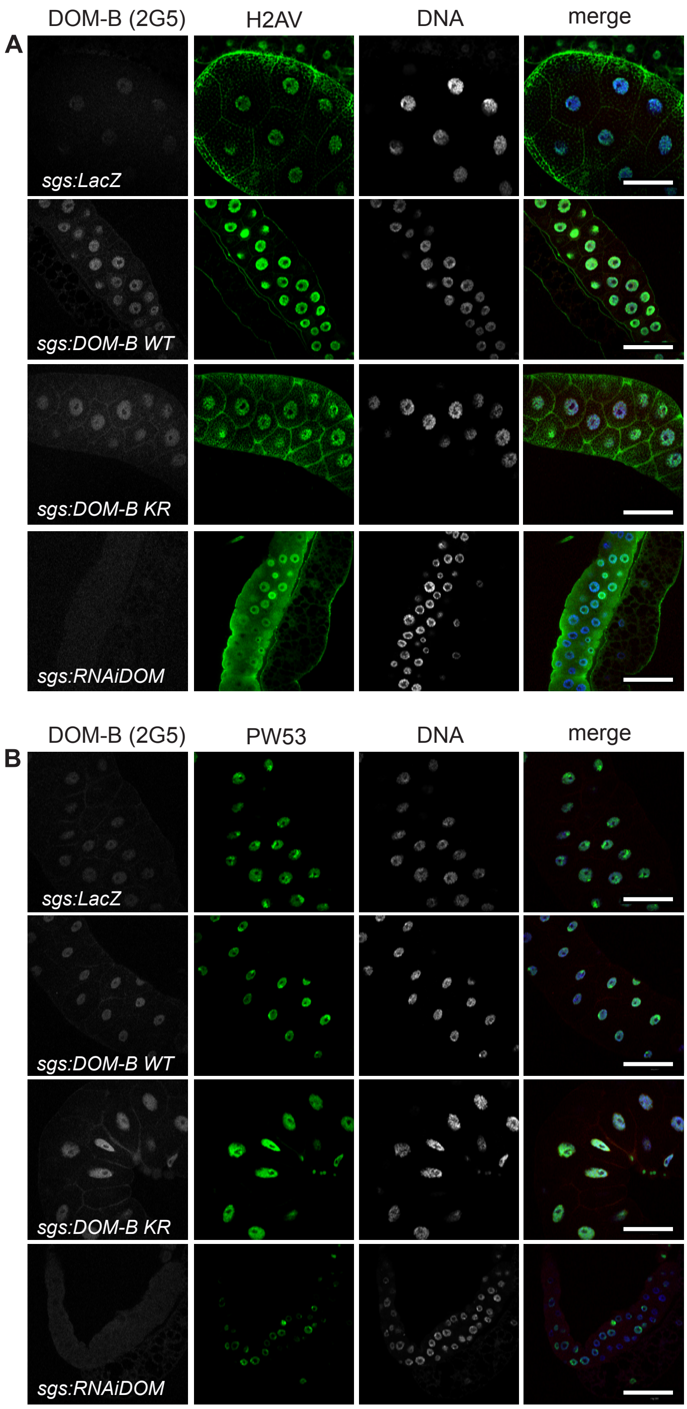
A
DOM-B (2G5)
H2AV
DNA
merge
sgs:LacZ
sgs:DOM-B WT
sgs:DOM-B KR
sgs:RNAiDOM
B
DOM-B (2G5)
PW53
DNA
merge
sgs:LacZ
sgs:DOM-B WT
sgs:DOM-B KR
sgs:RNAiDOM

Figure 3.13: Establishment of the specific α-DOM-B monoclonal rat antibody 2G5
(A) Immunofluorescence staining of whole-mount salivary glands using the *sgs-GAL4* driver. DOM-B (white, red in merge), H2AV (green), DNA stained by TO-PRO3 (white, blue in merge). Salivary glands of larvae expressing β-galactosidase as a control (*sgs:LacZ*) contained low levels of DOM-B. Ectopic expression of DOM-B WT or KR (*sgs:DOM-B WT/KR*) increased DOM-B signals in salivary glands. No signal was visible upon DOM depletion (*sgs:RNAiDOM*). DNA signals were optimized in these larvae. Signals of H2AV were found to be of variable intensity. **(B)** Salivary glands were prepared as in (A). Instead of α-H2AV, α-PW53 (green) specific antibody served as an internal reference. Scale bars represent 100 µm.

the immunofluorescence staining of whole mount salivary glands was repeated with α-DOM-B 2G5 antibody and α-PW53 antibody (kindly provided by Dr. Catherine Regnard; Adolf-Butenandt-Institute, Munich, Germany) (Figure 3.13.B). PW53 displayed a homogeneous staining pattern, while DOM-B signals were in line with previous observations. In all experiments (Figure 3.13.A and B), shape and structure of whole salivary glands were influenced by targeted expression of DOM-B WT and, especially, by RNAi-mediated DOM depletion. Salivary glands of these larvae lacking DOM-B were smaller than wildtype salivary glands and contained also smaller polytene chromosomes. DNA signals stained by TO-PRO3 were under the detection limit with microscope settings adjusted to the control, indicating putatively less condensed and not polytenized DNA. Thus, DNA signals were manually adjusted by increasing the laser intensity and optimized in glands of all *sgs:RNAiDOM* larvae (Figure 3.13.A and B) to allow appropriate visualization of the DNA. Defects due to DOM depletion were analyzed in higher detail and are described in Chapter 3.7.

3.5.3 Characterization of a New Specific α-DOM-B Polyclonal Chicken Antibody

New polyclonal chicken antibodies (for details *see* Chapter 2.5) were also tested in immunofluorescence experiments. The antibodies Ch35 and Ch36, specific for DOM-B, and Ch37 and Ch38, specific for both isoforms, were previously tested in Western blot analysis (*see* Chapters 3.1 and 3.2). Best results were obtained with the polyclonal antibody Ch35 in Western blot analysis as well as in immunofluorescence stainings (Figure 3.14). This antibody yielded specific signals for DOM-B in salivary glands of DOM-B WT

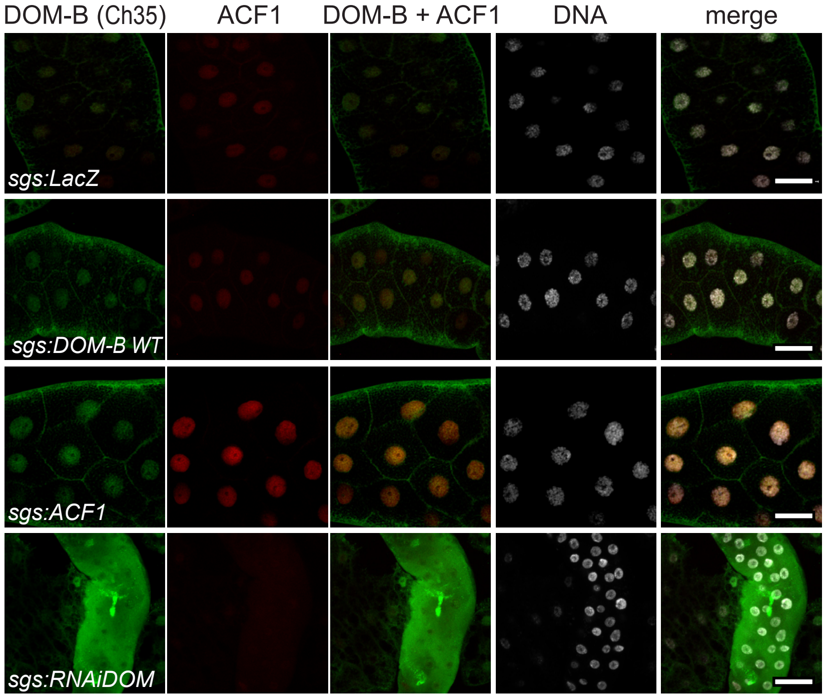

Figure 3.14: Establishment of the specific α-DOM-B polyclonal antibody Ch35
Immunofluorescence staining of whole-mount salivary glands using the *sgs-GAL4* driver. DOM-B (green), ACF1 (red), DNA stained by TO-PRO3 (white). Salivary glands of larvae expressing β-galactosidase as a control contained low levels of DOM-B and ACF1 (*sgs:LacZ*). Ectopic expression of DOM-B WT (*sgs:DOM-B WT*) increased DOM-B signals in salivary glands. No signal was visible upon DOM depletion besides a high background staining (*sgs:RNAiDOM*). Upon ectopic expression of ACF1 an increased signal of ACF1 and DOM-B was detected (*sgs:ACF1*). Scale bars represent 50 µm.

ectopically expressing larvae (*sgs:DOM-B WT)*, similar to monoclonal rat antibody 2G5 signals. The specificity of the antibody was confirmed by RNAi-mediated DOM depletion (*sgs:RNAiDOM*). However, higher background staining was obtained with the IgY (Immunglobolin Y) chicken antibodies. We were also interested in visualizing ACF1 in *Drosophila* where DOM-B was ectopically expressed or depleted, as ACF had been shown to cofractionate with a DOM-B-containing complex (Chapter 3.1). ACF1 is normally expressed at very low levels in *Drosophila* salivary glands (Chioda et al. 2010), similar to the observed DOM-B expression patterns (Figures 3.13 and 3.14). In agreement, ACF1 expression was observed near to the detection limit upon LacZ or DOM-B WT expression in salivary glands (*sgs:LacZ, sgs:DOM-B WT)* (Figure 3.14). RNAi-mediated DOM depletion (*sgs:RNAiDOM*) decreased or even abolished DOM-B staining from nuclei but gave rise to a strong background staining through the entire gland (Figure 3.14). In these glands also no ACF1 signal could be observed. Furthermore, DOM-B staining signal increased upon ACF1 ectopic expression (*sgs:ACF1*).

3.5.4 Ectopic Expression of ACF1 in Salivary Glands Upregulates DOM-B Signals

The hypothesis that DOM-B and ACF1 may interact leads to the question of a possible direct dependency of expression levels of both proteins in salivary glands. Indications favoring this notion could be already observed in salivary glands of ectopically ACF1 expressing larvae (*sgs:ACF1*),

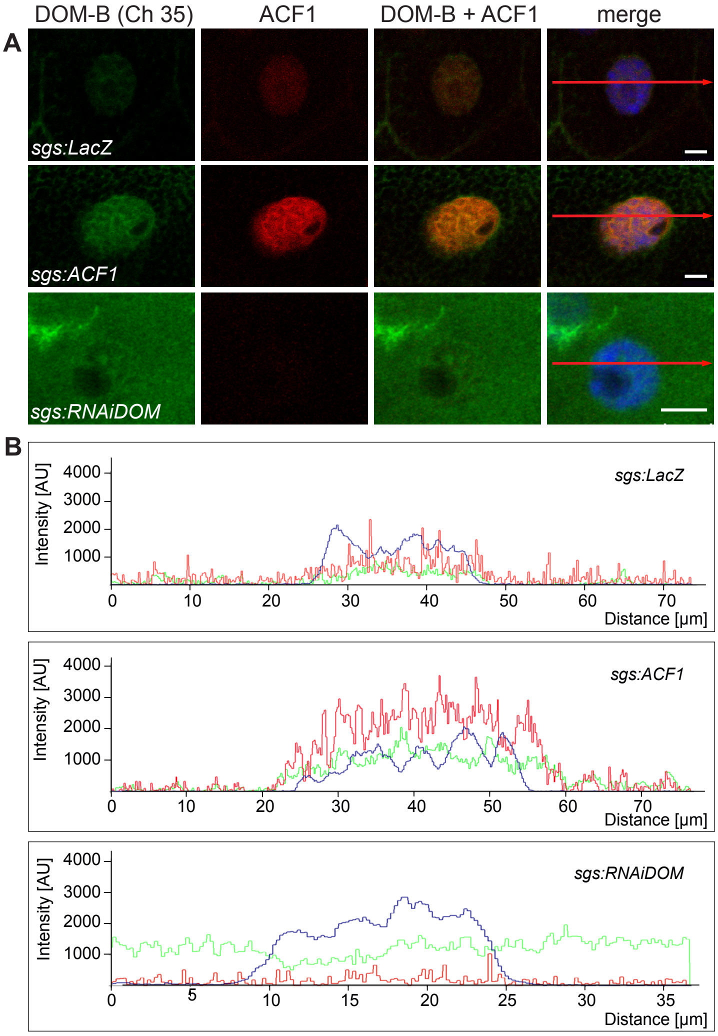
DOM-B (Ch 35)
ACF1
DOM-B + ACF1
merge
A
sgs:LacZ
sgs:ACF1
sgs:RNAiDOM
B
Intensity [AU]
4000
3000
2000
1000
sgs:LacZ
0
10
20
30
40
50
60
70
Distance [µm]
Intensity [AU]
4000
3000
2000
1000
sgs:ACF1
0
10
20
30
40
50
60
70
Distance [µm]
Intensity [AU]
4000
3000
2000
1000
sgs:RNAiDOM
0
5
10
15
20
25
30
35
Distance [µm]

Figure 3.15: Colocalization of DOM-B and ACF1 on chromatin of salivary glands
(A) Magnification of salivary gland nuclei stained for α-DOM-B (green) and α-ACF1 (red) specific antibodies, DNA stained by TO-PRO3 (blue in merge). Colocalization of signals appears orange in the overlay (DOM-B + ACF1). Scale bars represent 10 µm. **(B)** Line intensity profiles of salivary gland nuclei are indicated in A with red arrows and are generated by LSM image analyzing software. DOM-B (green), ACF1 (red), DNA (blue). Scans of intensity profiles are measured over a distance covering the nuclei and the immediate cytosol. Intensity is expressed as arbitrary units [AU].

in which signals for ACF1 and DOM-B were both found to be upregulated (Figures 3.14 and 3.15). In the chapter above (3.5.3) was shown that a knock-down of DOM-B (*sgs:RNAiDOM*) appears to abolish ACF1 immunofluorescence signals from chromatin (Figure 3.14). In addition, both proteins were detected in similar limited amounts on control salivary glands (*sgs:LacZ*) (Figure 3.14). This is visualized by a representative magnification of control nuclei (*sgs:LacZ*), costained with α-DOM-B and α-ACF1 specific antibodies, which show same weak staining signals on polytene chromosome as previously described (Figure 3.15.A). As seen above, ectopic expression of DOM-B WT (*sgs: DOM-B*) in salivary glands resulted in an increase of DOM-B, but not of ACF1 staining signals (Figure 3.14, 2nd panel). In contrast, targeted expression of ACF1 (*sgs:ACF1*) led to an increase of nuclear ACF1 and DOM-B signals (Figures 3.14 and 3.15). An overlay of both signals appeared orange suggesting a colocalization of DOM-B and ACF1 all-over the nuclei (*sgs:ACF1*) (Figure 3.14 and 3.15.A). Colocalization of DOM-B and ACF1 were analyzed by measuring an intensity profile of immunofluorescence staining signals over a distance covering the nuclei and the immediate cytosol (Figure 3.15.B). Low expression levels of DOM-B and ACF1 in nuclei of the control larvae (*sgs:LacZ*) was reflected by the low intensity of the profile. In contrast, ectopic expression of ACF1 (*sgs:ACF1*) led to a dramatic increase of nuclear ACF1 and DOM-B demonstrated by a higher intensity relative to the control signals. Interestingly, there was a tendency of DOM-B and ACF1 signals to be excluded from TO-PRO 3 stained DNA regions, suggesting a binding of both factors to less condensed chromatin. Upon DOM-B depletion, no labeling of either protein was observed on chromatin, besides the high background staining provoked by the IgY chicken antibody of DOM-B.

Taken together, the new α-DOM-B antibodies 2G5 and Ch35 were suitable for immunofluorescence experiments. Both were important tools for further *in vivo* studies. DOM-B was present at low levels on polytene chromosomes similar to ACF1. The expression of DOM-B and ACF1 appeared to be inter-dependent, which strengthens the idea of a functional *in vivo* interaction. Furthermore, DOM-B and ACF1 were found in association with less condensed chromatin, which led to further analyses of DOM-B as a potential factor for chromatin formation.

3.6 Chromatin Formation in Salivary Glands Is Disturbed by Ectopic Expression of DOM-B

To visualize effects on chromatin organization, whole-mount nuclei of salivary glands were stained with an α-HP1a-specific antibody. HP1 (heterochromatin protein 1) is a constitutive component of heterochromatin essential for heterochromatic gene silencing and heterochromatin stability (Shi et al., 2008). Under wildtype conditions, HP1a localizes preferentially to the pericentric heterochromatin, which is visible as the “chromocenter” in polytene chromosomes and is displayed by the bright nuclear domain in control larvae (*sgs:LacZ*) (Figure 3.16) (Swaminathan et al., 2005; Shi et al., 2008). Ectopic expression of DOM-B WT led to a reduction of HP1 staining signal at the chromocenter and to a more dispersed staining detectable all-over the nuclei (*sgs:DOM-B WT,* 2nd panel), suggesting a reduction of HP1 recruitment to the chromocenter. A similar staining pattern was observed upon DOM-B KR expression. Also in this case, the expression of DOM-B KR mutant gave rise to a reduction of HP1 foci (*sgs:DOM-B KR*, 4th panel). In addition, these salivary glands were costained with an α-H2AV-specific antibody, since previous immunofluorescence experiments had revealed a certain degree of variability (*see* Chapter 3.5.2), which in turn may point to an alteration of chromatin organization. H2AV

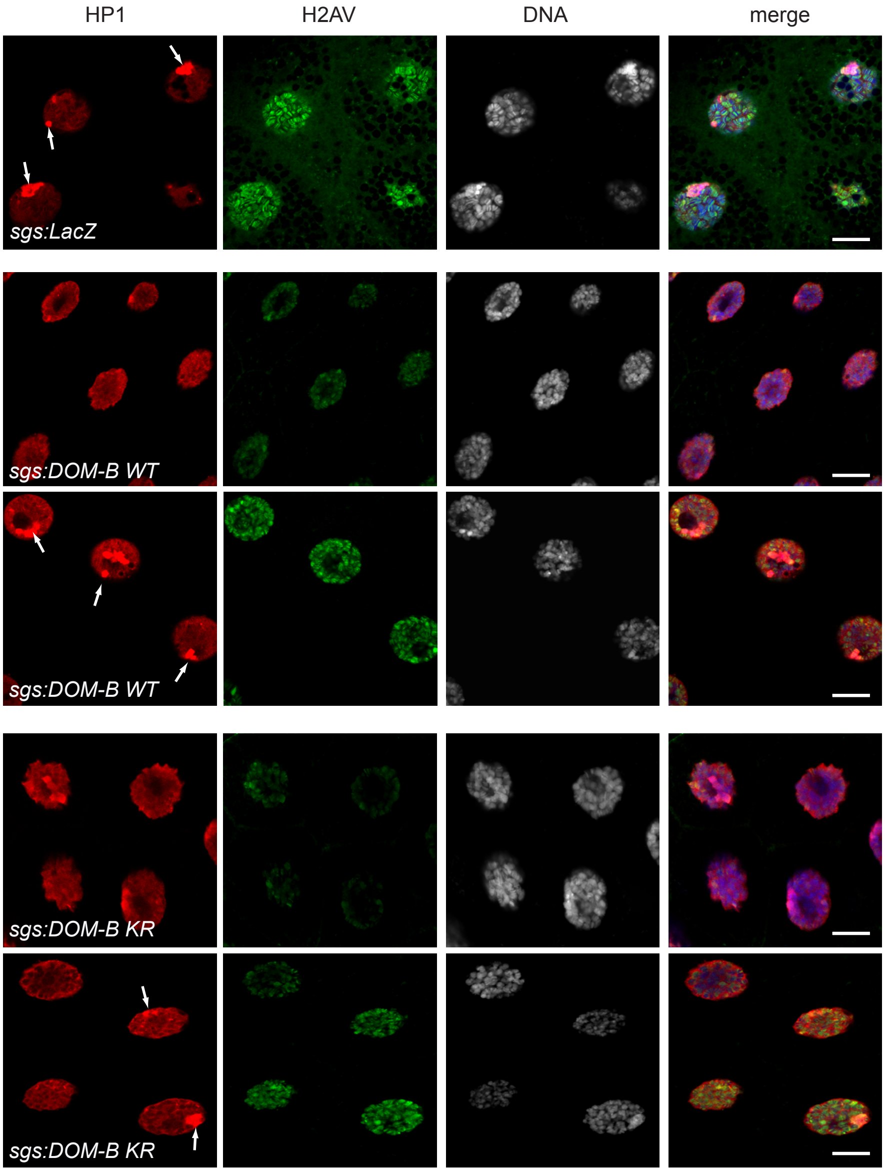

Figure 3.16: Ectopic expression of DOM-B leads to a disruption of chromatin organization
Immunofluorescence staining of whole-mount salivary glands using the *sgs-GAL4* driver. Salivary glands of larvae expressing β-galactosidase as a control (*sgs:LacZ*) display the normal staining pattern of HP1a (red) enriched on the chromocenter (marked with white arrows) and of H2AV (green); DNA stained by TO-PRO3 (white, blue in merge). Expression of DOM-B WT or KR in salivary glands varied from a normal HP1a distribution (white arrows) to a loss of HP1a on the chromocenter (*sgs:DOM-B WT, sgs:DOM-B KR*). In these nuclei, incorporation of H2AV into chromatin was decreased compared to the control. Scale bars represent 20 µm.

incorporation is known to be important for a proper establishment of chromatin and is required for the recruitment of HP1 (Swaminathan et al., 2005). Interestingly, nuclei lacking the characteristic HP1 foci also showed a reduction of H2AV staining signals. Alteration in the distribution of HP1 and H2AV staining signals was detected in the majority of salivary glands of ectopically DOM-B WT and DOM-B KR expressing larvae (*sgs:DOM-B WT/KR*, 2nd / 4th panel). In a few specimen, a distribution of H2AV and HP1 was observed comparable to the control line (*sgs:DOM-B WT/KR*, 3rd / 5th panel). Furthermore, wandering 3rd instar larvae ectopically expressing DOM-B WT or KR showed a developmental delay of 2-3 days compared to control larvae, which points to functional defects associated with an impaired nuclear organization.

3.7 DOM Depletion Disturbs Normal Development during Fly Morphogenesis

According to previous studies DOM plays an important role during fly development. Ruhf and colleagues demonstrated that various *dom* loss-of-function mutations derived by imprecise excision of P-elements gave rise to multiple defects or were lethal during morphogenesis (Ruhf et al., 2001). They further showed that DOM is necessary for cell viability and proliferation, as well as for oogenesis. To shed light on the specific role of DOM-B during fly development, effects and phenotypes of RNAi-mediated targeted depletion of DOM were analyzed.

3.7.1 Knock-Down of DOM in Salivary Glands Causes Pupal Lethality

For further studies, *dom* was depleted using transgenic RNA interference (RNAi). Therefore, *UAS-IR-DOM* flies were crossed to *sgs3-GAL4* flies for a salivary gland specific knock-down as previously done (*see* Chapter 3.5). This strategy did not allow distinguishing between effects of DOM-A and DOM-B knock-down, since both isoforms are depleted by this approach. As observed before (*see* Chapter 3.5) salivary glands lacking DOM (*sgs:RNAiDOM*) showed a remarkable reduction in size when compared to salivary glands of the control line (*sgs:LacZ*) (Figure 3.17). The fat body of DOM depleted salivary glands, which is attached to the glands, appeared to be normal in size and therefore serves as a reference.

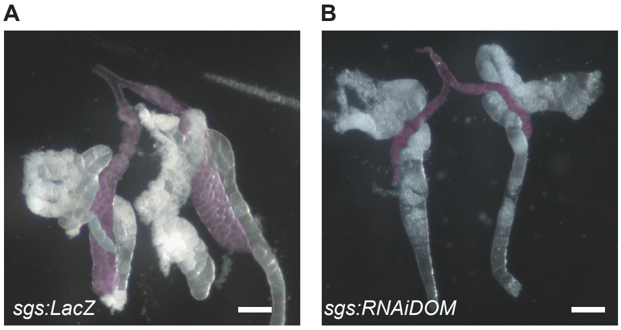

Figure 3.17: DOM depletion leads to a remarkable reduction in size of salivary glands
Salivary glands, in which DOM was depleted by RNAi-mediated interference (*sgs:RNAiDOM*) and salivary glands expressing β-galactosidase as a control (*sgs:LacZ*) were dissected under a binocular microscope. Images were taken with the Axiostar plus optic device-camera (Zeiss, Germany). Glands were artificially colored in pale red using Adobe Photoshop CS2. The white structure corresponds to the fat body. Scale bars represent 300 µm.

Since an inappropriate expression of DOM-B perturbs chromatin organization in salivary glands, nuclei of glands were also analyzed upon DOM depletion. As an indicator of proper chromatin formation, polytene chromosomes were stained for H2AV and HP1a as before (Chapter 3.6). The depletion of DOM in salivary glands resulted in an obvious reduction of the size of nuclei and an altered chromatin organization (Figure 3.18.A). Compared to the control (*sgs:LacZ*), nuclei lacking DOM (*sgs:RNAiDOM*) were only half the size or even smaller and misshaped (Figure 3.18.A, 2nd / 3rd panel). Defects in polytenic banding pattern were observed, suggesting that the polytene chromosomes may be under-replicated. In these nuclei, H2AV staining signals were reduced or even occasionally below the detection level, which can be caused by a reduced incorporation of H2AV into chromatin. Interestingly, HP1 signals were distributed similar to the control (Figure 3.18.A, 2nd panel). In addition, actin filaments were visualized by phalloidin staining to monitor the cell shape (Figure 3.18.B). Plasma membranes of DOM-depleted salivary glands appeared misshaped and have lost the cuboidal form. They displayed nearly a round shape around the nuclei in DOM-depleted cells, compared to control cells (*sgs:LacZ*).

Taken together, DOM depletion in salivary glands affects the size and shape of entire gland cells as well as the nuclei size and the banding pattern of polytene chromosomes.

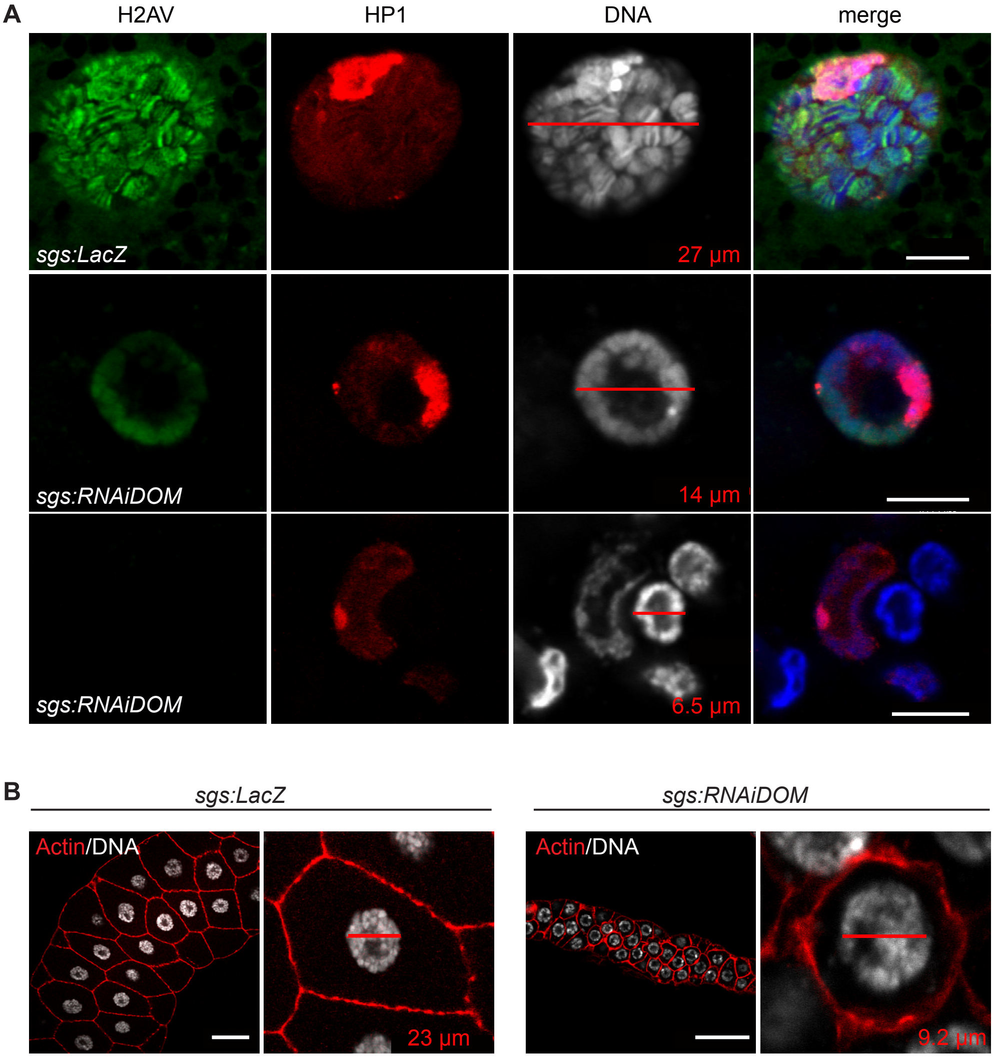

Figure 3.18: DOM depletion leads to a remarkable reduction of nuclei size
Immunofluorescence staining of whole-mount salivary glands using the *sgs-GAL4* driver. **(A)** Salivary glands expressing β-galactosidase as a control (*sgs:LacZ*) display the normal staining pattern of HP1a (red) and H2AV (green); DNA stained by TO-PRO3 (white, blue in merge). The depletion of DOM in salivary glands resulted in reduction of nuclei size and perturbation of chromatin organization (*sgs:RNAiDOM*). Diameter measurements of nuclei are indicated in red. Scale bars represent 10 µm. **(B)** Control salivary glands (*sgs:LacZ*) show the normal staining pattern for actin (stained by phalloidin, red); DNA stained byTO-PRO3 (white). After RNAi-mediated DOM depletion (*sgs:RNAiDOM*) plasma membranes of these salivary glands were misshaped and lost the cuboidal form. Diameter measurements of nuclei are indicated in red. Scale bars represent 50 µm.

A further consequence of DOM depletion was the pupal lethality observed in the *sgs:RNAiDOM* line: 136 dead pupae and only four adult flies ("escapers") were counted (Figure 3.19). Nearly fully developed adult flies were observed in pupal cases of dead individuals, which suggest a late pupal lethality (Figure 3.19.A/B). This phenotype was also observed by Ruhf and colleagues by certain P-element excisions of the *dom* gene leading to larval and late pupal lethality (Ruhf et al., 2001). Assuming

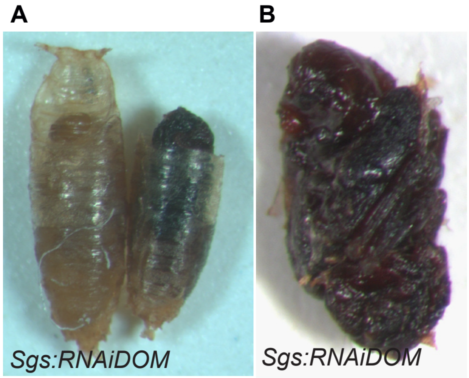

Figure 3.19: DOM depletion leads to late pupal lethality
(A) Dead pupae of RNAi-mediated targeted depletion of DOM in salivary glands by the *sgs3-GAL4* driver. *Dom* depletion in salivary glands leads to late pupal lethality. (**B**) Dead pupa with removed pupal case after DOM RNAi-mediated depletion. The fly is already fully developed. (**C**) The table presents the absolute numbers scored for adult flies (n) or dead pupae (n).

C

Genotype	Adult flies (n)	Dead pupae (n)
yw; +/+; UAS-IR-DOM/sgs-GAL4	4	136
yw; +/+; UAS-IR-ACF 1/sgs-GAL4	156	0

that ACF1 is present on chromatin in limited amounts, but plays an important role for chromatin formation and fly viability (Chioda et al., 2010), offspring of RNAi-mediated depletion of ACF1 in salivary glands were analyzed in parallel (Figure 3.19.C). No phenotypic abnormalities were observed, which indicates that defects in salivary glands and the late pupal lethality were due to depletion of DOM and not a result of indirect effects caused by reduced ACF1 levels.

3.7.2 Depletion of DOM during Eye Development Impairs Eye and Antenna Morphology

One of the best-understood examples of how molecular interactions and mechanisms generate adult structures is the development of the eye in *Drosophila*, which lends itself to explore the role of DOM during development. Hence, effects of an eye-specific knock-down were analyzed in offspring (F1) of *UAS-IR-DOM* flies crossed to a *eyeless-GAL4* (*ey-GAL4*) driver line (*ey:RNAiDOM*). The activation of the *eyeless* gene starts already at embryonic stage 4 (~2 h AED) in the eye primordia of embryos. In subsequent larval stages, *eyeless* continues to be expressed in the developing eye-antenna discs anterior to the morphogenetic furrow (MF) (*see* also Chapter 1.4.3). This gene is required for the initiation of photoreceptor development and their determination (Halder et al., 1995).

In contrast to the knock-down of DOM in salivary glands that resulted in a late pupal lethality, DOM depletion in larval eye-antenna discs did not interfere with fly viability. However, these flies lacking DOM in the eye-antenna disc during morphogenesis, showed many aberrations of adult compound eyes and antennae (*ey:RNAiDOM*) (Figure 3.20.A-C). The phenotypes ranged from mispositioning, loss or duplication of the antennae and abnormal eye morphology in about 58% of adult flies (Figure 3.20.F/G). This inappropriate formation of the antenna may be due to specific DOM-B depletion, since Ruhf and colleagues found only DOM-B to be expressed in the entire eye and antenna disc, whereas DOM-A expression appeared restricted to the photoreceptor precursor cells posterior to the MF in the eye disc (Ruhf et a., 2001). These eye and antennal aberrations were specific to the depletion of DOM, since they were never observed upon RNAi-mediated depletion of ACF1 in eye disc using the same *ey-GAL4* driver (*ey:RNAiACF1*) (Figure 3.20.D/E).

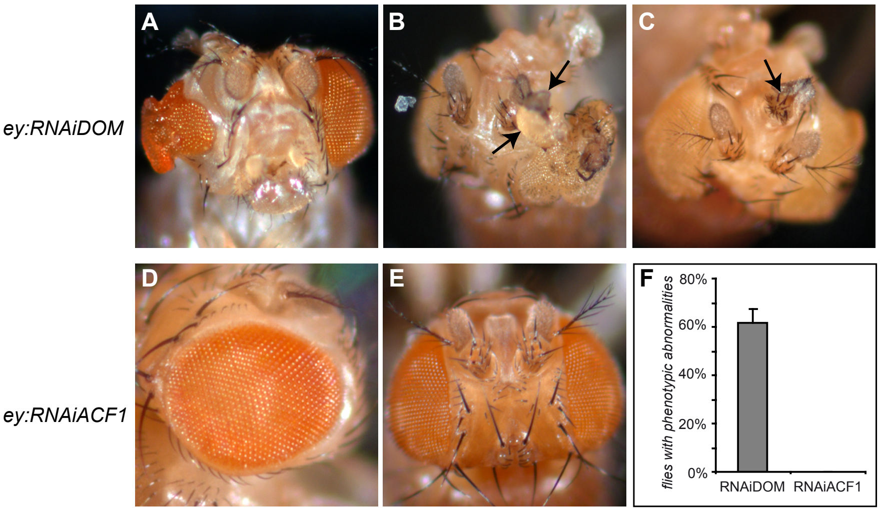

G

Fly line	Genotype	n	flies (n) with phenotypic abnormalities	%
RNAiDOM	*yw; +/+; UAS-IR-DOM/ey-GAL4*	181	112	62
RNAiACF1	*yw; +/+; UAS-IR-ACF1/ey-GAL4*	225	0	0

Figure 3.20: DOM depletion in eye-antenna discs disrupts morphogenesis of adult compound eyes and antennae
RNAi-mediated targeted depletion of DOM and ACF1 with the *eyeless-GAL4* driver in eye-antenna discs of *Drosophila*. **(A-C)** DOM depletion resulted in phenotypic abnormalities ranging from antennae mispositioning, loss or duplication and abnormal eye morphology (*ey:RNAiDOM*). **(D-E)** None of these phenotypes were observed when ACF1 (*ey:RNAiACF1*) was knocked-down as a control similar to *ey:LacZ* control flies (not shown). **(F)** The percentage of abnormal eye/antenna phenotypes is graphically presented in the histogram. **(G)** The percentages in (F) correspond to numbers of abnormal eyes and numbers of flies (n) scored for each genotype. Error bars represent SD of two biological replicates.

3.7.3 Differentiation of Precursor Cells in Imaginal Eye-Antenna Discs Is Perturbed by DOM Depletion

The observed phenotypic abnormalities in adult eyes resulting from RNAi-mediated targeted depletion of DOM might originate from altered differentiation processes that occur in the imaginal eye-antenna discs of larvae. As described above (Chapter 1.4.3), an adult compound eye results from the complex combination of cell cycle control and cell fate determination during morphogenesis in eye-antenna discs. These tissues are particularly suitable to study mechanisms and factors involved in cell proliferation and cell differentiation in *Drosophila*.

To uncover the causes of phenotypic abnormalities of adult compound eyes resulting from a knock-down of DOM, eye-antenna discs of third instar larvae were dissected for further analysis. The eye-antenna discs were immunofluorescence-stained with markers for different cell types and analyzed by confocal microscopy (Figure 3.21). The neuronal marker Dachshund (DAC) was used to identify undifferentiated neuronal precursor cells, which are normally restricted to a domain of the eye disc along the MF and to the inner circle of the posterior antennal lobe (Duong et al., 2008). A knock-down of ACF1 by RNAi-mediated depletion (*ey:RNAiACF1*) did not result in obvious phenotypic abnormalities of adult fly eyes (*see* Figure 3.20). The eye-antenna imaginal discs of corresponding third instar larvae displayed a normal distribution of DAC signals along the MF and in the posterior lobe (Figure 3.21) comparable to discs of wildtype flies (not shown) or control flies *ey:LacZ* (*see* Figure 3.23). In striking contrast, DOM depletion led to a deranged and irregular MF indicated by the abnormal distribution of DAC signals, suggesting neuronal differentiation along the MF was impaired. Additionally, a global distortion and increased size of *ey:RNAiDOM* eye discs were observed.

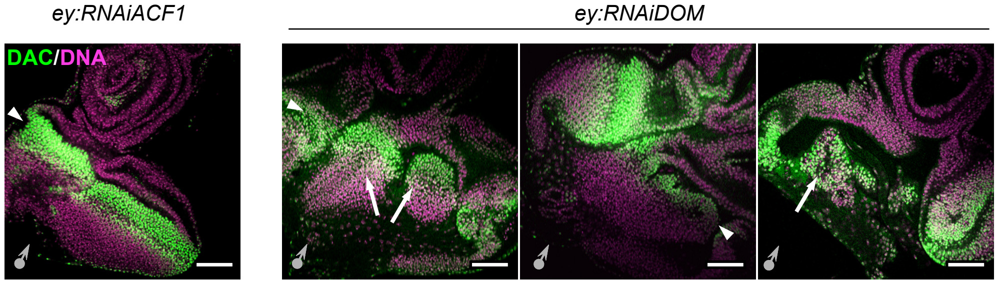

Figure 3.21: DOM depletion in eye-antenna discs affects cell differentiation
Immunofluorescence analysis of whole-mount larval imaginal eye-antenna discs, in which DOM or ACF1 was depleted by an RNAi-mediated knock-down. A white arrowhead indicates the location of the morphogenetic furrow (MF). The grey arrows demonstrate the orientation of the eye-antenna disc: the arrowhead shows the direction of the anterior antennal region, the tail indicates the posterior eye part. Immunofluorescence staining with Dachshund (DAC, green), a marker for undifferentiated neuronal precursors, is usually limited to a domain of the eye disc along MF in the posterior lobe (*ey:RNAiACF1*). DOM depletion (*ey:RNAiDOM*) resulted in a deranged and irregular morphogenetic furrow and aberrant distribution of DAC signals. DNA stained by TO-PRO3 (purple). Scale bars represent 50 µm.

Taken together, *dom* depletion resulted in defects of precursor cell differentiation along the MF. A loss of the regular organization and the tight coordination especially in the region along the MF of eye-discs during morphogenesis will lead to adult phenotypic abnormalities observed by RNAi-mediated knock-down of DOM (*see* Figure 3.20). In addition, defects of antennal structure (mispositioning, loss or duplication of antenna, Figure 3.20) were observed only upon *dom* depletion. DOM-B is known to be ubiquitously expressed in the eye as well as in the antennal part of the disc, and these abnormalities were neither observed upon ACF1 depletion nor upon ectopic expression of DOM or LacZ under the *ey-GAL4* driver, which will be described in the following (Chapter 3.8).

3.8 Ectopic Expression of DOM-B in Imaginal Eye-Antenna Discs Disturbs Eye Development

3.8.1 Ectopic Expression of DOM-B in Imaginal Eye-Antenna Discs Caused Phenotypic Abnormalities in Adult Compound Eyes

Encouraged by the finding that a developmental- and tissue-specific depletion of DOM in imaginal eye-antenna discs disturbs the eye development and impairs cell differentiation, DOM-B was ectopically expressed in these tissues to compare effects and potential phenotypic abnormalities to the ones observed upon DOM depletion. DOM-B WT and KR were expressed in eye-antenna discs using the *ey-GAL4* driver as in previous experiment. Adult flies expressing DOM-B WT (*ey:DOM-B WT*) displayed a high frequency of phenotypic abnormalities in their compound eyes (Figure 3.22.A-C). A dramatic increase of ectopic cells in distinct regions of the eye could be observed. In addition, flies showed eye duplications and outgrowing structures reminiscent of antennal structures frequently bearing ommatidia on the tip (Figure 3.22.A/B). Ectopic expression of DOM-B also led to altered eye morphology and complete deranged eyes (Figure 3.22.C). Major differences were monitored ectopically expressing the putative ATPase-deficient DOM-B KR mutant (Figure 3.22.D-F). Expression of DOM-B KR caused loss of cells in regions the eye part together with overgrowth of ommatidia in barrel-like structures and undefined tissue. Between 40-60% of adult flies showed these phenotypic abnormalities, regardless of the transgene insertion site (Figure. 3.22.H/I). These eye aberrations were specific for the ectopic expression of DOM-B WT and KR, as they were never observed in the control line (*eye:LacZ*) (Figure 3.23.G). Interestingly, the observed phenotypic abnormalities of the

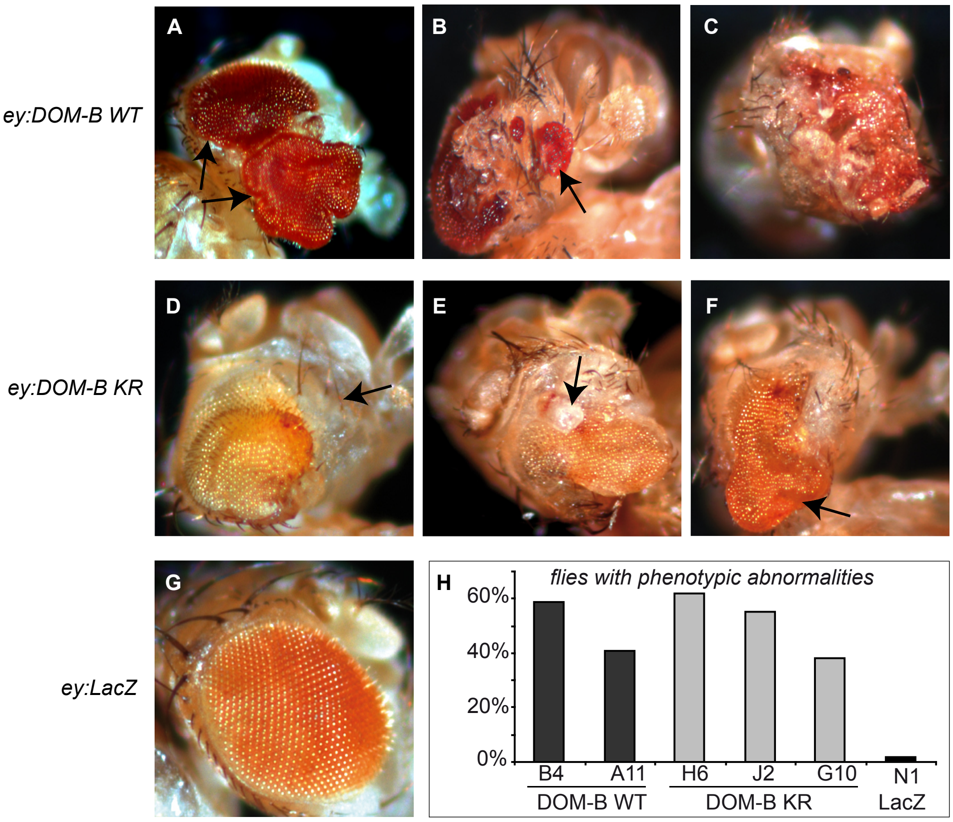

I

Fly line	Genotype	n	flies (n) with phenotypic abnormalities	%
B4	*yw; UAS-DOM-B WT/+; ey-GAL4/+*	257	150	60
A11	*yw; UAS-DOM-B WT/ey-GAL4*	162	65	41
H6	*yw, UAS-DOM-B KR/+; ey-GAL4 /+*	278	173	62
J2	*yw; UAS-DOM-B KR/+; ey-GAL4 /+*	321	175	55
G10	*yw; UAS-DOM-B KR/ey-GAL4*	258	98	38
N1	*yw; UAS-LacZ/ey-GAL4*	168	4	2

Figure 3.22: Ectopic expression of DOM-B in eye-antenna discs disrupts adult eye morphology
UAS-DOM-B WT, *UAS-DOM-B KR* and *UAS-LacZ* transgenic flies were crossed to *ey-GAL4* flies. The offspring (F1) was analyzed for potential phenotypic abnormalities in compound eyes of adult flies. **(A-C)** Ectopic expression of DOM-B WT (*ey:DOM-B WT*) leads to general increase in eye size and dramatic alteration of eye morphology. **(D-F)** Ectopic expression of DOM-B KR (*ey:DOM-B KR*) resulted in reduction and overgrowth of eye cells. **(G)** None of the phenotypes were observed in offspring (F1) of the control flies expressing β-galactosidase as a control (*ey:LacZ*). **(H)** The percentage of phenotypic abnormalities of one or both adult compound eyes is graphically represented in the histogram; Dark grey bars indicate two independent transgenic fly lines for *UAS-DOM-B WT* (B4, A11); Light grey bars indicate three independent fly lines for *UAS-DOM-B KR* (H6, J2, G10). N1 indicates the control fly line *UAS-LacZ*. **(I)** The table depicts the total numbers of flies scored (n), the number of flies with phenotypic abnormalities of one or both adult compound eyes and the percentage thereof.

putative ATPase-deficient DOM-B KR ectopically expressing flies corresponded to gross abnormalities in fly eyes resulting from ACF1 ectopic expression induced by ACF1 (Chioda et al., 2010). This suggests a genetic interaction and a potential *in vivo* interplay between DOM-B and ACF1.

3.8.2 Ectopic Expression of DOM-B Disturbes Cell Differentiation in Larval Imaginal Eye-Antenna Discs

To analyze the cause of the observed phenotypic abnormalities of compound eyes from flies overexpressing DOM-B and KR using the *ey-GAL4* driver line, imaginal discs of 3rd instar larvae were immunofluorescence-stained for the neuronal markers DAC and ELAV. DAC had already been used as marker in stainings of eye-antenna discs lacking DOM (*see* Chapter 3.7.3). The α-ELAV antibody stains differentiated photoreceptor cells posterior to the MF, as displayed by the control line (*ey:LacZ*) (Figure 3.23.A) (Duong et al., 2008). The regular staining pattern of ELAV was disturbed upon DOM-B WT expression (*ey:DOM-B WT*). Imaginal discs showed an irregular and diffuse ELAV staining (marked with white arrow) in certain regions posterior to the MF. This suggests that an unbalanced DOM-B WT expression in eye discs disturbs terminal differentiation of photoreceptors and correlates with a perturbed progression of the MF, as well as irregular photoreceptor cell clusters. Only minor alteration of the regular ELAV staining pattern was detected upon expression of DOM-B KR (*ey:DOM-B KR*), suggesting that the putative ATPase-deficient DOM-B KR protein has a weaker influence on

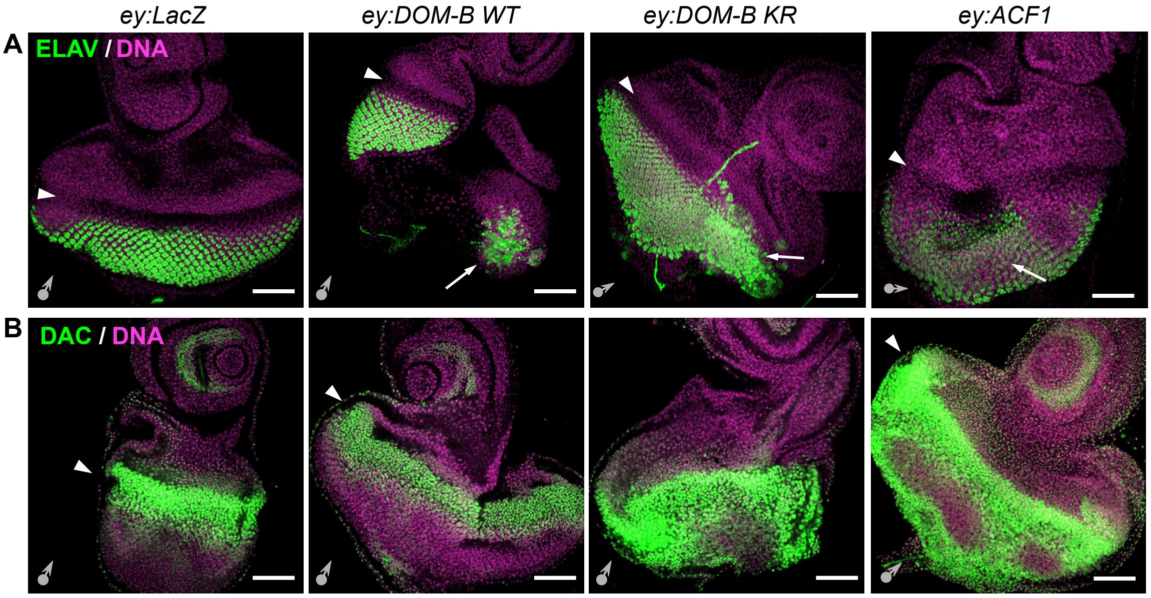

Figure 3.23: Ectopic expression of DOM-B WT and KR disturbs cell differentiation in eye-antenna discs
Immunofluorescence analysis of whole-mount imaginal eye-antenna discs of 3rd instar larvae after crossing *UAS-DOM-B WT*, *UAS-DOM-B KR* and *UAS-LacZ* as a control to *ey-GAL4* flies. A white arrowhead indicates the location of the morphogenetic furrow (MF). The grey arrows demonstrate the orientation of the eye-antenna disc: the arrowhead shows the direction of the anterior antennal region, the tail indicates the posterior eye portion. DNA was stained by TO-PRO 3 (purple). **(A)** Immunofluorescence staining with the α-ELAV antibody (green), a marker for differentiated photoreceptors as displayed by the control (*ey:LacZ*). An Irregular and diffused ELAV staining (marked with white arrows) was observed upon DOM-B WT/KR and ACF1 expression (*ey:DOM-B WT, ey:DOM-B KR, ey:ACF1*). **(B)** Immunofluorescence staining with α-DAC antibody (green), a marker for undifferentiated neuronal precursors, is usually limited to a domain of the eye disc along the MF in the posterior lobe, as displayed by eye discs of the control *ey:LacZ* or *ey:DOM-B WT*. Strong increase of DAC positive cells was monitored upon DOM-B KR and ACF1 expression (*ey:DOM-B KR, ey:ACF1*). Scale bars represent 50 μm.

cell differentiation than DOM-B WT. The DAC-marker was used to detect undifferentiated neuronal precursors. As displayed in the control line (*ey:LacZ*), DAC expression appears as a band along the MF and as a circle in the antennal part of the disc (Figure 3.23.B). Upon DOM-B WT expression the pattern of DAC was similar to control discs, suggesting that earlier stages of neuronal differentiation are not affected (*ey:DOM-B WT*). Strikingly, expression of DOM-B KR showed a clear increase of DAC - positive cells in the entire posterior region of eye discs (*ey:DOM-B KR*).

These data validate that DOM-B WT or the ATPase-deficient mutant DOM-B KR alters cell fate determination upon early ectopic expression in imaginal eye-antenna discs. Uncoupling the tight coordination between cell cycle progression and differentiation by DOM-B WT or KR reflects the phenotypes in adult compound eyes. A higher dose of DOM-B WT during morphogenesis disrupts cell differentiation and leads to deranged eyes with an altered morphology. By contrast, expression of the putative ATPase-deficient DOM-B KR leads on the one hand to additional ommatidia in some regions of the compound eye, but on the other hand to an increased amount of undifferentiated cells. This may lead finally to the altered structure of entire regions lacking eye cells along with overgrowing ommatidia. The similarity between phenotypic abnormalities in compound eyes of flies expressing DOM-B KR and phenotypic aberrations described for expression of ACF1 (Chioda et al., 2010) can be explained by the comparable DAC staining pattern in *ey:DOM-B KR* and *ey:ACF1* eye discs (Figure 3.23.B). Indeed, both eye discs displayed the same perturbed DAC pattern of a strong expansion of DAC - positive cells behind the MF. In addition, expression of ACF1 led to an irregular ELAV staining pattern as already shown by Chioda and colleagues (Chioda et al., 2010), which was similar to the disturbed ELAV staining of *ey:DOM-B WT* eye-discs (Figure 3.23.A). This supports again the hypothesis of a direct genetic interaction between DOM-B and ACF1 *in vivo*.

3.8.3 Ectopic Expression of DOM-B Delays Cell Cycle Progression during S-Phase and Perturbs Apoptotic Events

A misexpression of DOM-B during morphogenesis in imaginal eye-discs perturbs cell differentiation. Cell fate is precisely determined and controlled by a number of factors including cell cycle progression, synchronization and apoptotic events. In analogy to related phenomena upon ACF1 expression in eye-antenna discs (Chioda et al., 2010), expression of DOM-B during eye morphogenesis may also lead to an altered S-phase progression and cell proliferation. To gain deeper insights into the function of DOM-B during cell cycle, the S-phase progression in eye-antenna discs was visualized by bromodesoxyuridine (BrdU) incorporation.

A normal staining pattern of BrdU incorporation is characterized by a stripe of cells just posterior to the MF that replicate their genomes synchronously (Figure 3.24.A). Besides the defined band of BrdU-positive cells, some interommatidial cells divide more posterior (*see* also Chapter 1.4.3). Cells anterior to the MF undergo asynchronous cycles and also incorporate BrdU in agreement with earlier studies (Leong et al., 2009). This staining pattern could be detected in 80% of the control eye disc allowing incorporation of BrdU with a pulse of 30 minutes (*ey:LacZ*).

Reduced BrdU incorporation was detected in eye discs expressing *ey:DOM-B WT*. More than 60% of eye discs did not show a defined stripe of nuclei positive for BrdU incorporation (Figure 3.24.B), suggesting defects in S-phase progression and lack of synchronous DNA synthesis (*ey:DOM-B WT*). By contrast, upon DOM-B KR expression eye discs displayed normal BrdU signals along the MF comparable to the control discs (*ey:DOM-B KR*). In 20% of control discs less BrdU incorporation was monitored (Figure 3.24.B). This variability may be due to the precise time point when wandering larvae were dissected. Therefore, the ratio between eye discs exhibiting a normal BrdU labeling versus discs without BrdU incorporation was scored and calculated (Figure 3.24.B). Whereas DOM-B WT ectopic expression led to reduced BrdU incorporation, ectopic expression of DOM-B KR had a much smaller effect.

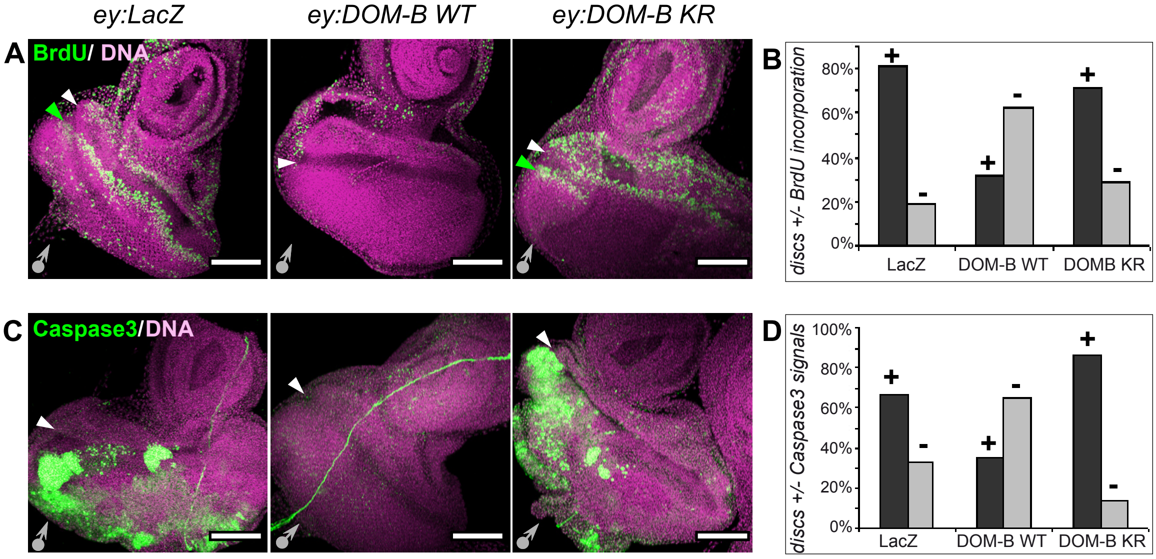

Figure 3.24: Ectopic expression of DOM-B delays S-phase progression and perturbs apoptotic events Immunofluorescence analysis of whole-mount imaginal eye-antenna discs of third instar larvae after crossing *UAS-DOM-B WT*, *UAS-DOM-B KR* and *UAS-LacZ* as a control to *ey-GAL4* flies. A white arrowhead indicates the location of the MF. The grey arrows demonstrate the orientation of the eye-antenna disc: the arrowhead shows the direction of the anterior antennal region, the tail indicates the posterior eye portion. DNA stained by TO-PRO 3 (purple) **(A)** Immunofluorescence staining with BrdU incorporation (green) with a pulse of 30 min. Most of control eye discs (*ey:LacZ*) displayed the regular pattern of BrdU incorporation posterior to the MF in a stripe of cells undergoing synchronous replication (green arrow). The white arrow points at irregular BrdU patterns typical of asynchronous cycles anterior to the MF. **(B)** The histogram shows the percentage of imaginal eye discs displaying a regular (+) or reduced (-) BrdU patterning scored for each genotype. **(C)** Apoptotic events were visualized using activated Caspase 3 as a marker (green). The white arrow shows the MF. **(D)** The histogram presents the percentage of imaginal eye discs displaying a significant amount of Caspase-3 signal (+) or a clear reduction thereof (-) scored for each genotype. Scale bars represent 50 µm.

To assess whether these defects in S-phase progression were due to a cell cycle block or just to a delay, BrdU incorporation was allowed for 60 minutes (data not shown). In this case, a defined stripe of BrdU-positive cells posterior to the MF was observed in all discs even in the presence of increased DOM-B WT or KR. This suggests that DOM-B expression leads to a delay and asynchrony of S-phase onset along the MF. Interestingly, a similar effect of S-phase perturbation is known from ectopically expressed ACF1, which also leads to a reduced BrdU labeling and impaired synchronization of DNA (Chioda et al., 2010). Based on these findings, both, DOM-B and ACF, appeared to play an important role during cell cycle progression and differentiation.

Another observed phenotype was the obvious lack of ommatidia in adult eyes generated by DOM-B KR, which might be linked to perturbation of scheduled apoptosis. Controlled cell death in eye discs normally occurs during eye differentiation and is essential for proper morphogenesis. Apoptotic cells can be visualized due to the presence of the cleaved (active) form of Caspase 3 (Figure 3.24.C/D). Normal levels of apoptosis (about 66%) are demonstrated by the control eye disc, where Caspase 3 positive cells most prominently appeared just posterior of the MF (*ey:LacZ*). 33% of monitored discs did not show a clear Caspase 3 signal. The opposite was observed upon expression of DOM-B WT, since more than 60% of discs lacked a Caspase 3 signal, which suggests a major decrease of apoptotic events (*ey:DOM-B WT*). In comparison to control discs, DOM-B KR expression resulted in eye discs with apoptotic cells in over 80% (*ey:DOM-B KR*). The ratio between imaginal eye discs positive for Caspase 3 to discs where no clear Caspase 3 signal was detectable (Figure 3.24.D) is consistent with the observed adult eye phenotypes. Overproliferation of ommatidia may be due to low levels of apoptotic events in more than 60% of imaginal eye discs. In contrast, a 20% increase in apoptosis of eye-discs expressing DOM-B KR was observed and might explain the abnormal lack of ommatidia in DOM-B KR flies.

3.9 Combined Ectopic Expression of DOM-B and ACF1 Leads to Major Defects and Lethality

Evidence for an association between DOM-B and ACF1 could already be obtained from *in vitro* studies (Chapter 3.1). Furthermore, the *in vivo* analysis pointed to a functional relationship between both proteins. DOM-B and ACF1 appeared to be both important for proper chromatin organization. Upon ectopic expression of ACF1, the protein level of DOM-B is increased (*see* Chapter 3.5). Inappropriate expression of DOM-B leads to numerous forms of defects during differentiation, which is also known for ACF1 (Chioda et al., 2010). Therefore, effects that originate from the combined expression of both proteins in various *Drosophila* tissues were examined. For that purpose, a transgenic fly line bearing *UAS-ACF1* on the first and *UAS-DOM-B WT* on the second chromosome was established and is referred to as "ACDC" fly line. In addition, a similar fly line termed as "ACKC" was designed with *UAS-ACF1* on the first in combination with *UAS-DOM-B KR* on the second chromosome to study phenomena due to expression of ACF1 with the putative ATPase-deficient mutant DOM-B KR. This strategy allowed an expression of both proteins at the same time in a tissue- and developmental-specific manner. Phenotypic abnormalities for ectopic coexpression of DOM-B and ACF1 regardless of the driver lines that will be described in the following had a tendency to become weaker after 2-3 generations of homozygosity, as already described for ACF1 (Chioda et al., 2010). Therefore, only transgenic flies homozygous for *UAS-ACDC* or *UAS-ACKC* between the 2nd to 5th generations were used.

3.9.1 Ectopic Expression of DOM-B in Fly Eyes Leads to a Rough Eye Phenotype

In order to drive the ectopic expression in different tissues and at various developmental stages, several *GAL4*-driver lines were required. The *glass-GAL4* driver was first used to study effects upon ACDC or ACKC expression during eye development. The *Drosophila glass* gene is activated at embryo stage 11-12 and is required in larval eye-antenna discs for the differentiation and survival of photoreceptors. *Glass* initiates at the morphogenetic furrow and extends to the posterior margin of the disc. It is functionally active only in the photoreceptors but not in cone cells (Moses and Rubin, 1991; Ellis et al., 1993). Expression of DOM-B WT in eye discs using the *glass* driver (*glass*:DOM-B WT) led to a rough eye phenotype with 100% penetrance (Figure 3.25). In a rough eye the repeating pattern of hexagonal facets (ommatidia) is disorganized. Only DOM-B WT expression altered the structure of the hexagonal pattern by disturbing the development of photoreceptors and their regular spacing. The general shape of the eye and of the antenna, respectively, was not affected. Perturbation of the eye was neither observed in the control line (*glass:LacZ*) nor in adult eyes expressing ACF1 (*glass:ACF1*). The eye development was also not influenced by the expression of the putative ATPase-deficient DOM-B KR (*glass:DOM-B KR*) alone or in combination with ACF1 (*glass:ACKC*). Interestingly, the rough eye phenotype appeared to be completely rescued by ACF1 in flies coexpressing DOM-B WT and ACF1 (*glass:ACDC*). In this case, the apparent functional antagonism between DOM-B and ACF1 indicates a genetic interaction of both proteins also *in vivo*. Moreover, expression of the ATPase-deficient dominant negative ISWI mutant (ISWI^{K159R}) in imaginal eye-discs resulted in a similar rough eye phenotype (Corona et al., 2002).

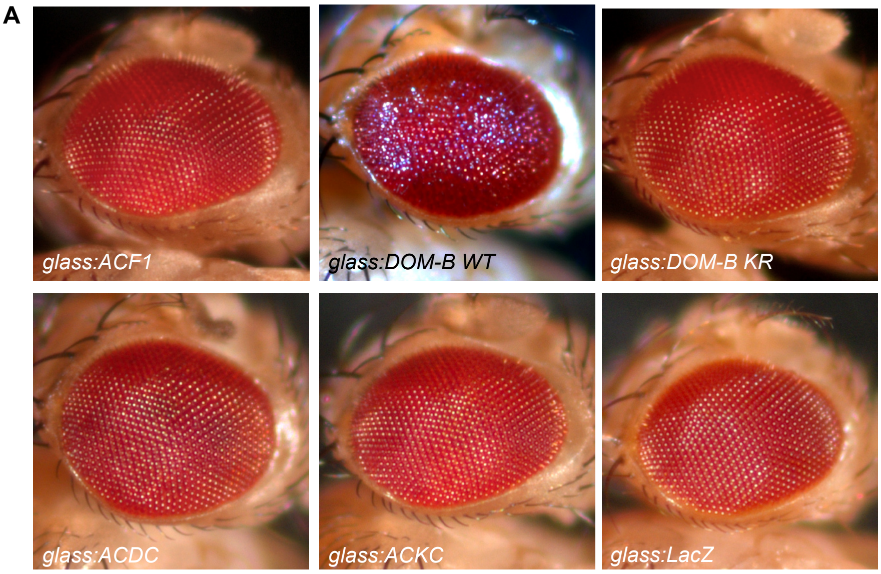

B

Fly line	Genotype	n	flies (n) with rough eyes	%
ACF1	*yw, UAS-ACF1/+ ; glass-GAL4/+*	156	0	0
WT	*yw; UAS-DOM-B WT/glass-GAL4*	160	160	100
KR	*yw; UAS-DOM-B KR/glass-GAL4*	167	0	0
ACDC	*yw, UAS-ACF1/+;UAS-DOM-B WT/glass-GAL4*	135	0	0
ACKC	*yw, UAS-ACF1/+;UAS-DOM-B KR/glass-GAL4*	162	0	0
LacZ	*yw; UAS-LacZ/glass-GAL4*	206	1	0

Figure 3.25: Ectopic expression of ACDC or ACKC using the *glass-GAL4* driver did not lead to eye perturbation
UAS-DOM-B WT, UAS-DOM-B KR, UAS-ACF1, UAS-ACDC, *UAS-ACKC* and *UAS-LacZ* as a control were crossed to the *glass-GAL4* driver line. The offspring (F1) was analyzed for potential phenotypic abnormalities in compound eyes of adult flies. **(A)** A rough eye phenotype was only observed expressing DOM-B WT alone (*glass: DOM-B WT*). **(B)** The table presents the absolute numbers of eyes scored (n) for each genotype, the absolute number of flies with rough eye phenotype and their percentage.

.

Comparing the strong phenotypic abnormalities observed upon expression of DOM-B WT, KR and ACF1 using the *ey-GAL4* driver (Chapter 3.8) with the relatively mild rough eye phenotype inducing by the *glass-GAL4* driver, exclusively DOM-B WT alone appeared to influence the eye formation also in later stages of development. The expression of the *eyeless* gene starts at stage 4 during embryogenesis, whereas *glass* is activated later between stages 11-12. This observation reflects also *in vivo* a developmentally regulated expression of DOM-B (*see* Chapter 3.1.1). To shed light on effects and interplay of the DOM-B WT and ACF1 coexpression in imaginal eye discs induced by *ey-GAL4* in comparison to previous observed phenotypic abnormalities resulting from single overexpression fly lines, homozygote flies containing DOM-B WT or KR and ACF1 were crossed to the *ey-GAL4* driver line (Figure 3.26). When coexpressing DOM-B WT and ACF1 (*ey:ACDC*) in larval eye imaginal discs, adult fly eyes displayed significant phenotypic abnormalities (Figure 3.26.A-C).

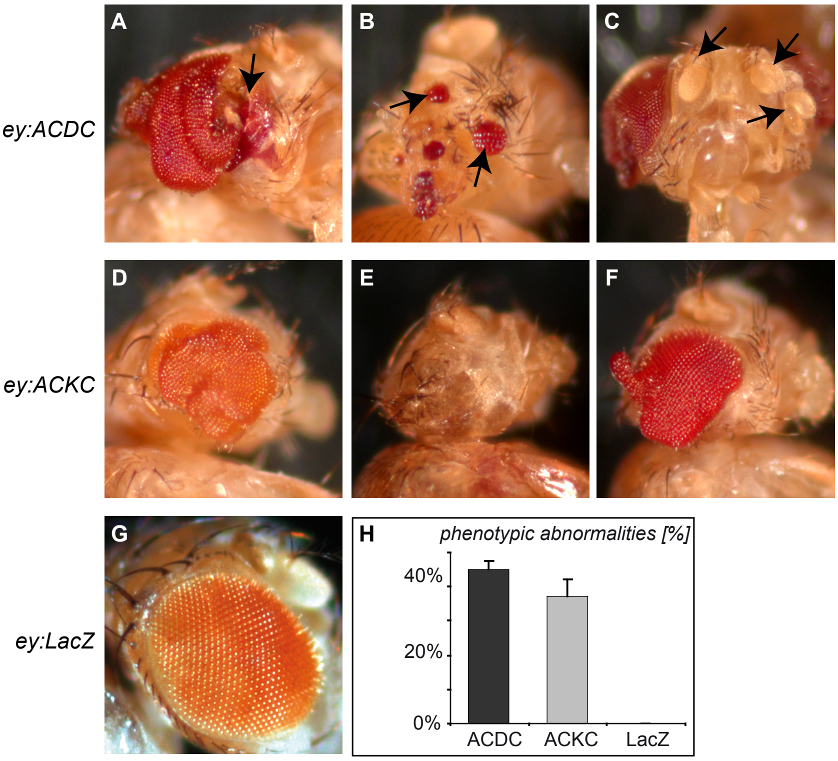

I

Fly line	Genotype	n	Abnormal eyes	%
ACDC	*yw, UAS-ACF1/+; UAS-DOM-B WT/+; ey-GAL4/+*	168	76	45
ACKC	*yw, UAS-ACF1/+; UAS-DOM-B KR/+; ey-GAL4/+*	373	140	37
LacZ	*yw; +/+; UAS-LacZ/ey-GAL4*	275	1	0

Figure 3.26: Expression of ACDC or ACKC using the *ey-GAL4* driver leads to major aberrations in adult compound eyes
UAS-ACDC, *UAS-ACKC* and *UAS-LacZ* as a control were crossed to *ey-GAL4* flies. The offspring (F1) was analyzed for potential phenotypic abnormalities in compound eyes of adult flies. **(A-C)** Coexpression of DOM-B WT and ACF1 (*ey:ACDC*) resulted in severe phenotypic abnormalities of eyes and antennae. **(D-F)** Combined expression of the DOM-B KR mutant and ACF1 (*ey*:ACKC) leads to a remarkable loss of cells in the eyes. **(G)** None of the phenotypes were observed when β-galactosidase (*ey:lacZ*) was expressed as a control. **(H)** The percentage of phenotypic abnormalities is graphically presented in the histogram. **(I)** The table presents the absolute numbers of flies scored (n) and the numbers of flies with phenotypic abnormalities corresponding to the percentages in (H). Error bars represent SD of three biological replicates.

A dramatic increase of ommatidia or undifferentiated cells in the compound eye was observed in 45% of analyzed flies similar to phenotypic abnormalities resulting from single expression of DOM-B WT such as gross abnormalities of the eye morphology ranging from overgrowing structures and ectopic tissues bearing ommatidia on the tip. In addition, coexpression of DOM-B WT and ACF1 resulted also in mispositioning and duplication of the antennae (*ey:ACDC*), which was never observed upon expression of DOM-B WT alone. Defects in antennal development were only monitored upon DOM depletion (*see* Chapter 3.7.2).

Major differences to the expression of DOM-B WT and ACF1 were observed upon coexpression of the putative ATPase-deficient mutant DOM-B KR and ACF1 (*ey:ACKC*) (Figure 3.26.D-F). *ey:ACKC* gave rise to a remarkable loss of ommatidia in the eyes similar to expression of *ey:DOM-B KR* alone that also corresponds to phenotypic abnormalities resulting from expressions of ACF1 (Chioda et al., 2010). In *ey:ACKC* flies a complete lack of ommatidia in the entire eye field was found, which was never observed before. In this case, DOM-B KR and ACF1 together led to an entirely loss of ommatidia. This supports again a genetic interaction between DOM-B and ACF1 *in vivo*. A further indication that both proteins synergize is the high lethality observed upon coexpression of DOM-B WT and ACF1.

Only 168 adult flies (*ey:ACDC*) were obtained in comparison to 275 adult flies from control crosses (*ey:LacZ*), in which no phenotypic abnormalities were detected (Figure 3.26.G/I). In contrast to ACDC, coexpression of DOM-B KR and ACF1 yielded 373 flies. This data indicate that inappropriate amounts of DOM-B and ACF1 lead to a 40% reduced viability. Expression of DOM-B KR and ACF1 generated phenotypic abnormalities in adult compound eyes, which did not result in lethality. Since a drastic decrease of fly viability was observed especially upon combined expression of DOM-WT and ACF1, adult fly numbers with respect to their control are evaluated in details in a separate chapter (*see* Chapter 3.12).

3.9.2 Coexpression of DOM-B and ACF1 Affects Cell Fate in Imaginal Eye-Antenna Discs

Phenotypic abnormalities generated by targeted expression of ACDC or ACKC originated from perturbation of patterning processes in imaginal eye-antenna discs. Therefore, imaginal discs of 3rd instar larvae coexpressing DOM-B WT or KR and ACF1 were dissected and subjected to immunofluorescence staining with the α-DAC antibody (*see* Chapter 3.8.2). Corresponding samples were analyzed by confocal microscopy (Figure 3.27). Surprisingly, expression of ACDC or ACKC showed in both cases a similar derangement of DAC -positive cells in the entire posterior region of eye discs (*ey:ACDC, ey:ACKC*). Furthermore, a defined MF could not be identified, since the entire disc shape was strikingly deformed in most eye discs ranging from a slightly misshaped structure to a dramatic derangement of the entire disc morphology. This perturbation of the eye-antenna disc shape was, hitherto, never observed in single expression of DOM-B WT, DOM-B KR or ACF1 (*see* Figures 3.23 and 3.24). In contrast to eye discs expressing ACKC, some ACDC expressing eye discs showed an additional antennal structure (marked with a white arrow) growing out of the anterior part of the disc in consistence with observed adult eye phenotypic abnormalities. This entire deformation of the imaginal disc structure points to a synergistic interaction of DOM-B WT and ACF1, since a similar defect in eye discs was never observed inducing LacZ, DOM-B WT, KR or ACF1 alone.

Taken together, combined expression of DOM-B and ACF1 leads to gain-of-function phenotypes. Assuming the dramatic deranged disc morphology upon ACDC or ACKC expression, a functional interaction of DOM-B and ACF1 is conceivable. In addition, the high lethality provoked especially by ACDC expression (*see* Figure 3.22.I) using the *ey-GAL4* driver line that is active during early development supports the idea of a novel “ACDC” complex with a defined biological function and which is developmentally regulated (*see* also Chapter 3.11). To gain deeper insight into an interdependency of DOM-B WT and ACF1 in early stages of *Drosophila* development, both proteins were analyzed in ovaries of adult female flies.

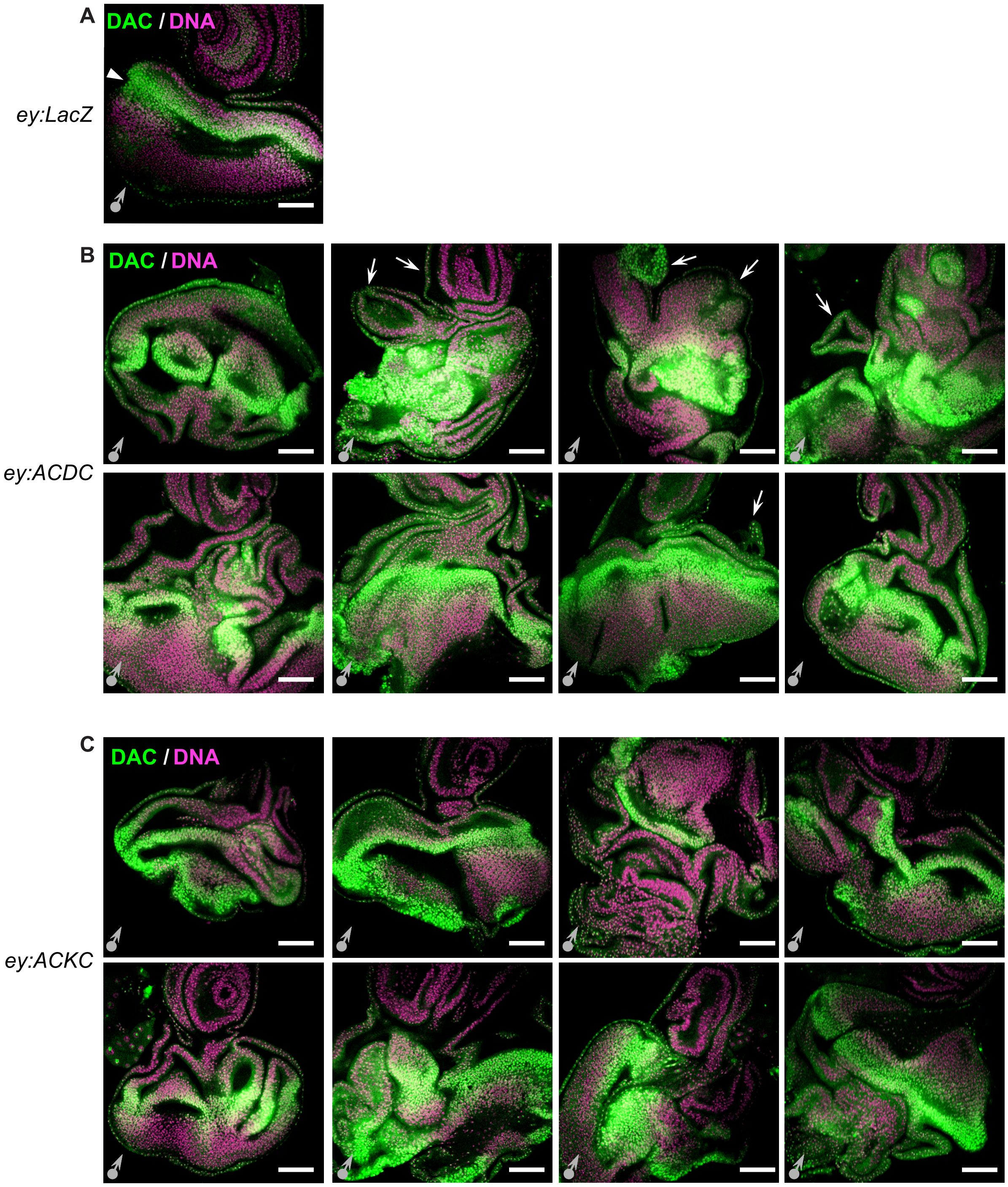

Figure 3.27: Ectopic expression of ACDC and ACKC disturb the entire eye-antenna disc morphology
Immunofluorescence analysis of whole-mount imaginal eye-antenna discs of third instar larvae after crossing *UAS-ACDC*, *UAS-ACKC* and *UAS-LacZ* as a control to *ey-GAL4* flies. A white arrowhead indicates the location of the morphogenetic furrow (MF). The grey arrows demonstrate the orientation of the eye-antenna disc: the arrowhead shows the direction of the anterior antennal region, the tail indicates the posterior eye portion. Immunostaining with Dachshund (DAC) (green), a marker for undifferentiated neuronal precursors, which is usually limited to a region of the eye disc along the MF in the posterior lobe as displayed by the control (*ey:lacZ*). DNA was stained by TO-PRO3 (purple). Combined expression of DOM-B WT/KR and ACF1 (*ey:ACDC*, *ey: ACKC*) resulted in gain-of-function phenotypes and synergistic effects. Additional antennal structures are marked with white arrows. Scale bars represent 50 µm.

3.10 DOM-B and ACF1 Are Important during Oogenesis

The germline cyst formation in *Drosophila* ovaries is especially helpful in developmental biology research, as it provides an ideal system to study the molecular basis of stem cell regulation as well as of cell proliferation and differentiation processes. An imbalance of factors that play an important role during oogenesis should lead to major defects and phenotypic abnormalities. To confirm that DOM-B and ACF1 are indeed important players in stem cell formation and maintenance - particularly if both share a functional dependency - they were further analyzed in female gonads.

The DOM-B isoform was already known to be expressed at higher levels in germ stem cells (GSCs) than in other cells of the germarium, even though the function of DOM-B was linked to somatic stem cell (SSC) self-renewal and not to GSCs maintenance so far (Ruhf et al., 2001; Xi and Xie, 2005). Xi and Xie showed that ISWI is present at high levels in nuclei of all cell types in the germarium, including GSCs and SSCs, but playes an essential role only for GSC self-renewal. They suggested that different stem cell types depend on different chromatin remodeling factors to control their self-renewal and require a unique constellation of genetic and epigenetic regulators. In embryos, the expression of the ISWI-interacting factor ACF1 persists at high levels in undifferentiated cells, including germ cell precursors and the gonadal anlagen (Chioda et al., 2010). Taking into account that ACF1 contributes to the initial establishment of chromatin structure diversity during early development, it is surprising that the expression of ACF1 in adult ovaries and its potential role during oogenesis is still not well understood.

To confirm a direct interplay and a synergistic effect of both proteins, ACF1 and DOM-B WT were coexpressed in combination with DOM-B KR in ovaries using a *vasa-GAL4* driver line (kindly provided by Sandy Mietzsch, laboratory of Prof. G. Reuter, Martin-Luther-University Halle-Wittenberg, Germany). *Vasa* is expressed from the beginning on of early embryogenesis (stage 1) at the posterior end of the embryo and marks the pole plasm (Extavour and Garcia-Bellido, 2001; Polesello et al., 2002). Vasa proteins are essential for the establishment of pole cells, which are the precursors of the *Drosophila* germ line and develop subsequently into the germ cells. In adult flies, *vasa* is active in ovaries of female flies including the ovariols with the germarium harboring GSCs, SSCs, nurse cells and oocytes (*see* also Chapter 1.4.4) (Hay et al., 1988; Extavour and Garcia-Bellido, 2001; Polesello et al., 2002). Ovaries from adult female flies ectopically expressing LacZ as a control, DOM-B WT, DOM-B KR and ACF1 as well as combinations thereof driven by *vasa-GAL4* were dissected under a binocular microscope and subjected to immunofluorescence staining with α-ACF1 and α-phosphorylated H2AV antibodies (*see* Chapter 2.7.1). The ovariols were carefully separated and analyzed by confocal microscopy. First, the expression and subcellular distribution of ACF1 was characterized in ovaries of the control line (*vasa: LacZ*). There, ACF1 appeared to be enriched in GSCs, cystoblasts (CBs) and oocytes (Figure 3.28). GSCs can be identified by their location (contact with cap cells), size, and spherical spectrosome (Xi and Xie, 2005). However, an unbiased distinction between GSCs and CBs was not possible, since further analysis with stem cell-specific markers was not performed in this study. Ovaries were costained with an antibody against the phosphorylated histone variant H2AV at S137, which is referred to as ɣ-H2AV. ɣ-H2AV is involved in DSB repair and recombination events (Madigan et al., 2002; Joyce and Kim, 2010). The latter occur especially in chromatin of 16-cell-cysts, where the pro-oocytes proceed through the pachytene stage of meiosis (Joyce and Kim, 2010). The staining pattern of ɣ-H2AV in control germaria reflects this event, as it was enriched on 16-cell-cysts (Figure 3.28.B). Furthermore, ɣ-H2AV could be detected on GSCs, follicle cells and nurse cells. Encouraged by the finding that ACF1

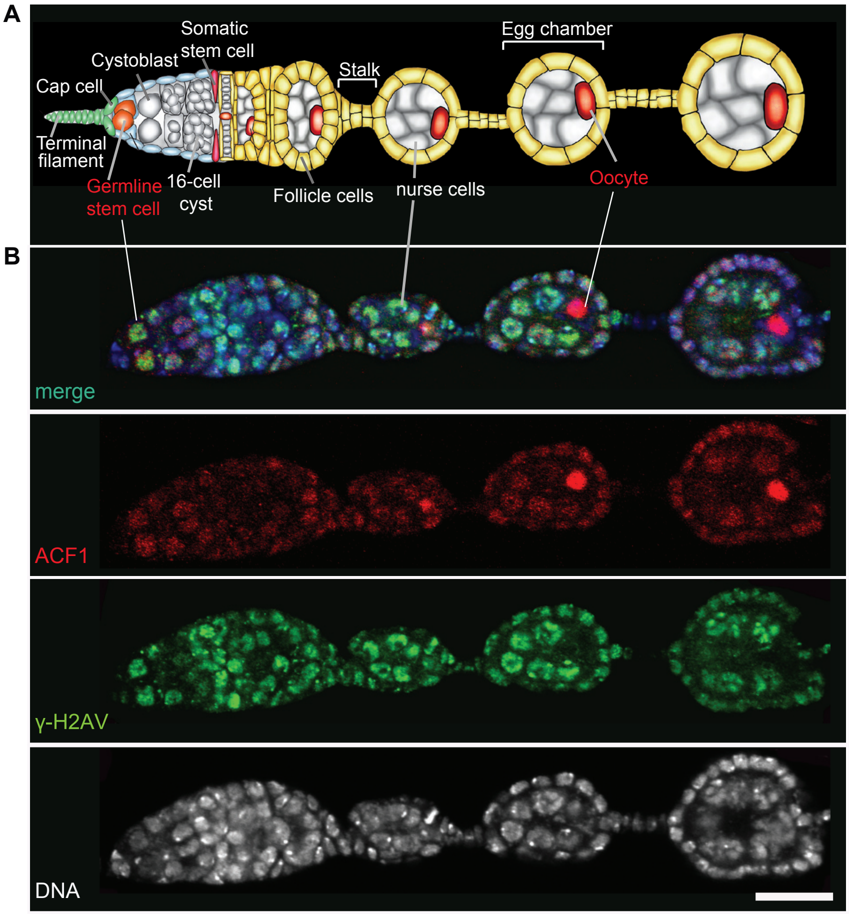

Figure 3.28: ACF1 is enriched in germline stem cells, cystoblasts and oocytes in *Drosophila* ovaries
(A) Schematic depiction of a *Drosophila* germarium and budding egg chambers (adapted from Hartman et al., 2010). **(B)** Confocal microscope image of a whole-mount ovariol expressing β-galactosidase as a control using the *vasa-GAL4* driver line. Immunofluorescence staining with α-ɣ-H2AV (green) and α-ACF1 (red). DNA stained by TO-PRO3 (white). ACF1 is enriched in GSCs, CBs and oocytes, while ɣ-H2AV localizes predominately in the 16-cell cyst as well as in GSCs, follicle cells and nurse cells. Scale bar represents 20 µm.

is enriched in GSCs and CBs and might be used as a putative marker for GSCs and CBs, phenotypic abnormalities generated by overexpression of DOM-B WT or KR and ACF1 were studied (Figure 3.29). After expressing DOM-B WT by the *vasa-GAL4* driver, germaria showed a reduced level of ACF1 immunofluorescence staining signals on GSCs, which could not clearly be distinguished from other cells such as CBs (*vasa:DOM-B WT*) (Figure 3.29.A). In this case it might also be that the number of GSCs is reduced, which was not clarified in this experiment. Moreover, the staining signals of ɣ-H2AV displayed a certain degree of variability, since ɣ-H2AV signals were decreased in some GSCs and enriched in a few cells of the 16-cell-cyts, which in turn may point to an alteration of chromatin organization. This observation is in line with the previous finding that chromatin formation is disturbed by expression of DOM-B WT in salivary glands (*see* Chapter 3.6). Taking into account that the subunit DOM-A of the TIP60 complex was found to catalyze the exchange of ɣ-H2AV, an influence of DOM-B on phosphorylation of histone variants is possible (Kusch et al., 2004). The unbalanced distribution of ɣ-H2AV especially in the 16-cell-cyt region is possible provoked by the perturbed expression of DOM-B WT, since DOM-B is contributed to the maintenance of SSCs and the generation of follicle cells in this region (Xi and Xie, 2005; Hartman et al., 2010). Upon DOM-B KR expression, germaria displayed a normal distribution of ACF1 immunofluorescence staining signals, while higher levels of ɣ-H2AV signals were detected in cells of the entire germarium, which might be due to a failure

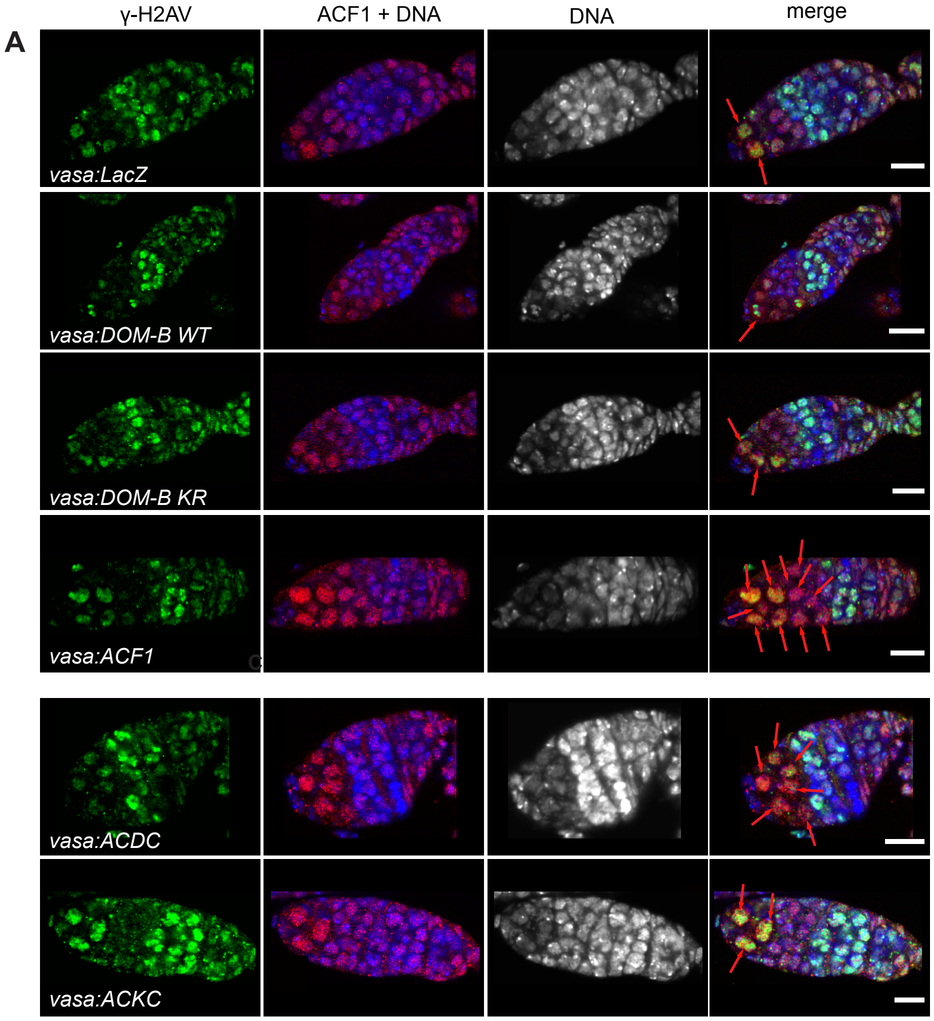

B

Fly line	Genotype	total numbers of flies
LacZ	*yw; +/+; UAS-LacZ/ vasa-GAL4*	143
DOM-B WT	*yw; UAS-DOM-B WT/+; vasa-GAL4/+*	152
KOM-B KR	*yw; UAS-DOM-B KR/+; vasa-GAL4/+*	130
ACF1	*yw, UAS-ACF1/+; +/+; vasa-GAL4/+*	160
ACDC	*yw, UAS-ACF1/+; UAS-DOM-B WT/+; vasa-GAL4/+*	60
ACKC	*yw, UAS-ACF1/+; UAS-DOM-B KR/+; vasa-GAL4/+*	144

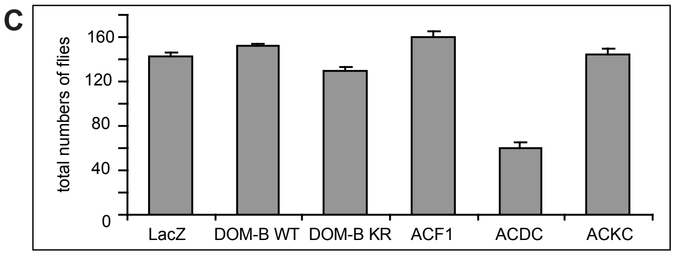

Figure 3.29: Ectopic expression of DOM-B WT and ACF1 in *Drosophila* ovaries affects oogenesis
UAS-DOM-B WT, UAS-DOM-B KR, UAS-ACF1, UAS-ACDC, UAS-ACKC and *UAS-LacZ* as a control were crossed to *vasa-GAL4* flies. Female progenies (F1) were crossed again to *vasa-GAL4* males and analyzed for potential phenotypic abnormalities in their ovaries. **(A)** Confocal images of whole-mount ovaries that were immunofluorescence stained with α-ɣ-H2AV (green) and α-ACF1 (red) antibodies. DNA stained by TO-PRO3 (white, blue in merge). GSCs (or putative CBs) are marked with red arrows. White arrows indicate putative apoptotic cells. Scale bars represent 10 µm. **(B)** The table displays the absolute numbers of flies (F1 generation) scored (n) for each genotype. **(C)** The total number of adult flies (F1) is graphically depicted in the histogram. Error bars represent SD of three biological replicates.

in ɣ-H2AV-removal by the potential impaired function of the DOM-B KR mutant (*vasa:DOM-B KR*). An obvious alteration of the ACF1 immunofluorescence staining signal was detected in germaria upon ACF1 expression (*vasa:ACF1*). In these ovaries ACF1 was upregulated in cells, which have features of GSCs as well as of CBs (marked with arrows). The level of ɣ-H2AV staining signal was not affected, but more than two cells in the stem cell niche region showed a ɣ-H2AV staining suggesting that more than two GSCs are present in these germaria.

In order to obtain a clear evidence for a synergistic effect of DOM-B and ACF1, both proteins were expressed in ovaries (*vasa:ACDC*) (Figure 3.29.A). Dramatic effects were monitored upon coexpression of DOM-B and ACF1 with the *vasa-GAL4* driver: these germaria contained higher numbers of GSCs or CBs (marked with red arrows) and often harbored putative apoptotic cells (marked with a white arrow), which are so far determined by a strong DNA signal indicating highly condensed chromatin that is characteristic for dying cells. However, further analysis with apoptosis-specific markers need to be proceeded to determine apoptosis within the germarium. Apoptotic cells were especially detected in the region where 16-cell-cysts get surrounded by follicle cells, which are generated by the SSCs (white arrow). This is in agreement with earlier studies, in which DOM-B was shown to be required for SSC self-renewal and a depletion of DOM-B gave rise to a reduced SSC maintenance ability of germaria (Xi and Xie, 2005). A perturbed function of SSCs and a putative cell death in the 16-cyst region might also explain the impaired shape of germaria, as they appeared thick and shorter in size compared to the control. This was already observed during dissection and mounting of these ovariols, since the entire ovaries were much smaller in size and difficult to dissect in comparison to other analyzed ovaries expressing LacZ, DOM-B WT or KR, ACF1 as well as ACKC. The latter appeared to rescue phenotypic abnormalities of ACDC expressing ovaries, since none of these abnormalities were monitored in germaria coexpressing the putative ATPase-deficient form DOM-B KR and ACF1 (*vasa:ACKC*). Furthermore, in ACKC expressing ovaries, higher levels of ɣ-H2AV were detected, like in *vasa:DOM-B KR* expressing flies. Again, this might originate from an improper function of the ATPase domain of DOM-B KR resulting in reduced exchange of ɣ-H2AV.

Taken together, phenotypic abnormalities observed especially upon expression of ACDC and the compensatory effects of ovaries expressing ACKC support the hypothesis of a direct interdependency of DOM-B WT and ACF1 in a putative ACDC-complex. A further hint of a functional interaction is displayed by the number of adult flies scored for each genotype (Figure 3.29.B/C). Compared to 143 flies expressing β-galactosidase as a control (*vasa:LacZ)*, only 60 flies survived after combined expression of DOM-B WT and ACF1 (*vasa:ACDC*). This indicates a dramatic decrease of fly viability upon expression of the putative ACDC-complex. A synergistic action thereof is supported by the fact that the coexpression of ACF1 and the putative ATPase-deficient mutant DOM-B KR (*vasa:ACKC*) resulted into the normal quantity of 144 flies, which is similar to the number scored for the control line (*vasa:LacZ*). Such a reduced number of adult flies was never observed in lines expressing DOM-B WT and DOM-B KR or ACF1 alone using the *vasa-GAL4* driver. However, similar effects were observed in previous experiments when transgenic fly lines were crossed to *ey-GAL4* driver (*see* Chapter 3.8 and 3.9). To gain further information of an influence of DOM-B and ACF1 on adult fly viability, offspring from each genotype and from each cross were scored and analyzed in comparison to each other in the following chapter.

3.11 Ectopic Coexpression of DOM-B and ACF1 Has a Dramatic Synergistic Effect on Fly Viability during Early *Drosophila* Development

Since a dramatic effect on the viability of flies coexpressing DOM-B and ACF1 using the *vasa-GAL4* driver was observed, the viability of flies crossed to other GAL4-driver lines was analyzed. Therefore, the ratio of offspring (F1) of transgenic fly lines (*UAS-LacZ, UAS-DOM-B WT, UAS-DOM-B KR, UAS-ACF1, UAS-ACDC and UAS-ACKC*) crossed to four different GAL4-driver lines (*vasa-GAL4, ey-GAL4, glass-GAL4, eng-GAL4*), was scored for each genotype and compared relative to the progenies of the control line (*UAS-LacZ*) (Figure 3.30). The viability was unaffected in flies expressing DOM-B WT, DOM-B KR or ACF1 by the *vasa-GAL4* driver line. In contrast, a dramatic reduction of about 60% of fly viability was observed after combined expression of ACDC by *vasa-GAL4* (*see* Chapter 3.10). This lethality was not observed upon expression of ACF1 and the putative ATPase-deficient mutant DOM-B KR. This indicates a strong synergistic effect of ACF1 and DOM-B WT during oogenesis and embryogenesis, since *vasa* is active in adult female ovaries and in pole cells of early embryos.

To study putative phenotypic abnormalities of DOM-B (WT and KR) and ACF1 in adult compound eyes, the *ey-GAL4* driver line was used (*see* Chapters 3.7; 3.8 and 3.9). Also in this case, a consistent synergistic effect upon DOM-B WT and ACF1 coexpression (*ey:ACDC*) of was observed: the viability was reduced in about 40%, which was not monitored upon coexpression of DOM-B KR and ACF1 (*ey:ACKC*). In contrast, the fly viability after the expression of DOM-B (WT or KR) and ACF1 alone was not affected compared to the control line (*ey:LacZ*).

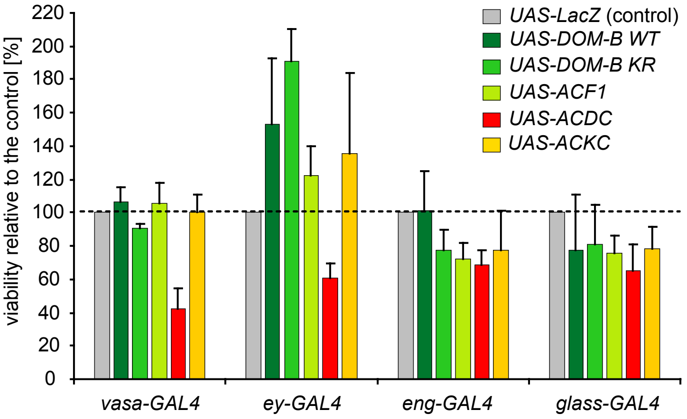

Figure 3.30: Ectopic expression of ACDC leads to drastic reduced fly viability Comparative analysis of adult transgenic fly viability relative to the control (*UAS-LacZ*). Bar charts indicate fly viability of different transgenic fly lines (*UAS-LacZ, UAS-DOM-B WT, UAS-DOM-B KR, UAS-ACF1, UAS-ACDC and UAS-ACKC*) crossed to four different GAL4-diver lines (*vasa-GAL4, ey-GAL4, eng-GAL4, glass-GAL4*). Error bars represent SD of three biological replicates (*vasa-Gal4* and *ey-Gal4*) or two biological replicates (*eng-GAL4* and *glass-GAL4*). A consistent synergistic effect was monitored upon coexpression of DOM-B WT and ACF1 (*UAS-ACDC*).

The drastic impact on fly viability by expression of ACDC is reduced in experiments using *eng-GAL4* or *glass-GAL4* driver lines. A mild reduction of adult fly viability was monitored in all fly lines compared to the control line. The lowest viability was monitored in ACDC offspring (F1), even the difference to other transgenic fly lines were smaller compared to experiments with *vasa-GAL4* or *ey-GAL4*, suggesting a higher importance of DOM-B and ACF1 during early development.

Taken together, a dramatic reduced adult fly viability was observed only by coexpression of DOM-B and ACF1, which indicates a synergistic effect of both factors, especially during early development. The “rescue” of viability by coexpression of ACF1 and the putative ATPase-deficient DOM-B KR mutant supports the hypothesis of the existence of a novel ACDC chromatin remodeling complex, which might play an important role during early stages of *Drosophila* development.

4 DISCUSSION

4.1 DOM-B Is a Subunit of the Putative Novel Chromatin Remodeling Complex ACDC

In yeast two remodeling complexes of the INO80/SWR1 family are known - INO80 and SWR1, whereas mammals contain three complexes: hINO80, SCRAP and TRRAP/TIP60 (Bao and Shen, 2007; Clapier and Cairns, 2009; Bao and Shen, 2011) (*see* also Table 1.1, Chapter 1.2.2). In *Drosophila*, only two chromatin remodeling complexes of this family are identified so far: the INO80-type remodeling complex Pho-dINO80 and the remodeling complex dTIP60 with the SWR1-type ATPase subunit DOM-A (Figure 4.1). This study found a third putative novel chromatin remodeling complex of the SWR1 family in *Drosophila*, which is referred to as “ACDC remodeling complex” with the isoform DOM-B as catalytic subunit and as possible “binding-platform” for other associated factors (Figure 4.1).

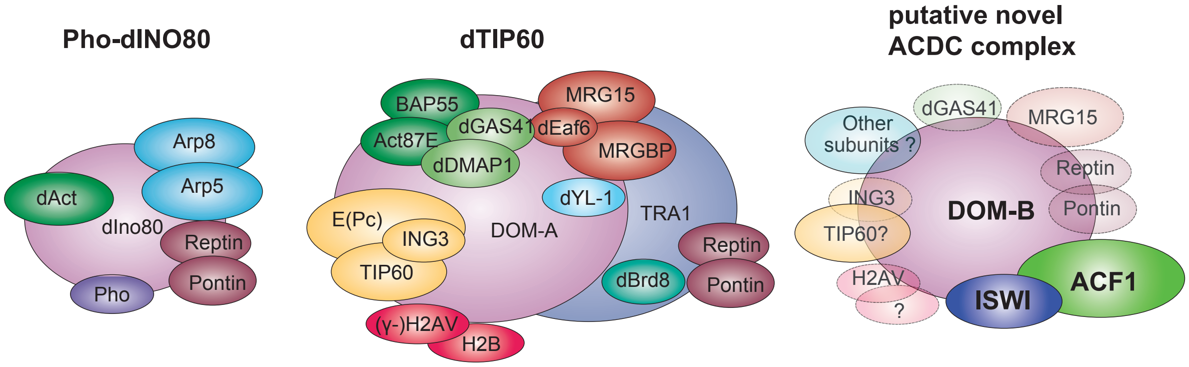

Figure 4.1: Model of the novel chromatin remodeling complex ACDC
Composition of the INO80 type chromatin remodeling complex Pho-dINO80 and dTIP60 of the SWR1 family in *Drosophila*, in comparison to the proposed homology model of the novel chromatin remodeling complex ACDC. Conserved subunits are color coded (*see* also Table 1.1). Putative subunits, which were found in the cofractionation of the ACDC complex, are represented in light colors, while ACF1 and ISWI were shown to bind directly to DOM-B.

By fractionating embryo extracts the association of DOM-B with ACF was one major observation (*see* Chapter 3.1). DOM-B, ACF1 and ISWI were predominately detected in preblastodermal embryos (0-2 h AED) (Figures 3.2). Considering that only the isoform DOM-B is ubiquitously present in early embryos, while DOM-A is not expressed until embryonic stage 10 (Ruhf et al., 2001), it can be hypothesized that DOM-B associates with ACF in preblastodermal embryos, while DOM-A exists as catalytic subunit of the TIP60 complex at later stages during embryogenesis. This does not exclude an association of DOM-B with TIP60 subunits, especially as both DOM isoforms differ only in their C-terminus. Indeed, in 0-12 h AED nuclear embryo extracts, DOM-B also cofractionated in different combination with five known subunits (H2AV, GAS41, MRG15, TIP60 and ING3) of the TIP60 complex as well as with ACF1 or ISWI using ion exchange chromatography (Figures 3.2 – 3.4). Notably, the association of DOM-B with the TIP60 subunit varies between distinct fractions (*see* Chapter 3.1.3). To our surprise, these data reveal that a so far unappreciated diversity of nucleosome remodeling complexes exist in parallel and vary in their composition and complexity during embryonic development. Future studies will have to specify the differential association and composition of ACDC as opposed to TIP60. The identification of all associated subunits with respect to different developmental stages will require, for example, affinity purification and mass spectrometry analysis. In addition, immunoprecipitations of DOM-B will confirm associated subunits of ACDC. Furthermore, after the establishment of α-DOM-B antibodies that work in ChIP protocols, DOM-B binding partners can also be identified using ChIP-chip.

The unforeseen diversity of nucleosome remodeling complexes leads to the question, why ACDC and other complexes were not identified so far. One possible reason could be that complexes like CHRAC and ACF were purified only from late embryos between 0-12 h or 0-16 h AED by a purification procedure established for CHRAC following the 500 mM fraction (Varga-Weisz et al., 1997; Eberharter et al., 2001). Are all these observed remodelers real multisubunit complexes or just associated proteins? According to Hargreaves and Crabtree, a complex is defined by (A) a stable association of subunits, which can only be disrupted by denaturation, (B) a distinct stoichiometry of subunits and (C) by the resistant to exchange with free factors (Hargreaves and Crabtree, 2011). On the one hand, the association of DOM-B and ACF resists four fractionation steps. The stoichiometry of DOM proteins is so far unknown and awaits further characterization. On the other hand, ACF1 and ISWI are subunits of e.g. ACF, CHRAC and ACDC and furthermore, ISWI is part of the RSF complex. Certain subunits can be found in more than one complex according to Hargreaves and Crabtree. They speculate that a combinatorial assembly is a feature of mammalian complexes to rapidly couple reactions and to provide mechanistic variation leading to the functional specialization (Hargreaves and Crabtree, 2011). For example, BAF complexes of the SWI/SNF family (orthologous to *Drosophila* BAP) are known for their combinatorial diversity and their unique composition at each developmental stage correlating with a specific gene expression program. BAF complexes contain at least seven different subunits, of which several isoforms exist that are required for a subset of complex functions (Wu et al., 2009; Hargreaves and Crabtree, 2011). The ATPase subunit BRG1 of BAF complexes for instance was found to collaborate with the CHD family member CHD7 (Hargreaves and Crabtree, 2011). This was recently ascribed to the association of CHD7 with PBAF to promote neural crest gene expression and cell migration in humans by Bajpai and colleagues (Bajpai et al., 2010). Also the INO80/SWR1 type complexes of higher vertebrates have lost, gained and shuffled subunits during their evolution and often contain more than 10 subunits (van Attikum and Gasser, 2005; Auger et al., 2008; Hargreaves and Crabtree, 2011). The notion that DOM proteins may engage in similar combinatorial diversity is therefore not without precedent.

The complexity of these remodelers might be due to their wide variety of chromatin-dependent nuclear transactions such as transcriptional regulation, DNA repair or histone replacement. Apparently, the function of histone exchange necessitates the use of multiprotein complexes as all of the remodelers involved in histone replacement harbor about 18 different components. For an optimal histone replacement it is crucial to access nucleosomal DNA, to disrupt histone-histone as well as histone-DNA contacts, to catalyze histone mobilization and finally to replace histone variants in a replication-independent manner (Kusch et al., 2004; Clapier and Cairns, 2009; Hargreaves and Crabtree, 2011). Remodelers of this function have to combine all these processes, which might explain the existence of two ATPase subunits in one complex, such as DOM-B and ISWI in ACDC. Remarkably, a direct physical interaction between DOM-B and ISWI could be reconstituted *in vitro* in this study (*see* Chapter 3.3).

The binding region of DOM-B to ACF1 was mapped to the split ATPase domain of DOM-B (Figure 3.9). Interestingly, the bipartite ATPase domain is the defining feature of all INO80/SWR1-type ATPases, as it contains a long insertion, to which also other components, like Pontin and Reptin (homologues of Rvb1/2), bind (Bakshi et al., 2004; Clapier and Cairns, 2009; Bao and Shen, 2011; Hargreaves and Crabtree, 2011). It can be speculated that this large linker region of DOM proteins might function as a “meeting and binding platform” for associated factors and other remodelers. This novel interaction between INO80-type chromatin remodelers and subunits of the ISWI family is only known from the fly RSF complex so far, which is a further example of combinatorial diversity. Hanai and colleagues immunoprecipitated dRSF-1 and ISWI proteins with α-DOM antibodies together with the TIP60 complex components E(Pc), dTIP60 and dMRG15 in *Drosophila* embryonic nuclear extracts (Hanai et al., 2008). They propose that RSF plays a role in silent chromatin formation by promoting histone H2AV replacement through the association with the TIP60 complex. This shows already the complexity of DOM interactors and their functions, as the DOM containing complex TIP60 is involved in DNA repair by exchanging ɣ-H2AV with unmodified H2AV (Kusch et a., 2004), while the macromolecular complex RSF-TIP60 possesses heterochromatin formation through the replacement of H2A with H2AV (Hanai et al., 2008). It is unknown, whether RSF can bind to DOM-B or ACDC and how the combinatorial assembly of complexes such as ACDC, RSF, TIP60 or ACF/CHRAC is restricted to certain developmental stages.

One tantalizing hypothesis could be that ACDC is a novel type of complex that combines two distinct remodeling principles: nucleosome sliding through the associated ACF complex and histone exchange by DOM-B and other interacting subunits. However, the mechanism is still unclear and the idea that ACDC might change chromatin dynamics through histone replacement needs further investigations, which will be discussed in chapter 4.5. However, several functional aspects of DOM-B were characterized in this study. DOM-B is involved in cell proliferation and differentiation, cell cycle progression and stem cell maintenance during *Drosophila* development. These can be derived from *in vitro* and *in vivo* obtained data of DOM-B and ACF1, which are discussed in the next chapters

4.2 Developmental Expression of DOM-B in *Drosophila* Is Similar to ACF1

Similar to the expression of DOM-B in preblastodermal embryos, ACF1 is known to be expressed at early stages of *Drosophila* development and is strongly diminished during embryogenesis (Ito et al., 1999; Chioda et al., 2010). The similarity between DOM-B and ACF1 was not only observed during embryogenesis, also in other tissues of different developmental stages both factors showed a significant correspondence. For example, immunofluorescence signals of DOM-B and ACF1 were barely detectable on salivary gland nuclei of 3rd instar larvae (*see* Section 3.5) (Chioda et al., 2010). DOM-B signals increased upon ACF1 ectopic expression and colocalized with ACF1, which point to an interdependence of both proteins. Furthermore, RNAi-mediated DOM depletion abolished DOM-B staining from nuclei of salivary glands and might remove also the weak immunofluorescence signals of ACF1 (s*ee* Figures 3.14 and 3.15).

All three factors, DOM-B, ACF1 and ISWI, are present in female ovaries (*see* Chapter 3.10). Ruhf and colleagues already observed the isoform DOM-B in female ovaries and did not find DOM-A in this tissue (Ruhf et al., 2001). Later on, DOM-B in germaria was characterized by Xi and colleagues, who detected DOM-B at higher levels in germ stem cells (GSCs) as compared to other cells of ovaries together with high levels of ISWI (Xi and Xie, 2005). Already Xi and colleagues suggested that different stem cell types in the germarium depend on distinct chromatin remodelers. A remodeling factor with important functions for stem cells could be ACF/ACDC, since it turned out that ACF1 is present in female ovaries and enriched on GSC or CBs and oocytes (Figures 3.28 and 3.29). The enrichment of ACF1 in these distinct cell types of ovaries was shown in this work with an α-ACF1 antibody. Future studies using α-DOM-B antibodies in concert with markers for different cell types in the germarium will address this question in details. However, in agreement with earlier studies, it can be speculated that

DOM-B, ACF1 and ISWI are combined in the putative ACDC complex significantly on GSCs, since all three appeared to be enriched especially on these cells.

Taken together, DOM-B, ACF1 and ISWI were predominantly found in early embryos and ovaries, in which the chromatin state is highly dynamic. This points to an important function of DOM-B and the ACDC complex during early *Drosophila* development, which will be discussed below. A misregulation of DOM-B during oogenesis or early embryogenesis had consequences for all further developmental stages.

4.3 DOM-B Plays an Important Role during *Drosophila* Development Similar to ACF1

4.3.1 DOM-B and ACF1 Influence the Stem Cell Maintenance in *Drosophila* Female Ovaries

Encouraged by the finding that DOM-B, ACF1 and ISWI are located in fly ovaries and assuming that different stem cell types in the germarium depend on different chromatin remodeling factors, led to the question of their functionality in this tissue. According to Xi and colleagues, ISWI is essential for the GSC maintenance, while DOM-B is important for the SSC-self renewal (Xi and Xie, 2005). The identification of ACF1 in oocytes and GSCs as well as CBs in germaria was hitherto unknown and opens up new lines of research. An overexpression of ACF1 in female ovaries using the *vasa-GAL4* driver resulted in increased ACF1 staining signals on GSCs and/or CBs and led to increased numbers of GSCs or CBs, which could not be clearly distinguished in this study. Further analysis with stem cell markers will address this question. However, GSCs can also be recognized by their location (contact with cap cells), size and their numbers, which are normally fixed to 2-3 (Xi and Xie, 2005). As more than three cells in the posterior region of the germarium contained ACF1 upon overexpression (Figure 3.29), it can be speculated that a higher dose of ACF1 might prevent these cells from differentiation and keep them in an undetermined status. This is in accordance with the previous hypothesis that ectopic expression of ACF1 reverts the signature of mature chromatin to more undefined structures. ACF1 is progressively downregulated once cells become determined towards a given cell fate (Chioda et al., 2010). In contrast to ACF1, overexpression of DOM-B resulted in lower staining levels of ACF1 on GSCs or CBs in many germaria.

Assuming an important role of DOM-B for cell fate determination and differentiation processes (*see* next chapter 4.3.3), one tantalizing hypothesis might be that higher levels of DOM-B may favor a premature differentiation of GSCs, due to reduced self-renewal. In this case, DOM-B and ACF1 might be antagonists that negotiate the tip of the balance between stem cell self-renewal and cell differentiation within the stem cell niche region. However, as this is pure speculation, the influence of ACF1, DOM-B and also the role of ISWI need further investigations. The expression of the DOM-B KR mutant resulted in higher levels of ɣ-H2AV immunofluorescence staining signals in germaria, which might be due to a failure of ɣ-H2AV-removal by the impaired ATPase function of DOM-B KR (Figure 3.29). This supports the notion of DOM-B KR as a dominant negative form *in vivo* and has to be verified in further studies.

In summary, both proteins DOM-B and ACF1 may fulfill important functions in *Drosophila* ovaries especially in the germarium. The presumed antagonistic function between DOM-B and ACF1 during oogenesis leads to the hypothesis of a regulatory interaction of both factors. It will be interesting to see, what future studies investigating in the fascinating field of stem cell maintenance and pluripotency will achieve in terms of the maintenance of stemness and differentiation processes through different chromatin remodelers like ACF and TIP60 or the putative ACDC.

4.3.2 DOM-B Is Important for Chromatin Formation at Larval Stage

Even though DOM-B proteins were found only in low amounts on whole mount salivary glands of *Drosophila* 3rd instar larvae similar to ACF1, a depletion of DOM in this larval tissue using the *sgs3-GAL4* driver line caused pupal lethality, whereas the ACF1 knock-down had no effect (*see* Chapter 3.7). After manual removal of the pupal cases, nearly fully developed flies were observed suggesting lethality at a late pupal stage (Figure 3.19). Such a strong phenotype has already been described by Ruhf and colleagues using several P-element excisions of the *dom* gene, which also resulted in larval and pupal lethality (Ruhf et al., 2001). Analyzing the DOM-depleted salivary glands of 3rd instar larvae might give one possible explanation for the observed phenotype: the size of entire salivary gland cells as well as the size of nuclei and polytene chromosomes was strongly reduced. Additionally, the banding patterning of polytene chromosomes and their chromatin organization were perturbed, as visualized by immunofluorescence staining with H2AV (Figure 3.18). In nuclei lacking DOM, H2AV signals were significantly reduced or even abolished in the majority of cells while HP1 signals were not affected and found to be distributed similar to the control. This might be caused by a diminished incorporation of H2AV into chromatin and points to a function of DOM-B as a histone exchange factor to regulate chromatin formation similar to RSF, which replaces H2A with H2AV (Hanai et al., 2008). Assuming that DOM-A is not expressed in nuclei of larval salivary glands according to Ruhf and colleagues (Ruhf et al., 2001), the presence of an RSF-associated DOM-A complex might be ruled out in this case.

On the other hand, it can be speculated that reduced H2AV distribution originates from an underreplication of chromatin as a consequence of DOM knock-down. The giant polytene chromosomes originate in the secretory cells of salivary glands by multiple rounds of DNA replication without subsequent nuclei division (Andrew et al., 2000). Salivary glands differentiate without further cell division and increase in size simply by increasing the volume of individual cells (Andrew et al., 2000). Consequently, underreplicated nuclei lead to the observed small gland tubes upon DOM knock-down. In addition, cells with misshaped and highly condensed chromatin were observed (Figure 3.18. A, last row), indicating apoptotic events in these cells. Therefore, the late pupal lethality upon DOM depletion might be related to underreplicated chromosomes, which normally are essential to increase metabolic requirements of these cells during morphogenesis.

In contrast to the pupal lethality caused by DOM depletion, ectopic expression of DOM-B yielded phenotypic abnormalities of the salivary glands but did not result in lethality. Ectopic expression of DOM-B WT or KR disrupted the chromatin organization in the majority of larval salivary glands, as a certain variation of H2AV distribution was observed in these salivary glands (Figure 3.16). This result is reminiscent of previous studies on ACF1, when ectopic expression of ACF1 led to a global derangement of chromatin organization (Chioda et al., 2010). Considering the colocalization profile of DOM-B and ACF1 on nuclei of whole mount salivary glands (Figure 3.15), both proteins appeared to associate with less condensed chromatin. It can be speculated, that an association of DOM-B and ACF1 to decondensed chromatin may reflect a more general function on euchromatic regions and strengthens the idea of a function on dynamic chromatin. These observations are in line with earlier studies. DOM-B was found on a large number of euchromatic sites on polytene chromosomes, which is consistent with a regulatory role in transcription (Ruhf et al., 2001). Furthermore, a recent study described a functional overlap of the *Drosophila dom* and the *elp3* gene (Walker et al., 2011). Walker and colleagues monitored a strong similarity between phenotypes of Elp3- and DOM-depleted flies. Elp3 is known to associate with active genes and participates in RNA polymerase II transcript elongation. Since they found a similarity between gene expression profiles of ELP3- and DOM-depleted mutants, a contribution of DOM to transcriptional regulation is more conceivable.

4.3.3 DOM-B Is Essential for Cell Differentiation and Cell Cycle Progression

In order to test whether DOM-B influences cell differentiation or cell cycle progression, DOM-B was depleted or expressed in imaginal eye-antenna discs, as these tissues provide a useful system to study cell differentiation in coordination with cell proliferation. Regardless of whether DOM-B was expressed or depleted, abnormalities of the eye-antenna imaginal discs were monitored (*see* Chapters 3.7.3 and 3.8). The failure of photoreceptor differentiation (visualized with ELAV immunofluorescence staining) in concert with significant delays in cell cycle progression and perturbed apoptosis (studied with BrdU incorporation and Caspase 3 staining, respectively) caused by DOM-B overexpression indicates the role of DOM-B in cell fate determination and cell cycle progression during morphogenesis. Cell proliferation was not affected by DOM-B, as the DAC distribution was normal.

Expression of the putative ATPase-deficient mutant DOM-B KR showed different defects compared to DOM-B WT in eye-antenna discs: While minor perturbation in the photoreceptor differentiation pattern was detected, a large number of proliferating cells, indicated by wide-spread DAC distribution in the posterior part of the eye-discs, was detected, which might be due to dominant negative effects of DOM-B KR. In accordance with earlier studies, these cells might fail to adopt a neural fate and are likely to remain in an undifferentiated state (Mardon et al., 1994). Furthermore, these cells undergo apoptosis, which is seen by the higher number of DOM-B KR expressing discs positive for Caspase 3. In contrast to DOM-B WT, DOM-B KR did not influence the cell cycle progression at the MF, since the BrdU staining was similar to that scored in control discs, suggesting that the observed defects cannot be explained by simple titration of DOM-B associated factors. The abnormalities upon DOM-B KR expression were reminiscent of ectopic expression of ACF1, which also resulted in a strongly perturbed DAC distribution and slightly disorganized ELAV patterning (Chioda et al., 2010).

This similarity between DOM-B KR and ACF1 during eye development led to the exploration of a functional interaction between DOM-B and ACF1 *in vivo*. Deletion of subunits of one complex often results in similar phenotypes according to Hargreaves and Crabtree, while different phenotypes can emerge if a subunit is employed in another complex or is only required for a subset of complex functions (Hargreaves and Crabtree, 2011). For example, a depletion of ACF1 in eye-antenna discs, which is barely expressed in this tissue (Chioda et al., 2010), had no effect, while a knock-down of DOM perturbed the DAC distribution in eye-antenna discs. This could indicate a distinct function of DOM-B and ACF1 required for a special subset of complex functions during morphogenesis. The different abnormalities in eye-antenna discs provoked by expression or depletion of DOM-B WT and KR correlate well with defects observed in the adult compound eyes (*see* Chapters 3.7.3 and 3.8). The reduced differentiation combined with the delay of cell replication and decreased apoptotic events in the eye-antenna discs upon DOM-B WT expression might explain the phenotypic abnormalities in adult compound eyes ranging from extra tissues in the eye field and the enlargement of eyes to their complete derangement. Whereas the high number of precursor cells positive for DAC, remaining in an undifferentiated state and undergoing apoptosis in eye-antenna discs, might explain the significant loss of ommatidia in entire regions of the adult eye by DOM-B KR-targeted expression. Also phenotypic abnormalities of DOM-depleted eyes such as a striking loss of ommatidia and antennal cells as well as mispositioning of antennae can be derived from the perturbed DAC distribution in these eye discs. Considering that DOM-B is expressed in the entire eye-antennal disc, while DOM-A is only present in the eye part (Ruhf et al., 2001), defects of the antenna formation can be related specifically to the depletion of DOM-B, whereas aberration of the compound eye might originate from loss of both isoforms.

However, phenotypic aberrations upon DOM knock-down can be linked to ectopic expression of ACF1, which perturbs normal eye development as well as antennal growth and positioning (Chioda et al., 2010). Furthermore, Chioda and colleagues showed that the ectopic expression of ACF1 in the eye disc altered nuclear programs (timing of S phase, apoptosis and differentiation) similar to expression of DOM-B KR or to DOM-B knock-down (Chioda et al., 2010). Assuming that deletion of subunits often results in similar phenotypes (Hargreaves and Crabtree, 2011), this might be a further evidence for a functional crosstalk between DOM and ACF1.

It can be speculated that DOM-B and ACF1 are not only required for an individual subset of complex functions, but also may interact as antagonists at certain stages of development. An earlier study found an opposite effect of p400 (homologues of DOM) and TIP60 in cell cycle progression and p21 expression (Tyteca et al., 2006). The p21 protein is a major regulator of cyclin/cdk activity and governs cell cycle arrest. Tyteca and colleagues showed in U2OS cells that p400/Domino represses p21 expression and thereby allowing cell cycle progression, while TIP60 favours the expression of p21 through the activation of p53 resulting in cell cycle arrest. They propose that this antagonism relies on the inhibition of TIP60 function by p400 (Tyteca et al., 2006). A similar antagonistic role might be considered for DOM-B and ACF, which awaits further analysis.

In summary, loss-of-function phenotypes and gain-of-function phenotypes of DOM-B, DOM-B KR and ACF1 in eye-antenna imaginal discs or salivary glands indicate that the levels of these factors are carefully balanced during development. The significant similarity of the distribution and the phenotypic abnormalities as described support the notion of a crosstalk between ACF1 and DOM-B. Furthermore, the putative antagonism between ACF1 and DOM-B during oogenesis or during eye-development indicates a biological interplay between both of them. Therefore, the consequences of a coexpression of DOM-B and ACF1 in various tissues were analyzed.

4.4 Synergistic Effects upon DOM-B and ACF1 Overexpression Are Restricted to Oogenesis and Early Embryogenesis

Studying phenotypic abnormalities provoked by coexpression of DOM-B and ACF1 pointed to a strong synergistic effect, which supports the hypothesis of the novel putative ACDC complex (*see* Chapter 3.11). Interestingly, the synthetic lethality was restricted to oogenesis and early embryogenesis as it was predominantly monitored using GAL4 driver lines that are active during early stages of fly development as well as during oogenesis. For example, to drive the coexpression of DOM-B and ACF1 in female ovaries, the *vasa-GAL4* driver line was used. *Vasa* belongs to the posterior group of maternal effect genes and is active in female ovaries in GSCs, SSCs, nurse cells and oocytes. During embryogenesis, *vasa* is transcribed from the beginning of stage 1 at the posterior end of the embryo marking the pole plasm (Figure 4.2) (Hay et al., 1988; Extavour and Garcia-Bellido, 2001; Polesello et al., 2002). *Vasa* is necessary for pole cell formation in embryos and subsequent germ line

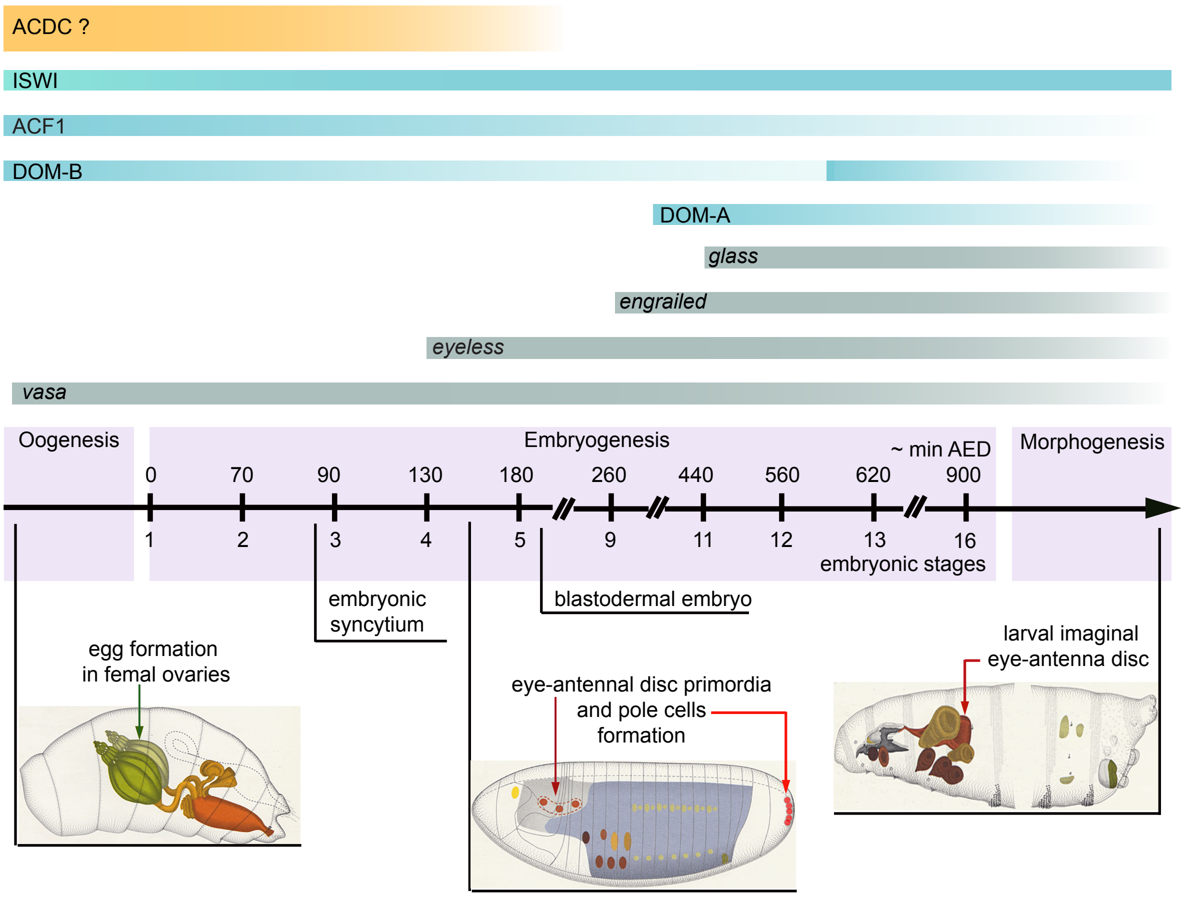
ACDC ?
ISWI
ACF1
DOM-B
DOM-A
glass
engrailed
eyeless
vasa
Oogenesis
Embryogenesis
~ min AED
Morphogenesis
0
70
90
130
180
260
440
560
620
900
1
2
3
4
5
9
11
12
13
16
embryonic stages
embryonic syncytium
blastodermal embryo
egg formation in femal ovaries
eye-antennal disc primordia and pole cells formation
larval imaginal eye-antenna disc

Figure 4.2: The putative novel chromatin remodeling complex ACDC is restricted to oogenesis and early embryonic stages
Expression patterns of ISWI, ACF1 and DOM (blue) and of the putative ACDC complex (yellow) in comparison with expression patterns of used GAL4-drivers (grey). *Vasa* is expressed in female ovaries and during the entire embryogenesis. *Eyeless* starts at embryonic stage 4, *engrailed* between stage 9 and 10 and *glass* begins at embryonic stage 11. Bottom: Schematic drawings depict major structures: the female abdomen including ovaries, eye-antennal disc primordial in an embryo between stage 4 and 5 and larval imaginal discs (adapted from Hartenstein, 1993).

development until adult stage. The combined expression of DOM-B and ACF1 using *vasa-GAL4* resulted in a dramatic decrease of viability, which was never observed upon individual expressions of DOM-B or ACF1 (Figure 3.30). This indicates a strong influence of DOM-B and ACF1 in combination during oogenesis and earliest stages of embryogenesis, where both factors appeared to play important roles. For example, TIP60-p400/Domino is suggested to be essential for embryonic stem cell self-renewal, pluripotency and differentiation (Fazzio et al., 2008). ACF1 is enriched throughout embryogenesis in the pole cells in the gonadal anlagen (Chioda et al., 2010). Indeed, the few adult escapers from this cross (*vasa:ACDC*, Figure 3.29) showed significant defects in their gonads, which might originate from failure during embryonic germ line development provoked by coexpression of DOM-B and ACF1. Structure and shape of entire ovaries were deranged and diminished, which made their dissection difficult. The increased number of GSCs or CBs in the germaria might be due to higher ACF1 levels, which was already discussed upon expression of ACF1 alone (Chapter 4.3.1). The bright DNA staining signals in some cells within the 16-cell-cyst region are an indication of highly condensed DNA in these cells that presumably undergo apoptosis. This 16-cell-cyst region comprises also the SSC niche where DOM-B is important for the self-renewal of these stem cells. An earlier study showed that the depletion of DOM-B in adult ovaries leads to a loss of SSCs because of defective self-renewal (Xi and Xie, 2005). It can be speculated that the observed abortion of cyst cells might be a consequence of unbalanced DOM-B expression in SSCs, which subsequently fail to generate the follicular monolayer around the cysts. In parallel, the upregulation of ACF1 in the GSCs/CBs prevents their differentiation and disrupts the progression of CBs towards the 16-cell-cyst. As a consequence, GSCs and CBs accumulate in an undetermined status and finally undergo apoptosis. The disturbed function of DOM-B and ACF1 in ovaries provokes the gross phenotypic abnormalities in ovaries of adult flies.

Notably, the combined expression of ACF1 and the putative ATPase-deficient DOM-B KR had a no effect. The fly viability was similar to the control and ovaries displayed a normal morphology except higher levels of ACF1 and ɣ-H2AV staining signals. Even though staining signals of ACF1 were increased upon expression of ACF1 and DOM-B KR, the number of GSCs was fixed to two or three as similar to the control. The higher levels of ɣ-H2AV might be generated by a defective ATPase function of DOM-B KR, which was already discussed for the expression of DOM-B KR alone and confirms that DOM-B KR acts properly as a dominant negative form *in vivo*.

Dramatically decreased fly viability and synthetic phenotypes were also observed upon coexpression of DOM-B and ACF1 using the *eyeless-GAL4* driver. *Eyeless* belongs to the group of selector genes and starts its expression early during embryogenesis at stage 4 in the anterior part of the preblastodermal embryo, where the eye-antennal primordia are set aside as small cell clusters of 20-40 cells (Figure 4.2). There, *eyeless* is required for the establishment of cells in the eye-antennal primordia and later on for photoreceptor determination in larval stages (*see* Chapter 1.4.3) (Halder et al., 1995). The coexpression of DOM-B and ACF1 induced by the *eyeless-GAL4* driver resulted not only in a failure of photoreceptor differentiation and cell cycle progression in larval eye-antenna imaginal discs, also a strong decrease of adult fly viability was scored (Figure 3.30). It can be speculated that the observed adult fly lethality, regardless of *eyeless-* or *vasa-GAL4* driver lines, might be due to changes of altered preblastoderm chromatin in early embryos. The nuclei in these embryos accumulate in the cytoplasm of a multinucleate syncytium (*see* Chapter 1.4.2), which is largely unstructured and where no morphological distinction between euchromatin and heterochromatin exists. Preblastoderm nuclei are characterized by highly dynamic chromatin in which many replication events occur. The upregulation of both factors (DOM-B and ACF1) during early stages of development could lead to a major disruption and inappropriate preblastodermal chromatin organisation with far-reaching consequences for all further developmental stages. This synergistic interplay or gain-of-function of DOM-B and ACF1 supports the possible existence of a novel ACDC complex, as most severe phenotypic abnormalities manifest upon combined expression of both factors.

A further example for a functional crosstalk between DOM-B and ACF1 are the observed misshaped and completely deranged imaginal eye-antenna discs of 3rd instar larvae provoked by coexpression of DOM-B WT (KR) and ACF1 (Figure 3.27). This pronounced hyperproliferation of imaginal eye discs tissue, accompanied by deregulation of epithelial architecture was never observed upon individual expression of DOM-B WT, DOM-B KR or ACF1 or upon DOM or ACF1 depletion. Such a general perturbation of an organ size and shape can only be achieved by altered signaling pathways and gene expression patterns in early stages of development, in which the eye-antenna disc primordia are formed. In this case, ACDC might play a role in cell proliferation and growth or cell signaling. In multicellular organisms like humans and flies, organs develop according to an instructive model where proliferation is regulated by extracellular signals (Kango-Singh and Singh, 2009). Kango-Singh and Singh documented a dramatic increase of interommatidial cells in *Drosophila* eyes, when the Hippo pathway was perturbed. They revealed that this phenotype results because Hippo pathway mutant cells proliferate faster than surrounding wild-type cells and do not terminate proliferation when imaginal tissues have reached their normal size (Kango-Singh and Singh, 2009). Another example is the mitogenic JAK-STAT pathway, which is specifically activated in mutant tissue (Classen et al., 2009). Classen and colleagues monitored a severe overproliferation of imaginal eye discs, which are reminiscent of the observed misshaped eye discs upon ACDC (or ACKC) expression. They revealed pronounced hyperproliferation of imaginal eye discs tissue upon mutation of *Drosophila* Polycomb Group (PcG) genes. PcG proteins are known to maintain cell identity by repressing alternative differentiation programmes, and play an oncogenic role in human cancer. This study showed further that a conventional PcG complex can also have a potent tumor suppressor activity mediated by JAK-STAT signaling and that PcG proteins are involved in growth control by silencing mitogenic signaling pathways (Classen et al., 2009). Interestingly, *dom* loss-of-function mutations enhance PcG mutations according to Ruhf and colleagues (Ruhf et al., 2001). They suggest a functional convergence between DOM and PcG members and described a repressive effect of *dom* on homeotic genes via interactions with PcG members. An influence of DOM-B and ACF1 on proliferation and cell signaling is, therefore, conceivable and should be revealed through further studies.

Another hypothesis to explain the severe phenotypic abnormalities in tissues like eye-antenna primordia or ovaries might be a perturbance of other chromatin remodeling complexes like TIP60, ACF or CHRAC by ACDC (or ACKC). An upregulation of DOM-B and/or ACF1 could favor the incorporation of both proteins in the ACDC complex and alter the formation and function of other remodelers like ACF or TIP60. Remarkably, the presumed interaction of DOM-B and ACF in the putative ACDC complex combines two distinct remodeling principles, histone variant exchange through the motorprotein DOM-B, and nucleosome sliding through the subunits ACF1 and ISWI, which is only known from the RSF complex so far. However, as this is pure speculation, further studies will address these questions.

Upregulating DOM-B and ACF1 with *engrailed-GAL4* or *glass-GAL4* driver lines revealed viable adult flies without any phenotypic abnormality. *Engrailed* belongs to the segment polarity genes and is expressed in the eye-antennal primordia between embryonic stage 7 and 9, while *glass* is expressed even later at stage 11 (Moses and Rubin, 1991; Ellis et al., 1993). Both are predominantly active in larval eye discs and necessary for a proper photoreceptor development. Only ectopic expression of DOM-B WT yielded a rough eye phenotype, whereas no abnormality was monitored upon expression of ACDC. This observation that coexpression of ACF1 with DOM-B WT prevented the rough-eye phenotype may point to an inhibitory effect of ACF1 association with DOM-B. The rough eye phenotype was not observed upon the expression of the putative ATPase-deficient mutant DOM-B KR. This shows that catalysis is required for the effects, as opposed to just interactions or titrations. Phenotypic abnormalities were also not observed upon overexpression of ACF1 or ACKC.

Comparing the expression patterns of different driver lines with the expression of DOM-B, ACF1 and ISWI (Figure 3.1) in a developmental context, the restriction of the putative ACDC complex to certain developmental stages can be understood (Figure 4.2). DOM-B, ISWI and ACF1 are mainly expressed in preblastodermal embryos until approximately stage 5. DOM-B was not found in embryos between 3 h and 9 h AED, while ACF was diminished during embryogenesis, in agreement with previous studies, in which ACF was detected in 0-12 h AED and to a lesser extend in 12-15 h AED old *Drosophila* embryos (Elfring et al., 1994; Ito et al., 1999). The association of DOM-B, ACF1 and ISWI at earliest stages (between stage 1 and 5), in which *vasa* and *eyeless* are predominantly active, correlates in an interesting way with the developmental time at which an overexpression leads to phenotypic abnormalities. Considering that preblastodermal embryos contain high levels of ACF1-containing complexes like CHRAC/ACF, which might relate to a 'hyperdynamic' chromatin state (Meshorer and Misteli, 2006; Chioda et al., 2010), a similar contribution of ACDC to undetermined chromatin is conceivable. It can be speculated that ACDC fulfills important function during earliest stages of development involved in chromatin determination, while TIP60 acts as histone exchange factor at later stages in context of DNA repair. This hypothesis does not exclude a function for ACDC in context of a histone replacement, but might point to different roles of ACDC during different developmental stages. In addition, DOM-B was found not associated with ACF1 in late embryos between stage 12 and 17, which might explain the rough eye phenotype specific for DOM-B WT using the *glass-GAL4* driver line.

The challenge of further studies will be to elucidate the mechanism and function of the putative ACDC complex in context with developmental processes. The complexity of cell fate determination in combination with chromatin remodeling reveals additional analyses *in vitro* as well as *in vivo*.

4.5 Outlook

4.5.1 Future *in Vivo* and *in Vitro* Studies of DOM-B and ACDC

A step towards a deeper understanding of ACDC function during *Drosophila* oogenesis will be the precise localization of ACF1, DOM-B and ISWI in different cell types during oogenesis using specific stem cell markers by immunofluorescence staining. Furthermore, the targeted depletion of DOM-B, ACF1 and ISWI in female ovaries is indispensable. Appropriate *UAS-IR* fly lines depleting these factors in ovaries were not available during this study, but have been offered recently from the Bloomington stock center. Loss-of-function phenotypes in ovaries and the number of offspring will be analyzed and contrasted to gain-of-function phenotypes. Further immunofluorescence analysis of germaria with antibodies against H2AV and ɣ-H2AV will possibly shed light on ACDC as a chromatin remodeler involved in histone exchange. Since ACDC appeared to play an important role during early embryogenesis, a colocalization of DOM-B, ACF1 and ISWI in precisely staged embryos will be necessary. Changes of their expression patterns provoked by expression with different *UAS-GAL4* lines (e.g. *vasa-GAL4, eyeless-GAL4*) may give information about their functional contribution during early embryogenesis. Another approach will be to study DOM-B and ACF1 expression from their endogenous promoter in transgenic fly lines and marked with different (fluorescent) tags, like GFP or RFP. An elegant method to analyze ACDC during development is live cell imaging of embryos or ovaries following the fluorescent tags of DOM-B and ACF1.

Data obtained *in vivo* about the putative ACDC complex should be complemented by further *in vitro* analyses exploring the mechanisms of ACDC. As mentioned, affinity purification, mass spectrometry and ChIP-chip analyses will contribute to identify all associated subunits of ACDC and their binding sites (*see* Chapter 4.1). In addition, protein purification from female gonads and their subsequent characterization will address the question of ACDCs function during oogenesis. Immunoprecipitations of DOM-B (e.g. using nuclear extracts of embryos or ovaries) will verify associated subunits of ACDC during different developmental stages. Knowing which subunits belong to the ACDC complex leads to the question of their function and mechanism. This can be tested further in *in vitro* assays.

For example, it was shown in this work that the ATPase activity of DOM-B is blocked by its C-terminus suggesting a hitherto unknown function of the C-terminal end, which awaits further characterization (Figure 3.10). ATPase hydrolysis of DOM-B was only detectable in experiments with truncated versions lacking the C-terminus. All attempts to modulate the ATPase activity of DOM-B were without success, as the derivatives were either inactive or active without a substrate, be it assembled chromatin, recombinant H2A or H2AV histones or DNA (*see* Chapter 3.4.1). Partial reconstitution of DOM-B complexes from recombinant subunits may shed light on the stimulation of DOM-B and hence, ACDC. As a further consequence of the C-terminal blockade, the DOM-B KR mutant could not be clearly verified as ATPase-deficient form. Both full length proteins, DOM-B WT and DOM-B KR, did not show any ATPase hydrolysis. Therefore, a derivative similar to DOM Δ6 comprising only the split ATPase domain, but containing the KR point mutation may prove that DOM-B KR is inactivated. Additionally, point mutations introduced in the DOM-B linker region to which ACF1 and other subunit may bind to, will give further information about whether these factors affect the ATPase activity.

4.5.2 The Connection between DOM-Containing Nucleosome Remodelers and ACF/CHRAC Might Be the Metabolism of H2AV

As already discussed (Chapter 4.1), DOM-A appeared to be involved in two different functions – chromatin formation through H2AV incorporation (RSF) and DNA repair (TIP60) through histone exchange of ɣ-H2AV with H2AV (Kusch et al., 2004; Hanai et al., 2008). Both complexes share, besides DOM, the subunits TIP60, E(Pc) and MRG15. In *Drosophila*, the histone acetyltransferase TIP60 acetylates ɣ-H2AV at Lys^5 in a DSB-dependent manner before ɣ-H2AV can be exchanged with H2AV (Kusch et al., 2004). This reaction was not detected in S2 cell extracts lacking TIP60 or MRG15. The exact function and mechanism of MRG15, as well as of E(Pc) during histone replacement are still unknown. TIP60 and p400/Domino synergistically interact during DNA damage and are both required for UV-induced apoptosis (Tyteca et al., 2006). Notably, TIP60 and p400/Domino play antagonistic roles during cell cycle progression. According to Tyteca and colleagues, p400/Domino can inhibit the function of TIP60, a property that is abolished following DNA damage (Tyteca et al., 2006). As recently described, also ACF1 is involved in DNA damage response in humans (Sanchez et al., 2011). Sanchez and colleagues observed that hACF1 is quickly enriched together with ɣ-H2AX at sites of

UV laser-induced damage. After depletion of hACF1, ɣ-H2AX was diminished in response to UV- and X-rays. Furthermore, ACF1 is required for proper H2AV incorporation and chromatin organisation during development. Chioda and colleagues found a variegated incorporation of H2AV upon ectopic expression and incomplete and defective H2AV integration after ACF1 depletion, accompanied by faulty chromatin formation (Chioda et al., 2010). Also RSF governs heterochromatin formation via H2AV replacement and requires the sliding function of ISWI and the association with TIP60 subunits for this reaction (Hanai et al., 2008).

What is the interception of all these subunits and complexes? First, proteins like ACF1, ISWI, MRG15, H2AV and TIP60 cofractionated in this study with DOM-B and may be part of the novel SWR1/INO80-type ACDC complex (*see* Chapter 3.1.3). Second, all referred factors appeared to be involved in H2AV-metabolism. In yeast and mammals, some features of SWR1/INO80-class complexes include the special affinity for the histone variants H2AZ and H2AX as recently reviewed by Hargreaves and Crabtree (Hargreaves and Crabtree, 2011). Notably, in flies H2AV is the only known variant of H2A and a chimeric molecule consisting of the H2AZ and H2AX (see Chapter 1.1.3). Therefore, a tantalizing hypothesis might be that ACDC combines functions and mechanisms of H2AZ and H2AX remodelers in context of developmental and cell-specific processes. A crosstalk between ACDC and other remodeling complexes (e.g. TIP60, ACF/CHRAC or RSF) takes place via the H2AV-metabolism restricted to different developmental processes (Figure 4.3).

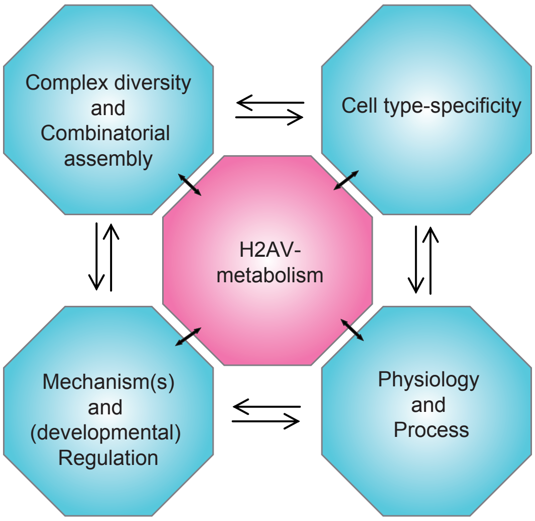
Complex diversity and Combinatorial assembly
Cell type-specificity
H2AV-metabolism
Mechanism(s) and (developmental) Regulation
Physiology and Process

Figure 4.3: The intersection of DOM-containing nucleosome remodeling complexes
The functional crosstalk of DOM-containing complexes like ACDC, TIP60 and RSF might be via H2AV-metabolism.

This would be an effective way to rapidly couple mechanisms to provide a functional specialization as proposed by Hargreaves and Crabtree (Hargreaves and Crabtree, 2011). For example, ACDC might be required for chromatin formation during earliest stages of embryonic development, while in ovaries ACDC is important for stem cell maintenance and the balance between cell proliferation and differentiation. *In vivo* analysis of female ovaries gave also the first hint about a relationship between DOM-B and histone exchange, as ɣ-H2AV appeared to be enriched and not removed by the ATPase-defective DOM-B KR (Chapters 4.3.1 and 4.4). The hypothesis of a selective histone exchange function of DOM-B might be clarified with *in vitro* assays. To this end, H2A or H2AV-containing nucleosomal arrays bound to paramagnetic beads, can be incubated with free recombinant histones

H2AV and H2A, respectively, as well as ACDC subunits including DOM-B, chaperones and other components and ATP. Subsequent analysis of bound material compared to the supernatant may give further information of a histone replacement. Another elegant way to verify direct physical interactions of DOM-B and ACDC subunits with H2AV will be given by GFP-binder affinity purification using the *Drosophila* transgenic fly line *GFP-H2AV*. For that purpose, embryonic nuclear extracts of *GFP-H2AV* flies can be subjected to GFP affinity purification. GFP-H2AV associated proteins might be identified by western-blot analysis. In addition, GFP-bound and purified material can be used in *in vitro* assays to see a putative histone exchange. Moreover, three transgenic fly lines homozygous for DOM-B WT, DOM-B KR or ACF1 and homozygous for GFP-H2AV were generated during this work (*yw; DOM-B WT; GFP-H2AV*, *yw; DOM-B KR; GFP-H2AV*, *yw, ACF1; +/+; GFP-H2AV*). These fly lines allow an ectopic expression of DOM-B (WT or KR) or ACF1 and H2AV in a tissue-and developmental-specific manner using different GAL4 driver lines. Whole mount immunofluorescence analysis will possibly shed light on a direct interaction between DOM-B and H2AV compared to ACF1 and H2AV. Also in this case, GFP-binder affinity purification is possible.

Taken together, further studies will address the questions, whether ACDC is more involved in transcription and proliferation/differentiation programs, whether in DNA repair mechanisms or whether in chromatin formation. It might be that ACDC governs more than one function depending from its combinatorial association with other subunits in specific cell-types and in accordance with developmental stages.

5 ABBREVIATIONS

6 BIBLIOGRAPHY

7 LIST OF FIGURES AND TABLES

8 CURRICULUM VITAE

ABBREVIATIONS

α	Anti
aa	amino acids
A	Adenine
ACDC	ACF1 Domino B-containing complex
ACKC	ACF1 Domino B KR-containing complex
ACF	ATP-utilizing chromatin assembly and remodelling factor
ADP	Adenosindiphosphate
AED	After egg deposition
A/P	Anterior-posterior
ATP	Adenosintriphosphate
BAF	BRG1-associated factors
BAP	Brahma-associated proteins
Bcg	Black cell glass
bp	Basepairs
BPTF	Bromodomain PHD finger transcription factor
BrdU	Bromdesoxyuridin
BRM	Brahma
BRG1	Brahma-related gene 1
BSA	Bovine serum albumin
C	Cytosine
CAB	Chromatin assembly buffer
CB	Cystoblast
CHD	Chromodomain-helicase-DNA-binding
ChIP	Chromatin IP
CHRAC	Chromatin accessibility complex
Cyo	Curly of oyster
dATP	Desoxyadenosintriphosphate
DAC	Dachshund
DB	Dialysis buffer
DBP	DNA-binding protein
dCTP	Desoxycytosintriphosphate
dGTP	Desoxyguanidintriphosphate
Dls1	Dpb3-like subunit
DMSO	Dimethylsulfoxide
DNA	Desoxyribonucleic acid
DNMT	DNA methyltransferase
dNTP	Desoxyribonucleotidetriphosphate
DOM	Domino
DOM-A/B	Domino A/B
DOM-B KR	Domino K945 → R
Drosophila	*Drosophila melanogaster*
DTT	Dithiothreitol
dTTP	Desoxythymidintriphosphate
D/V	Dorso-ventral
E. coli	*Escherichia coli*
EB	Embryo buffer
ECM	Extracellular matrix
EDTA	Ethylendiamintetraacetate
EGF	Epidermal growth factor
EGTA	Ethylenglycol-bis(2-aminoethyl)-N,N,N',N'-tetraacetic acid
ELP3	Elongator complex protein 3

EM	Electron microscopy
Eng	*Engrailed*
E(Pc)	Enhancer of Polycomb
EtBr	Ethidiumbromide
EW	Embryo wash
Ey	*eyeless*
FM	First X chromosome
FPLC	Fast protein liquid chromatography
fw	Forward
G	Guanine
GAS41	Glioma-amplified sequence-41
Gcn5	General control non-derepressible
GSC	Germ stem cells
GST	Gluthtione-S-tranferase
H	Hour
H2A	Histone 2A
H2AV	H2A variant
HAT	Histone acetyltransferase
HDAC	Histone deacetylase
HFD	Histone fold domain
HEPES	(N-(2-Hydroxyethyl)piperazine-H’-(2-ethanesulfonic acid)
HMT	Histone methyltransferase
HP1	Heterochromatin protein 1
HRP	Horseradish peroxidase
Ig	Immunoglobulin
ING3	Inhibitor of growth protein 3
INO80	Inositol requiring
IP	Immunoprecipitation
IPTG	1-isopropyl-β-D-1-thiogalacto-pyranoside
IR	Inverted repeats
ISW1/ISW2	Imitation switch (*Sacharomyces cerevisiae*)
ISWI	Imitation switch (*Drosophila*, *Xenopus*)
JAK-STAT	Janus Kinase-Signal Transducer and Activator of Transcription
kb	Kilobase
kDa	Kilo Dalton
KLH	Keyhole limpet hemocyanin
M	Molar
MBD3	Methyl-binding protein 3
MDa	Mega Dalton
MF	Morphogenetic furrow
min	Minute
Mi-2	dermatomyositis autoantigen 2
ml	Milliliter
mM	Millimolar
MNase	Micrococcal nuclease
MORF	Mortality factor
MRG15	MORF4 related factor on human chromosome 15
mRNA	Messenger RNA
MW	Molecular weight
NAP-1	Nucleosome assembly protein 1
NLS	Nuclear localization sequence
NoRC	Nucleolar remodeling complex
NURD	Nucleosome remodeling and deacetylation
NURF	Nucleosome remodeling factor
OD	Optical density
o/n	over night

P	P-element
PAGE	Polyacrylamide gel electrophoresis
PBAF	Polybromo-associated BAF
PBAP	Polybromo-associated BAP
PBS	Phosphate buffered saline
PcG	Polycomb Group
PCR	Polymerase chain reaction
PEST	Proline (P), Glutamic acid (E), Serine (S), and Threonine (T).
PFA	Paraformaldehyde
PHD	Plant homeo domain
PMSF	Phenylmethanesulfonyl fluoride
PTM	Posttranslational modification
PVDF	Polyvinylidene Fluoride
R	Photoreceptor
RDGN	Retinal determination gene network
Rh	Rhabdomere
Rhod. Red	Rhodamine Red
RNA	Ribonucleic acid
RNAi	RNA interference
rpm	Revoltations per minute
RSC	Remodels the structure of chromatin
RSF	Remodelling and spacing factor
RT	Room temperature
Rv	Reverse
SANT	SWI3, ADA2, N-CoR and TFIIIB B
SCRAP	SNF-2-related CREB-binding protein activator protein
SDS	Sodiumdodecylsulfate
Sf9	*Spodoptera Frugiperda 9*
Sgs	Salivary glands
SHL	Superhelical location
SLIDE	SANT-like ISWI domain
SirT1	Sirtuin (silent mating type information regulation 2 homolog1)
S/MAR	Scaffold/matrix attachement region
SNF2	Sucrose non-fermenting protein 2 homolog
SNF2H	Sucrose non-fermenting protein 2 homolog
SNF2L	Sucrose non-fermenting protein 2-like
SSC	Somatic stem cell
Sth1	Snf two homologous 1
SUMO	Small ubiquitin-related modifier
SWI/SNF	Switch/sucrose non-fermenting
SWR1	Swi2/Snf2-related 1
T	Thymine
Temed	N,N,N’,N’-Tetramethylethylenediamine
TIP60	Tata interactive protein
TLC	Thin layer chromatography
TM3	Third multiple 3
TRAX	*Drosophila* embryo nuclear extract
Tris	Tris(hydroxymethyl)aminomethane
TrxG	Trithorax Group
UAS	Upstream activating sequence
UV	Ultraviolet
V	Volts
v/v	Volume per volume
WICH	WSTF-ISWI chromatin remodelling complex
WSTF	Williams syndrome transcription factor
WT	Wildtype
w/v	Weight per volume

Xenopus	*Xenopus laevis*
Yw	*Yellow white*
µg	Microgramm
µl	Microliter
µM	Micromolar
ɣ-H2AV	phosphorylated H2AV at S137

BIBLIOGRAPHY

Ables, E. T., and Drummond-Barbosa, D. (2010) The steroid hormone ecdysone functions with intrinsic chromatin remodeling factors to control female germline stem cells in Drosophila, *Cell Stem Cell 7*, 581-592.

Alberts, B., Johnson. A., Lewis, J., Raff, M., Roberts, K., and Walter, P., (2002) Molecular biology of the cell, *New York: Garland Science*, 4th Edition.

Annunziato, A. (2008) DNA packaging: Nucleosomes and chromatin. *Nature Education 1*, 1

Atkins, M., and Mardon, G. (2009) Signaling in the third dimension: the peripodial epithelium in eye disc development, *Dev Dyn 238*, 2139-2148.

Auger, A., Galarneau, L., Altaf, M., Nourani, A., Doyon, Y., Utley, R. T., Cronier, D., Allard, S., and Cote, J. (2008) Eaf1 is the platform for NuA4 molecular assembly that evolutionarily links chromatin acetylation to ATP-dependent exchange of histone H2A variants, *Mol Cell Biol 28*, 2257-2270.

Avery, O. T., Macleod, C. M., and McCarty, M. (1944) Studies on the Chemical Nature of the Substance Inducing Transformation of Pneumococcal Types : Induction of Transformation by a Desoxyribonucleic Acid Fraction Isolated from Pneumococcus Type Iii, *J Exp Med 79*, 137-158.

Bajpai, R., Chen, D. A., Rada-Iglesias, A., Zhang, J., Xiong, Y., Helms, J., Chang, C. P., Zhao, Y., Swigut, T., and Wysocka, J. (2010) CHD7 cooperates with PBAF to control multipotent neural crest formation, *Nature 463*, 958-962.

Bakshi, R., Prakash, T., Dash, D. and Brahmachari, V., (2004) In silico characterization of the INO80 subfamily of SWI2/SNF2 chromatin remodeling proteins. *Biochem Biophys Res Commun 320*, 197-204.

Bao, Y., and Shen, X. (2007) SnapShot: chromatin remodeling complexes, *Cell 129*, 632.

Bao, Y., and Shen, X. (2007a) Chromatin remodeling in DNA double-strand break repair, *Curr Opin Genet Dev 17*, 126-131.

Bao, Y., and Shen, X. (2011) SnapShot: Chromatin remodeling: INO80 and SWR1, *Cell 144*, 158-158 e152.

Becalska, A. N., and Gavis, E. R. (2009) Lighting up mRNA localization in Drosophila oogenesis, *Development 136*, 2493-2503.

Becker, P. B. (2002) Nucleosome sliding: facts and fiction, *EMBO J 21*, 4749-4753.

Becker, P. B., and Horz, W. (2002) ATP-dependent nucleosome remodeling, *Annu Rev Biochem 71*, 247-273.

Bernstein, E., and Hake, S. B. (2006) The nucleosome: a little variation goes a long way, *Biochem Cell Biol 84*, 505-517.

Bochar, D. A., Savard, J., Wang, W., Lafleur, D. W., Moore, P., Cote, J., and Shiekhattar, R. (2000) A family of chromatin remodeling factors related to Williams syndrome transcription factor, *Proc Natl Acad Sci USA 97*, 1038–1043.

Bonisch, C., Nieratschker, S. M., Orfanos, N. K., and Hake, S. B. (2008) Chromatin proteomics and epigenetic regulatory circuits, *Expert Rev Proteomics 5*, 105-119.

Brand, A. H., and Perrimon, N. (1993) Targeted gene expression as a means of altering cell fates and generating dominant phenotypes, *Development 118*, 401-415.

Braun, A., Lemaitre, B., Lanot, R., Zachary, D., and Meister, M. (1997) Drosophila immunity: analysis of larval hemocytes by P-element-mediated enhancer trap, *Genetics 147*, 623-634.

Brown, E., Malakar, S., and Krebs, J. E. (2007) How many remodelers does it take to make a brain? Diverse and cooperative roles of ATP-dependent chromatin-remodeling complexes in development, *Biochem Cell Biol 85*, 444-462.

Butler, L. C., Blanchard, G. B., Kabla, A. J., Lawrence, N. J., Welchman, D. P., Mahadevan, L., Adams, R. J., and Sanson, B. (2009) Cell shape changes indicate a role for extrinsic tensile forces in Drosophila germ-band extension, *Nat Cell Biol 11*, 859-864.

Cherbas, L., Hu, X., Zhimulev, I., Belyaeva, E., and Cherbas, P. (2003) EcR isoforms in Drosophila: testing tissue-specific requirements by targeted blockade and rescue, *Development 130*, 271-284.

Cherry, C. M., and Matunis, E. L. (2010) Epigenetic regulation of stem cell maintenance in the Drosophila testis via the nucleosome-remodeling factor NURF, *Cell Stem Cell 6*, 557-567.

Chioda, M., and Becker, P. B. (2010) Soft skills turned into hard facts: nucleosome remodelling at developmental switches, *Heredity 105*, 71-79.

Chioda, M., Vengadasalam, S., Kremmer, E., Eberharter, A., and Becker, P. B. (2010) Developmental role for ACF1-containing nucleosome remodellers in chromatin organisation, *Development 137*, 3513-3522.

Clapier, C. R., and Cairns, B. R. (2009) The biology of chromatin remodeling complexes, *Annu Rev Biochem 78*, 273-304.

Classen, A. K., Bunker, B. D., Harvey, K. F., Vaccari, T., and Bilder, D. (2009) A tumor suppressor activity of Drosophila Polycomb genes mediated by JAK-STAT signaling, *Nat Genet 41*, 1150-1155.

Conaway, R. C., and Conaway, J. W. (2009) The INO80 chromatin remodeling complex in transcription, replication and repair, *Trends Biochem Sci 34*, 71-77.

Corona, D. F., Clapier, C. R., Becker, P. B., and Tamkun, J. W. (2002) Modulation of ISWI function by site-specific histone acetylation, *EMBO Rep 3*, 242-247.

Corona, D. F., and Tamkun, J. W. (2004) Multiple roles for ISWI in transcription, chromosome organization and DNA replication, *Biochim Biophys Acta 1677*, 113-119.

Deuring, R., Fanti, L., Armstrong, J. A., Sarte, M., Papoulas, O., Prestel, M., Daubresse, G., Verardo, M., Moseley, S. L., Berloco, M., Tsukiyama, T., Wu, C., Pimpinelli, S., and Tamkun, J. W. (2000) The ISWI chromatin-remodeling protein is required for gene expression and the maintenance of higher order chromatin structure in vivo, *Mol Cell 5*, 355-365.

Dulac, C. (2010) Brain function and chromatin plasticity, *Nature 465*, 728-735.

Duong, H. A., Wang, C. W., Sun, Y. H., and Courey, A. J. (2008) Transformation of eye to antenna by misexpression of a single gene, *Mech Dev 125*, 130-141.

Eberharter, A., Ferrari, S., Langst, G., Straub, T., Imhof, A., Varga-Weisz, P., Wilm, M., and Becker, P. B. (2001) Acf1, the largest subunit of CHRAC, regulates ISWI-induced nucleosome remodelling, *EMBO J 20*, 3781-3788.

Eberharter, A., Ferreira, R., and Becker, P. (2005) Dynamic chromatin: concerted nucleosome remodelling and acetylation, *Biol Chem 386*, 745-751.

Eberharter, A., Langst, G., and Becker, P. B. (2004) A nucleosome sliding assay for chromatin remodeling factors, *Methods Enzymol 377*, 344-353.

Eberharter, A., Vetter, I., Ferreira, R., and Becker, P. B. (2004a) ACF1 improves the effectiveness of nucleosome mobilization by ISWI through PHD-histone contacts, *EMBO J 23*, 4029-4039.

Elfring, L. K., Deuring, R., McCallum, C. M., Peterson, C. L., and Tamkun, J. W. (1994) Identification and characterization of Drosophila relatives of the yeast transcriptional activator SNF2/SWI2, *Mol. Cell Biol. 14*, 2225–2234.

Ellis, M. C., O'Neill, E. M., and Rubin, G. M. (1993) Expression of Drosophila glass protein and evidence for negative regulation of its activity in non-neuronal cells by another DNA-binding protein, *Development 119*, 855-865.

Extavour, C., and Garcia-Bellido, A. (2001) Germ cell selection in genetic mosaics in Drosophila melanogaster, *Proc Natl Acad Sci U S A 98*, 11341-11346.

Fazzio, T. G., Huff, J. T., and Panning, B. (2008) An RNAi screen of chromatin proteins identifies Tip60-p400 as a regulator of embryonic stem cell identity, *Cell 134*, 162-174.

Fetting, J. L., Spencer, S. A., and Wolff, T. (2009) The cell adhesion molecules Echinoid and Friend of Echinoid coordinate cell adhesion and cell signaling to regulate the fidelity of ommatidial rotation in the Drosophila eye, *Development 136*, 3323-3333.

Flaus, A., Martin, D. M., Barton, G. J., and Owen-Hughes, T. (2006) Identification of multiple distinct Snf2 subfamilies with conserved structural motifs, *Nucleic Acids Res 34*, 2887-2905.

Foe, V. E., and Alberts, B. M. (1983) Studies of nuclear and cytoplasmic behaviour during the five mitotic cycles that precede gastrulation in Drosophila embryogenesis, *J Cell Sci 61*, 31-70.

Foley, K., and Cooley, L. (1998) Apoptosis in late stage Drosophila nurse cells does not require genes within the H99 deficiency, *Development 125*, 1075-1082.

Frankfort, B. J., and Mardon, G. (2002) R8 development in the Drosophila eye: a paradigm for neural selection and differentiation, *Development 129*, 1295-1306.

Frescas, D., Mavrakis, M., Lorenz, H., Delotto, R., and Lippincott-Schwartz, J. (2006) The secretory membrane system in the Drosophila syncytial blastoderm embryo exists as functionally compartmentalized units around individual nuclei, *J Cell Biol 173*, 219-230.

Fuchs, M., Gerber, J., Drapkin, R., Sif, S., Ikura, T., Ogryzko, V., Lane, W. S., Nakatani, Y., and Livingston, D. M. (2001) The p400 complex is an essential E1A transformation target, *Cell 106*, 297-307.

Fujii, T., Ueda, T., Nagata, S., and Fukunaga, R. (2010) Essential role of p400/mDomino chromatin-remodeling ATPase in bone marrow hematopoiesis and cell-cycle progression, *J Biol Chem 285*, 30214-30223.

Fuks, F. (2005) DNA methylation and histone modifications: teaming up to silence genes, *Curr Opin Genet Dev 15*, 490-495.

Fyodorov, D. V., Blower, M. D., Karpen, G. H., and Kadonaga, J. T. (2004) Acf1 confers unique activities to ACF/CHRAC and promotes the formation rather than disruption of chromatin in vivo, *Genes Dev 18*, 170-183.

Gangaraju, V. K., and Bartholomew, B. (2007) Mechanisms of ATP dependent chromatin remodeling, *Mutat Res 618*, 3-17.

Grune, T., Brzeski, J., Eberharter, A., Clapier, C. R., Corona, D. F., Becker, P. B., and Muller, C. W. (2003) Crystal structure and functional analysis of a nucleosome recognition module of the remodeling factor ISWI, *Mol Cell 12*, 449-460.

Guschin, D., Geiman, T. M., Kikyo, N., Tremethick, D. J., Wolffe, A. P. and Wade, P. A. (2000) Multiple ISWI ATPase complexes from Xenopus laevis: functional conservation of an ACF/CHRAC homolog, *J. Biol. Chem 275*, 35248-35255.

Halder, G., Callaerts, P., and Gehring, W. J. (1995) Induction of ectopic eyes by targeted expression of the eyeless gene in Drosophila, *Science 267*, 1788-1792.

Hanai, K., Furuhashi, H., Yamamoto, T., Akasaka, K., and Hirose, S. (2008) RSF governs silent chromatin formation via histone H2Av replacement, *PLoS Genet 4*, e1000011.

Hargreaves, D. C., and Crabtree, G. R. (2011) ATP-dependent chromatin remodeling: genetics, genomics and mechanisms, *Cell Res 21*, 396-420.

Hartenstein, V., (1993) Atlas of *Drosophila* development, *Cold Spring Harbor Laboratory Press.*

Hartman, T. R., Zinshteyn, D., Schofield, H. K., Nicolas, E., Okada, A., and O'Reilly, A. M. (2010) Drosophila Boi limits Hedgehog levels to suppress follicle stem cell proliferation, *J Cell Biol 191*, 943-952.

Hay, B., Jan, L. Y., and Jan, Y. N. (1988) A protein component of Drosophila polar granules is encoded by vasa and has extensive sequence similarity to ATP-dependent helicases, *Cell 55*, 577-587.

Held, L. I. (2005) Imaginal Discs: The Genetic and Cellular Logic of Pattern Formation, *Cambridge University Press.*

Ho, L., and Crabtree, G. R. (2010) Chromatin remodelling during development, *Nature 463*, 474-484.

Hsiung, F., and Moses, K. (2002) Retinal development in Drosophila: specifying the first neuron, *Hum Mol Genet 11*, 1207-1214.

Huynh, V. A., Robinson, P. J., and Rhodes, D. (2005) A method for the in vitro reconstitution of a defined "30 nm" chromatin fibre containing stoichiometric amounts of the linker histone. *J Mol Biol 345*, 957-968.

Ikura, T., Ogryzko, V. V., Grigoriev, M., Groisman, R., Wang, J., Horikoshi, M., Scully, R., Qin, J., and Nakatani, Y. (2000) Involvement of the TIP60 histone acetylase complex in DNA repair and apoptosis, *Cell 102*, 463-473.

Isogai, Y., Keles, S., Prestel, M., Hochheimer, A. and Tjian, R. (2007) Transcription of histone gene cluster by differential core-promoter factors. *Genes Dev*. 21, 2936-2949.

Ito, T., Bulger, M., Pazin, M. J., Kobayashi, R., and Kadonaga, J. T. (1997) ACF, an ISWI-containing and ATP-utilizing chromatin assembly and remodeling factor, *Cell 90*, 145-155.

Ito, T., Levenstein, M. E., Fyodorov, D. V., Kutach, A. K., Kobayashi, R., and Kadonaga, J. T. (1999) ACF consists of two subunits, Acf1 and ISWI, that function cooperatively in the ATP-dependent catalysis of chromatin assembly, *Genes Dev 13*, 1529-1539.

Janody, F., Sturny, R., Catala, F., Desplan, C., and Dostatni, N. (2000) Phosphorylation of bicoid on MAP-kinase sites: contribution to its interaction with the torso pathway, *Development 127*, 279-289.

Jin, J., Cai, Y., Li, B., Conaway, R. C., Workman, J. L., Conaway, J. W., and Kusch, T. (2005) In and out: histone variant exchange in chromatin, *Trends Biochem Sci 30*, 680-687.

Joyce, E. F., and McKim, K. S. (2010) Chromosome axis defects induce a checkpoint-mediated delay and interchromosomal effect on crossing over during Drosophila meiosis, *PLoS Genet 6*.

Kango-Singh, M., and Singh, A. (2009) Regulation of organ size: insights from the Drosophila Hippo signaling pathway, *Dev Dyn 238*, 1627-1637.

Kasten, M. M., Clapier, C. R., and Cairns, B. R. (2011) SnapShot: Chromatin remodeling: SWI/SNF, *Cell 144*, 310 e311.

Keenen, B., Qi, H., Saladi, S. V., Yeung, M., and de la Serna, I. L. (2010) Heterogeneous SWI/SNF chromatin remodeling complexes promote expression of microphthalmia-associated transcription factor target genes in melanoma, *Oncogene 29*, 81-92.

Keller, R. (2006) Mechanisms of elongation in embryogenesis, *Development 133*, 2291-2302.

Kenyon, K. L., Ranade, S. S., Curtiss, J., Mlodzik, M., and Pignoni, F. (2003) Coordinating proliferation and tissue specification to promote regional identity in the Drosophila head, *Dev Cell 5*, 403-414.

Kobor, M. S., Venkatasubrahmanyam, S., Meneghini, M. D., Gin, J. W., Jennings, J. L., Link, A. J., Madhani, H. D. and Rine, J. (2004). A protein complex containing the conserved Swi2/Snf2-Related ATPase Swr1p deposits histone variant H2A.Z into euchromatin. *PLoS. Biol.* 2, E131.

Konev, A. Y., Tribus, M., Park, S. Y., Podhraski, V., Lim, C. Y., Emelyanov, A. V., Vershilova, E., Pirrotta, V., Kadonaga, J. T., Lusser, A., and Fyodorov, D. V. (2007) CHD1 motor protein is required for deposition of histone variant H3.3 into chromatin in vivo, *Science 317*, 1087-1090.

Korber, P., and Becker, P. B. (2010) Nucleosome dynamics and epigenetic stability, *Essays Biochem 48*, 63-74.

Kumar, J. P. (2001) Signalling pathways in Drosophila and vertebrate retinal development, *Nat Rev Genet 2*, 846-857.

Kusch, T., Florens, L., Macdonald, W. H., Swanson, S. K., Glaser, R. L., Yates, J. R., 3rd, Abmayr, S. M., Washburn, M. P., and Workman, J. L. (2004) Acetylation by Tip60 is required for selective histone variant exchange at DNA lesions, *Science 306*, 2084-2087.

Längst, G., and Becker, P. B. (2001) Nucleosome mobilization and positioning by ISWI-containing chromatin-remodeling factors, *J Cell Sci 114*, 2561-2568.

Längst, G., and Becker, P. B. (2004) Nucleosome remodeling: one mechanism, many phenomena?, *Biochim Biophys Acta 1677*, 58-63.

Lasko, P. (2011), Posttranscriptional regulation in Drosophila oocytes and early embryos. *Wiley Interdisciplinary Reviews: RNA*, 2: 408–416.

Leach, T. J., Mazzeo, M., Chotkowski, H. L., Madigan, J. P., Wotring, M. G., and Glaser, R. L. (2000) Histone H2A.Z is widely but nonrandomly distributed in chromosomes of Drosophila melanogaster, *J Biol Chem 275*, 23267-23272.

Leong, G. R., Goulding, K. R., Amin, N., Richardson, H. E., and Brumby, A. M. (2009) Scribble mutants promote aPKC and JNK-dependent epithelial neoplasia independently of Crumbs, *BMC Biol 7*, 62.

Lin, H. (2002) The stem-cell niche theory: lessons from flies, *Nat Rev Genet 3*, 931-940.

Lorch, Y., Maier-Davis, B., and Kornberg, R. D. (2006) Chromatin remodeling by nucleosome disassembly in vitro, *Proc Natl Acad Sci U S A 103*, 3090-3093.

Lorch, Y., Maier-Davis, B., and Kornberg, R. D. (2010) Mechanism of chromatin remodeling, *Proc Natl Acad Sci U S A 107*, 3458-3462.

Luger, K., and Hansen, J. C. (2005) Nucleosome and chromatin fiber dynamics, *Curr Opin Struct Biol 15*, 188-196.

Lusser, A., Urwin, D. L., and Kadonaga, J. T. (2005) Distinct activities of CHD1 and ACF in ATP-dependent chromatin assembly, *Nat Struct Mol Biol 12*, 160-166.

Madigan, J. P., Chotkowski, H. L., and Glaser, R. L. (2002) DNA double-strand break-induced phosphorylation of Drosophila histone variant H2Av helps prevent radiation-induced apoptosis, *Nucleic Acids Res 30*, 3698-3705.

Maier, V. K., Chioda, M., Rhodes, D., and Becker, P. B. (2008) ACF catalyses chromatosome movements in chromatin fibres, *EMBO J 27*, 817-826.

March-Diaz, R., and Reyes, J. C. (2009) The beauty of being a variant: H2A.Z and the SWR1 complex in plants, *Mol Plant 2*, 565-577.

Mardon, G., Solomon, N. M. and Rubin, G. M. dachshund encodes a nuclear protein required for normal eye and leg development in Drosophila, *Development 120*, 3473-3486 (1994).

Martinez-Arias, A., and Lawrence, P. A. (1985) Parasegments and compartments in the Drosophila embryo, *Nature 313*, 639-642.

McDaniel, I. E., Lee, J. M., Berger, M. S., Hanagami, C. K., and Armstrong, J. A. (2008) Investigations of CHD1 function in transcription and development of Drosophila melanogaster, *Genetics 178*, 583-587.

Meshorer, E., and Misteli, T. (2006) Chromatin in pluripotent embryonic stem cells and differentiation, *Nat Rev Mol Cell Biol 7*, 540-546.

Mizuguchi, G., Shen, X., Landry, J., Wu, W. H., Sen, S., and Wu, C. (2004) ATP-driven exchange of histone H2AZ variant catalyzed by SWR1 chromatin remodeling complex, *Science 303*, 343-348.

Mohrmann, L., and Verrijzer, C. P. (2005) Composition and functional specificity of SWI2/SNF2 class chromatin remodeling complexes, *Biochim Biophys Acta 1681*, 59-73.

Morata, G. (2001) How Drosophila appendages develop, *Nat Rev Mol Cell Biol 2*, 89-97.

Morillo-Huesca, M., Clemente-Ruiz, M., Andujar, E., and Prado, F. (2010) The SWR1 histone replacement complex causes genetic instability and genome-wide transcription misregulation in the absence of H2A.Z, *PLoS One 5*, e12143.

Morrison, A. J., and Shen, X. (2009) Chromatin remodelling beyond transcription: the INO80 and SWR1 complexes, *Nat Rev Mol Cell Biol 10*, 373-384.

Moses, K., and Rubin, G. M. (1991) Glass encodes a site-specific DNA-binding protein that is regulated in response to positional signals in the developing Drosophila eye, *Genes Dev 5*, 583-593.

Moshkin, Y. M., Mohrmann, L., van Ijcken, W. F., and Verrijzer, C. P. (2007) Functional differentiation of SWI/SNF remodelers in transcription and cell cycle control, *Mol Cell Biol 27*, 651-661.

Niki, Y., Yamaguchi, T. and Mahowald, A.P. (2006) Establishment of stable cell lines of Drosophila germ-line stem cells. *Proc Natl Acad Sci USA 103*, 16325-16330.

Oberdoerffer, P., and Sinclair, D. A. (2007) The role of nuclear architecture in genomic instability and ageing, *Nat Rev Mol Cell Biol 8*, 692-702.

Park, S. W., Oh, H., Lin, Y. R., and Park, Y. (2010) MSL cis-spreading from roX gene up-regulates the neighboring genes, *Biochem Biophys Res Commun 399*, 227-231.

Olins, D. E. and Olins, A. L. (2003) Chromatin history: our view from the bridge, *Nat Rev Mol Cell Biol 4(10)*: 809-814.

Peterson, C. L., and Herskowitz, I. (1992) Characterization of the yeast SWI1, SWI2, and SWI3 genes, which encode a global activator of transcription, *Cell 68*, 573-583.

Polesello, C., Delon, I., Valenti, P., Ferrer, P., and Payre, F. (2002) Dmoesin controls actin-based cell shape and polarity during Drosophila melanogaster oogenesis, *Nat Cell Biol 4*, 782-789.

Popov, V. M., Wu, K., Zhou, J., Powell, M. J., Mardon, G., Wang, C., and Pestell, R. G. (2010) The Dachshund gene in development and hormone-responsive tumorigenesis, *Trends Endocrinol Metab 21*, 41-49.

Potter, C. J., Turenchalk, G. S., and Xu, T. (2000) Drosophila in cancer research. An expanding role, *Trends Genet 16*, 33-39.

Probst, A. V., Dunleavy, E., and Almouzni, G. (2009) Epigenetic inheritance during the cell cycle, *Nat Rev Mol Cell Biol 10*, 192-206.

Quivy, J. P., and Becker, P. B. (1997). Genomic footprinting of Drosophila embryo nuclei by linker tag selection LM-PCR. *Methods 11*, 171-179.

Reiter, L. T., Potocki, L., Chien, S., Gribskov, M., and Bier, E. (2001) A systematic analysis of human disease-associated gene sequences in Drosophila melanogaster, *Genome Res 11*, 1114-1125.

Roberts, C. W., and Orkin, S. H. (2004) The SWI/SNF complex--chromatin and cancer, *Nat Rev Cancer 4*, 133-142.

Roignant, J. Y., and Treisman, J. E. (2009) Pattern formation in the Drosophila eye disc, *Int J Dev Biol 53*, 795-804.

Roth, S., and Lynch, J. A. (2009) Symmetry breaking during Drosophila oogenesis, *Cold Spring Harb Perspect Biol 1*, a001891.

Rudolph, T., Yonezawa, M., Lein, S., Heidrich, K., Kubicek, S., Schafer, C., Phalke, S., Walther, M., Schmidt, A., Jenuwein, T., and Reuter, G. (2007) Heterochromatin formation in Drosophila is initiated through active removal of H3K4 methylation by the LSD1 homolog SU(VAR)3-3, *Mol Cell 26*, 103-115.

Ruhf, M. L., Braun, A., Papoulas, O., Tamkun, J. W., Randsholt, N., and Meister, M. (2001) The domino gene of Drosophila encodes novel members of the SWI2/SNF2 family of DNA-dependent ATPases, which contribute to the silencing of homeotic genes, *Development 128*, 1429-1441.

Sambrook, J., and Russell, D.W. (2001). Molecular Cloning - A Laboratory Manual, *Cold Spring Harbor Laboratory Press*, 3rd Edition.

Sánchez-Molina, S., Mortusewicz, O., Bieber, B., Auer, S., Eckey, M., Leonhardt, H., Friedl, A.A. and Becker, P.B. (2011) Role for hACF1 in the G2/M damage checkpoint, *Nucleic Acids Research*, epub ahead of print

Sarma, K., and Reinberg, D. (2005) Histone variants meet their match, *Nat Rev Mol Cell Biol 6*, 139-149.

Schmitt, S., Prestel, M. and Paro, R. (2005) Intergenic transcription through a polycomb group response element counteracts silencing. *Genes Dev. 19*, 697-708.

Schroeder, M. D., Pearce, M., Fak, J., Fan, H., Unnerstall, U., Emberly, E., Rajewsky, N., Siggia, E. D., and Gaul, U. (2004) Transcriptional control in the segmentation gene network of Drosophila, *PLoS Biol 2*, E271.

Sheng, S., Czajkowsky, D.M., and Shao, Z. (2006). Localization of linker histone in chromatosomes by cryo-atomic force microscopy. *Biophys J 91*, L35-37.

Shi, S., Larson, K., Guo, D., Lim, S. J., Dutta, P., Yan, S. J., and Li, W. X. (2008) Drosophila STAT is required for directly maintaining HP1 localization and heterochromatin stability, *Nat Cell Biol 10*, 489-496.

Sims, J. K., and Wade, P. A. (2011) SnapShot: Chromatin remodeling: CHD, *Cell 144*, 626-626 e621.

Spradling, A., Drummond-Barbosa, D., and Kai, T. (2001) Stem cells find their niche, *Nature 414*, 98-104.

St Johnston, D. (2002) The art and design of genetic screens: Drosophila melanogaster, *Nat Rev Genet 3*, 176-188.

St Johnston, D., and Nusslein-Volhard, C. (1992) The origin of pattern and polarity in the Drosophila embryo, *Cell 68*, 201-219.

Sullivan, W., Ashburner, M., and Hawley, S. (2000) Drosophila Protocols, *Cold Spring Harbor Laboratory Press.*

Swaminathan, J., Baxter, E. M., and Corces, V. G. (2005) The role of histone H2Av variant replacement and histone H4 acetylation in the establishment of Drosophila heterochromatin, *Genes Dev 19*, 65-76.

Talbert, P. B., and Henikoff, S. (2010) Histone variants--ancient wrap artists of the epigenome, *Nat Rev Mol Cell Biol 11*, 264-275.

Thomas, J. O. and Kornberg, R.D. (1974) Chromatin structure; oligomers of the histones. *Science 184(139)*:865–868

Tremethick, D. J. (2007) Higher-order structures of chromatin: the elusive 30 nm fiber, *Cell 128*, 651-654.

Tsukiyama, T., and Wu, C. (1995) Purification and properties of an ATP-dependent nucleosome remodeling factor, *Cell 83*, 1011-1020.

Ueda, T., Watanabe-Fukunaga, R., Ogawa, H., Fukuyama, H., Higashi, Y., Nagata, S., and Fukunaga, R. (2007) Critical role of the p400/mDomino chromatin-remodeling ATPase in embryonic hematopoiesis, *Genes Cells 12*, 581-592.

van Attikum, H., Fritsch, O., and Gasser, S. M. (2007) Distinct roles for SWR1 and INO80 chromatin remodeling complexes at chromosomal double-strand breaks, *EMBO J 26*, 4113-4125.

van Holde, K.E. (1988) Chromatin, *Springer*, New York.

Varga-Weisz, P. D. (2010) Insights into how chromatin remodeling factors find their target in the nucleus, *Proc Natl Acad Sci U S A 107*, 19611-19612.

Varga-Weisz, P. D., Wilm, M., Bonte, E., Dumas, K., Mann, M., and Becker, P. B. (1997) Chromatin-remodelling factor CHRAC contains the ATPases ISWI and topoisomerase II, *Nature 388*, 598-602.

Vidal, M., and Cagan, R. L. (2006) Drosophila models for cancer research, *Curr Opin Genet Dev 16*, 10-16.

Walker, J., Kwon, S. Y., Badenhorst, P., East, P., McNeill, H., and Svejstrup, J. Q. (2011) Role of Elongator Subunit Elp3 in Drosophila melanogaster Larval Development and Immunity, *Genetics 187*, 1067-1075.

Wang, G. G., Allis, C. D., and Chi, P. (2007) Chromatin remodeling and cancer, Part II: ATP-dependent chromatin remodeling, *Trends Mol Med 13*, 373-380.

Wang, Y., Zhang, H., Chen, Y., Sun, Y., Yang, F., Yu, W., Liang, J., Sun, L., Yang, X., Shi, L., Li, R., Li, Y., Zhang, Y., Li, Q., Yi, X., and Shang, Y. (2009) LSD1 is a subunit of the NuRD complex and targets the metastasis programs in breast cancer, *Cell 138*, 660-672.

Wiedemann, S. M., Mildner, S. N., Bonisch, C., Israel, L., Maiser, A., Matheisl, S., Straub, T., Merkl, R., Leonhardt, H., Kremmer, E., Schermelleh, L., and Hake, S. B. (2010) Identification and characterization of two novel primate-specific histone H3 variants, H3.X and H3.Y, *J Cell Biol 190*, 777-791.

Wolffe, A. (1998). Chromatin - Structure & Function, *London, Academic Press*, 3rd Edition.

Wolpert, L., Jessell, Th., Lawrence, P., Meyerowitz, E., Robertson, E., Smith, J. (2007) Principles of Development, *Oxford University Press*, 3rd Edition.

Wong, M. M., Cox, L. K., and Chrivia, J. C. (2007) The chromatin remodeling protein, SRCAP, is critical for deposition of the histone variant H2A.Z at promoters, *J Biol Chem 282*, 26132-26139.

Wood, W., and Jacinto, A. (2007) Drosophila melanogaster embryonic haemocytes: masters of multitasking, *Nat Rev Mol Cell Biol 8*, 542-551.

Woodcock, C. L., and Ghosh, R. P. (2010) Chromatin higher-order structure and dynamics, *Cold Spring Harb Perspect Biol 2*, a000596.

Wu, J. I., Lessard, J., and Crabtree, G. R. (2009) Understanding the words of chromatin regulation, *Cell 136*, 200-206.

Wu, W. H., Alami, S., Luk, E., Wu, C. H., Sen, S., Mizuguchi, G., Wei, D., and Wu, C. (2005) Swc2 is a widely conserved H2AZ-binding module essential for ATP-dependent histone exchange, *Nat Struct Mol Biol 12*, 1064-1071.

Xi, R., and Xie, T. (2005) Stem cell self-renewal controlled by chromatin remodeling factors, *Science 310*, 1487-1489.

Xiao, A., Li, H., Shechter, D., Ahn, S. H., Fabrizio, L. A., Erdjument-Bromage, H., Ishibe-Murakami, S., Wang, B., Tempst, P., Hofmann, K., Patel, D. J., Elledge, S. J., and Allis, C. D. (2009) WSTF regulates the H2A.X DNA damage response via a novel tyrosine kinase activity, *Nature 457*, 57-62.

Xu, Y., Sun, Y., Jiang, X., Ayrapetov, M. K., Moskwa, P., Yang, S., Weinstock, D. M., and Price, B. D. (2010) The p400 ATPase regulates nucleosome stability and chromatin ubiquitination during DNA repair, *J Cell Biol 191*, 31-43.

Yadon, A. N., and Tsukiyama, T. (2011) SnapShot: Chromatin remodeling: ISWI, *Cell 144*, 453-453 e451.

Zink, D. and Paro, R. (1995) Drosophila Polycomb-group regulated chromatin inhibits the accessibility of a trans-activator to its target DNA. *EMBO J 14*, 5660–5671.

LIST OF FIGURES

1.1 The major structures in DNA compaction....8
1.2 Epigenetic mechanisms involved in chromatin modifications....9
1.3 Canonical core histones and their major variants....11
1.4 Major histone variants of the H2A family in different species....12
1.5 Mechanisms of ATP-driven chromatin remodeling....14
1.6 Families of ATP-dependent chromatin remodelers and their basic domains....15
1.7 Chromatin remodeling complexes of the ISWI family and their homologous subunits....18
1.8 Major chromatin remodeling complexes of the INO80 family and their homologous subunits....20
1.9 The two isoforms of Domino and their domains....21
1.10 The life cycle of *Drosophila melanogaster*....24
1.11 The three major stages during *Drosophila* embryogenesis....26
1.12 Imaginal discs in the *Drosophila* larva and corresponding structures in an adult fly....28
1.13 Schematic fate map of the eye-antenna disc and the corresponding structures....29
1.14 Differentiation of photoreceptors in the *Drosophila* eye imaginal disc....30
1.15 Cells in one ommatidium of an adult compound eye in *Drosophila*....30
1.16 The *Drosophila* ovariole....31
1.17 The *Drosophila* germarium....32
1.18 Proposed model of a stem cell niche....34

3.1 DOM-B expression is developmentally regulated in *Drosophila* embryos....62
3.2 DOM-B, ACF1 and ISWI cofractionate in nuclear protein extracts of early embryos....63
3.3 DOM-B is part of a high molecular weight complex in *Drosophila* Embryos....64
3.4 DOM-B is part of a high molecular weight complex in *Drosophila* Embryos....65
3.5 Overview of DOM-B derivatives investigated in this study....67
3.6 DOM-B derivatives can be generated in *E.coli* and purified via GST-tag....68
3.7 DOM-B proteins can be expressed in *Sf9* cells and purified via FLAG-tag....69
3.8 Recombinant DOM-B associates directly with ACF1 and ISWI *in vitro*....70
3.9 Mapping the ACF1 interacting domain of DOM-B....71
3.10 ATPase activities of DOM-B WT or KR, DOM-B derivatives and in combination with ACF1....73
3.11 The *UAS-GAL4* system for targeted expression or deletion of proteins in *Drosophila*....75
3.12 Establishment of a new α-H2AV antibody on larval tissues....76
3.13 Establishment of the specific α-DOM-B monoclonal rat antibody 2G5....78
3.14 Establishment of the specific α-DOM-B polyclonal antibody Ch35....79
3.15 Colocalization of DOM-B and ACF1 on chromatin of salivary glands....80
3.16 Ectopic expression of DOM-B leads to a disruption of chromatin organization....82
3.17 DOM depletion leads to a remarkable reduction in size of salivary glands....83
3.18 DOM depletion leads to a remarkable reduction of nuclei size....84
3.19 DOM depletion leads to late pupal lethality....85
3.20 DOM depletion in eye-antenna discs disrupts morphogenesis of adult compound eyes and antennae....86

3.21 DOM depletion in eye-antenna discs affects cell differentiation..................................87
3.22 Ectopic expression of DOM-B in eye-antenna discs disrupts adult eye morphology................88
3.23 Ectopic expression of DOM-B WT and KR disturbs cell differentiation in eye-antenna discs...89
3.24 Ectopic expression of DOM-B delays S-phase progression and perturbs apoptotic events...91
3.25 Ectopic expression of ACDC or ACKC using the *glass-GAL4* driver did not lead to eye perturbation...93
3.26 Expression of ACDC or ACKC using the *ey-GAL4* driver leads to major aberrations in adult compound eyes...94
3.27 Ectopic expression of ACDC and ACKC disturb the entire eye-antenna disc morphology...96
3.28 ACF1 is enriched in germline stem cells, cystoblasts and oocytes in *Drosophila* ovaries........98
3.29 Ectopic expression of DOM-B WT and ACF1 in *Drosophila* ovaries affects oogenesis............99
3.30 Ectopic expression of ACDC leads to drastic reduced fly viability..101

4.1 Model of the novel chromatin remodeling complex ACDC..104
4.2 The putative novel chromatin remodeling complex ACDC is restricted to oogenesis and early embryonic stages...111
4.3 The intersection of DOM-containing nucleosome remodeling complexes..............................116

LIST OF TABLES

1.1 Subfamilies of main chromatin remodeling complexes and their orthologous subunits 16

2.1 Chromatin assembly by gradually reducing the salt concentration..47
2.2 Primary antibodies and their dilution used in this study for Western blot analyses...................48
2.3 Novel established transgenic fly lines for *UAS-DOM-B WT-FLAG* and *UAS-DOM-B KR-FLAG*...55
2.4 Dilutions of primary antibodies and their appropriate secondary antibodies............................57
2.5 Dilutions of primary antibodies and their appropriate secondary antibodies............................58

CURRICULUM VITAE

Sandra Vengadasalam

Birth name: Vengadasalam
Date of birth: July 23rd 1980
Place of birth: München

Education

11/2006 - present	**PhD thesis at the Ludwig-Maximilians-University of Munich** Adolf-Butenandt-Institute Professor Dr. Peter Becker, Group of Dr. Anton Eberharter Project: Physical and Functional Interaction between DOM-B and ACF1. The Interception of Two Distinct Nucleosome Remodeling Principles
05/2005 - 03/2006	**Diploma thesis at the Ludwig-Maximilians-University of Munich** Professor Dr. Lutz Eichacker Project: Spektroskopische Untersuchungen zur NADPH: Protochlorophyllid-Oxidoreduktase
10/2000 - 03/2006	**Studies in biology at the Ludwig-Maximilians-University of Munich**
09/1991 - 06/2000	**Secondary school: Gymnasium Max-Josef-Stift München** Abitur

Publications

Sandra Vengadasalam, Mariacristina Chioda, Elisabeth Kremmer, Natascha Kunert, Anton Eberharter and Peter B. Becker, Physical and functional interactions of ACF and a DOMINO complex in cell fate specification, *In preparation*

Mariacristina Chioda, **Sandra Vengadasalam**, Elisabeth Kremmer, Anton Eberharter and Peter B. Becker, (2010) Developmental role for ACF1-containing nucleosome remodellers in chromatin organisation, *Development 137*, 3513-3522.